Bridging HIV neutralization sensitivities and Env dynamic phenotypes across genetically diverse variants

Edgar A. Hodge

A dissertation

Submitted in partial fulfillment of the

Requirements for the degree of

Doctor of Philosophy

University of Washington

2023

Reading Committee

Kelly Lee, Chair

Abhinav Nath

Shiu-Lok Hu

Program Authorized to Offer Degree:

Medicinal Chemistry

University of Washington

Abstract

Bridging HIV neutralization sensitivities and Env dynamic phenotypes across genetically diverse variants

Edgar A. Hodge

Chair of the Supervisory Committee

Kelly Lee

Medicinal Chemistry

The envelope glycoprotein (Env) is the sole target for neutralizing antibodies against HIV and the most rapidly evolving, variable part of the virus. High-resolution structures of Env trimers captured in the prefusion, closed conformation have revealed a high degree of structural similarity across diverse isolates. Biophysical data, however, indicate that Env is highly dynamic, and the level of dynamics and conformational sampling are believed to vary dramatically between HIV isolates. Dynamic differences likely influence neutralization sensitivity, receptor activation, and overall trimer stability. The primary objective of this dissertation is to understand how sequence diversity impacts dynamics, and better understand how differences in dynamics impact antibody recognition. After briefly introducing the HIV Env fusion protein, chapter 1 will review one of the primary biophysical techniques I use throughout this dissertation to characterize dynamics-- hydrogen-deuterium exchange mass spectrometry (HDX-MS) -- and highlight recent advances pertaining to its use in structural biology. In chapter 2 I use HDX-MS to map local dynamics across five native-like Env trimers from diverse isolates selected for their high yields, stability, and ability to be purified to a high degree of purity. We demonstrate that significant differences in epitope structural ordering are observed across most sites targeted by

broadly neutralizing antibodies (bnAbs). We also observe isolate-dependent conformational switching that occurs over a broad range of timescales. Lastly, we report that hyper-stabilizing mutations that dampen dynamics in some isolates have little effect in others. In chapter 3 I show that variation in structural ordering in the V1/V2 apex of Env across a widely used panel of HIV-1 isolates is a major source of isolate-specific antigen variation that results in a marked effect on antibody association rates. With help from collaborators, we also report cryo-EM reconstructions of the apex-targeting PGT145 bnAb bound to two divergent Env that exhibit dramatically different degrees of structural ordering throughout much of the trimer structure. Parallel HDX-MS experiments demonstrate that the PGT145 bnAb has an exquisitely focused binding footprint at the apex and is unaffected by local and global structural fluctuations throughout the trimers. In chapter 4 we extend our characterization of Env dynamic phenotypes across trimers derived from isolates in a global panel that is representative of the vast genetic diversity of HIV-1. These data highlight the impact of extreme sequence diversity on dynamic phenotype, elucidates a structure-dynamic link between local dynamics and neutralization phenotype, and provides a mechanistic explanation for IgG recognition of Env trimers.

Table of Contents

List of Figures

Acknowledgements

This project would not have been possible without the encouragement, support and guidance from many people.

First and foremost, I'd like to express my gratitude to my supervisor, Dr. Kelly Lee. His guidance and feedback has been invaluable. Whether writing a manuscript or making a presentation Kelly always encouraged me to focus on the story and cater to the audience. His support allowed me to branch out and learn about other viral systems outside of my main thesis on HIV Env; including interesting projects on RSV, EBV, and SARS-CoV2 that contributed to the breadth of my learning.

I would like to extend my gratitude to my committee for their guidance and support: Dr. Abhi Nath, Dr. Shiu-Lok Hu, Dr. Miklos Guttman, and Dr. Neil King. Their thoughtful feedback and critical insights have helped me to improve my research and shaped my thinking. I also thank them for their time and effort in reviewing and evaluating my work. Dr. Miklos Guttman in particular was the first person to train me on HDX-MS during my lab rotations and his help troubleshooting mass spec instrumentation has been invaluable.

I am grateful for the support of the University of Washington, which provided me with access to resources and facilities that were essential to the success of this research. I would like to thank the Mass Spectrometry Center and Dale Whittington, for his support and encouragement throughout my studies. Additionally, Priska von Haller at the University of Washington's Proteomics Resource was a frequent source of technical support. I'm especially grateful for Rick Harkewicz's help in the construction and plumbing of an HDX LC box that was more user-friendly than the original Waters system I was first trained on and contributed to the overall quality of my HDX-MS data.

I also want to thank my colleagues and friends who supported me throughout this journey. Their encouragement and support were essential in helping me to stay motivated during the more challenging moments of this project. I am fortunate to have such an incredible group of people in my life. Alex Mileant and James Williams spent a considerable amount of time training me on the SOSIP purification method during my Lee lab rotation. After which, Mark Benhaim spent many hours hand-holding and training me on HDX-MS after I first joined the lab. This project required non-stop protein purification, and I am especially grateful to Gajendra Naika for joining the lab and taking over many protein purification duties to streamline the process for several years. Other Lee lab members including; Nancy Hom, Long Gui, Vidya Prasad, Adam Nguyen, Sally Kephart, Klaus Lovendahl, Chengbo Chen, Mint Laohajaratsang, Jake Croft, Mason Saunders, Meghan McGrath, Vada Becker, and Nastassia Parker, have all been a great group of early career scientists that have helped me grow and contributed to a fun environment.

Finally, I would like to express my heartfelt gratitude to my family. Their unconditional love and unwavering support have been the foundation of my success. I am grateful for their patience and encouragement, which have allowed me to pursue my academic goals. Their support has been a constant source of strength and inspiration, and I am blessed to have them in my life.

Dedication

To my dearest wife Aysu,

During the tail end of my academic journey as I asked myself whether grad school had been a reasonable or terrible decision and I endlessly waffled, reminding myself that grad school is where I met you always worked to correct my perspective. You are an endless source of kindness, patience, and love in sunny or gloomy times. I am forever grateful to you.

Chapter 1. Introduction

Portions of the text in this chapter have been modified with permissions from:

Hodge EA, Benhaim MA, Lee KK. Bridging Protein Structure, Dynamics, and Function using Hydrogen/Deuterium-Exchange Mass Spectrometry. Protein Sci. 2019 Nov 13. doi: 10.1002/pro.3790. Review. PMID: 31721348

1.1 Overview

The surfaces of enveloped viruses are decorated with dynamic fusion proteins. For example, influenza viruses present the HA fusion protein, corona viruses display the S spike fusion protein, and HIV is decorated with the HIV envelope glycoprotein (Env) (Figure 1.1) [1]. Functionally these proteins all serve a similar purpose: to merge the lipid bilayer that surrounds the virus with the target cell membrane and allow the virus entry into the target cell. In order to merge the two membranes these fusion machines undergo dramatic structural rearrangements from a meta-stable pre-fusion state to a post-fusion conformation (typically a 6-helix bundle). Since the transition from the pre-fusion to post-fusion state is irreversible, this transition has evolved to rely on some sort of trigger, such as binding to receptors and/or a change in pH. Because fusion proteins are exposed on the virus surface, they are targeted by immune cells and antibodies. Neutralizing antibodies (nAbs) prevent infection by blocking fusion protein structural rearrangements, or blocking interactions with receptors. Viruses are often under immense immune pressure to evade antibody mediated neutralization. Evasion can include changes in a fusion protein's epitope sequence, epitope charge, length of variable loops that conceal binding sites, conformational masking, heterogeneous glycosylation, and latency [2, 3]. HIV utilizes all of these immune evasion strategies. Hence since its discovery over 40 years ago there is still no successful vaccine.

Promisingly there are nAbs capable of neutralizing over 90% of circulating HIV strains (broadly neutralizing antibodies; bnAbs) that arise in some individuals after a few years of infection [4]. But attempts to elicit these bnAbs via vaccination strategies have fallen flat. Successful vaccine design will likely require Env based immunogens that recapitulate the sequence diversity, native glycosylation, and optimal epitope conformations that bind and trigger rare progenitor B-cells capable of generating HIV bnAbs [5]. However the field is still lacking an understanding of how the genetic diversity across HIV viral isolates impacts Env local epitope structural dynamics, and how dynamic motions impact antibody recognition. Below, the HIV Env fusion protein structure and function will be briefly discussed, along with a detailed introduction to a biophysical technique I primarily use to characterize Env trimer dynamics throughout this dissertation; hydrogen-deuterium exchange mass spectrometry (HDX-MS).

1.1 HIV-1 Genetic Diversity

In comparison to many other enveloped viruses, HIV stands out due to the remarkable amount of genetic diversity it contains, where this diversity primarily manifests in its surface Env fusion protein. During the current SARS-CoV-2 pandemic even the lay public have become accustomed to thinking about genetic diversity. Every few weeks major news outlets publish articles warning of a new SARS-CoV-2 variant that is genetically distinct from previous variants. The amount of genetic diversity in SARS-CoV-2, however, is dwarfed by the amount of genetic diversity in HIV-1 [3]. Similarly the amount of viral genetic diversity in a single HIV infected individual can be on par with the global genetic diversity of the influenza virus in humans in a given year [6]. Arguably this may not be a fair comparison because the majority of influenza virus diversity is concentrated in birds [7].

HIV-1 isolates have been classified into different genetic subtypes and circulating recombinant forms (CRF's) based on differences and similarities in their genetic sequences, where different subtypes can differ by as much as 35% [8]. These diverse isolates have further been shown to exhibit a broad range of sensitivities to neutralization using pooled sera from infected donors [9]. It is poorly understood how the enormous amount of genetic diversity in HIV affects virus protein structure and behavior.

1.2 Env Structure and Function

While the influence of sequence variation on protein motions is enigmatic, the structures of many diverse Env trimers have been resolved. Structurally Env is a trimer of heterodimers consisting of three apex receptor (CD4) and co-receptor (CCR4 or CXCR5) binding subunits (gp120) noncovalently bound to three gp41 fusion subunits that sit at the membrane surface and house the hydrophobic fusion peptide [10]. Env binding to the receptor CD4 triggers a transition to an open conformation; involving reorganization of gp120 to form a 4-stranded bridging sheet, displacement of the variable loops 1 and 2 (V1/V2) to the sides of the trimer, and exposure of the tip of the third variable loop (V3) [11]. In this open state the exposed 4-stranded bridging sheet and the tip of the V3 act as the binding site for co-receptor (CCR5 or CXCR4). Binding of co-receptor induces the transition to the post-fusion conformation driving membrane fusion and virus entry into the target cell. Many of the initial challenges to solving the structural details of these flexible trimers were overcome thanks to mutations that stabilize Env in the pre-fusion conformation. Saunders et al. designed the SOSIP construct that includes truncation of the C-terminal transmembrane region to increase solubility, insertion of a disulfide bridge between gp120 and gp41 (SOS), and mutation of an isoleucine to a proline (IP) in the HR1 helix in gp41 to prevent the transition to the post-fusion state (Figure 1.2) [12, 13]. There are now scores of

high resolution structures of Env, including structures from different HIV isolates. While some of these structures are of Env presented on a membrane, the vast majority of our most detailed structural understanding of Env has come from high resolution electron microscopy or x-ray crystal structures of soluble, pre-fusion stabilized Env constructs usually bound to Fabs that lock in one static conformation [14].

1.3 Env Structural Dynamics

While these high-resolution three-dimensional structures have deepened our understanding of Env's assembly and construction, proteins are dynamic molecules that are constantly in motion. These motions range from small fluctuations in local structure to large scale conformational rearrangements between distinct structural states. Indeed, when you align pre-fusion closed Env structures from different viral isolates on top of each other (Figure 1.3), the shared structural homology belies the large differences in sequence and neutralization sensitivities that we know exist. Env trimers, including native-like trimers such as SOSIPs, are known to spontaneously and reversibly transition between at least three distinct pre-fusion conformations, even in the absence of receptor (Figure 1.4) [15]. Furthermore, high-resolution models are usually only available for the endpoints of dynamic processes and one can only infer what takes place regarding protein motion and conformational changes. In order to fully understand how a protein functions, we need to understand the dynamic structural changes that lead to functionally distinct conformations. Importantly, the prevailing hypothesis is that the frequency that Env samples an open conformation determines the virus neutralization phenotype [16]. The propensity of Env to sample distinct conformations has been shown to be isolate dependent using single molecule Forester Resonance Energy Transfer (smFRET) [15]. However, trimer dynamics have only been characterized across a limited number of isolates, and smFRET tracks changes in the distance between inserted fluorophores that span many regions of interest across the trimer structure. The

field is still lacking a full mechanism of the allosteric network that controls the reversible transition between Env conformational states. In this dissertation I have used hydrogen/deuterium exchange mass spectrometery (HDX-MS) to compare dynamic variation across trimers derived from isolates in a global panel that is representative of the vast diversity of HIV-1. In the remainder of this chapter I will provide a primer on HDX-MS and discuss how HDX-MS has been used to interrogate challenging biological problems and extract information that was otherwise not available. I will show how the HDX-MS data enabled the researchers to reach their conclusions and highlight the power of HDX-MS as a tool to study diverse biological systems and protein structures. In addition, pulse labeling HDX-MS has recently been used to study protein folding mechanisms and the structures of intrinsically disordered proteins; areas of structural biology where conventional high-resolution structural techniques have shown limited success. I will also review how HDX-MS can be used to resolve and monitor conformational changes in integral membrane proteins and large protein complexes. These recent works demonstrate the power and versatility of HDX-MS as a solution state structural technique and highlight how the technique has rapidly evolved over the recent years.

1.4 The Biophysics of HDX-MS

Protein motion is constant and ranges from large-scale, slower structural rearrangements to rapid, transient fluctuations in local structure[17]. These innate, often subtle, dynamic motions across the protein backbone are fundamental to protein function but cannot be probed readily by most structural techniques [18]. The intrinsic chemical rate of deuterium exchange of a residue's amide group is primarily dependent on temperature, pH, and the particular type of amino acid. On top of this, HDX-MS applied to proteins is sensitive to the accessibility, or exposure, of backbone amide hydrogens resulting from a protein's conformation and can change in response to protein motion and structural dynamics [19, 20]. In native proteins, the accessibility of a backbone amide

hydrogen is largely dependent on hydrogen bonding and local secondary structure, as well as solvent accessibility [20, 21]. Backbone amide hydrogens more exposed to deuterated solvent will exchange faster than those occluded in the protein core. Similarly, those amide hydrogens engaged in stable hydrogen bonds are protected from deuterium and will exchange more slowly. Local fluctuations in protein structure transiently expose backbone amide hydrogens to deuterium. The propensity for exposed amide hydrogens in a peptide segment to exchange with deuterium is related to how frequently and for how long they exist in an exposed, exchange-competent state with respect to the chemical rate of exchange [20]. These transitions are monitored under equilibrium conditions during continuous labeling HDX-MS experiments [22]. Briefly, in such an experiment, a protein is diluted into a deuterated solution for various amounts of time, ranging from seconds to hours or days. The exchange reaction is then quenched by dropping the solution pH to 2.5 and 0°C, where the labeling rate is at its minimum [20, 23-25]. The labeled protein is digested into peptide fragments which are separated and analyzed by LC-MS. The reverse phase LC separation must be performed quickly and under quench conditions to limit back exchange of the deuterium label with water in solution. The extent of labeling is straightforward to analyze by mass spectrometry as uptake of a single deuteron produces a one Dalton increase in mass.

Under physiological conditions, the majority of local protein motion is faster than the HDX labeling rate and thus leads to gradual incorporation of deuterium onto the peptide backbone (Figure 1.5A). So-called “EX2 kinetics” are observed when the interconversion rate between a peptide’s protected, exchange-incompetent and exposed, exchange-competent state is faster than the labeling rate [20, 26, 27]. In this case, rapid opening and closing events allow only a subset of the collectively exposed amide hydrogens to exchange during any single transition to the exchange competent state. These rapid fluctuations are characterized by unimodal mass spectra envelopes that gradually shift to higher masses with time. Over time the entire peptide segment will become deuterated after repeatedly sampling the exposed, exchange-competent state. The rate and extent of a peptide’s deuterium uptake under EX2 kinetics is interpretable in

terms of local structural dynamics, motion, and flexibility (Figure 1.5 A). Furthermore, by characterizing how this exchange profile changes with environment, upon ligand binding, or between homologous proteins, one can begin to appreciate and dissect the structural basis for protein function and behavior.

Large scale structural rearrangements, including reversible interconversion between conformations, can also be monitored by HDX-MS (Figure 1.5 B). As a protein changes conformation, the rate and extent of HDX will shift in accordance with the local structure of each state. These types of protein motion are typically slow (on the order of milliseconds to seconds) and highly correlated across segments of the amide backbone. In an HDX labeling experiment, this behavior manifests as multimodal isotopic distributions with unique HDX populations for each structural state, and is termed EX1 kinetics [27-30]. For example, if a region in a protein reversibly interconverts between a “closed” protected (exchange-incompetent) and an “open” exposed (exchange-competent) state, with the residues in this segment switching conformations in a concerted manner, this would be readily apparent by HDX-MS (Figure 1.5 B). The amide hydrogens in the “closed” state would be protected from exchange and visible as a lower mass population in the spectra, whereas those that had transitioned to the exposed state would be evidenced as a deuterated higher mass population in the spectra. As the protein reversibly transitions between these states, the individual HDX populations will ultimately converge on the fast-exchanging exposed state, enabling one to determine the rate of conversion between states and their relative half-lives (Figure 1.5 B). More generally, EX1 kinetics is indicative of correlated local structural changes or motion occurring slower than the labeling rate; meaning multiple amide hydrogens in a peptide segment adopt a relatively long-lived exchange competent state and become deuterated together [27, 31]. In reality, EX1 exchange kinetics are rarely observed under physiological conditions because one’s ability to resolve EX1 kinetics is dependent on the rate of interconversion between the protected-exchange incompetent and exposed-exchange competent state being slower than the labeling rate [27, 31].

EX1 kinetics are also often misidentified during analysis [28, 32-34]. Determining the presence and root cause of EX1 behavior requires careful interrogation and analysis of the data using the proper analytical tools. Most commonly, HDX-MS data is analyzed by centroid fitting, where the centroid of a mass envelope is identified and tracked over time [35]. While centroid fitting may be sufficient for analysis of clean EX2 kinetics data, it is insufficient for the analysis and extraction of accurate structural dynamic information when EX1 kinetics are present. More importantly, centroid fitting fails to identify all but the most blatantly obvious EX1 exchange data where the two HDX states are dramatically different. EX1 exchange kinetics commonly manifests as abnormally broad mass envelopes, where the two HDX states are not dissimilar enough from one another to produce visually distinct populations. Analysis by binomial fitting is sensitive to changes in mass envelope width and can therefore detect the presence of two similar, coexisting HDX states and characterize their individual exchange profiles through bimodal deconvolution (For a more expansive explanation of bimodal deconvolution and binomial fitting the reader is referred here [28, 34].

The presence of bimodal spectra in HDX-MS data does not always correspond to EX1 kinetics arising from large scale conformational changes, reversible interconversion between states, or local coordinated motion. It can also be indicative of conformational heterogeneity resulting from sample impurity or degradation, mixed populations from unsaturated ligand binding, and even back exchange from chromatographic carryover and improper sample handling [24, 36, 37]. Similarly where EX2 kinetics are observed, it does not necessarily prove that the local protein motion across those residues is uncorrelated, only that it is occurring faster than the labeling rate [27, 38]. Critical analysis of HDX-MS data using the proper and most robust analytical tools is essential for making meaningful conclusions about protein structural dynamics and motion. Below, we highlight some notable examples where HDX-MS has been used to investigate protein motions and conformational changes, revealing novel insights into their behavior and functions.

1.5 HDX-MS Approaches to Studying Conformational Sampling & Protein Folding

The mechanism by which proteins fold in solution remains the subject of intense debate [39-41]. An unfolded protein must rearrange in solution to find its final native conformation amongst a vast conformational space. Exactly how proteins find this proverbial “needle in a haystack” is still unclear; are there multiple discrete folding pathways for a given protein, or does folding occur through a single distinct pathway [41, 42]? Biology has evolved a solution to the protein folding problem and encoded it in each protein’s sequence. However, we have yet to elucidate these solutions for ourselves. Classical high-resolution structural techniques, such as cryo-EM and X-ray crystallography, are not amenable to studying protein folding. While folding can often be directly monitored by spectroscopic methods, these approaches lack the structural and temporal resolution needed to resolve and appreciate the mechanism of protein folding [26, 39].

Pulse labeling HDX-MS enables direct monitoring of active events such as protein folding with high structural and temporal resolution. During folding the protein is rapidly pulsed with deuterium, effectively capturing a snapshot of the protein’s structure as it transitions to the native folded state. Using a short, fixed, often millisecond, labeling time abrogates the contributions of structural dynamics to exchange as the labeling rate is faster than folding can occur; thus the acquisition of structure during folding is the primary factor contributing to HDX [22, 43]. Walters et al. sought to determine the mechanism of protein folding for maltose binding protein (MBP), a large multidomain protein, using pulse labeling HDX-MS [42]. An obligate folding intermediate was observed soon after folding was initiated (Figure 1.6A). This intermediate was comprised of two structurally adjacent helices that form long range contacts in the native folded state, as seen in the crystal structure (Figure 1.6 C-D). Together with these helices, the adjacent sheets form the structural core of MBP. As these helices formed, they became protected from exchange resulting in clear bimodal isotopic distributions representing both a protected helical state and an exposed

unfolded state (Figure 1.6 E-F). Following formation of this intermediate, multiple slow but distinct folding events were observed. These sequential folding events began nearest to the obligate intermediate's structural core and concluded in the most distant parts of the protein (Figure 1.6 B). While Walters et al. were unable to resolve individual discrete folding intermediates from within these events, it was clear that folding radiated outwards from the structural core that was present in the fast folding intermediate. The authors of this protein folding pulse deuteration study concluded that for MBP, folding occurs through a single distinct pathway where the obligate fast folding intermediate acts as a seed for the subsequent folding events. Bimodal deconvolution allowed the researchers to resolve how, and on what time scale, each peptide segment folds. If MBP folded by multiple discrete pathways, they would have manifested in the data as uncorrelated and temporally blurred folding events. Each discrete folding event would not be resolvable from one another, therefore the observable folding kinetics for each peptide would be the combination of all folding pathways. Their conclusions are further supported by a subsequent study where Ye et al. examined the effect of mutations on the folding mechanism for MBP by HDX-MS [44]. Mutations made in the hydrophobic cluster of the fast folding intermediate and structural core resulted in dramatically slower folding for the intermediate and all subsequent folding events. The folding rate for the intermediate was roughly 20x slower, whereas the subsequent folding events were only two-fold slower thus supporting their earlier conclusions that formation of the intermediate is required for folding to occur [44]. They also demonstrated using HDX-MS, that folding aided by a chaperone abrogated the mutation's effect on folding. HDX-MS is a sensitive tool to probe the conformational space proteins navigate through. It has been successfully used to identify partially folded intermediate conformations during the protein folding process. The time-resolved monitoring of structure formation throughout the protein can be used to understand the mechanism of protein folding and unfolding in solution and deepen our understanding of how large, multidomain proteins fold and how this process is modulated by chaperones. HDX-MS combines high structural resolution with the temporal resolution of quench-

flow spectroscopic techniques enabling for the precise elucidation of how and when folding occurs in proteins.

1.6 Monitoring Transiently Preferred Conformational States in Intrinsically Disordered Proteins

While it had long been believed that proteins require a well-folded, ordered native structure to carry out their functions, recent research revealed the ubiquitous nature of intrinsically disordered proteins (IDPs) that play essential roles in cellular signaling, regulation, and have been implicated in disease pathogenesis [45]. IDPs are critical for a number of diverse cellular processes and individual IDPs are often functionally promiscuous. The large range of IDP functionalities are likely derived from their inherent conformational plasticity [46]. IDPs are challenging to study using HDX-MS for a number of reasons; significant flexibility and a lack of secondary structure means IDPs require very short, rapid deuteration time points under physiological conditions. IDPs have been shown to rapidly interconvert between ensembles of conformational states and this structural heterogeneity poses additional hurdles during data analysis [47]. For example, if an ensemble of conformations are present in solution, multimodal spectra may make ascribing which population in the spectra belongs to which conformer a challenging task [48].

The combination of rapid conformational switching along with a lack of secondary structure often means most IDPs are maximally deuterated in mere seconds. In order to get any dynamic information from proteins with such rapid deuteration times researchers have made use of quench-flow devices to detect transient conformational states of IDPs at very short timeframes [49, 50]. Even without access to quench-flow instrumentation, adjusting the pH can dramatically increase the time window covered by HDX [51, 52]. Decreasing the pH by one unit slows the exchange rate 10 fold, enabling one to probe differences in HDX for even the most exposed amide hydrogens [20, 21, 53]. By reducing the pH during the exchange reaction,

Goswami et al. were able to compare the dynamics of an IDP responsible for regulating nuclear receptors, PGC-1α, in the presence and absence of the nuclear receptor PPARγ [51]. Initially, they were unable to detect differences in HDX at physiological conditions, however, at pH 6.0 where the labeling rate is dramatically slower, they were able to see how regions of PGC-1α rapidly fold upon receptor binding. This study is an excellent example of how labeling times may be adjusted to capture protein dynamics that occur on very fast time-scales, however care should be taken to ensure the protein's structural dynamics and conformational bias are not altered by lowering the pH.

Pulse labeling HDX has enabled researchers to better understand the mechanism of aggregation for the clinically important IDPs Aβ (amyloid beta) and AS (alpha-synuclein) [54, 55]. Aggregation of Aβ and AS is closely linked with progression of their neurological diseases, Alzheimer and Parkinson's disease respectively. By monitoring the structure of these IDPs during aggregation, researchers were able to understand how the appearance of early structural features contribute to the initiation and kinetics of the aggregation cascade. By HDX-MS these structural seeds for aggregation are visualized as the formation of a long-lived protected population. Identification of these preferential structural features is critical for understanding the progression of disease and developing effective therapeutics [54, 55]. The presence of multiple conformers/ oligomeric states frequently generates complex multimodal spectra. While discerning which population belongs to a certain conformer may be very challenging, typically a shift in mass to more protected populations is observed as a result of aggregation [54, 55]. Aggregation, especially fibril formation, can cause poor protein sequence coverage due to decreased proteolysis efficiency in bottom-up HDX-MS approaches where the protein is proteolyzed before analysis [47, 54, 56, 57]. In addition, typically, HDX-MS data for a given peptide is an average of all states present in the population, meaning if multiple unique states exist but are not resolvable by bottom-up HDX-MS workflows, they remain undetected. Furthermore, if all protein states are not proteolyzed with similar efficiencies the resulting

distributions seen during analysis can be artificially skewed and misrepresentative of what existed in solution. More recent technological innovations have allowed for combining top-down HDX-MS workflows, where the intact protein is ionized into the mass spectrometer, with the gas phase fragmentation technique, electron capture dissociation (ECD) to isolate and analyze individual conformers from within a population. ECD functions by fragmenting a protein or peptide inside the mass spectrometer that has been selected for based on mass and charge enabling analysis of the peptide fragments without proteolytic digestion having occluded which unique conformer they originated from. When ionized in a mass spectrometer different protein conformations take on charge differently due to their size and shape, thus allowing one to isolate and analyze target conformers and their peptide fragments [58-60]. ECD also enables fragmentation of a peptide without scrambling of the deuterium label, as is the case with other fragmentation methods, meaning deuterium uptake can be analyzed with single amino acid resolution [58, 61, 62]. Pan et al were able to take advantage of different conformers' preferences for different charge states and select for specific isotopically labeled Aβ42 conformers using pre-cursor ion selection and analysis of the Aβ42 oligomer's HDX profile with single amino acid resolution using ECD [62].

The innate conformational plasticity of IDPs enables them to engage multiple partners and modulates a diverse range of functionalities. However, it has proven difficult to understand or identify specific structural features or conformations present in IDPs that give rise to these functions. Interactions with IDPs are often accompanied by a disorder-to-order transition, which can be directly monitored by HDX-MS [63, 64]. Like many proteins, CyaA, an adenylate cyclase toxin from bacteria, contains a large intrinsically disordered region (IDR) [65]. Binding of calmodulin (CaM) to CyaA activates its enzymatic activity, generating toxic levels of cAMP. HDX-MS was used by O'Brien et al. to elucidate the mechanism of CyaA activation through ligand binding. While no crystal structure of unbound CyaA was available, HDX-MS revealed an IDR encompassing a 75 amino acid stretch of fast exchanging peptides previously thought to

primarily be helical based on the ligand bound crystal structure. Upon binding CaM, large regions of the C-terminus displayed significant increases in backbone amide protection, suggesting formation of secondary structure confirmed to be helical via CD. This ligand-induced gain of structure is likely important for adopting a catalytically active conformational state. Regions distal to the binding location, such as around the catalytic site became rigidified upon CaM binding, while the catalytic loop remained highly disordered and solvent accessible (Figure 1.7 A-B). The authors posit that balancing a more ordered catalytic site with a flexible loop may optimize substrate binding and product release, and that structural disorder in CyaA is a mechanism used to inhibit enzymatic activity. To illustrate the benefit of pairing high-resolution atomic models with a solution state technique, the authors noted a rigid G helix in the ligand bound crystal structure was shown to be highly flexible in solution by HDX-MS (Figure 1.7 C-D). They surmise the rigidity in the crystal structure may be an artifact of symmetric crystal packing and not representative of the native environment [65]. HDX-MS can be used to characterize structural transitions that often define protein function and control protein-protein interactions. Though HDX data does not provide a three-dimensional structure of a protein, it provides useful information on how proteins dynamically move in solution and is a more powerful tool when combined with high resolution structures. This ligand induced structural rearrangement is an excellent example of how HDX-MS can be used to characterize structural transitions that often define protein function and control protein-protein interactions.

1.7 Conformational Switching Through Correlated Motions

It is well appreciated that a protein's 3-dimensional structure dictates its function and induced or spontaneous changes in that structure are critical to that function. Typically, static high-resolution models are used to visualize protein structure and its related function. However, functionally relevant dynamic changes in protein structure are not always apparent by these

methods. One of the powers of HDX-MS is the ability to identify and resolve induced conformational changes distal to the ligand binding site. A better understanding of allosteric effects can provide important details on protein function. Conversely it can complicate epitope mapping since it is not always apparent what changes in HDX result from protection at the binding site or long range compensatory structural changes. Deng et al demonstrated that HDX data generated from a typical HDX-MS experiment, where an antibody was pre-incubated with myoglobin (Mb) and allowed to reach equilibrium, provided data that was unable to differentiate changes in peptide amide protection caused by antibody binding at the immediate binding site from distal allosteric changes [66]. In order to better differentiate between the antigen binding site and allosteric effects, the authors utilized a novel kinetic labeling approach using microfluidic chips to perform mixing of small solution volumes. In this configuration, the antibody, antigen, and deuterium were mixed simultaneously prior to quenching and enzymatic digestion. The authors demonstrate the kinetic labeling approach can distinguish the epitope of an antibody against Mb from distal allosteric changes because local allosteric changes in HDX were generally not detectable until ~200 milliseconds, where peptides in regions involved directly in binding Ab displayed an immediate decrease in HDX. It thus appears that the allosteric communication leading to detectable changes in structure may occur more slowly than the immediate increase in protection resulting from a ligand binding event [66]. The authors note that this approach proved successful here, however it has limited scope as the allosteric change they observed was markedly slower than the initial binding event. It will be interesting to determine if this kinetic labeling approach is generalizable to other protein systems as well, or if rates of allosteric propagation in other proteins takes place on timescales too rapid to parse out allosteric changes from ligand binding using HDX-MS.

Protein-protein interactions can alter a protein's conformational landscape giving rise to new conformational states, and the subsequent changes are often critical for a diverse range of protein functions, including those involved in cellular signaling [17]. Tulsian et al used HDX-MS

along with supporting techniques to probe such binding induced conformational changes in the ternary complex of protein kinase A (PKA), phosphodiesterase (PDE), and cAMP to better understand how cells terminate cellular signaling [67]. The two cAMP binding sites on PKA have been well characterized, however, the mechanism of cAMP hydrolysis by PDE was poorly understood. It had puzzled researchers how cAMP tightly bound to PKA could be hydrolyzed by PDE. Monitoring peptides in the cAMP binding sites confirmed PKA alone could only bind cAMP but not hydrolyze it. Following the addition of PDE, they observed hydrolysis and release of cAMP resulting in bimodal mass spectra representing a protected, cAMP bound state, and an exposed apo state. However, over time they observed increased broadening of the mass envelope indicating the presence of a unique conformational state distinct from the apo and cAMP bound states of this ternary complex. The observed HDX profile could not be attributable to linear combinations of spectra corresponding to any individual assembly (Figure 1.8 top right spectrum). The authors suggest this unique HDX state may arise from an additional structural rearrangement in the RIα-PDE-cAMP complex that forms a substrate channel linking the cAMP binding site to the PDE catalytic site as a method to shuttle bound cAMP to the catalytic site for enzymatic hydrolysis.

It has been shown that many proteins require a lipid environment to properly fold into their native functional conformation and many essential protein-protein interactions occur on the surface of membranes with integral and peripheral membrane proteins [63, 68]. It is known that this amphipathic environment can have profound effects on the native structure and dynamics of proteins [69]. Researchers have tried to recapitulate the native environments of integral and peripheral membrane proteins in vitro using detergent solubilization, lipid micelles and bicelles, liposomes, and lipid nanodiscs [68, 70, 71]. While it is not well understood how each of these synthetic lipid systems influence or perturb a protein's structure, dynamics, or function these synthetic systems are invaluable experimental tools for the study of membrane protein structure and function. Recently, the atomic structures of an increasing number of integral and

peripheral membrane proteins, often solubilized in detergent, have been solved; and while these structures have proved invaluable in furthering our understanding of membrane protein structure they do not fully convey how these dynamic proteins function. One such integral membrane protein, the P-glycoprotein ABCB1 transporter (Pgp) facilitates the active transport of a myriad of small molecules across the cell membrane, including drugs, peptides, and lipid-like molecules through a dynamic conversion between inward and outward facing conformations (Figure 1.9 C) [72]. Using HDX-MS to study the conformational dynamics of Pgp, Li et al identified multiple peptides across Pgp displaying bimodal spectra likely resulting from the inward and outward facing conformations (Figure 1.9 A) (62). HDX-MS was performed in both detergent and lipid nanodiscs to mimic the native environment of this integral membrane protein and to attempt to understand how different synthetic lipid systems influence protein structure, dynamics, and function. A larger number of peptides exhibiting bimodal spectra suggestive of mixed EX1/EX2 kinetics were identified in the nanodiscs compared to detergent (Figure 1.9 B). This observation may suggest the more native membrane-like nanodisc environment slowed the conformational interconversion rate in local regions enough to resolve multiple conformational states. It is also possible that the lipid packing in nanodiscs restricts protein motion in a way that is not present in detergent [73]. Meanwhile, the conformational switching in detergent likely takes place on a faster time scale effectively masking certain peptides indicative of dynamic conformational transitions. Peptides from ligand-free Pgp displayed bimodals on different timescales; fast conformationally interconverting peptides only displayed bimodals at the earliest time points (10 seconds and 1 minute), moderate peptides displayed bimodals up to 1 hour, and peptides suggesting the slowest conformational transitions displayed bimodal spectra up to 4 hours (Figure 1.9 A). The presence of mixed EX1/EX2 kinetics enabled the authors to extract approximate half-lives for these intermediate conformations. The authors deduced that the presence of peptides exhibiting structural transitions on different timescales likely implies that

Pgp exists not only as the inward or outward facing conformation but instead is more dynamic and fluidly undergoes multiple conformational transitions.

While often a protein's functional structure is visualized as a single discrete state, this static image does not represent the ensemble of states present in solution that contribute to that protein's functionality. This is especially relevant for promiscuous proteins, such as the Pgp transporter, which has an incredibly diverse substrate pool or may interact with multiple partners and ligands. By using HDX-MS to study changes in protein structure, it becomes possible to start to identify and link specific structural changes to specific functional events, to characterize the timescales of protein motion during a conformational change, and to shift the perspective on protein dynamics and conformational change away from a static image to one that captures a fluid, dynamic entity.

1.8 Summary

HDX-MS has evolved into a powerful and versatile solution state biophysical and structural technique capable of probing protein structure and motion under native conditions and in complex assemblies. Recent advancements have enabled the investigation of protein folding intermediates, the characterization of transient structure in IDPs, and the real-time observation of large integral membrane proteins during catalysis. These studies demonstrate how HDX-MS can be readily applied to study protein structural dynamics in systems with a scale and complexity where other techniques have struggled. As the field continues to evolve, the technique is becoming increasingly powerful and accessible, further expanding the scale and complexity of systems capable of being studied. For example, HDX-MS has recently been used to study the structural dynamics of proteins on intact enveloped viruses such as dengue virus and influenza virus [74-76]. Similarly, the structural characterization of integral membrane proteins in native membrane environments by HDX-MS has become commonplace. What were

once considered pipedreams of structural biology are now within reach. Furthermore, as HDX-MS becomes used by a larger population of researchers, significant efforts have been made across the field to standardize experimental procedures and data processing and reporting practices [36, 77]. A major focus of this dissertation utilizes continuous labeling HDX-MS to characterize strain specific differences in Env trimer dynamics, particularly focusing on regions targeted by bnAbs. In combination with other biophysical tools, structural mass spectrometry is used here to investigate the consequences of extreme sequence variation on dynamics, and assess how differences in epitope flexibility impact antibody recognition.

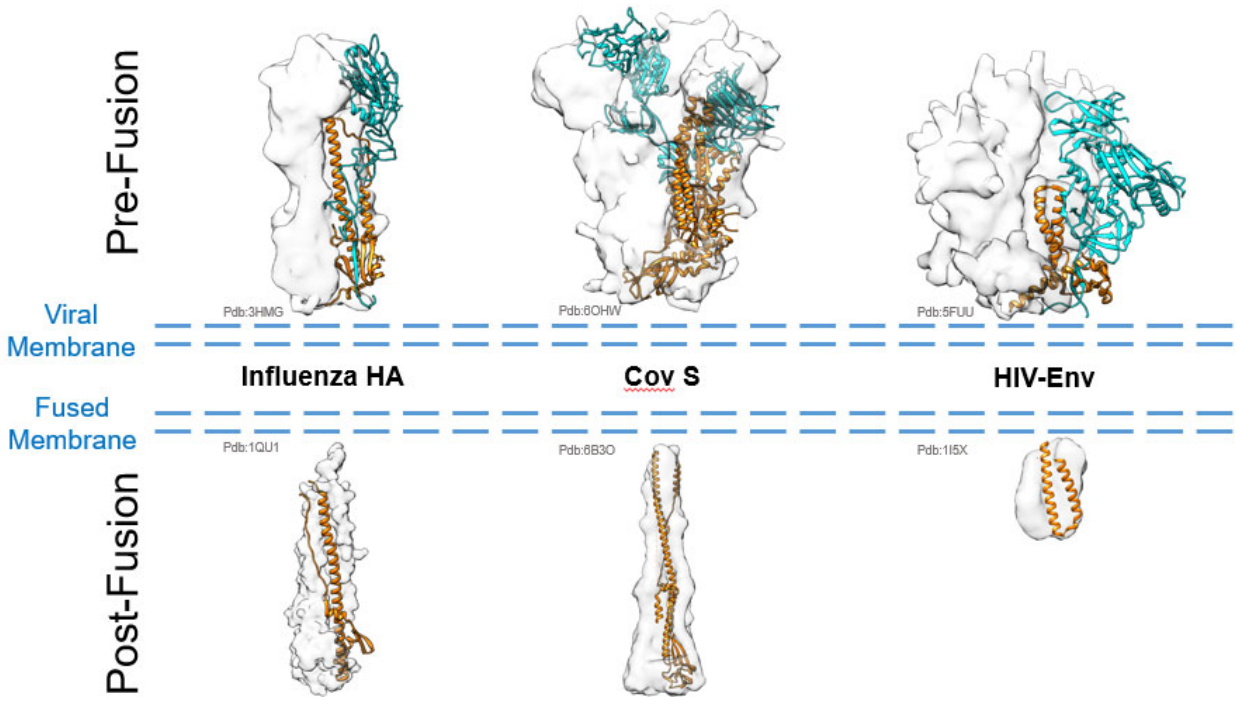

Figure 1. 1. Enveloped viruses display trimeric fusion proteins in order to merge virus and target cell membranes. The hemagglutinin (HA) fusion protein (PDB 3HMG), the coronavirus spike (S) fusion protein (PDB 6OHW), and the HIV Envelope (Env) fusion protein (PDB 5FUU) are displayed on top in their pre-fusion conformations. 2/3 of the protomers are displayed in white surface, and 1 protomer is displayed in ribbon representation, where the receptor binding subunits are colored in cyan and the base fusion subunits are colored in orange. After membrane fusion these fusion proteins exist in a stable six-helix bundle post-fusion conformation displayed on the bottom of the figure. Again with 2/3 of the fusion subunits displayed in white surface, and 1 displayed in ribbon across the 3 different proteins (PDB 1QU1, 6B3O, 1I5X).

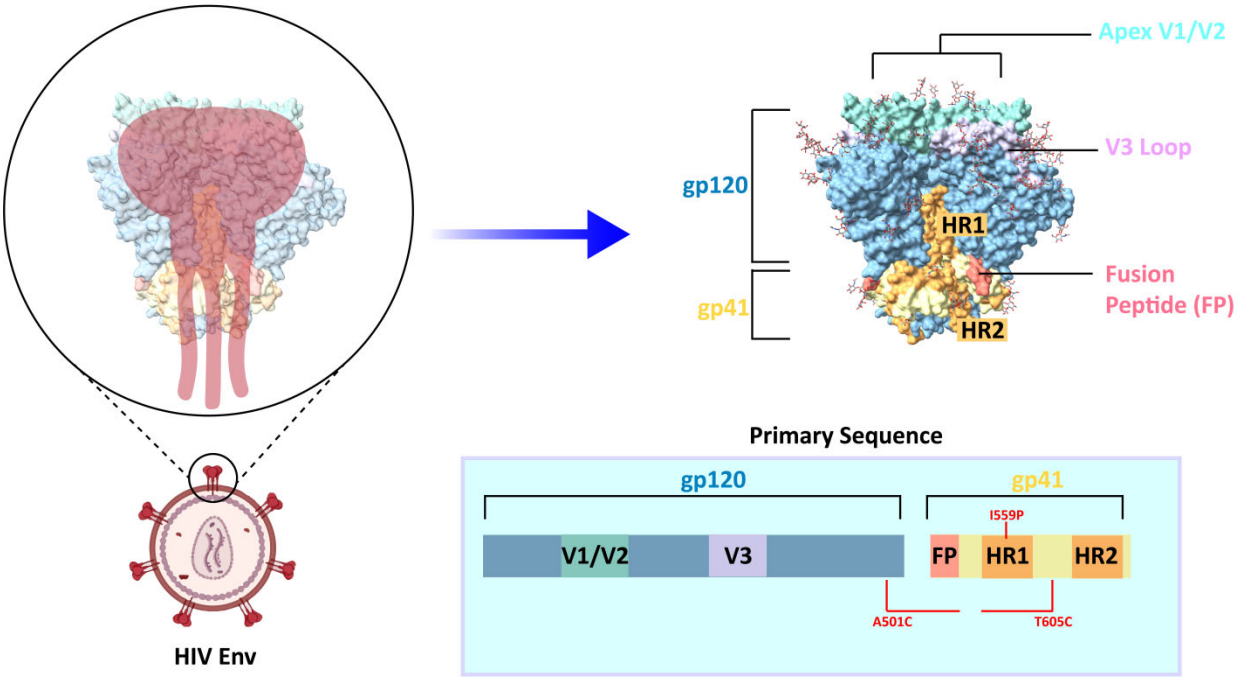

Figure 1. 2. HIV Env SOSIP stabilizing mutations. SOSIP stabilizing mutations are highlighted in the primary sequence box in the bottom right corner and include truncation at the C-terminal end of gp41 to make Env more soluble and less prone to aggregation, an added disulfide bridge (SOS) connecting gp41 and gp120 (A501C and T605C), and an isoleucine to proline mutation (IP) in HR1 of gp41 to lock Env in the pre-fusion state. The env trimer is displayed (PDB 5ACO) in the top right in surface representation with the three gp120 subunits colored in blue, the apex V1/V2 loops colored in teal, the V3 loop colored in purple, the three gp41 subunits colored in orange, and the fusion peptide (FP) colored in red.

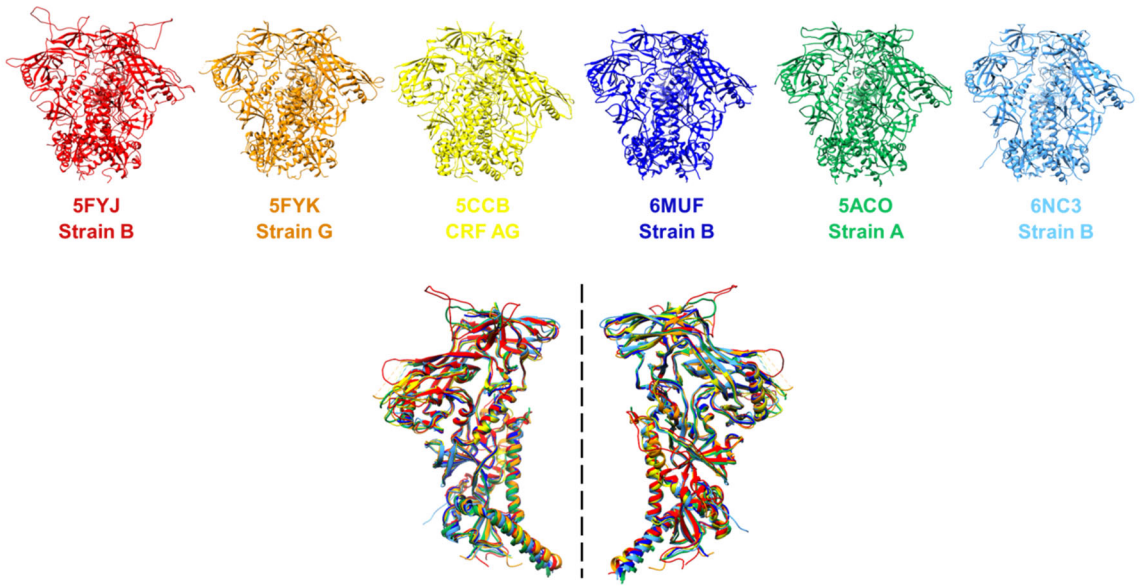

Figure 1. 3. Env trimers share a high degree of structural homology despite genetic diversity. High resolution EM and crystal structures (PDB's listed above) of Env trimers in the pre-fusion closed conformation are lined up and colored differently. On the bottom one protomer (gp120 and gp41) from each structure were aligned in chimera.

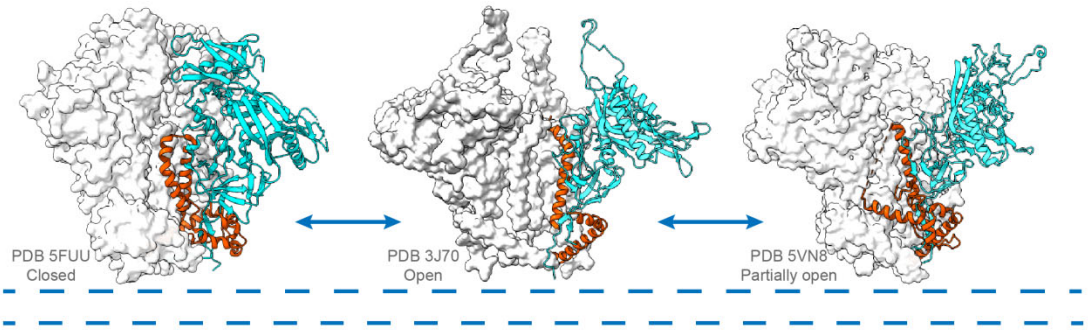

Figure 1. 4. Env trimers spontaneously and reversibly sample at least three distinct conformations. fAb bound trimers in a closed (PDB 5FUU), open (PDB 3J70), and an intermediate conformation (PDB 5VN8) are shown. 2/3 protomers are displayed in white surface representation, and one protomer is displayed in ribbon with gp120 colored cyan and gp41 colored orange.

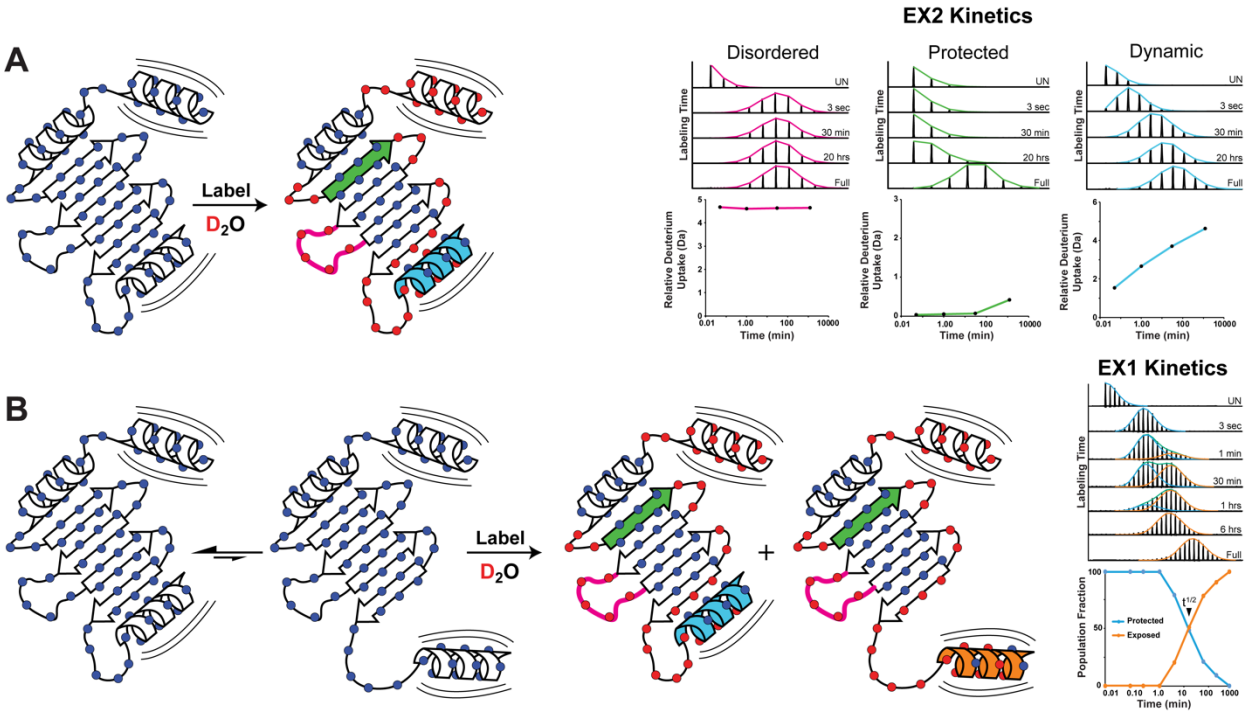

Figure 1. 5. Protein structural dynamics and motion monitored by HDX-MS. Continuous labeling HDX-MS probes the accessibility of backbone amide hydrogens (blue circles) by their exchange with deuterium in solution. Under equilibrium conditions the majority of protein structural dynamics and motion manifests as “EX2 kinetics” (A) where deuterium is gradually incorporated across the protein backbone in a manner directly related to the local structural dynamics and changes in amide accessibility. Peptide segments in highly structured regions with strong hydrogen bonding networks (green beta sheet) take up deuterium more slowly than

regions with exposed and accessible amides (pink loop) and those undergoing dynamic motions (blue helix) that occur faster than the labeling rate. (B) When these dynamic structural changes are slower than the labeling rate (e.g. a reversible interconversion or conformational change) they produce unique and resolvable HDX states that manifest as “EX1 kinetics”.

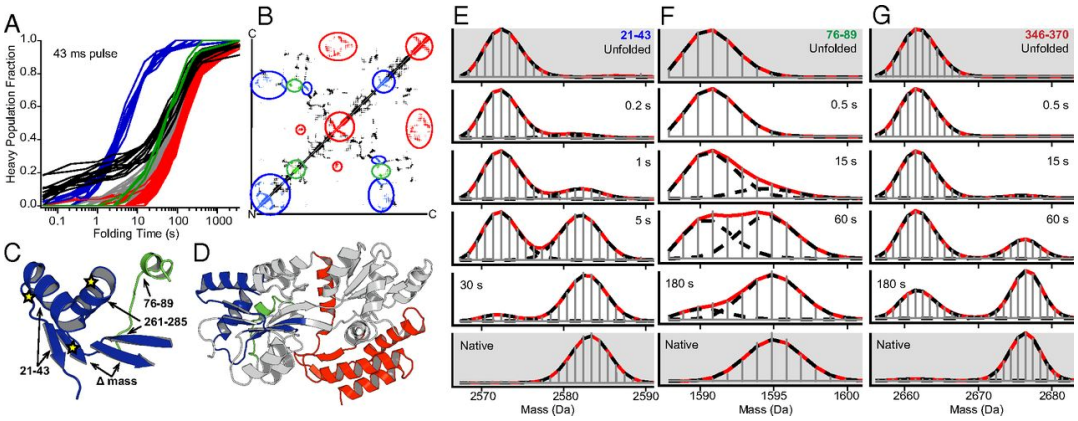

Figure 1. 6. Elucidating the mechanism of protein folding by pulse labeling HDX-MS. The folding of maltose binding protein (MBP) was monitored by pulse labeling HDX-MS where unfolded and fully deuterated MBP was diluted to initiate folding. Using a quench flow system the samples were rapidly labeled during folding with a ~millisecond pulse of H2O (D-H exchange) resulting in bimodal isotopic distributions showing the formation of secondary structure, and resistance to exchange, as each peptide folds (E-G). Analysis of all peptides folding kinetics revealed the formation of an obligate “fast folding” intermediate state (blue traces and highlights A-E). Subsequent folding events radiated outward from the structural core formed by the fast folding intermediate and only a single distinct folding pathway was observed (A, B, and D). Figure adapted from reference (Walters PNAS, 2013) with permission.

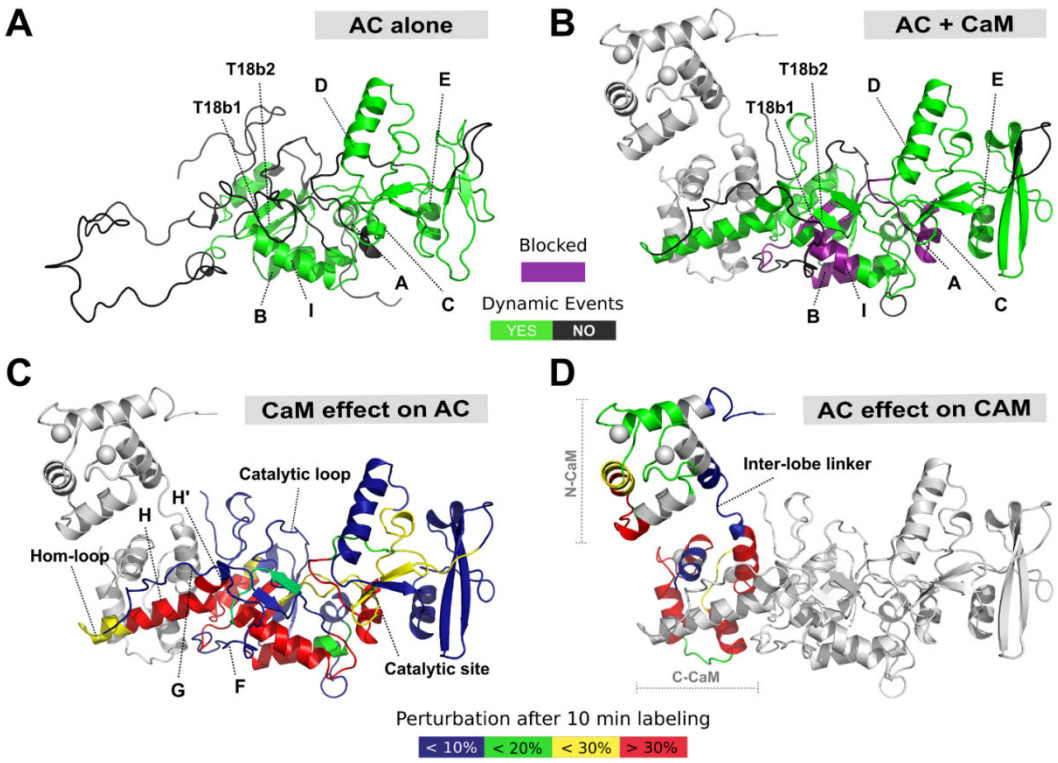

Figure 1. 7. Ligand induced disorder to order transition is critical for catalytic function in CyaA. The structure of free CyaA eluded previous structural characterization. By HDX-MS it was observed that a 75 amino acid long region, previously seen as helical in the ligand bound structure, was intrinsically disordered in the apo state and becomes ordered upon binding with CaM (A-D). Purple indicates helices with dramatic increases in protection from deuteration, and green indicates regions that became more dynamic upon ligand binding. Figure C & D map differences in percent deuteration on AC and CaM upon binding, respectively. Figure adapted from reference (O'Brien PLOS Biology, 2017) with permission.

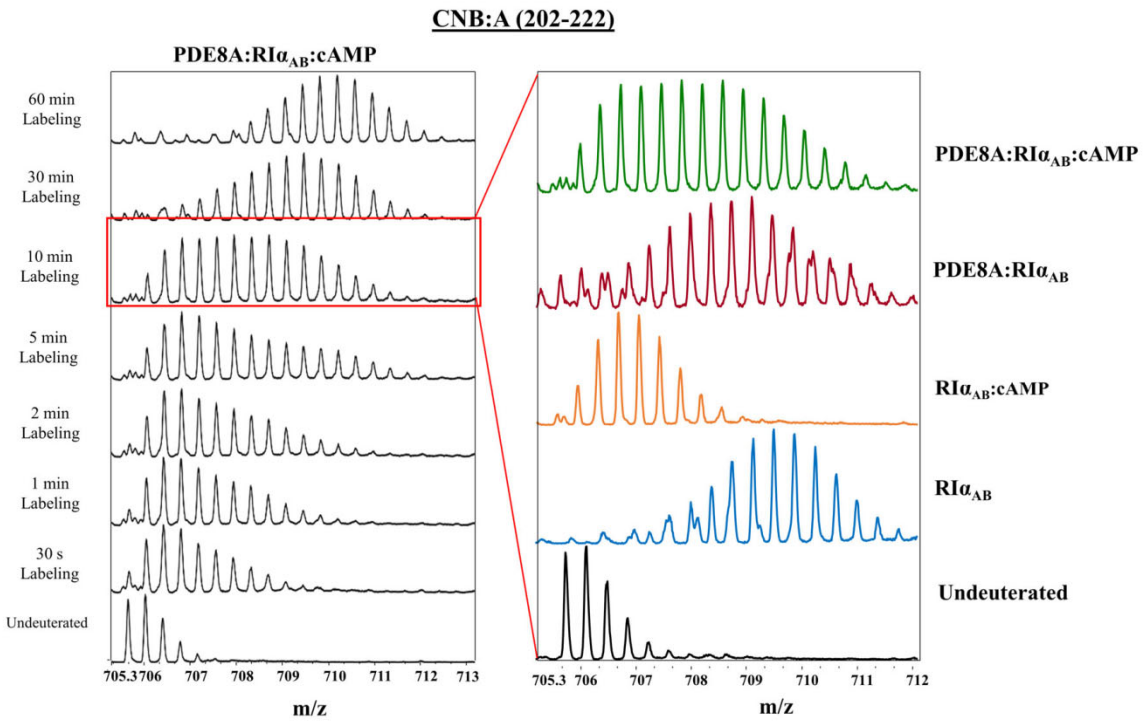

Figure 1. 8. HDX-MS reveals novel functional state in protein kinase A ternary complex. Hydrolysis of cAMP by the protein kinase A (PKA) and phosphodiesterase (PDE) ternary complex was monitored in real time by HDX-MS. A highly broad mass envelope appeared over time in the ternary complex (top right spectra). Analysis of each component and their possible assemblies could not explain the distribution seen in the ternary complex indicating this is a unique and catalytically active structural state. Figure adapted from reference (Tulsian Biophysical Journal, 2017) with permission.

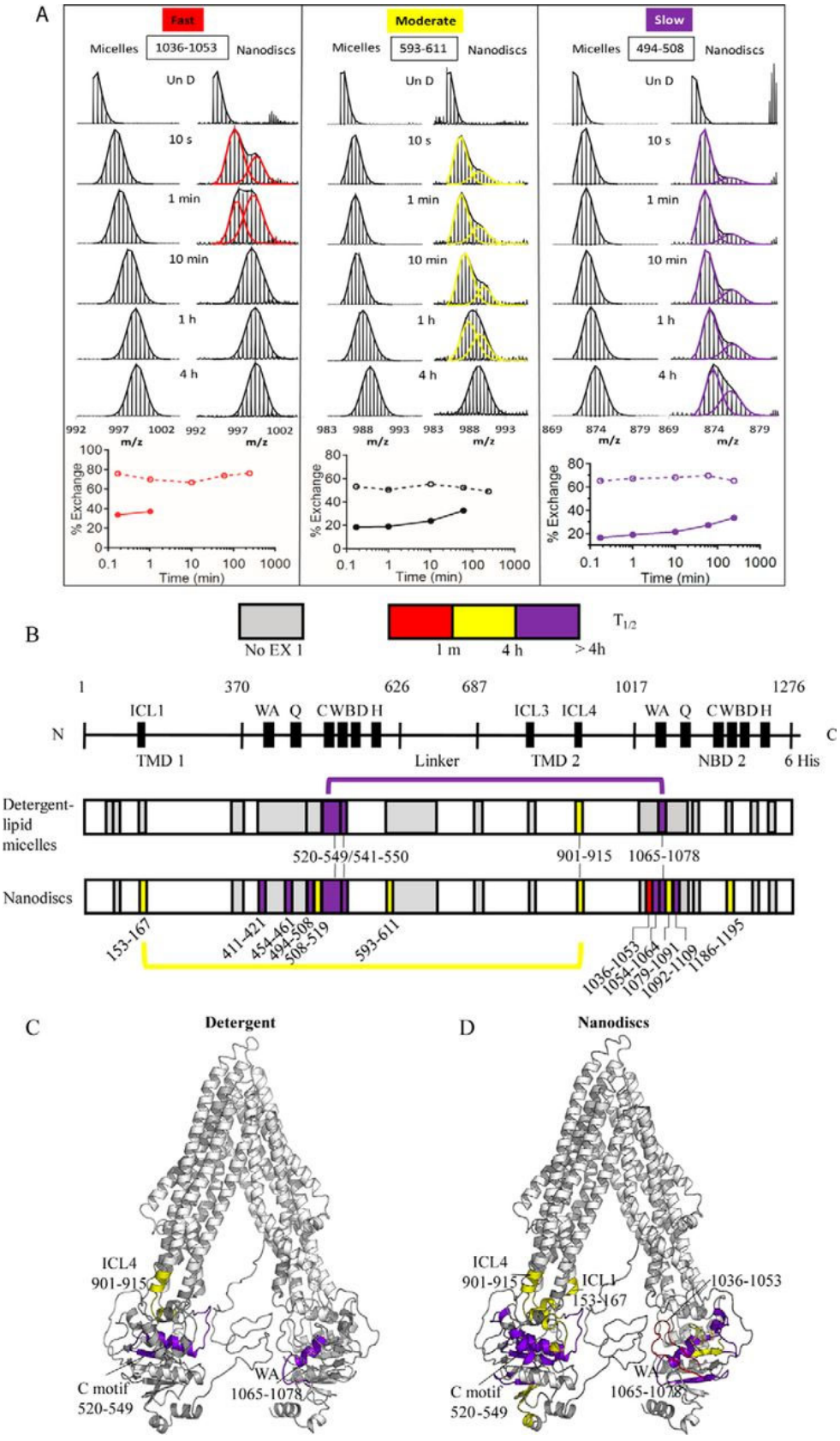
A
Fast
Micelles
1036-1053
Nanodiscs
Moderate
593-611
Slow
494-508
Un D
10 s
1 min
10 min
1 h
4 h
m/z
% Exchange
Time (min)
B
No EX 1
1 m
4 h
>4h
T1/2
1
370
626
687
1017
1276
ICL1
WA
Q
CWBD
H
ICL3
ICL4
N
C
TMD 1
Linker
TMD 2
NBD 2
6 His
Detergent-lipid micelles
520-549/541-550
901-915
1065-1078
Nanodiscs
153-167
411-421
454-461
494-508
508-519
593-611
1036-1053
1054-1064
1079-1091
1092-1109
1186-1195
C
Detergent
D
Nanodiscs
ICL4
901-915
C motif
520-549
WA
1065-1078
ICL1
153-167
1036-1053

Figure 1. 9. Dynamic conformational changes in the integral membrane protein Pgp. The ABCB1 transporter P-glycoprotein P (Pgp) reversibly interconverts between inward and outward facing conformational states to facilitate transport of ligand across the cell membrane. HDX-MS of Pgp in lipid nanodics and detergent revealed conformational transitions occurring on multiple timescales across Pgp indicating the presence of more than two discrete conformational states (A-C). Binomial fitting of bimodal isotopic distributions enabled the deconvolution of multiple coexisting HDX populations and analysis of their conformational kinetics (A-B). Figure adapted from reference (Li JBC, 2018) with permission.

References

1. Benhaim, M.A. and K.K. Lee, *New Biophysical Approaches Reveal the Dynamics and Mechanics of Type I Viral Fusion Machinery and Their Interplay with Membranes.* Viruses, 2020. **12**(4).
2. Bricault, C.A., et al., *HIV-1 Neutralizing Antibody Signatures and Application to Epitope-Targeted Vaccine Design.* Cell Host Microbe, 2019. **25**(1): p. 59-72 e8.
3. Duerr, R., et al., *SARS-CoV-2 Portrayed against HIV: Contrary Viral Strategies in Similar Disguise.* Microorganisms, 2021. **9**(7).
4. Stamatatos, L., M. Pancera, and A.T. McGuire, *Germline-targeting immunogens.* Immunol Rev, 2017. **275**(1): p. 203-216.
5. Jardine, J., et al., *Rational HIV Immunogen Design to Target Specific Germline B Cell Receptors.* Science, 2013. **340**(6133): p. 711-716.
6. Korber, B., et al., *Evolutionary and immunological implications of contemporary HIV-1 variation.* British Medical Bulletin, 2001. **58**(1): p. 19-42.
7. Palese, P., *Influenza: old and new threats.* Nat Med, 2004. **10**(12 Suppl): p. S82-7.
8. Seaman, M.S., et al., *Tiered Categorization of a Diverse Panel of HIV-1 Env Pseudoviruses for Assessment of Neutralizing Antibodies.* Journal of Virology, 2010. **84**(3): p. 1439-1452.
9. deCamp, A., et al., *Global panel of HIV-1 Env reference strains for standardized assessments of vaccine-elicited neutralizing antibodies.* Journal of virology, 2014. **88**(5): p. 2489-2507.
10. Guttman, M., et al., *CD4-Induced Activation in a Soluble HIV-1 Env Trimer.* Structure, 2014. **22**(7): p. 974-984.
11. Wang, H., et al., *Partially Open HIV-1 Envelope Structures Exhibit Conformational Changes Relevant for Coreceptor Binding and Fusion.* Cell Host & Microbe, 2018. **24**(4): p. 579-5920000.
12. Julien, J.-P., et al., *Crystal Structure of a Soluble Cleaved HIV-1 Envelope Trimer.* Science, 2013. **342**(6165): p. 1477-1483.
13. Sanders, R.W., et al., *A Next-Generation Cleaved, Soluble HIV-1 Env Trimer, BG505 SOSIP.664 gp140, Expresses Multiple Epitopes for Broadly Neutralizing but Not Non-Neutralizing Antibodies.* PLoS Pathogens, 2013.

14. Ward, A.B. and I.A. Wilson, *The HIV-1 envelope glycoprotein structure: nailing down a moving target.* Immunological Reviews, 2017. **275**(1): p. 21-32.
15. Munro, J.B., et al., *Conformational dynamics of single HIV-1 envelope trimers on the surface of native virions.* Science, 2014. **346**(6210): p. 759-763.
16. Montefiori, D.C., et al., *Neutralization tiers of HIV-1.* Current Opinion in HIV and AIDS, 2018. **13**(2): p. 128.
17. Bu, Z. and D. Callaway, *Chapter 5 Proteins MOVE! Protein dynamics and long-range allostery in cell signaling.* Advances in Protein Chemistry and Structural Biology, 2011. **83**: p. 163-221.
18. Percy, A.J., et al., *Probing protein interactions with hydrogen/deuterium exchange and mass spectrometry—A review.* Analytica Chimica Acta, 2012. **721**: p. 7-21.
19. Bai, Y., et al., *Primary structure effects on peptide group hydrogen exchange.* Proteins: Structure, Function, and Bioinformatics, 1993. **17**(1): p. 75-86.
20. Weis, D.D., *Hydrogen Exchange Mass Spectrometry of Proteins: Fundamentals, Methods, and Applications.* wiley, 2016: p. 295-321.
21. Zhang, Z. and D.L. Smith, *Determination of amide hydrogen exchange by mass spectrometry: A new tool for protein structure elucidation.* Protein Science, 1993. **2**(4): p. 522-531.
22. Deng, Y., Z. Zhang, and D.L. Smith, *Comparison of continuous and pulsed labeling amide hydrogen exchange/mass spectrometry for studies of protein dynamics.* Journal of the American Society for Mass Spectrometry, 1999. **10**(8): p. 675-684.
23. Marcsisin, S.R. and J.R. Engen, *Hydrogen exchange mass spectrometry: what is it and what can it tell us?* Analytical and bioanalytical chemistry, 2010. **397**(3): p. 967-972.
24. Hamuro, Y. and S.J. Coales, *Optimization of Feasibility Stage for Hydrogen/Deuterium Exchange Mass Spectrometry.* Journal of The American Society for Mass Spectrometry, 2018. **29**(3): p. 623-629.
25. Chalmers, M.J., et al., *Differential hydrogen/deuterium exchange mass spectrometry analysis of protein–ligand interactions.* Expert Review of Proteomics, 2014. **8**(1): p. 43-59.
26. Chamberlain, A.K., T.M. Handel, and S. Marqusee, *Detection of rare partially folded molecules in equilibrium with the native conformation of RNaseH.* Nature structural biology, 1996. **3**(9): p. 782-787.
27. Ferraro, D.M., N.D. Lazo, and A.D. Robertson, *EX1 hydrogen exchange and protein folding.* Biochemistry, 2004. **43**(3): p. 587-594.
28. Weis, D.D., et al., *Identification and characterization of EX1 kinetics in H/D exchange mass spectrometry by peak width analysis.* Journal of The American Society for Mass Spectrometry, 2006. **17**(11): p. 1498-1509.
29. Smith, D.L., Y. Deng, and Z. Zhang, *Probing the Non-covalent Structure of Proteins by Amide Hydrogen Exchange and Mass Spectrometry.* Journal of Mass Spectrometry, 1997. **32**(2): p. 135-146.
30. Sivaraman, T. and A.D. Robertson, *Kinetics of conformational fluctuations by EX1 hydrogen exchange in native proteins.* Methods in molecular biology (Clifton, N.J.), 2001. **168**: p. 193-214.
31. Malhotra, P. and J.B. Udgaonkar, *Tuning Cooperativity on the Free Energy Landscape of Protein Folding.* Biochemistry, 2015. **54**(22): p. 3431-3441.
32. Engen, J.R. and T.E. Wales, *Analytical Aspects of Hydrogen Exchange Mass Spectrometry.* Annual Review of Analytical Chemistry, 2015. **8**(1): p. 1-22.
33. Wales, T.E., M.J. Eggertson, and J.R. Engen, *Considerations in the analysis of hydrogen exchange mass spectrometry data.* Methods Mol Biol, 2013. **1007**: p. 263-88.

34. Guttman, M., et al., *Analysis of Overlapped and Noisy Hydrogen/Deuterium Exchange Mass Spectra.* Journal of The American Society for Mass Spectrometry, 2013. **24**(12): p. 1906-1912.
35. Zhang, J., et al., *H/D Exchange Centroid Monitoring is Insufficient to Show Differences in the Behavior of Protein States.* Journal of The American Society for Mass Spectrometry, 2013. **24**(3): p. 450-453.
36. Hudgens, J.W., R. Huang, and E. D'Ambro, *Method validation and standards in hydrogen/deuterium exchange mass spectrometry.* Hydrogendeuterium exchange mass spectrometry: Fundamentals, techniques and applications, 2016: p. 40-50.
37. Wu, Y., S. Kaveti, and J.R. Engen, *Extensive deuterium back-exchange in certain immobilized pepsin columns used for H/D exchange mass spectrometry.* Analytical chemistry, 2006. **78**(5): p. 1719-1723.
38. Li, K.S., et al., *Orthogonal Mass Spectrometry-Based Footprinting for Epitope Mapping and Structural Characterization: The IL-6 Receptor upon Binding of Protein Therapeutics.* Anal Chem, 2017. **89**(14): p. 7742-7749.
39. Englander, W.S., *PROTEIN FOLDING INTERMEDIATES AND PATHWAYS STUDIED BY HYDROGEN EXCHANGE.* Annual Review of Biophysics and Biomolecular Structure, 2000. **29**(1): p. 213-238.
40. Englander, W.S., et al., *Protein Folding—How and Why: By Hydrogen Exchange, Fragment Separation, and Mass Spectrometry.* Annual Review of Biophysics, 2015. **45**(1): p. 1-18.
41. Finkelstein, A.V., *50+ Years of Protein Folding.* Biochemistry (Mosc), 2018. **83**(Suppl 1): p. S3-S18.
42. Walters, B.T., et al., *Folding of a large protein at high structural resolution.* Proceedings of the National Academy of Sciences, 2013. **110**(47): p. 18898-18903.
43. Gardner, N.W., et al., *A cooperative folding unit as the structural link for energetic coupling within a protein.* Biochemistry, 2017. **56**(50): p. 6555-6564.
44. Ye, X., et al., *Folding of maltose binding protein outside of and in GroEL.* Proceedings of the National Academy of Sciences, 2018. **115**(3): p. 519-524.
45. Dunker, K.A., et al., *Flexible nets.* FEBS Journal, 2005. **272**(20): p. 5129-5148.
46. Fonin, A.V., et al., *Intrinsically disordered proteins in crowded milieu: when chaos prevails within the cellular gumbo.* Cellular and Molecular Life Sciences, 2018. **75**(21): p. 3907-3929.
47. Mandell, J.G., et al., *Measurement of solvent accessibility at protein-protein interfaces.* Methods in molecular biology (Clifton, N.J.), 2005. **305**: p. 65-80.
48. Wang, G., et al., *Conformer-specific characterization of nonnative protein states using hydrogen exchange and top-down mass spectrometry.* Proceedings of the National Academy of Sciences, 2013. **110**(50): p. 20087-20092.
49. Al-Naqshabandi, M.A. and D.D. Weis, *Quantifying protection in disordered proteins using millisecond hydrogen exchange-mass spectrometry and peptic reference peptides.* Biochemistry, 2017. **56**(31): p. 4064-4072.
50. Keppel, T.R. and D.D. Weis, *Analysis of Disordered Proteins Using a Simple Apparatus for Millisecond Quench-Flow H/D Exchange.* Analytical Chemistry, 2013. **85**(10): p. 5161-5168.
51. Goswami, D., et al., *Time Window Expansion for HDX Analysis of an Intrinsically Disordered Protein.* Journal of The American Society for Mass Spectrometry, 2013. **24**(10): p. 1584-1592.
52. Coales, S.J., et al., *Expansion of time window for mass spectrometric measurement of amide hydrogen/deuterium exchange reactions.* Rapid communications in mass spectrometry : RCM, 2010. **24**(24): p. 3585-3592.

53. Englander, W.S., *Hydrogen exchange and mass spectrometry: A historical perspective.* Journal of The American Society for Mass Spectrometry, 2006. **17**(11): p. 1481-1489.
54. Zhang, Y., et al., *Pulsed hydrogen–deuterium exchange mass spectrometry probes conformational changes in amyloid beta (Aβ) peptide aggregation.* Proceedings of the National Academy of Sciences, 2013. **110**(36): p. 14604-14609.
55. Illes-Toth, E., D.L. Rempel, and M.L. Gross, *Pulsed Hydrogen-Deuterium Exchange Illuminates the Aggregation Kinetics of α-Synuclein, the Causative Agent for Parkinson's Disease.* ACS chemical neuroscience, 2018. **9**(6): p. 1469-1476.
56. Kheterpal, I., et al., *Abeta amyloid fibrils possess a core structure highly resistant to hydrogen exchange.* Proceedings of the National Academy of Sciences of the United States of America, 2000. **97**(25): p. 13597-13601.
57. Kheterpal, I., et al., *Abeta protofibrils possess a stable core structure resistant to hydrogen exchange.* Biochemistry, 2003. **42**(48): p. 14092-14098.
58. Pan, J., et al., *Characterizing short-lived protein folding intermediates by top-down hydrogen exchange mass spectrometry.* Analytical chemistry, 2010. **82**(20): p. 8591-8597.
59. Pan, J., et al., *Conformer-Specific Hydrogen Exchange Analysis of Aβ(1–42) Oligomers by Top-Down Electron Capture Dissociation Mass Spectrometry.* Analytical Chemistry, 2011. **83**(13): p. 5386-5393.
60. Pan, J., et al., *Higher-order structural interrogation of antibodies using middle-down hydrogen/deuterium exchange mass spectrometry.* Chemical Science, 2015. **7**(2): p. 1480-1486.
61. Benhaim, M., K.K. Lee, and M. Guttman, *Tracking Higher Order Protein Structure by Hydrogen-Deuterium Exchange Mass Spectrometry.* Protein and peptide letters, 2019. **26**(1): p. 16-26.
62. Pan, J., et al., *Conformer-specific hydrogen exchange analysis of Aβ(1-42) oligomers by top-down electron capture dissociation mass spectrometry.* Analytical chemistry, 2011. **83**(13): p. 5386-5393.
63. Dyson, H.J. and P.E. Wright, *Coupling of folding and binding for unstructured proteins.* Current Opinion in Structural Biology, 2002. **12**(1): p. 54-60.
64. Keppel, T.R., B.A. Howard, and D.D. Weis, *Mapping unstructured regions and synergistic folding in intrinsically disordered proteins with amide H/D exchange mass spectrometry.* Biochemistry, 2011. **50**(40): p. 8722-8732.
65. O'Brien, D.P., et al., *Calmodulin fishing with a structurally disordered bait triggers CyaA catalysis.* PLOS Biology, 2017. **15**(12).
66. Deng, B., et al., *Suppressing allostery in epitope mapping experiments using millisecond hydrogen / deuterium exchange mass spectrometry.* mAbs, 2017. **9**(8): p. 1327-1336.
67. Tulsian, N.K., S. Krishnamurthy, and G.S. Anand, *Channeling of cAMP in PDE-PKA Complexes Promotes Signal Adaptation.* Biophys J, 2017. **112**(12): p. 2552-2566.
68. Vadas, O., et al., *Chapter Seven Using Hydrogen–Deuterium Exchange Mass Spectrometry to Examine Protein–Membrane Interactions.* Methods in Enzymology, 2017. **583**: p. 143-172.
69. Muller, D.J., N. Wu, and K. Palczewski, *Vertebrate membrane proteins: structure, function, and insights from biophysical approaches.* Pharmacol Rev, 2008. **60**(1): p. 43-78.
70. Martens, C., et al., *Direct protein-lipid interactions shape the conformational landscape of secondary transporters.* Nature Communications, 2018. **9**(1): p. 4151.
71. Redhair, M., A.F. Clouser, and W.M. Atkins, *Hydrogen-Deuterium Exchange Mass Spectrometry of Membrane Proteins in Lipid Nanodiscs.* Chemistry and Physics of Lipids, 2019. **220**(Proceedings of the National Academy of Sciences 114 2017): p. 14-22.

72. Li, M., M. Guttman, and W.M. Atkins, *Conformational dynamics of P-glycoprotein in lipid nanodiscs and detergent micelles reveal complex motions on a wide time scale.* Journal of Biological Chemistry, 2018. **293**(17): p. 6297-6307.
73. Harrison, R.A. and J.R. Engen, *Conformational insight into multi-protein signaling assemblies by hydrogen-deuterium exchange mass spectrometry.* Curr Opin Struct Biol, 2016. **41**: p. 187-193.
74. Garcia, N.K., et al., *Dynamic Changes during Acid-Induced Activation of Influenza Hemagglutinin.* Structure, 2015: p. 665-676.
75. Lim, X.-X.X., et al., *Epitope and Paratope Mapping Reveals Temperature-Dependent Alterations in the Dengue-Antibody Interface.* Structure (London, England : 1993), 2017. **25**(9): p. 1391-1402000.
76. Wijesinghe, K.J., et al., *Detection of lipid-induced structural changes of the Marburg virus matrix protein VP40 using hydrogen/deuterium exchange-mass spectrometry.* Journal of Biological Chemistry, 2017. **292**(15): p. 6108-6122.
77. Masson, G.R., et al., *Recommendations for performing, interpreting and reporting hydrogen deuterium exchange mass spectrometry (HDX-MS) experiments.* Nat Methods, 2019. **16**(7): p. 595-602.

Chapter 2. Structural Dynamics Reveal Isolate-specific Differences at Neutralization Epitopes on HIV Env

The text in this chapter has been reproduced in its entirety with permissions from:

Edgar A. Hodge et al. Structural dynamics reveal isolate-specific differences at neutralization epitopes on HIV Env. iScience. 2022 May 23; doi: 10.1016/j.isci.2022.104449

2.1 Introduction

The HIV-1 envelope glycoprotein (Env) is a major determinant of viral tropism, pathogenesis, and neutralization. It is the only virally encoded protein displayed on the surface of the virus and the sole target for neutralizing antibodies (nAbs). Due to intense immune pressures in each infected individual, Env evolves rapidly, making it the most variable part of the virus. While high-resolution structures have provided a blueprint of Env's protein and glycan architecture, the extent of Env structural and functional variation are only beginning to be grasped [1-5]. One fundamental but poorly characterized feature of Env that impacts its immune recognition is the high level of intrinsic dynamics embodied in the trimer at equilibrium even prior to CD4 receptor activation [6]. Env exhibits dynamic conformational switching that exposes non-protective immunodominant epitopes and disrupts the presentation of conformational epitopes, while local structural flexibility can lead to disordered epitopes that reduce antibody affinities [7-9]. At present, we lack an understanding of the extent of differences in these cryptic traits among diverse HIV isolates due to the challenges associated with measuring local dynamics in such a complex antigenic target.

An indication that different HIV isolates can exhibit significant differences in conformational dynamics was provided by single-molecule Förster resonance energy transfer

(sm-FRET) experiments [6]. Env trimers were shown to spontaneously interconvert between at least three distinct states, and the relative population bias differed significantly between a lab adapted and a primary isolate. Dipole electron-electron resonance (DEER) spectroscopy analysis of Env trimers also revealed marked differences in the conformational states and structural heterogeneity displayed by engineered native-like “SOSIP” trimers from two isolates [10]. Both sm-FRET and DEER spectroscopy, however, only provide information about the relative positioning of the respective fluorescent or spectroscopic probes. In order to draw a link between structure and antigenicity, it is necessary to probe local structure at specific epitope positions in different Env trimers.

Hydrogen/Deuterium-exchange Mass Spectrometry (HDX-MS) offers a powerful means of probing local structural dynamics in proteins under native solution conditions [11]. This technique measures the kinetics of deuterium uptake from solvent by amide groups on the protein backbone. Amides that are occluded from solvent or protected by hydrogen bonding, such as in forming secondary structure, become deuterated more slowly, while those in dynamic regions of the protein exhibit more rapid deuteration. Coupled with proteolysis and mass spectrometry, one can monitor local protein dynamics with sequence-specific resolution. Our previous HDX-MS analysis of HIV Env demonstrated that isolate-specific differences in local epitope flexibility are apparent in isolated gp120 receptor binding subunits and in two early generation subtype A SOSIP trimers [8, 12-14]. The studies of the gp120 subunits also demonstrated that local dynamics impact binding of antibodies targeting conformational epitopes [12].

Indeed, most HIV-1 antibody epitopes on native Env are conformational and in some cases involve quaternary structural features. Broadly neutralizing antibodies (bnAbs) with exceptional breadth are known to target conserved regions on Env such as the V1/V2 loop apex, base of the V3 loop, CD4 receptor binding site, fusion peptide, and the gp120/gp41

interface [15, 16]. The majority of these bnAbs recognize conformational epitopes displayed by the closed, prefusion form of the trimer [13, 17, 18].

Here we utilized HDX-MS to characterize dynamic phenotypes in native-like SOSIP.664 Env trimers across five divergent strains to characterize the impact of large sequence variations on structural dynamics and to determine whether differences in Env dynamics impact its recognition by antibodies. We examined trimers from the isolates BG505, B41, AMC008, JR-FL, and CE1176, all stabilized by the 'SOSIP.664' modifications that help the trimer maintain a native-like prefusion form [2]. These types of soluble trimers have been shown to closely mimic the native structure and antigenic profile of Env on virus [2, 19, 20]. Whereas cryo-EM structures show a high degree of structural homology [18, 21], HDX-MS analysis presented here reveals substantial dynamic differences that impact structural ordering of nearly all bnAb epitopes present on the ectodomain (Figure 2.1) including: the V1/V2 apex targeted by bnAbs such as PGT145 and VRC26 [22, 23]; the CD4 binding site targeted by VRC01 class bnAbs [24]; the V3 loop targeted by PGT121 class bnAbs [25, 26]; and the gp120/gp41 interface that includes the fusion peptide and is the target of bnAbs such as 35022, PGT151, and VRC34 [27-29].

We also observed conformational sampling between deuterium-exchange protected and exposed states at multiple sites and found that the sampling timescales were not correlated across the trimer, indicating that regional trends in sub-domain behavior predominate rather than all parts of the trimer switching in concert. This aspect of the Env's architecture may impact mechanisms of neutralization and cooperativity of antibodies that target distinct epitopes across this complex antigenic target.

Lastly, a recent trend in viral immunogen design has been toward increasing stabilization of the closed conformational state, reducing conformational flexibility and increasing antigenicity [30-34]. Since the original SOSIP modifications were introduced [35-37], additional stabilizing mutations have been tested with the aim of increasing trimer stability and reducing exposure of

non-protective immunodominant epitopes such as the V3 loop and portions of the V1/V2 loops [30, 38, 39]. We thus also examined the consequences for antibody binding kinetics and affinity resulting from suppressing protein dynamics by introducing additional hyperstabilizing mutations into the Env trimer.

Collectively, we find that isolate-specific differences in Env structural dynamics impact the display and recognition of conserved epitopes by bnAbs. With this type of information, we can optimize the design of stabilized immunogens to suppress dynamics as well as aid in the selection of immunogens with desirable structural and dynamic properties.

2.2 Materials and Methods

2.2.1 Cell lines for antibody production

HEK293F cells (ThermoFisher Scientific) used for expression of antibodies were grown at 37°C, 8% CO2, with shaking at 125 rpm in Freestyle 293 media (ThermoFisher Scientific) without additives. The cell lines were not authenticated within our lab, however a certificate of analysis from the manufacturer is available. The gender of the 293F cell line is female.

2.2.2 Cell lines for SOSIP production

HEK293F cells (ThermoFisher Scientific) used for expression of SOSIP Env glycoproteins were grown at 37°C, 8% CO2, with shaking at 125 rpm in Freestyle 293 media (ThermoFisher Scientific) without additives. The cell lines were not authenticated within our lab, however a certificate of analysis from the manufacturer is available. The gender of the HEK293F cell line is female.

2.2.3 Protein expression and purification

SOSIPs were produced and purified as previously described by Verkerke et al and briefly below. The JR-FL SOSIP was kindly provided by the Shiu-Lok Hu lab. Briefly, HEK293F cells were transiently transfected at a density between 0.8 and 1.2 million cells/mL using polyethylenimine (PEI) with plasmids encoding each SOSIP isolate co-transfected with furin in pcDNA.3 at a ratio of three SOSIPs to one furin to ensure proteolytic cleavage between gp120 and gp41 subunits during production. After roughly six days the cell supernatants were cleared by centrifugation and filtered through a 0.2-micron vacuum filtration unit and supplemented with protease inhibitors (Roche) and sodium azide to prevent microbial growth. Glycosylated trimers were extracted using Galanthus nivalis lectin (GNL) coupled to agarose beads overnight at 4°C and washed with 20 mM Tris (pH 7.4), 1 mMEDTA, 1 mM EGTA, 0.02% azide, and 120 mM NaCl; glycoproteins were eluted with 7 to 10 column volumes of 1 M alphamethyl-mannopyrannoside dissolved in 20 mM Tris (pH 7.4), 1 mM EDTA, 1 mM EGTA,0.02% azide, and 120 mM NaCl. GNL eluates were concentrated using Amicon ultrafiltration units (nominal molecular mass cutoff of 100 kDa) and buffer exchanged into DEAE low-salt buffer (20 mM Tris [pH 8.0], 100 mM NaCl) before anion-exchange chromatography using a DEAE column. Following 10 min of isocratic flow in 100 mM NaCl, a gradient to 1 M NaCl was initiated and fractions were collected through-out to remove protein aggregates. The DEAE flowthrough was buffer exchanged into 2 M ammonium sulfate– 0.1 M phosphate (pH 7.4) via dialysis and loaded onto a 5mL HIC HiTrap Phenyl HP column. A step-wise gradient of 2M to 0M ammonium sulfate in 0.1 M phosphate (pH 7.4) over 90 min was used to separate trimers from dimers and monomers. The early-eluting fractions (containing native-like trimers) were concentrated prior to being loaded onto a Superdex S200PG size exclusion chromatography (SEC) column in PBS (20mM sodium phosphate [pH 7.4], 150 mM sodium chloride, 0.02% sodium azide). Peak fractions were concentrated and characterized by DLS, SDS, BN-PAGE, and negative stain EM (Figure S2.3) to ensure homogenous, pure trimer populations immediately prior to HDX and BLI experiments.

The V2i and V3 tip IgG Abs were kindly provided by Susan Zolla-Pazner for BLI experiments. VRC01, and PG16 were provided by NIH AIDS Research and Reference Reagent Program. The other antibodies were produced by transient co-transfection of plasmids containing heavy and light chain fragments at a 1:1 ratio in HEK293F cells. Cultures were allowed to grow for approximately 6 days before harvesting. Secreted IgG was isolated and purified by affinity chromatography using a Hi-Trap Protein A column and eluted using 100mM Glycine pH2.0 and neutralized by addition of 1M Tris pH8.0. Purity was assessed by SDS-PAGE

2.2.4 SDS-PAGE and BN-PAGE

SDS denaturing PAGE and blue native PAGE (BN-PAGE) analyses with precast gels (Novex) were performed to assess the oligomeric species present throughout purification and immediately prior to experiments. Typically, between 10 and 15μg of protein was loaded per lane for BN-PAGE analysis and 5μg per lane was loaded for SDS-PAGE analysis.

2.2.5 Dynamic light scattering (DLS)

Dynamic light scattering (DLS) measurements were performed on a Dynapro Nanostar (Wyatt Technologies). Trimer samples were diluted to 1 mg/ml in PBS and centrifuged at 15,000xg for 20 min prior to loading of 10μl into a low-volume quartz cuvette. The mean estimated hydrodynamic radius, and polydispersity were generated from 30 acquisitions of 5 s at 20°C.

2.2.6 Hydrogen/Deuterium exchange mass spectrometry

5 μgs (42 pmol) per timepoint of each protein were incubated in deuterated buffer (20mM PBS, 85% D2O, pH*7.52) for 3s, 1min, 30min, and 20hrs at room temperature. The reaction was stopped via diluting 1:1 in ice-cold quench buffer (200 mM tris(2-chlorethyl) phosphate (TCEP), 8 M urea, 0.2% formic acid) to a final pH of 2.5 and flash frozen in liquid nitrogen followed by storage in -80°C prior to analysis. Online pepsin digestion was performed and analyzed by LC-

MS-IMS utilizing a Waters Synapt G2-Si Q-TOF mass spectrometer as described previously utilizing a 15 minute gradient and a home-made HDX cold box that maintains the pepsin digestion at 4°C and the LC plumbing at 0°C [14, 40]. Pepsin digest eluates from undeuterated sample LC-MS runs were collected, dried by speed vac, incubated in deuteration buffer for 1 hour at 65°C, and quenched as described above to prepare fully deuterated controls. Pepsin digest eluates from undeuterated sample LC-MS runs were also collected, dried by speed vac, resuspended in mobile buffer for peptide identification using nano LC-MS on an Orbitrap Fusion mass spectrometer. A 2 cm trapping column and a 35 cm analytical column were freshly prepared in fused silica (100 μm ID) with 5 μM ReproSil-Pur C18 AQ beads (Dr. Maisch). 8 μL of sample was injected and run using a 60-minute linear gradient from 2% to 30% acetonitrile in 0.1% FA, followed by 10 minutes of 80% acetonitrile. An EThcD method was optimized as follows: ion source: 2.1 kV for positive mode; ion transfer tube temperature: 350 °C; resolution: MS1 = 120000, MS2 = 30000; AGC target: MS1 = 2e5, MS2 = 1e5; and injection time: MS1 = 50 ms, MS2 = 60 ms. Orbitrap Fusion data was processed using Byonic (Version 3.8, Protein Metrics Inc.) to obtain a peptide reference list and identify peptic glycopeptides and glycosylation sites. Deuterium uptake analysis was performed with HD-Examiner (Version 2.5, Sierra Analytics) followed by HX-Express v2 for binomial fitting [41, 42]. The percent exchange was normalized to the fully deuterated samples. The well characterized BG505 SOSIP was exchanged alongside each new construct as a positive control sample and Internal exchange standards (Pro-Pro-Pro-Ile [PPPI] and Pro-Pro-Pro-Phe [PPPF]) were included in each reaction to control for variations in ambient temperature during the labeling reactions. For isolates that were exchanged independently, the differences in %deuteration of each homologous peptide with the same number of exchangeable amides were only considered significant if the differences were greater than the variability observed in that homologous peptide across the BG505 controls on a peptide-by-peptide basis.

2.2.7 Biolayer interferometry

The binding kinetics of the SOSIP constructs against a panel of IgG's were determined via BLI on an Octet Red system (FortèBio). Anti-human IgG Fc capture biosensors were presoaked in binding buffer (phosphate-buffered saline (PBS pH 7.4) supplemented with 0.1% BSA, 0.005% Tween 20, and 0.02% NaN3) for 10 minutes. The hydrated tips were then loaded with purified IgG prepared at 8µg/mL in binding buffer for 80 seconds. After reaching a stable baseline, antibody-immobilized biosensors were moved into wells containing a 2-fold dilution series of SOSIP trimer to monitor association for 3 mins, then biosensors were moved back into wells containing binding buffer to monitor dissociation for 3 mins. Responses were calculated and double referenced against the buffer reference signal and non-specific binding of analyte to biosensor in absence of IgG. Kinetic data were analyzed by using FortéBio Data Analysis 11.0 software and were smoothed by Savitzky-Golay filtering prior to fitting using a 1:1 binding model. Reported values are averages of data repeated in at least two independent experiments.

2.2.8 Glycan profiling

To identify the occupancy of glycans at each glycosite and assess the relative heterogeneity of glycoforms at each site bottom up mass spectrometry (MS) was utilized. SOSIPs (0.02mgs) were denatured in a solution containing 25 mM Tris (pH 8.0), 7 M guanidinium chloride (GdnHCl) and 50 mM dithiothreitol (DTT) at 90°C for 30 min (20µL of 1mg/mL SOSIP, 26mg of GdnHCl, 1µL of 1M Tris HCl pH 8.0, 2µL of 1M DTT). Reduced cysteines were alkylated by adding fresh iodoacetamide (IAA) to 100 mM (4µL of a fresh solution of 0.5M iodoacetamide) and incubating at room temperature for 1 h in the dark. 50 mM excess DTT was then added to quench the remaining IAA (2µL of 1M DTT). The GndHCl concentration was reduced to 0.6 M by diluting the samples 11-fold with a 10 mM Tris (pH 8.0), 2 mM calcium chloride solution (corresponds to bringing the ~50µL to final volume of 550µL. Samples were then divided in two

(two 225μL tubes) and digested using trypsin, and chymotrypsin separately at a ratio of 1:30 (w/w) for 4 h at 37°C, or a combination of Lys-C and Glu-C at a ratio of 1:30 (w/w). Each SOSIP was digested first by Lys-C for 4 h at 37°C followed by an overnight digestion of Glu-C 37°C. All proteases were MS grade (Promega) and the digestion reactions were quenched by the addition of 5μL of 10% formic acid to ea 225μL sample. The digested samples were desalted by Sep-Pak C18 cartridges (Waters) following the manufacturer's suggested protocol. Glycoform determination was performed via nano LC-MS using an Orbitrap Fusion mass spectrometer (Thermo Fisher) as described above in the HDX-MS method section using EThcD and the processing software Byonic (Version 3.8, Protein Metrics Inc.) using a 6 ppm precursor and 10 ppm fragment mass tolerance. Glycopeptides were searched using the N-glycan 309 mammalian database in Protein Metrics PMI-Suite and scored based on the assignment of correct c- and z- fragment ions. The true-positive entities were further validated by the presence of glycan oxonium ions m/z at 204 (HexNAc ions) and 366 (HexNAcHex ions). Glycoforms were categorized as either high mannose: HexNAc(2)Hex(9-5); Hybrid: HexNAc(3)Hex(5-6); or complex (data presented in table S5 in [43]).

2.3 Results

2.3.1 Isolate-specific differences in trimer structural dynamics

In order to investigate isolate-specific differences in Env conformation and local dynamics, HDX-MS was used to track the dynamic behavior of peptides in SOSIP.664 trimers from five HIV-1 isolates: subtype A BG505, subtype B AMC008, B41, and JR-FL, and subtype C CE1176 [44-47]. With the exception of AMC008, these isolates have been characterized as "tier 2" resistant to neutralization by pooled sera from HIV infected individuals [47, 48]. AMC008, by

contrast is a tier 1B, moderately neutralization-sensitive isolate [30]. Pairwise sequence variation across isolates ranged from 12% to 27%.

HDX-MS heatmaps for each isolate in Figure 2.2 show the deuterium exchange levels per peptide after one minute incubation in deuterated buffer, providing an overall dynamic portrait of each Env trimer ectodomain; complete reporting of all HDX-MS data can be found in Figures S2.6-2.8, Table S2.1. Figure S2.1 describes the HDX analysis workflow. Overall coverage of each trimer was roughly 60%, with the largest gaps in coverage resulting from reduced intensity of glycopeptides in the variable loops [49]. We note that the heatmaps include non-homologous peptides, thus these overview data are best interpreted qualitatively in terms of regional differences in dynamics. Many regions across each structure showed similar backbone amide protection that suggests conservation of structural ordering, however, key regions with substantial differences in dynamics were also observed covering the base of V1, the V2 and V3 loops, and the HR2 motif at the trimer's base (Figure 2.2). Many of these regions showing differences span sites of vulnerability targeted by bnAbs (Figure 2.1).

In cases where homologous peptides could be tracked in the different trimers, quantitative comparisons of deuterium uptake kinetics among isolates were possible (Figures 2.3 and 2.4). Trimers from the well-characterized isolate, BG505 [13, 30, 50], were purified and exchanged as a reference control alongside each batch of non-BG505 trimer. We set a threshold that any apparent difference in deuterium uptake between isolates exchanged independently was considered significant if the differences were greater than the variability (% standard deviation) observed in that homologous peptide between BG505 biological replicates from independent protein preparations (Figure S2.2); we note the experimental error from technical replicates (plotted as error bars in deuterium uptake plots) is far smaller than this threshold.

Exchange reactions were carried out immediately after protein purification without subjecting the fragile trimer specimens to freeze-thaw cycles. To verify the homogeneity of the

trimers and ensure that the samples were free of dissociated or misfolded species, samples were analyzed by blue native-PAGE, SDS-PAGE, DLS, and negative stain EM (Figure S2.3).

We further confirmed that the samples were composed of native-like prefusion trimers by examining HDX signatures for peptides covering the gp120 N and C-termini (Figure 2.3A, peptides 1 and 2) that showed significant protection from deuterium exchange, consistent with the trimers embodying well-formed gp120-gp41 interfaces [14, 50, 51]. Other well-ordered regions of the trimers also showed similar exchange protection. For example, the inner domain layer 2 of gp120 was relatively protected in all isolates over time points up to 20 hours (peptide 3, Figure 2.3A), consistent with the peptide adopting a well-ordered helix as observed in high-resolution structures. Differences in protection were detected at 20 hours, however, where transient disruption of backbone amide H-bonds led to greater deuteration over time in some isolates compared to others. Here this inner domain segment was more protected in the isolates JR-FL and B41, and slightly less protected in CE1176 and the tier 1B isolate AMC008.

Other regions across the gp120 subunit showed larger differences in local peptide dynamics (Figure 2.3), for instance, the V1/V2 apex region including peptides 4-5. This region is a target of bnAbs, such as PGT145, PG9, and VRC26 [22, 52, 53]. The base of V1 (peptide 4), which also forms part of the bridging sheet upon CD4-induced structural rearrangements, was considerably more protected in B41 but highly dynamic in CE1176. At the trimer apex, the V2 loop likewise was highly dynamic in CE1176 as well as AMC008 as reflected by peptide 5 with sequence FYRL that lies directly upstream of a proposed integrin binding site and V2i antibody epitope (V2 epitope overlapping the integrin binding site). Interestingly, all FYR/KL peptides start off similarly protected, but their backbone amide protection varies dramatically with time, suggesting a similar ground state level of amide protection. The differences in the rate of deuterium uptake for this peptide among different Env trimers would indicate differences in transient backbone exposure of the V2 loop, departing from the more protected ground state configuration. Indeed, the V2 loop has been shown to be capable of adopting different

conformations (a 4 stranded beta barrel, a partial helical-loop conformation, and a more protected beta sheet conformation in the open state) [54]. Envs with greater sampling among such conformations would take on deuterium more readily and the structural fluctuations would likely influence how V2i antibodies and integrins bind this region.

The third variable loop (V3), one of the most immunodominant regions on Env, is sequestered underneath V2 in all available closed, prefusion trimer structures. It has been suggested, however, that V3 can “flicker” out from underneath V2 without disrupting the V1/V2 apex ordering [54, 55]. V3 loop dynamics control the accessibility of the V3 crown/tip epitope to antibodies that bind this region. From HDX-MS analysis, significant differences in V3 exchange kinetics were observed. CE1176 exhibited the most protected V3 loop while JR-FL exhibited a rapidly exchanging V3 loop (peptide 6, Figure 2.3). AMC008, while paralleling CE1176’s dynamic profile in many areas, broke with CE1176 in exhibiting a V3 loop that more frequently samples an exchange accessible conformation.

Interestingly, in similar fashion to the FYR/KL peptide in V2, despite differences in overall deuterium exchange kinetics for these peptides in V1, V2, and V3, they all exhibited similar levels of exchange at the earliest time point but then diverged over the time courses. These trends indicate that these loops adopt similar ground state configurations in the trimers from the panel of isolates, even in the relatively dynamic CE1176 and AMC008 trimers, but they exhibit significant differences in their frequency of sampling more exposed conformations, giving rise to differences in the slope of the deuterium uptake plots [11].

The CD4 binding site, including peptides 7-9, also exhibited significant differences in structural dynamics. Greater protection was observed in AMC008 and JR-FL relative to BG505 and B41 for two homologous peptides in gp120 containing residues that are direct binding contacts with CD4 and the bnAb VRC01 (peptides 7 and 8; Figure 2.3). Conversely, CE1176 is more dynamic in these same regions. The trend with similar exchange at early time points and divergent exchange kinetics over time mirrors what was observed for the variable loops in the

apex, again suggesting a similar ground state peptide environment with isolate-specific differences in frequency of sampling more exposed configurations.

By contrast, peptide 9, which forms a beta-hairpin turn that projects toward CD4 when it is bound, at early time points showed divergent deuteration levels with BG505 taking on nearly saturating levels of deuteration and AMC008 exhibiting more protection (Figure 2.3). The variance in deuterium exchange at the earliest time points for this key CD4 binding site peptide, indicates that this site is intrinsically more disordered or accessible at equilibrium in BG505 than the other Env trimers.

Other peptides also show differences in deuterium exchange at the earliest time points, highlighting intrinsic differences in local ordering across isolates. This is observed for example, in the pivotal gp120 inner domain layer 1 peptide 10 that has been shown to help regulate CD4 activation; this also is a region where stabilizing modifications can shift the conformational equilibrium of Env towards the closed state [30, 56].

While the largest isolate-specific differences in local structural dynamics were concentrated in the gp120 subunit, peptides in gp41 also exhibited structural differences in dynamics despite the relatively high sequence conservation of this subunit. The N-terminal fusion peptide of gp41 (peptide 1, Figure 2.4) was rapidly deuterated in all strains, in agreement with this region's high degree of flexibility and solvent accessibility suggested by a lack of density in nearly all structures of unliganded Env [5, 57, 58]. By contrast the adjacent fusion peptide proximal region (FPPR, peptides 2 and 3; Figure 2.4) showed gradual deuterium uptake over 20 hours, which suggests that it samples exposed conformations infrequently, and the extent of the dynamic sampling differed among isolates. Peptides at the N-terminal end of HR1 (e.g. peptide 4, Figure 2.4) were highly dynamic in all strains. This region is disordered in most SOSIP crystal and cryo-EM structures likely due to the helix disrupting proline point mutation (I559P) designed to prevent transition to a rigid helix in the post fusion form. The segment was observed to exist as a rigid helix in a non-SOSIP prefusion JR-FL strain Env structure [59, 60].

Notably, while high resolution crystal and cryo-EM structures indicate that the core HR1 segment is part of a stable helical bundle, our HDX-MS data suggests that the degree of structural order of this helix can vary across isolates. For example in the B41 isolate, the central stretch of HR1 (peptide 5, Figure 2.4) shows greater exchange protection than the other four, which behaved similarly. The C-terminal end of the HR1 helix (peptide 6) is similarly protected from exchange in all strains at the earliest two time points, but isolate-specific differences became apparent at later time points. At the very base of the trimer, the dynamic profile of HR2 suggests differences in helix stability across the isolates, where again B41 exhibited the most exchange-protected HR2 segment (peptide 8).

From the comparison of homologous peptides it is clear that divergent Env trimers exhibit a broad range of local structural dynamics at key functional and antigenic sites despite appearing nearly identical in static structures.

2.3.2 Isolate-specific differences in conformational switching

We also investigated whether HDX-MS could identify signatures of large-scale conformational switching across Env that may relate to the dynamic changes reported by sm-FRET [6, 11]. Signatures of conformational transitions manifest as broadened or bimodal mass spectral envelopes, indicative of the peptide populating states with differences in backbone amide protection. Bimodal spectra were fit to two populations using the HX-Express analysis program [41, 42]. Bimodal spectra arise from slow (relative to the deuterium labeling rate) concerted motions where multiple backbone amides become deuterated in an exchange-competent state before the peptide has a chance to return to the more protected state. In this exchange regime (so-called EX1 kinetics) the rate of exchange equals the rate of conformational opening to a state with greater amide accessibility to solvent [61, 62].

In the Env HDX-MS data, if bimodal spectra were detected for a given peptide and the overall population transitioned to the exposed state within 1 minute, those were categorized as fast transitions driven by frequent conformational switching. If the protected population exhibits signs of a mixed population even after hours (as evidenced by persistent bimodal spectra at the late time points), those transitions were categorized as slow or infrequent switching events. A number of peptides also exhibited intermediate timescales for the kinetics of population transitions. Examples of peptides that show bimodal spectra indicative of conformational sampling on the different timescales are presented in Figure 2.5.

In AMC008, bimodal spectra were detected for the V3 peptide (Figures 2.5, 2.6B, Figure S4), but only at the earliest time point, after which the populations converged to a more exposed state. This suggests V3 in AMC008 undergoes a rapid sampling between protected and exposed states. Bimodal spectra from a peptide spanning residues 413-426 in the bridging sheet report on a transition to a more exposed state on an intermediate timescale. By contrast, the helix in layer 2 of AMC008 gradually samples a more exposed state over a long timescale, where even after 20 hours a population that has not sampled an exposed state can be resolved. Overall, AMC008 displayed the greatest number of bimodal spectra indicative of conformational transitions across the apex and trimer base, while B41 and JR-FL appear to be the most conformationally fixed with no bimodal peptides identified across the timescales we probed. Isolate-specific differences in structural and conformational dynamics thus extend beyond local peptide flexibility to include movement of larger sub-domains that sample distinct conformational states over a broad range of timescales.

The majority of peptides exhibiting bimodal profiles were found in the gp41 subunit (Figure 2.6). Two distinct populations in the mass spectra for peptides located in gp41's HR2 were resolvable only at the earliest time point for BG505, CE1176, and AMC008 trimers (Figure 2.6A-C, Figure S2.4). Similarly, peptides at the N-terminal end of HR1 exhibited bimodal spectra in early time points in BG505 and AMC008 (Figure 2.6A,B) suggesting this region may

frequently interconvert between a well-ordered helix and a more backbone accessible conformation. CE1176 displayed a broader range of timescales of structural transitions in gp41 compared to BG505 and AMC008. The FPPR of CE1176 transitions from a protected state to a more exchange-competent state on an intermediate timescale, up to 30 minutes (Figure 2.6C). The more C-terminal end of HR1 in CE1176 by contrast appears to sample two distinct conformations considerably less frequently than the FPPR, where even after 20 hours a fraction of the protected population did not yet transition to the exposed state (Figure 2.6C). Based upon the wide range of timescales observed for conformational switching at different sites in the trimer, the individual regions do not necessarily appear to be moving in concert with each other. Instead, more modular, regional conformational sampling is occurring.

Despite the lack of apparent coordination between sites that exhibit conformational switching, the localization of these peptides are consistent with regions that respond to CD4-induced changes that we previously mapped out by HDX-MS [50]. For example, in response to CD4 binding, the FPPR and HR2 became less protected, while the C-terminal end of HR1 became more protected in the transition from the closed to the CD4-induced open state (Figure 2.6D) [50]. The trends and clustering of bimodal HDX-MS spectra throughout gp41 are also in agreement with DEER spectroscopy work that reported conformational heterogeneity in gp41 [63].

2.3.3 Stabilizing mutation effects on local dynamics and conformational switching

Given the differences in local epitope dynamics and order we had observed, we sought to investigate the effect of Env structural dynamics on antibody affinity. Env sequence differences between the divergent isolates confound direct quantitative comparisons, however. To overcome this limitation, we examined the structural dynamic and antigenic profiles of SOSIP.664 compared against isolate-matched hyperstabilized forms of three of the Env—

AMC008, BG505, and B41— that showed dramatic differences in intrinsic structural and conformational dynamics. CE1176 was also examined, but the stabilizing mutations described below failed to produce sufficient native-like trimer for analysis. HDX-MS was first used to test the ability of additional stabilizing mutations to abrogate localized trimer dynamics in these three Envs. Next, biolayer interferometry (BLI) was used to characterize the antigenic effect of those changes in epitope flexibility.

We previously examined differences in dynamics between minimally engineered SOSIP.664 trimers and SOSIPv4.1 and 4.2 (mutations described below) for the subtype A BG505 isolate [30]. Here we confirmed the stabilizing v4.1 and v4.2 mutation effects on dynamics first in BG505 as a control, and then extended the analysis to the highly dynamic Env AMC008 as well as the relatively well-ordered B41 trimer. Because AMC008 and B41 previously were shown to form well folded trimers with good yields after inserting SOSIPv4 mutations, and they exhibited such starkly different dynamic phenotypes, we decided they would serve as informative cases to compare and contrast how abrogated epitope dynamics influence antibody recognition. The SOSIPv4 changes added on top of the SOSIP.664 modifications include E64K (v4.1) or H66R (v4.2) in the gp120 layer 1 inner domain to stabilize the closed state, A316W (both in v4.1 and v4.2) to lock the V3 loop under the trimer apex, and I535M and L543N in gp41 to match the residues in the base of BG505, which have been shown to boost trimer yield and thermostability [30].

In agreement with our previous analysis of BG505, we confirmed that the v4 mutations in the BG505 reference trimer resulted in only minor changes in dynamics proximal to the stabilizing mutations (Figure S2.6) [30, 39]. In the context of B41, which generally exhibits greater local order relative to BG505, the v4 modifications likewise yielded minimal differences in dynamics across the three SOSIP versions (Figure S2.7). Even a peptide containing the E64K/H66R mutation in the gp120 layer 1 inner domain did not exhibit a major change in protection as a result of the SOSIPv4 residue substitutions in B41. Although no significant

changes in dynamics were observed in BG505 and B41, it has been shown the thermostability and yields slightly increase upon v4 stabilization [30].

By comparison, the AMC008 isolate showed a dramatic response to v4 stabilizing modifications (Figure 2.7, Figure S2.8). Increases in deuterium exchange protection were observed in the gp120 inner domain, the bridging sheet, the V2 loop, and the V3 loop, including a peptide spanning the A316W mutation site. The increased protection observed in the V3 loop peptides suggests the A316W mutation indeed helped sequester the V3 loop. Whereas AMC008 SOSIP.664 exhibited multiple regions with bimodal spectra, the majority of regions with coverage in v4.1 and v4.2 constructs exhibited unimodal spectra suggesting the v4 constructs were locked into one conformational state (Figure S2.5). The exception to this suppression of conformational sampling was at the N-terminal end of HR1 (residues 538-546), which contains the L543N mutation and exhibited a persistent bimodal spectrum at the earliest time point.

2.3.4 Antigenic consequences of suppressed dynamics in Env trimers

In order to link antigenicity with the effects of reduced structural dynamics, a panel of antibodies specific for different conformational states and regions on Env were used for BLI experiments. In addition to antibodies (Abs) specific for the closed conformation (PGT145 and PG16), the open conformation (17b), and a partially open conformation (b12), three V3 tip binding Abs (447-52D, 3869, and 3074) and two V2i Abs (830A and 2158) were used here [64-66]. 447-52D and 3074 have been called ‘best in class’ V3 Abs, and the three V3 tip Abs are broadly reactive and can neutralize tier 1 and 2 psuedotyped HIV viruses across diverse subtypes [55, 67, 68]. mAbs 830A and 2158 bind discontinuous epitopes that overlap a potential integrin binding site on the V2 loop and fall into the class of Abs that correlated with protection against HIV infection in the RV144 vaccine trial but are not potent neutralizers [55, 69, 70].

Across all the isolates, the antibody 17b against the CD4-induced coreceptor binding site was only able to bind the AMC008.664 construct, but its binding was abrogated in the v4.2 trimer, consistent with the modifications stabilizing a closed conformation of the trimer. Likewise, nAb b12 against a partially open form of the CD4 binding site was able to bind the AMC008.664 trimer relatively tightly, but binding was suppressed in AMC008v4.2. All three V3 tip binding and V2i antibodies showed abrogated binding to the AMC008v4.2 construct, which demonstrates that these epitopes were sequestered or less frequently exposed in the stabilized constructs, which is in agreement with the loss of localized regions exhibiting bimodal spectra in the HDX data (Figure 2.8A, Table S2.2-2.4).

In contrast to the dramatic shift in binding profiles for the antibodies above, the bnAbs VRC01, 35022, and PGT121 demonstrated modest changes in binding between AMC008.664 and v4.2 constructs, with increases in K_D on the order of 2 to 4-fold, suggesting they are less susceptible to conformational variation in their antigenic targets. For the V1/V2 apex-targeting bnAb PGT145, though affinity increased against the stabilized v4.2 SOSIP, the antibody binding remained relatively weak. This is consistent with the still relatively dynamic, though slightly more protected, nature of the V2 apex in AMC008v4.2 trimers.

In the highly stable B41 background, binding of bnAbs PGT145, PG16, VRC01, 35022, and PGT121 were even less altered by V4.2 mutations (Figure 2.8C, Table S2.2-2.4). nAb b12, and the V3 tip specific Abs likewise were less affected by v4.2 stabilization in B41 with similar affinities of 3869 and 447-52D, while binding of 3074 was not detectable in the stabilized construct. The V2i Ab 2158 was unable to bind B41, and the affinity of 830A was comparable between B41.664 and v4.2. These results indicate that for trimers such as B41 that are already relatively fixed in the prefusion conformation, the additional SOSIPv4.2 modifications do not have major local or global impacts on structural ordering or antigenicity.

As with AMC008 and B41, binding of bnAbs PGT145, PG16, VRC01, 35022, and PGT121 were relatively unaffected comparing BG505.664 and BG505V4.2. Unexpectedly, however, b12

affinity for BG505 increased for the v4.2 construct. It has been shown via neutralization assays that alanine amino acid substitutions in the V3 loop at locations near the A316W mutation in the v4 constructs (such as F317A and Y318A in the crown of V3) can increase the neutralization potency of b12 for psuedotyped virus, but a structure-based explanation for this phenomenon is not available at present [71].

All three V3 tip binding Abs showed abrogated binding to the BG505v4.2 construct. The attenuated binding was largely driven by a decrease in k_{on}, with little change in k_{off}, which suggests the weakened V3 tip binding is likely due to decreased epitope accessibility (Table S2-4). Alternatively, the A316W mutation is adjacent to direct binding contact residues for 447-52D, 3074 and 3869, thus it is possible the mutation influences the binding of these antibodies. However, this may be less likely for 3869 and 447-52D because the A316W mutation did not alter the binding kinetics in B41. BLI reported weak binding for 830A and 2158 against BG505.664, but there was no measurable signal in the v4.2 construct using similarly high concentrations. We note that HDX-MS did not show a difference in deuterium exchange for these regions resulting from the SOSIP.v4 mutations, thus reflecting a limitation of the method for capturing some specific differences in structure that are present in SOSIP.664 and v4 trimers.

In summary, a comparison of these three isolates against their stabilized counterparts suggests strains that are more inherently flexible, such as AMC008, may be more susceptible to attenuating the binding of antibodies specific for the open conformation, the tip of V3, and parts of the V2 loop through mutation induced conformational fixation. In addition, the potent bnAbs that have the greatest documented neutralization breadth among the antibodies we examined were only modestly impacted in their binding, perhaps reflecting their impressive cross-reactivity and ability to tolerate extreme levels of structural and sequence variation in their cognate antigen targets.

2.4 Discussion

HIV Env exhibits tremendous genetic sequence diversity as a result of its rapid mutation rate and intense selective immune pressures. Here we sought to identify the structural and dynamic manifestations of sequence diversity, adding an important dimension to our understanding of HIV Env as an antigenic target that complements available static high-resolution information. Isolate-specific differences in local epitope organization and conformational equilibria have been challenging to characterize in the past. Indeed, structures of Env are most often determined with stabilizing antibody fragments bound and are the end result of stringent selection of sub-populations of particles in single particle cryo-EM analysis and conformational fixation in X-ray crystallography. These factors lock in conformational states and suppress protein dynamics. Biophysical techniques such as smFRET and DEER spectroscopy reveal dynamic motions and conformational heterogeneity but are limited in resolution, and at present a clear assignment of spectroscopically defined sm-FRET states to Env structures remains ambiguous [10, 72].

Here we used HDX-MS to bridge structure and dynamics in the Env trimer and demonstrate that substantial differences in local structural dynamics are evident in Env derived from five HIV isolates. The results of this study provide the first detailed analysis of structural variation among divergent HIV Env trimers and reveals structural properties such as regional conformational switching and differences in local epitope order.

We observed peptides indicative of conformational switching in regions previously shown to map to two distinct allosteric networks upon CD4 binding [50] (Figure 2.6D). In this case, however, the local structural changes are occurring in the absence of CD4. This suggests that the trimers are in equilibrium between the closed prefusion and a more open conformation that is largely consistent with a CD4 receptor-bound conformation. These transitions occur across timescales ranging from seconds to hours depending on the isolate and allow us to

compare the relative rates of Env opening motions across distinct isolates. Furthermore, the distinct timescales for different regions suggest that these motions are not concerted across the trimer, instead a degree of modularity appears to govern conformational dynamics. Widely separated sites such as V3, HR1 and HR2 peptides sample distinct conformations on the timescale of seconds, while the bridging sheet and gp120 inner domain helix undergo much less frequent conformational transitions with kinetics measured in hours.

It is interesting to speculate about the extent to which glycans may play a role in strain specific differences in dynamics and conformation. Glycosylation has been suggested to influence dynamics in Env and more recently in the SARS-CoV2 spike protein [73]. For example, loss of the N301 glycan seems to increase V3 loop flexibility [54], and loss of the N160 glycan has been posited to increase the V1V2 loop flexibility in turn destabilizing the V3 pocket making it easier for V3 crown targeting antibodies to bind [23, 74]. From our mass spectrometry data we did a relative isolate comparison of the glycan occupancy and glycan heterogeneity using different proteases (Table S5 in [43]). The majority of glycosylation differences were in the highly variable V1 loop (which explains the missing coverage in the HDX-MS data in this region), but heterogenous glycoforms were present across all isolates at N301 and N160 (although we did not have coverage here in JR-FL). From our glycoprofiling data we did not observe any correlations between glycosylation and conformational switching that were immediately recognizable.

Our results shed light on a structural model that has been proposed to explain the basis for neutralization resistant phenotypes [13, 47, 75]. In this model Env from neutralization resistant isolates adopt a closed prefusion conformation while sensitive isolates sample an open conformation more readily. From our analysis, surprisingly, the tier 2 CE1176 isolate exhibited a highly dynamic phenotype similar to AMC008. However, unlike AMC008, we observed that CE1176 has in fact the most highly protected V3 loop (Figure 2.3). The neutralization sensitive AMC008 isolate by contrast exhibits a relatively dynamic V3 loop. These data may thus help

explain the neutralization resistant tier 2 assignment of CE1176 and neutralization sensitive designation for AMC008 using pooled human serum from infected donors that is rich in V3-specific antibodies [67, 75, 76]. Isolate-specific differences in local epitope flexibility and global conformational switching in Env trimers may help provide a structure-based explanation for differences in antigenicity and neutralization sensitivities in addition to the more immediately recognizable differences in glycosylation and sequence variation. Further analysis of diverse HIV isolates is warranted to test the hypothesis that neutralization sensitivity is directly correlated with Env open/closed equilibria [47, 48].

These differences in epitope rigidity likely contribute to differences in antigenicity between isolates, but variability in Env sequences and glycosylation are clearly important contributing factors as well. By examining the effect of conformational fixation in a given Env background, we have been able to characterize the impact on dynamics and antigenicity. Our data suggests that the stabilizing v4 SOSIP mutations can suppress dynamics but appear more effective when applied to conformationally dynamic Env trimers such as AMC008. The effect of the SOSIPv4 mutations depends on the background Env to which it is introduced as reflected by the muted effect observed by HDX-MS comparisons of B41 and BG505 SOSIP.664 and v4 trimers. The lack of any change in dynamics in B41 after introduction of the v4 mutations could be because B41 was generally more structurally fixed than the other four isolates, including a region spanning the E64K/H66R mutation sites meant to lock Env in the closed state (Figure 2.3, peptide 10). Increased protection in the gp120 layer 1 suggests B41 may more stably maintain the short helix seen in many gp120 core crystal structures [77]. The antigenic effects were observed most potently in reduction in non-neutralizing antibody binding, which is critical for reducing immune responses against immunodominant but non-protective epitopes. Surprisingly, however, mature bnAbs in many cases only exhibited modest increases in binding to the more stabilized forms of the trimers. Perhaps over the course of their development they

evolved to tolerate extreme levels of structural and dynamic variation in their targets, much as they evolved to recognize conserved residues while skirting sites that vary among isolates.

Beyond v4 SOSIPs, other hyperstabilized SOSIPs and Env constructs have been designed to further abrogate the inherent trimer flexibility [18, 31, 38, 39, 78]. This strategy of stabilizing the prefusion protein structure, which is the primary target for nAbs, originated in the HIV Env SOSIP design, but has since been adopted for stabilization of prefusion conformations in respiratory syncytial virus [32] and SARS-CoV-2 spike trimers [79, 80] where the improvement in potent neutralization activity appears directly a result of the fixation of the prefusion conformations [81]. As is now appreciated, however, in the case of a hypervariable antigenic target such as HIV Env, achieving neutralization breadth requires not only maintaining a prefusion conformation for the viral protein, but also training of the immune system to focus on conserved epitopes while avoiding potentially immunodominant, distracting isolate-specific epitopes [82, 83].

A better understanding of how sequence diversity affects the structural dynamic behavior of Env provides a foundation to better understand structural correlates of antibody neutralization of HIV. Lastly, an understanding of the dynamic antigenic target and how structure-based modifications modulate dynamics and epitope exposure can help guide future Env-based HIV vaccine designs.

Figures

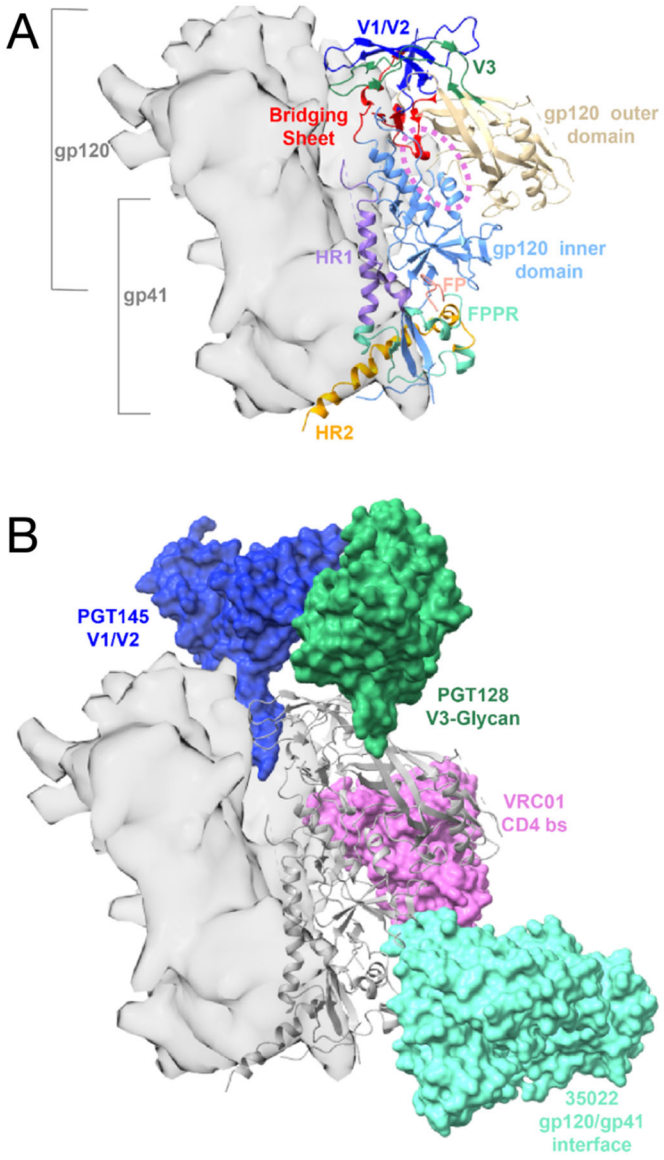

Figure 2.1. HIV Env domain organization and sites targeted by broadly neutralizing antibodies. (A) Localized regions are highlighted on the Env BG505 EM structure (PBD 5ACO; one Env protomer is displayed in ribbon representation, while the other 2 protomers are displayed as a gray surface). Each of the three protomers consists of three gp120 receptor binding subunits at the apex, and three gp41 subunits at the base that house the fusion peptide.

The gp120 outer domain is colored wheat, the gp120 inner domain is colored light blue, the CD4 binding site is outlined by a pink circle, the bridging sheet is colored in red, the V1/V2 apex is colored dark blue, and the V3 loop in green. In the base gp41 subunit, heptad repeat 1 (HR1) is colored purple, heptad repeat 2 (HR2) is colored orange, the fusion peptide (FP) is colored salmon, and the fusion peptide proximal region (FPPR) is colored teal. **(B)** Fabs from bnAbs that recognize four sites of vulnerability on Env are shown (PBD 5ACO for the Env ectodomain aligned with 5V8L, 5W6D, and 6VI0 PDB models in surface representation). bnAb PGT128 (green) targets the V3 base and N332 glycan, PGT145 (blue) binds the V1/V2 apex, VRC01 (pink) targets the CD4 binding site, and 35022 (teal) binds the gp120/gp41 interface.

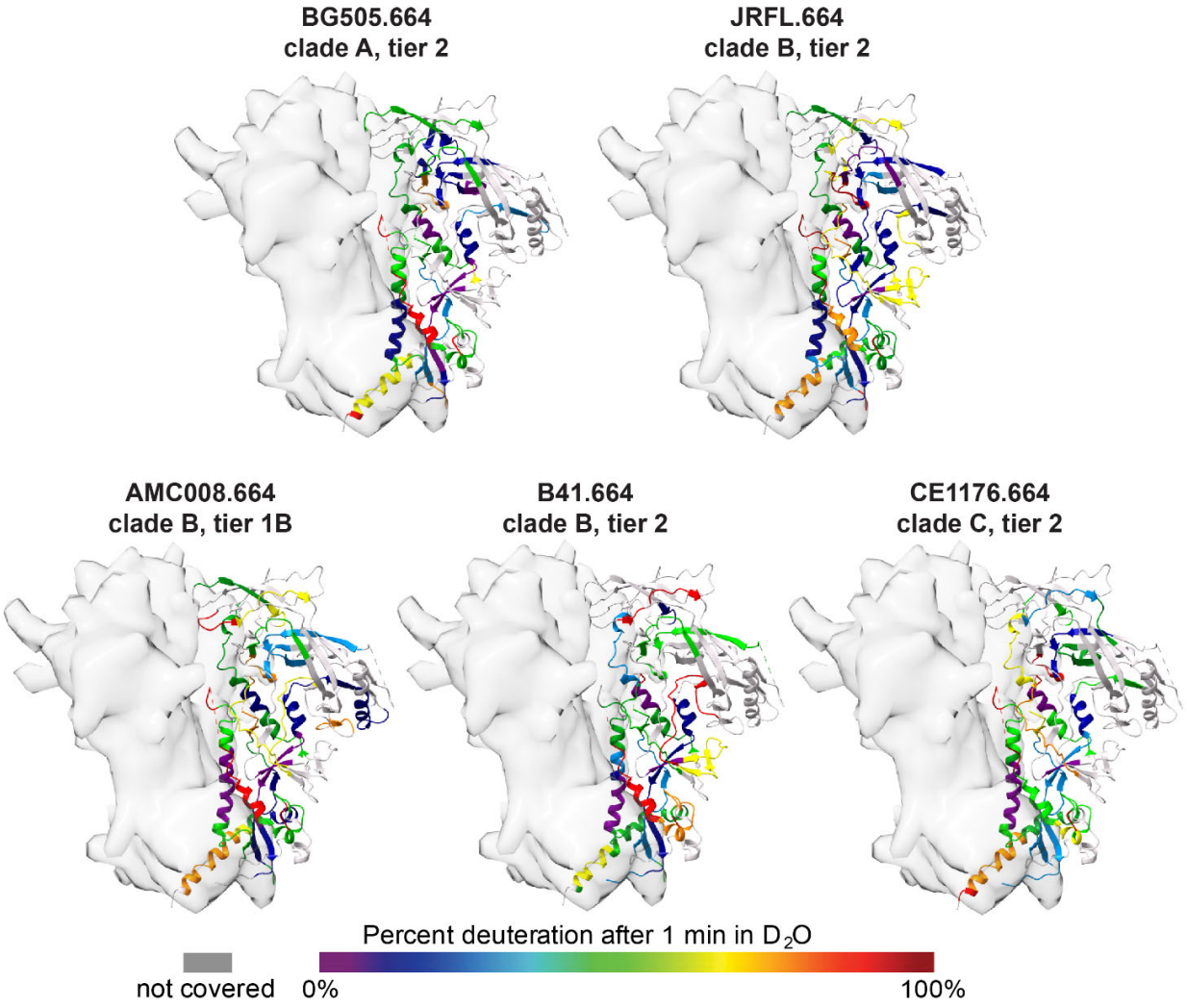

Figure 2. 2. HDX heatmaps show isolate-specific differences in Env structural dynamics in regions including epitopes targeted by broadly neutralizing antibodies. Percent deuteration after 1 minute of exchange for the five Env in our panel mapped on to the 5ACO Env structure (2/3 protomers shown in gray surface representation, 1 protomer displayed as a ribbon color coded according to the HDX heatmap). Cooler colors indicate regions that are more protected from exchange, warmer colors indicate regions that are more exposed and take up deuterium more readily.

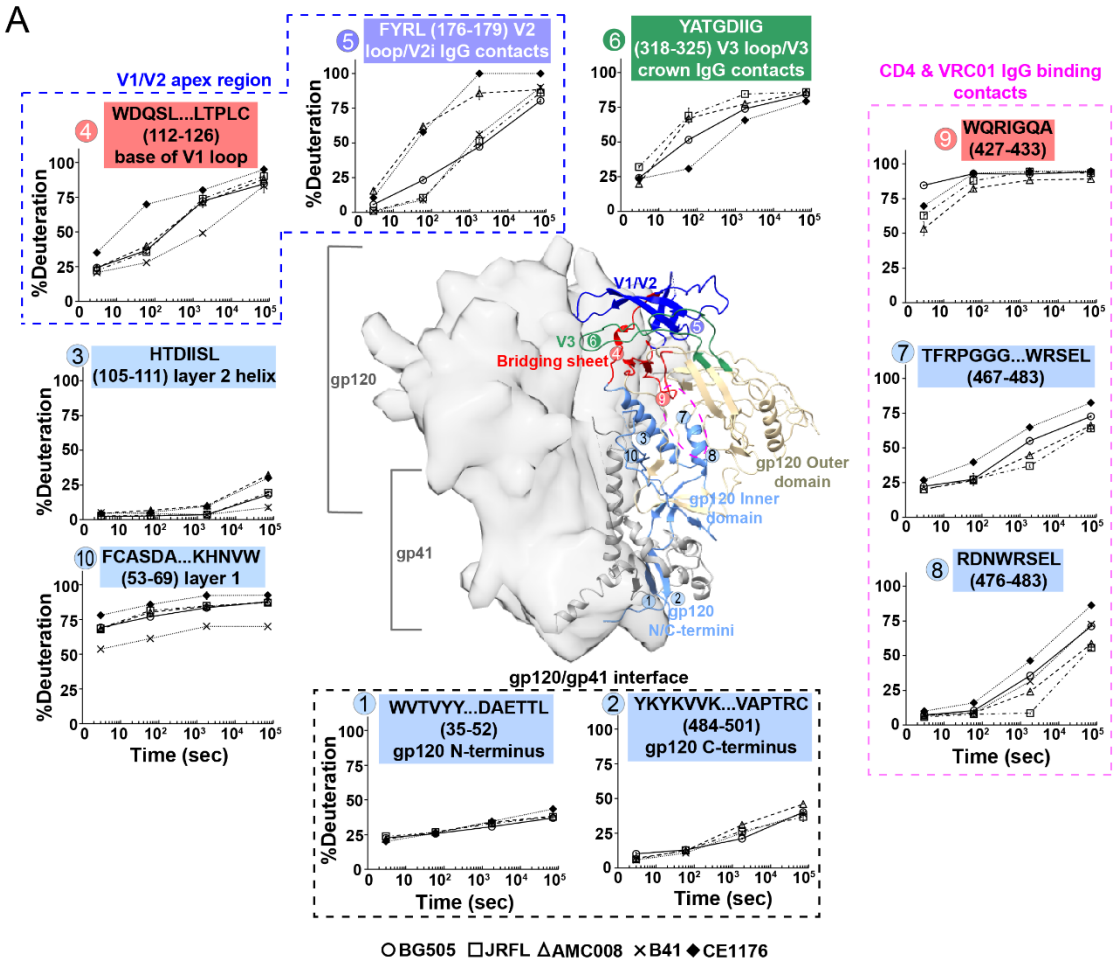
A
V1/V2 apex region
4 WDQSL...LTPLC (112-126) base of V1 loop
5 FYRL (176-179) V2 loop/V2i IgG contacts
6 YATGDIIG (318-325) V3 loop/V3 crown IgG contacts
CD4 & VRC01 IgG binding contacts
9 WQRIGQA (427-433)
7 TFRPGGG...WRSEL (467-483)
8 RDNWRSEL (476-483)
3 HTDIISL (105-111) layer 2 helix
10 FCASDA...KHNVW (53-69) layer 1
%Deuteration
Time (sec)
V1/V2
V3
Bridging sheet
gp120
gp41
gp120 Outer domain
gp120 Inner domain
gp120 N/C-termini
gp120/gp41 interface
1 WVTVYY...DAETTL (35-52) gp120 N-terminus
2 YKYKVVK...VAPTRC (484-501) gp120 C-terminus
BG505 JRFL AMC008 B41 CE1176
B
gp120 N-terminus Layer 1
Layer 2
Bridging Sheet
V1 loop
V2 loop
7-stranded Beta Sandwhich
V3 loop
Bridging Sheet
Layer 3
gp120 C-termini
BG505 WVTVYYGVPVWKDAETTLFCASDAKAYETEKHNVWATHACVPTDPNPQEIHLENVTEEFNMWKNNMVEQMHTDIISLWDQSLKPCVKLTPLCVTLQCTNVT 135
AMC008 WVTVYYGVPVWKEATTTLFCASDAKAYDTEVHNVWATHACVPTDPSPQEVILENVTENFNMWTNNMVEQMHEDIISLWDQSLKPCVKLTPLCVTLNCTNEL
B41 WVTVYYGVPVWKEATTTLFCASDAKAYDTEVHNVWATHACVPTDPNPQEIVLGNVTENFNMWKNNMVEQMHEDIISLWDQSLKPCVKLTPLCVTLNCNNVN
JRFL WVTVYYGVPVWKEATTTLFCASDAKAYDTEVHNVWATHACVPTDPNPQEVVLENVTEHFNMWKNNMVEQMQEDIISLWDQSLKPCVKLTPLCVTLNCKDVN
CE1176 WVTVYYGVPVWKEAKTTLFCASDAKAYEKEVHNVWATHACVPTDPNPQEMVLENVTENFNMWKNDMVDQMHEDVISLWDQSLKPCVKLTPLCVTLTCTNTT
BG505 NNITD----------DMRGELKNCSFNMTTELRDKKQKVYSLFYRLDVVQINENQGNRSNNSNKEYRLINCNTSAITQACPKVSFEPIPIHYCAPAGFAIL 226
AMC008 KNT--TKTNNS----SWGGEMKNCSFNVTTSIRDKVQKEYALFYKLDIVPIDDDN------NTSNYRLINCNTSVITQACPKITFEPIPIQFCTPAGFAIL
B41 TNNTNNSTNATISDWEKMGEMKNCSFNVTTSIRDKIKKEYALFYKLDVVPLENKN-NINNTNITNYRLINCNTSVITQACPKVSFEPIPIHYCAPAGFAIL
JRFL ATNTTNDSEGT----MERGEIKNCSFNITTSIRDEVQKEYALFYKLDVVPIDNN--------NTSYRLISCDTSVITQACPKISFEPIPIHYCAPAGFAIL
CE1176 VSNGSSNSN------ANFEEMKNCSFNATTEIKDKKKNEYALFYKLDIVPLNNS--------SGKYRLINCNTSAIAQACPKVTFEPIPIHYCAPAGYAIL
BG505 KCKDKKFNGTGPCPSVSTVQCTHGIKPVVSTQLLLNGSLAEEEVMIRSENITNNAKNILVQFNTPVQINCTRPNNNTRKSIR--IGPGQAFYATGDIIGDI 326
AMC008 KCNNKKFNGKGPCTNVSTVQCTHGIRPVVSTQLLLNGSLAEEEVIIRSDNFTDNAKTIIVQLNESVVINCTRPNNNTRKSIN--IGPGRAFYTTGEIIGDI
B41 KCNSKTFNGSGPCTNVSTVQCTHGIRPVVSTQLLLNGSLAEEEIVIRSENITDNAKTIIVQLNEAVEINCTRPNNNTRKSIH--IGPGRAFYATGDIIGNI
JRFL KCNDKTFNGKGPCKNVSTVQCTHGIRPVVSTQLLLNGSLAEEEVVIRSDNFTNNAKTIIVQLKESVEINCTRPNNNTRKSIH--IGPGRAFYTTGEIIGDI
CE1176 KCNNKTFNGTGPCNNVSTVQCTHGIKPVVSTQLLLNGSLAEKEIIIRSENLTNNAKTIIIHFNESVGIVCTRPSNNTRKSIR--IGPGQTFYATGDIIGDI
BG505 RQAHCNVSKATWNETLGKVVKQLRKHFGNNTIIRFANSSGGDLEVTTHSFNCGGEFFYCNTSGLFNSTWISNTS-VQGSNSTGSNDSITLPCRIKQIINMW 427
AMC008 RQAHCNLSRTQWNNTLKQIAIKLREQFEN-KTIVFNQSSGGDPEIVMHSFNCGGEFFYCNTTKLFNSTWNDT---DIRGNNTEGNDTITIPCRIKQIVNMW
B41 RQAHCNISKARWNETLGQIVAKLEEQFPN-KTIIFNHSSGGDPEIVTHSFNCGGEFFYCNTTPLFNSTWNNT---RTDDYPTGGEQNITLQCRIKQIINMW
JRFL RQAHCNISRAKWNDTLKQIVIKLREQFEN-KTIVFNHSSGGDPEIVMHSFNCGGEFFYCNSTQLFNSTWNNN---TEGSNNTEG-NTITLPCRIKQIINMW
CE1176 RQAHCNVSKQNWNRTLQQVGRKLAEHFPN-RNITFNHSSGGDLEITTHSFNCRGEFFYCNTSGLFNGTYHPNGTY--NETAVNSSDTITLQCRIKQIINMW
BG505 QRIGQAMYAPPIQGVIRCVSNITGLILTRDGGSTNSTTETFRPGGGDMRDNWRSELYKYKVVKIEPLGVAPTRCKRRVVG 507
AMC008 QEVGKAMYAPPIRGQIRCSSNITGLLLTRDGGSESNTTEIFRPGGGDMRDNWRSELYKYKVVRIEPLGVAPTKCKRRVVQ
B41 QGVGKAMYAPPIRGQIRCSSNITGLLLTRDGGRDQNGTETFRPGGGNMRDNWRSELYKYKVVKIEPLGIAPTACKRRVVQ
JRFL QEVGKAMYAPPIRGQIRCSSNITGLLLTRDGGINENGTEIFRPGGGDMRDNWRSELYKYKVVKIEPLGVAPTKCKRRVVQ
CE1176 QEVGRAMYAPPIAGNITCNSTITGLLLTRDGGINQTGEEIFRPGGGDMRDNWRNELYKYKVVEIKPLGIAPTKCKRRVVR

Figure 2. 3. Dynamic differences in gp120 subunits within SOSIP.664 trimers mapped by HDX-MS. (A) Deuterium uptake plots of homologous peptides in gp120 are shown**.** Each HDX uptake plot consists of the average percent deuteration of at least two replicates after 3 seconds, 1 minute, 30 minutes, and 20 hours of exchange normalized to a fully deuterated control. All homologous peptides contain the same number of exchangeable backbone amides across the five strains (BG505 circle, JR-FL square, AMC008 triangle, CE1176 diamond, and B41 indicated by x). In each uptake plot, the homologous peptide sequence (from reference BG505 isolate) is shown and color-coded to match the region on the SOSIP structure and sequence **(B)**. All gp120 inner domain peptides (including layers 1-3) are colored light blue, V1/V2 loops dark blue, V3 loop green, bridging sheet red, the outer domain wheat, and the CD4 binding site is outlined by a pink circle.

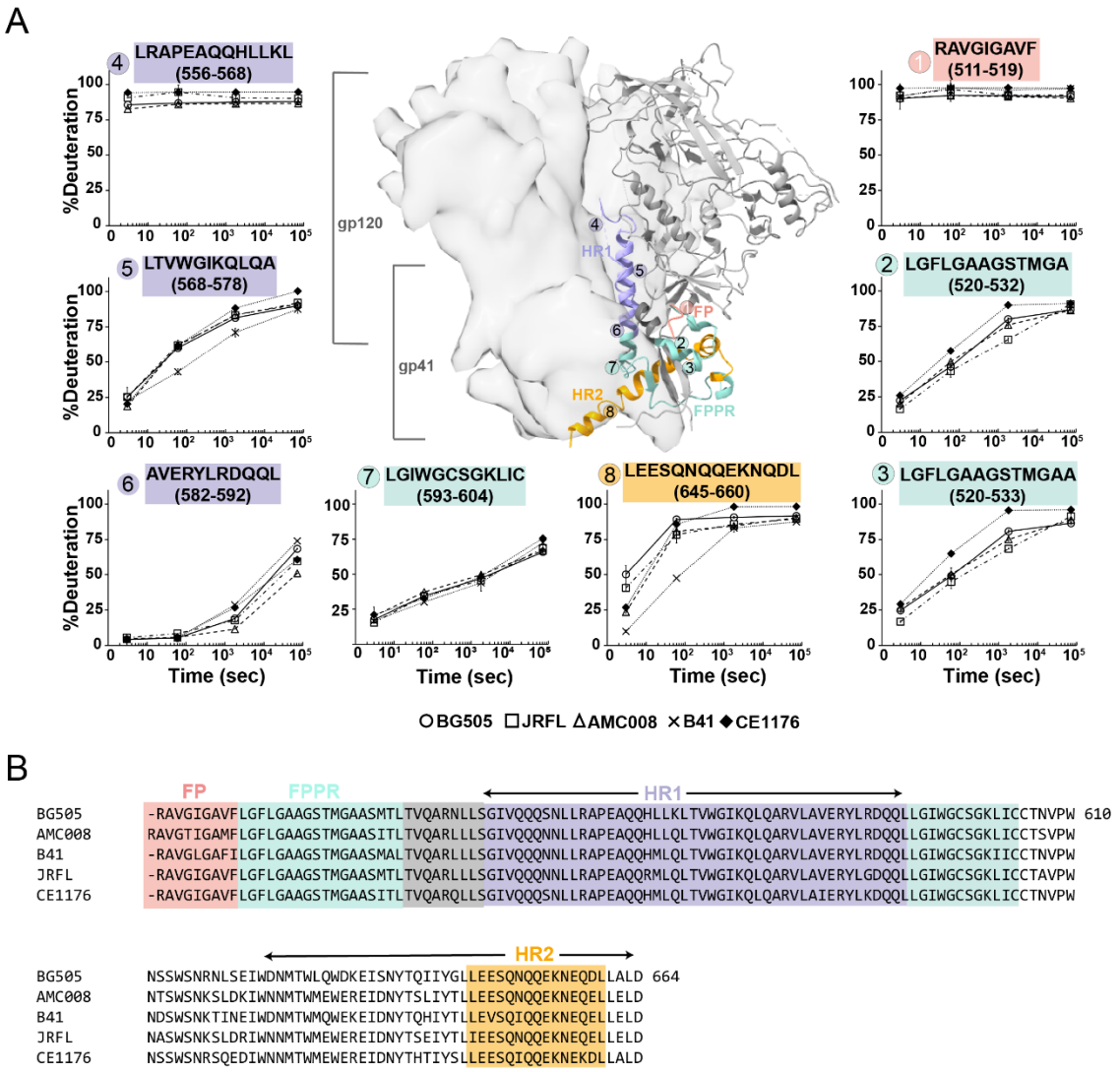

Figure 2. 4. Dynamic differences in gp41 subunits within SOSIP.664 trimers mapped by HDX-MS. (A) Deuterium uptake plots of homologous peptides in gp41 are shown. Each HDX uptake plot consists of the average percent deuteration of at least two replicates after 3 seconds, 1 minute, 30 minutes, and 20 hours of exchange normalized to a fully deuterated control. All homologous peptides contain the same number of exchangeable backbone amides across the five strains (BG505 circle, JR-FL square, AMC008 triangle, CE1176 diamond, and B41 indicated by x). In each uptake plot, the homologous peptide sequence (from reference BG505 isolate) is shown and color-coded to match the region on the SOSIP structure and sequence **(B)**. Homologous peptides found spanning the fusion peptide are colored salmon, the

fusion peptide proximal region (FPPR) in cyan, HR1 is colored purple, and HR2 is colored orange.

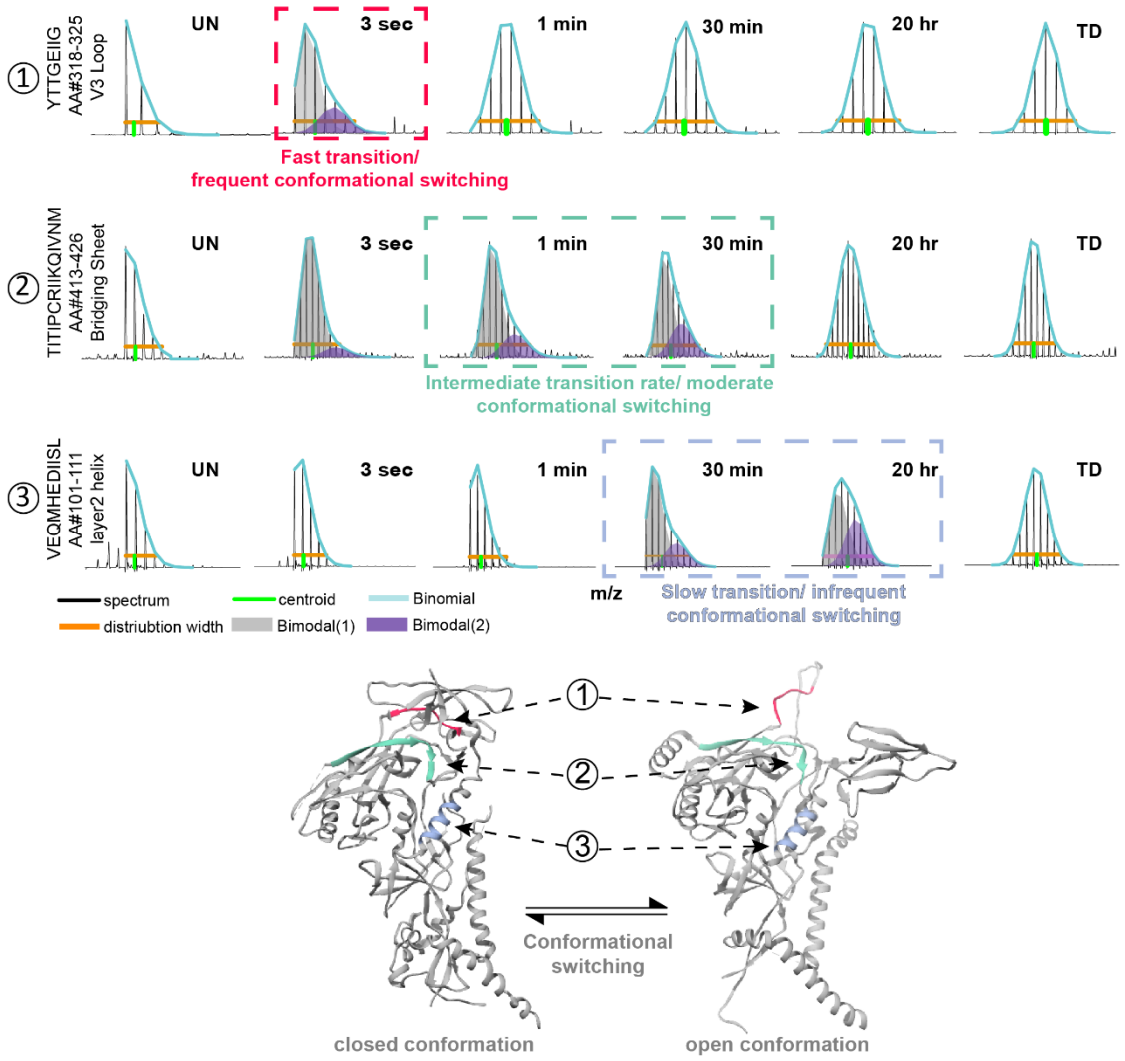

Figure 2. 5. Bimodal mass spectra in three AMC008 gp120 peptides reveal spontaneous local conformational switching that occurs on different timescales. Conformational sampling rates occur frequently (red), over intermediate timescales (green) and infrequently (blue) for peptides in different regions. Bimodal mass envelopes were binomially fit to two populations; a more protected, lighter in mass population in gray, and a more exposed, deuterated population in purple. The three peptides (a V3 peptide, a peptide in the gp120 inner domain helix 2, and a peptide that's part of the bridging sheet/ CD4i epitope) are highlighted

according to the relative rate of opening on the structure of Env in the closed conformation (PDB 5ACO with one protomer in ribbon representation) and on a theoretical structure of Env in an open conformation (PDB 3J70 with one protomer in ribbon representation) to illustrate a hypothetical example of how conformational switching may alter localized structure and give rise to bimodal spectra.

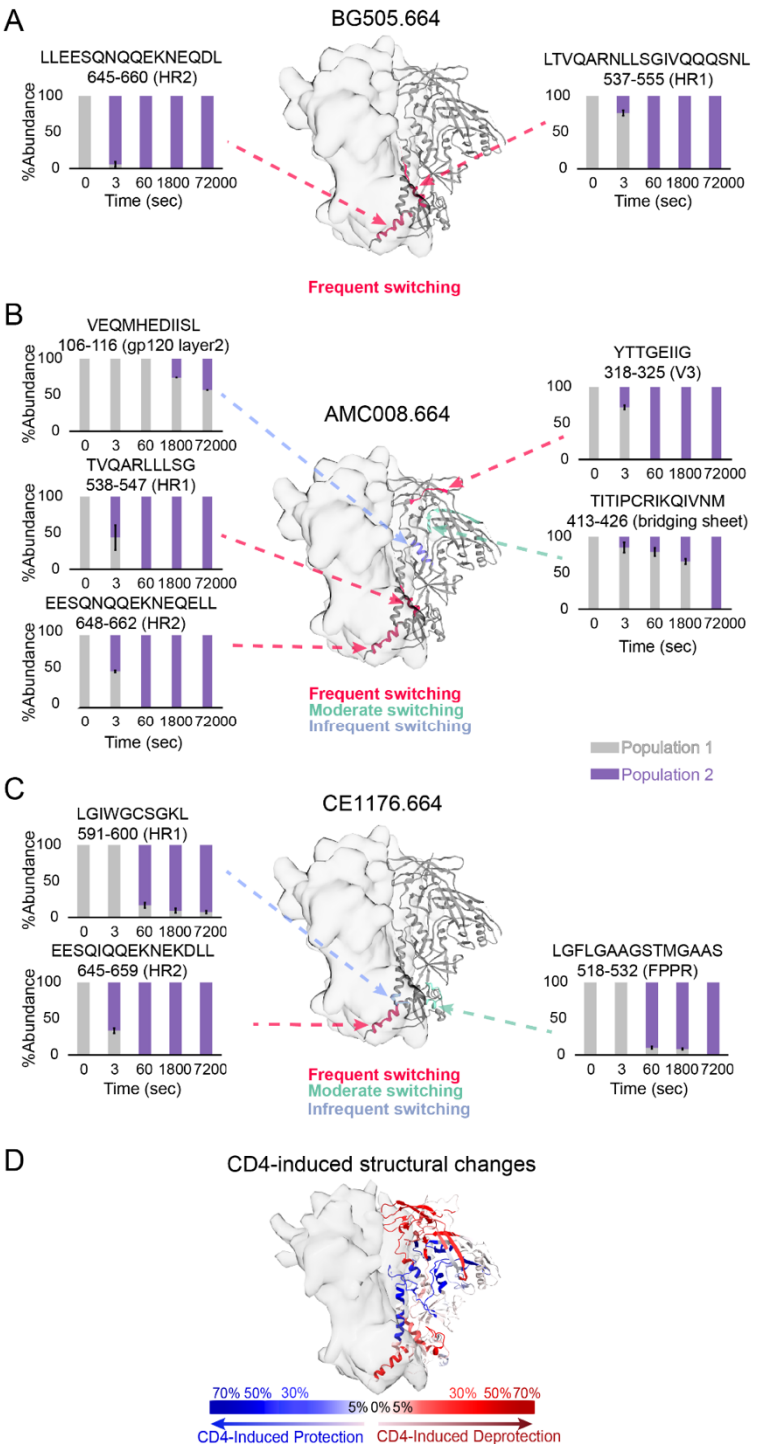

Figure 2. 6. Localized regions across the trimer base and apex undergo spontaneous conformational transitions over a broad range of timescales and in an isolate-specific fashion. Purple and gray bars indicate average population percentages of conformational

states for specific peptides indicated in BG505 **(A)**, AMC008 **(B)**, and CE1176 **(C)** SOSIP.664 trimers with standard deviation error bars (also see Figure S2.4). As in Figure 2.5, peptides sample exposed conformations on a range of time scales ranging from very frequent (red; bimodals only observed in 3sec time points) to very infrequent (blue; bimodals persist after hours). **(D)** Most peptides exhibiting bimodal behavior align with regions involved in CD4-induced conformational changes as shown in HDX-MS heatmap showing the %difference in exchange of unbound and CD4 bound BG505 SOSIP characterized by Guttman et al 2014.

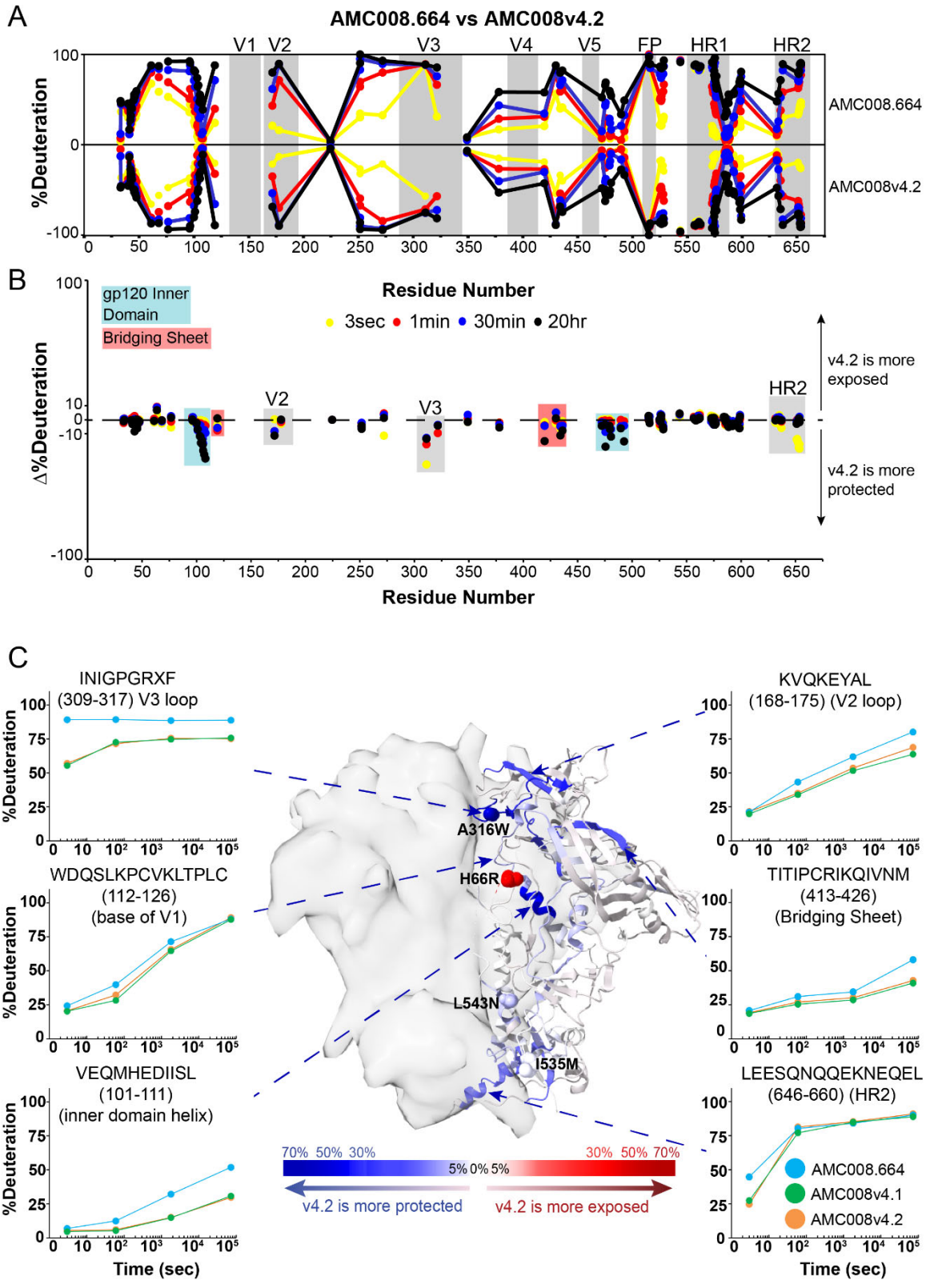
A
AMC008.664 vs AMC008v4.2
V1 V2 V3 V4 V5 FP HR1 HR2
%Deuteration
AMC008.664
AMC008v4.2
B
gp120 Inner Domain
Bridging Sheet
Residue Number
3sec 1min 30min 20hr
v4.2 is more exposed
v4.2 is more protected
Δ%Deuteration
Residue Number
C
INIGPGRXF
(309-317) V3 loop
WDQSLKPCVKLTPLC
(112-126)
(base of V1)
VEQMHEDIISL
(101-111)
(inner domain helix)
KVQKEYAL
(168-175) (V2 loop)
TITIPCRIKQIVNM
(413-426)
(Bridging Sheet)
LEESQNQQEKNEQEL
(646-660) (HR2)
A316W
H66R
L543N
I535M
70% 50% 30%
5% 0% 5%
30% 50% 70%
v4.2 is more protected
v4.2 is more exposed
AMC008.664
AMC008v4.1
AMC008v4.2
%Deuteration
Time (sec)

Figure 2. 7. Stabilizing mutations quench dynamics across the AMC008 structure. (A) HDX-MS butterfly plot showing the profile of dynamics for SOSIP.664 (top) and SOSIPv4.2 (bottom) trimers. The mid-point of each homologous peptide is plotted to show deuterium uptake at each time point (3sec yellow, 1min red, 30min blue, and 20h black). **(B)** Differential plot showing % difference in exchange between AMC008.664 and v4.2. Points below the axis are peptides that are more protected in the v4.2 construct, and peptides above the axis are more exposed in the v4.2 construct (also see Figure S2.8) **(C)** Sum of the differences in backbone amide dynamics between AMC008.664 and v4.2 across time are mapped onto the BG505 SOSIP structure (PDB 5ACO). Regions colored blue are more protected from exchange in v4.2, and regions colored red are regions that are more exposed. Residues with space filling rendering indicate positions of v4.2 stabilizing mutations including H66R in the gp120 inner domain layer 1, A316W in the V3 loop, I535M and L543N in gp41. Deuterium uptake plots comparing differences in backbone amide protection across time (3secs, 1min, 30min, 20hr) in AMC008.664, v4.1, and v4.2 (cyan, green, and orange circles respectively). Each point on the plot is the average percent deuteration of two replicates normalized to a fully deuterated control with standard deviation bars. An X in the peptide sequence is used to indicate mutation sites.

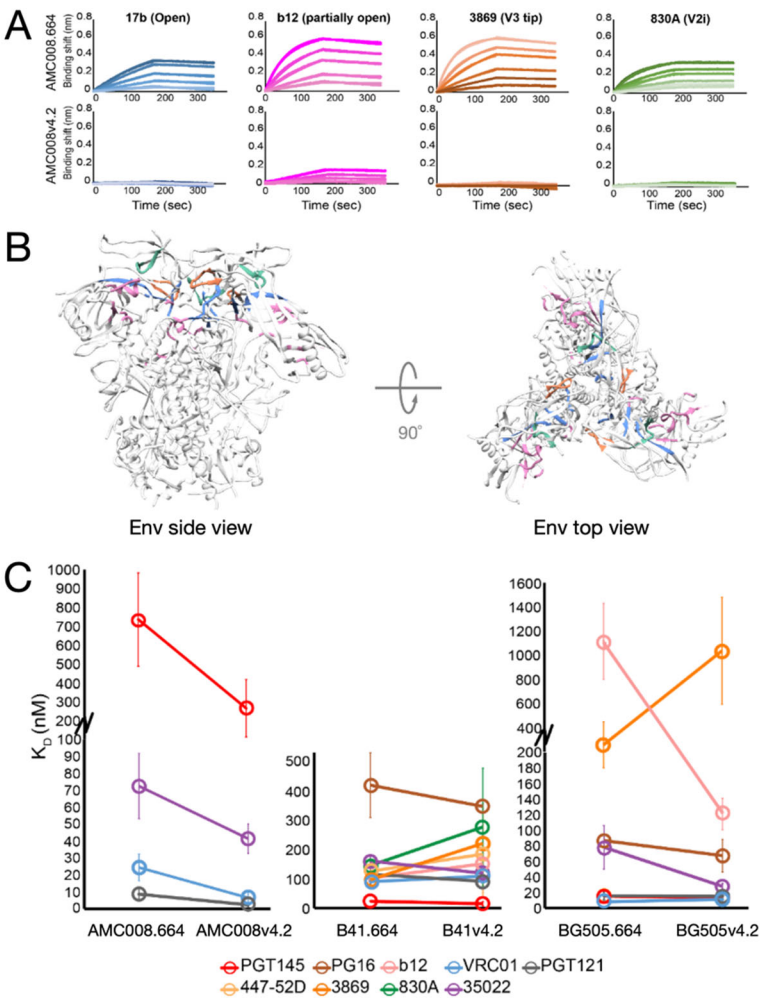

Figure 2. 8. Antigenic consequences of quenched dynamics in three divergent Env trimers. **(A)** BLI sensorgrams reporting on monoclonal antibody (mAb)-Env binding for mAbs that are specific for the open conformation (17b), a partially open conformation (b12), the tip of V3 (3869), and the V2i epitope (830A) of AMC008.664 and the v4.2 construct shows the antigenic effects of reduced flexibility (also see Tables S2-4). The color of each sensorgram corresponds to the epitope of the antibody that is highlighted on the SOSIP structure in the closed conformation (PDB 5ACO) **(B)**; side view (left) and top-down view (right). **(C)** For antibodies where K_D's could be determined, line plots were used to compare differences in binding affinities between the minimally engineered SOSIP and the v4.2 construct across

AMC008, B41, and BG505. Binding affinities are the average of two independent experiments and error bars are the standard deviations.

References

1. Li, Z., et al., *Subnanometer structures of HIV-1 envelope trimers on aldrithiol-2-inactivated virus particles.* Nature structural & molecular biology, 2020: p. 1-9.
2. Julien, J.-P., et al., *Crystal Structure of a Soluble Cleaved HIV-1 Envelope Trimer.* Science, 2013. **342**(6165): p. 1477-1483.
3. Pancera, M., et al., *Structure and immune recognition of trimeric pre-fusion HIV-1 Env.* Nature, 2014. **514**(7523): p. 455.
4. Struwe, W.B., et al., *Site-Specific Glycosylation of Virion-Derived HIV-1 Env Is Mimicked by a Soluble Trimeric Immunogen.* Cell reports, 2018. **24**(8): p. 1958-196600000.
5. Mangala Prasad, V., et al., *Cryo-ET of Env on intact HIV virions reveals structural variation and positioning on the Gag lattice.* Cell, 2022. **185**(4): p. 641-653 e17.
6. Munro, J.B., et al., *Conformational dynamics of single HIV-1 envelope trimers on the surface of native virions.* Science, 2014. **346**(6210): p. 759-763.
7. Liang, Y., et al., *Changes in Structure and Antigenicity of HIV-1 Env Trimers Resulting from Removal of a Conserved CD4 Binding Site-Proximal Glycan.* Journal of Virology, 2016. **90**(20): p. 9224-9236.
8. Davenport, T.M., et al., *Isolate-Specific Differences in the Conformational Dynamics and Antigenicity of HIV-1 gp120.* Journal of Virology, 2013. **87**(19): p. 10855-10873.
9. Kwong, P.D., et al., *HIV-1 evades antibody-mediated neutralization through conformational masking of receptor-binding sites.* Nature, 2002. **420**(6916): p. 678-682.
10. Stadtmueller, B.M., et al., *DEER Spectroscopy Measurements Reveal Multiple Conformations of HIV-1 SOSIP Envelopes that Show Similarities with Envelopes on Native Virions.* Immunity, 2018. **49**(2): p. 235-2460000.
11. Hodge, E.A., M.A. Benhaim, and K.K. Lee, *Bridging protein structure, dynamics, and function using hydrogen/deuterium-exchange mass spectrometry.* Protein Sci, 2020. **29**(4): p. 843-855.
12. Liang, Y., et al., *Probing the Impact of Local Structural Dynamics of Conformational Epitopes on Antibody Recognition.* Biochemistry, 2016. **55**(15): p. 2197-2213.
13. Guttman, M., et al., *Antibody potency relates to the ability to recognize the closed, pre-fusion form of HIV Env.* Nature Communications, 2015. **6**(1): p. 6144.
14. Verkerke, H.P., et al., *Epitope-Independent Purification of Native-Like Envelope Trimers from Diverse HIV-1 Isolates.* Journal of virology, 2016. **90**(20): p. 9471-9482.
15. Wibmer, C., P.L. Moore, and L. Morris, *HIV broadly neutralizing antibody targets.* Current Opinion in HIV and AIDS, 2015. **10**(3): p. 135-143.
16. Chuang, G.-Y., et al., *Structural Survey of Broadly Neutralizing Antibodies Targeting the HIV-1 Env Trimer Delineates Epitope Categories and Characteristics of Recognition.* Structure (London, England : 1993), 2018. **27**(1): p. 196-206000000.
17. Chuang, G.-Y., et al., *Structure-Based Design of a Soluble Prefusion-Closed HIV-1-Env Trimer with Reduced CD4 Affinity and Improved Immunogenicity.* Journal of Virology, 2017: p. 16.
18. Ward, A.B. and I.A. Wilson, *The HIV-1 envelope glycoprotein structure: nailing down a moving target.* Immunological Reviews, 2017. **275**(1): p. 21-32.

19. Sanders, R.W., et al., *A Next-Generation Cleaved, Soluble HIV-1 Env Trimer, BG505 SOSIP.664 gp140, Expresses Multiple Epitopes for Broadly Neutralizing but Not Non-Neutralizing Antibodies.* PLoS Pathogens, 2013.
20. Ringe, R.P., et al., *SOS and IP Modifications Predominantly Affect the Yield but Not Other Properties of SOSIP.664 HIV-1 Env Glycoprotein Trimers.* Journal of virology, 2019.
21. Lai, Y.T., et al., *Lattice engineering enables definition of molecular features allowing for potent small-molecule inhibition of HIV-1 entry.* Nat Commun, 2019. **10**(1): p. 47.
22. Doria-Rose, N.A., et al., *Developmental pathway for potent V1V2-directed HIV-neutralizing antibodies.* Nature, 2014. **509**(7498): p. 55-62.
23. Lee, J.H., et al., *A broadly neutralizing antibody targets the dynamic HIV envelope trimer apex via a long, rigidified, and anionic β-hairpin structure.* A broadly neutralizing antibody targets the dynamic HIV envelope trimer apex via a long, rigidified, and anionic β-hairpin structure, 2017.
24. Wu, X., et al., *Focused evolution of HIV-1 neutralizing antibodies revealed by structures and deep sequencing.* Science, 2011. **333**(6049): p. 1593-602.
25. Pejchal, R., et al., *A potent and broad neutralizing antibody recognizes and penetrates the HIV glycan shield.* Science, 2011. **334**(6059): p. 1097-103.
26. Mouquet, H., et al., *Complex-type N-glycan recognition by potent broadly neutralizing HIV antibodies.* Proc Natl Acad Sci U S A, 2012. **109**(47): p. E3268-77.
27. Kong, R., et al., *Fusion peptide of HIV-1 as a site of vulnerability to neutralizing antibody.* Science (New York, N.Y.), 2016. **352**(6287): p. 828-833.
28. Xu, K., et al., *Epitope-based vaccine design yields fusion peptide-directed antibodies that neutralize diverse strains of HIV-1.* Nat Med, 2018. **24**(6): p. 857-867.
29. Huang, J., et al., *Broad and potent HIV-1 neutralization by a human antibody that binds the gp41-gp120 interface.* Nature, 2014. **515**(7525): p. 138-42.
30. de Taeye, S.W., et al., *Immunogenicity of Stabilized HIV-1 Envelope Trimers with Reduced Exposure of Non-neutralizing Epitopes.* Cell, 2015. **163**(7): p. 1702-1715.
31. Torrents de la Pena, A. and R.W. Sanders, *Stabilizing HIV-1 envelope glycoprotein trimers to induce neutralizing antibodies.* Retrovirology, 2018. **15**(1): p. 63.
32. McLellan, J.S., et al., *Structure-based design of a fusion glycoprotein vaccine for respiratory syncytial virus.* Science, 2013. **342**(6158): p. 592-8.
33. Hsieh, C.L., et al., *Structure-based Design of Prefusion-stabilized SARS-CoV-2 Spikes.* bioRxiv, 2020.
34. Pallesen, J., et al., *Immunogenicity and structures of a rationally designed prefusion MERS-CoV spike antigen.* Proc Natl Acad Sci U S A, 2017. **114**(35): p. E7348-E7357.
35. Binley, J.M., et al., *A recombinant human immunodeficiency virus type 1 envelope glycoprotein complex stabilized by an intermolecular disulfide bond between the gp120 and gp41 subunits is an antigenic mimic of the trimeric virion-associated structure.* Journal of virology, 2000. **74**(2): p. 627-643.
36. Sanders, R.W., et al., *A next-generation cleaved, soluble HIV-1 Env trimer, BG505 SOSIP. 664 gp140, expresses multiple epitopes for broadly neutralizing but not non-neutralizing ….* A next-generation cleaved, soluble HIV-1 Env trimer, BG505 SOSIP. 664 gp140, expresses multiple epitopes for broadly neutralizing but not non-neutralizing …, 2013.
37. Sanders, R.W., et al., *Stabilization of the soluble, cleaved, trimeric form of the envelope glycoprotein complex of human immunodeficiency virus type 1.* Journal of virology, 2002. **76**(17): p. 8875-8889.
38. Rawi, R., et al., *Automated Design by Structure-Based Stabilization and Consensus Repair to Achieve Prefusion-Closed Envelope Trimers in a Wide Variety of HIV Strains.* Cell Rep, 2020. **33**(8): p. 108432.

39. de la Peña, A., et al., *Improving the Immunogenicity of Native-like HIV-1 Envelope Trimers by Hyperstabilization.* Cell Reports, 2017. **20**(8): p. 1805-1817.
40. Watson, M.J., et al., *Simple Platform for Automating Decoupled LC-MS Analysis of Hydrogen/Deuterium Exchange Samples.* J Am Soc Mass Spectrom, 2021. **32**(2): p. 597-600.
41. Guttman, M., et al., *Analysis of Overlapped and Noisy Hydrogen/Deuterium Exchange Mass Spectra.* Journal of The American Society for Mass Spectrometry, 2013. **24**(12): p. 1906-1912.
42. Weis, D.D., et al., *Identification and characterization of EX1 kinetics in H/D exchange mass spectrometry by peak width analysis.* Journal of The American Society for Mass Spectrometry, 2006. **17**(11): p. 1498-1509.
43. Hodge, E.A., et al., *Structural dynamics reveal isolate-specific differences at neutralization epitopes on HIV Env.* iScience, 2022. **25**(6): p. 104449.
44. Daar, E.S., et al., *High concentrations of recombinant soluble CD4 are required to neutralize primary human immunodeficiency virus type 1 isolates.* Proc Natl Acad Sci U S A, 1990. **87**(17): p. 6574-8.
45. Hoffenberg, S., et al., *Identification of an HIV-1 clade A envelope that exhibits broad antigenicity and neutralization sensitivity and elicits antibodies targeting three distinct epitopes.* J Virol, 2013. **87**(10): p. 5372-83.
46. Pugach, P., et al., *A native-like SOSIP.664 trimer based on an HIV-1 subtype B env gene.* J Virol, 2015. **89**(6): p. 3380-95.
47. deCamp, A., et al., *Global panel of HIV-1 Env reference strains for standardized assessments of vaccine-elicited neutralizing antibodies.* Journal of virology, 2014. **88**(5): p. 2489-2507.
48. Seaman, M.S., et al., *Tiered Categorization of a Diverse Panel of HIV-1 Env Pseudoviruses for Assessment of Neutralizing Antibodies.* Journal of Virology, 2010. **84**(3): p. 1439-1452.
49. Stavenhagen, K., et al., *Quantitative mapping of glycoprotein micro-heterogeneity and macro-heterogeneity: an evaluation of mass spectrometry signal strengths using synthetic peptides and glycopeptides.* J Mass Spectrom, 2013. **48**(6): p. 627-39.
50. Guttman, M., et al., *CD4-Induced Activation in a Soluble HIV-1 Env Trimer.* Structure, 2014. **22**(7): p. 974-984.
51. Guttman, M. and K.K. Lee, *A functional interaction between gp41 and gp120 is observed for monomeric but not oligomeric, uncleaved HIV-1 Env gp140.* J Virol, 2013. **87**(21): p. 11462-75.
52. Lee, J.H., et al., *A Broadly Neutralizing Antibody Targets the Dynamic HIV Envelope Trimer Apex via a Long, Rigidified, and Anionic beta-Hairpin Structure.* Immunity, 2017. **46**(4): p. 690-702.
53. Sok, D., et al., *Recombinant HIV envelope trimer selects for quaternary-dependent antibodies targeting the trimer apex.* Proceedings of the National Academy of Sciences of the United States of America, 2014. **111**(49): p. 17624-17629.
54. Powell, R.L.R.L.R., et al., *Plasticity and Epitope Exposure of the HIV-1 Envelope Trimer.* Journal of virology, 2017. **91**(17).
55. Pan, R., et al., *The V1V2 Region of HIV-1 gp120 Forms a Five-Stranded Beta Barrel.* Journal of virology, 2015. **89**(15): p. 8003-8010.
56. Finzi, A., et al., *Topological Layers in the HIV-1 gp120 Inner Domain Regulate gp41 Interaction and CD4-Triggered Conformational Transitions.* Molecular cell, 2010. **37**(5): p. 656-667.
57. Kumar, S., et al., *Capturing the inherent structural dynamics of the HIV-1 envelope glycoprotein fusion peptide.* Nature Communications, 2019. **10**(1): p. 763.

58. Ananthaswamy, N., et al., *A sequestered fusion peptide in the structure of an HIV-1 transmitted founder envelope trimer.* Nature Communications, 2019. **10**(1): p. 873.
59. Pan, J., et al., *Cryo-EM structure of full-length HIV-1 Env bound with the Fab of antibody PG16.* bioRxiv, 2019: p. 730333.
60. Lee, J.H., G. Ozorowski, and A.B. Ward, *Cryo-EM structure of a native, fully glycosylated, cleaved HIV-1 envelope trimer.* Science (New York, N.Y.), 2016. **351**(6277): p. 1043-1048.
61. Benhaim, M., K.K. Lee, and M. Guttman, *Tracking Higher Order Protein Structure by Hydrogen-Deuterium Exchange Mass Spectrometry.* Protein and peptide letters, 2019. **26**(1): p. 16-26.
62. Nielsen, A., et al., *Substrate-induced conformational dynamics of the dopamine transporter.* Nature Communications, 2019. **10**(1): p. 2714.
63. Wang, H., et al., *Partially Open HIV-1 Envelope Structures Exhibit Conformational Changes Relevant for Coreceptor Binding and Fusion.* Cell Host & Microbe, 2018. **24**(4): p. 579-5920000.
64. McLellan, J.S., et al., *Structure of HIV-1 gp120 V1/V2 domain with broadly neutralizing antibody PG9.* Nature, 2011. **480**(7377): p. 336-43.
65. Kwong, P.D., et al., *Structure of an HIV gp120 envelope glycoprotein in complex with the CD4 receptor and a neutralizing human antibody.* Nature, 1998. **393**(6686): p. 648-59.
66. Zhou, T., et al., *Structural definition of a conserved neutralization epitope on HIV-1 gp120.* Nature, 2007. **445**(7129): p. 732-737.
67. Han, Q., et al., *Difficult-to-neutralize global HIV-1 isolates are neutralized by antibodies targeting open envelope conformations.* Nature Communications, 2019. **10**(1): p. 2898.
68. Hioe, C.E., et al., *Anti-V3 Monoclonal Antibodies Display Broad Neutralizing Activities against Multiple HIV-1 Subtypes.* PLoS ONE, 2010. **5**(4).
69. Duerr, R. and M.K. Gorny, *V2-Specific Antibodies in HIV-1 Vaccine Research and Natural Infection: Controllers or Surrogate Markers.* Vaccines, 2019. **7**(3): p. 82.
70. Mayr, L.M., et al., *Epitope mapping of conformational V2-specific anti-HIV human monoclonal antibodies reveals an immunodominant site in V2.* PloS one, 2013. **8**(7).
71. Falkowska, E., et al., *PGV04, an HIV-1 gp120 CD4 Binding Site Antibody, Is Broad and Potent in Neutralization but Does Not Induce Conformational Changes Characteristic of CD4.* Journal of Virology, 2012. **86**(8): p. 4394-4403.
72. Pan, J., et al., *Cryo-EM Structure of Full-length HIV-1 Env Bound With the Fab of Antibody PG16.* J Mol Biol, 2020. **432**(4): p. 1158-1168.
73. Sztain, T., et al., *A glycan gate controls opening of the SARS-CoV-2 spike protein.* Nat Chem, 2021. **13**(10): p. 963-968.
74. Andrabi, R., et al., *Identification of Common Features in Prototype Broadly Neutralizing Antibodies to HIV Envelope V2 Apex to Facilitate Vaccine Design.* Immunity, 2015. **43**(5): p. 959-973.
75. Montefiori, D.C., et al., *Neutralization tiers of HIV-1.* Current Opinion in HIV and AIDS, 2018. **13**(2): p. 128.
76. Hraber, P., et al., *A single, continuous metric to define tiered serum neutralization potency against HIV.* eLife, 2018. **7**.
77. Kwon, Y.D., et al., *Unliganded HIV-1 gp120 core structures assume the CD4-bound conformation with regulation by quaternary interactions and variable loops.* Proc Natl Acad Sci U S A, 2012. **109**(15): p. 5663-8.
78. Georgiev, I.S., et al., *Single-Chain Soluble BG505.SOSIP gp140 Trimers as Structural and Antigenic Mimics of Mature Closed HIV-1 Env.* J Virol, 2015. **89**(10): p. 5318-29.
79. Wrapp, D., et al., *Cryo-EM structure of the 2019-nCoV spike in the prefusion conformation.* Science, 2020. **367**(6483): p. 1260-1263.

80. Hsieh, C.L., et al., *Structure-based design of prefusion-stabilized SARS-CoV-2 spikes.* Science, 2020. **369**(6510): p. 1501-1505.
81. Sanders, R.W. and J.P. Moore, *Virus vaccines: proteins prefer prolines.* Cell Host Microbe, 2021. **29**(3): p. 327-333.
82. D'Souza, M.P., et al., *Engineering immunity for next generation HIV vaccines: The intersection of bioengineering and immunology.* Vaccine, 2020. **38**(2): p. 187-193.
83. Derking, R. and R.W. Sanders, *Structure-guided envelope trimer design in HIV-1 vaccine development: a narrative review.* J Int AIDS Soc, 2021. **24 Suppl 7**: p. e25797.

Supplemental Figures

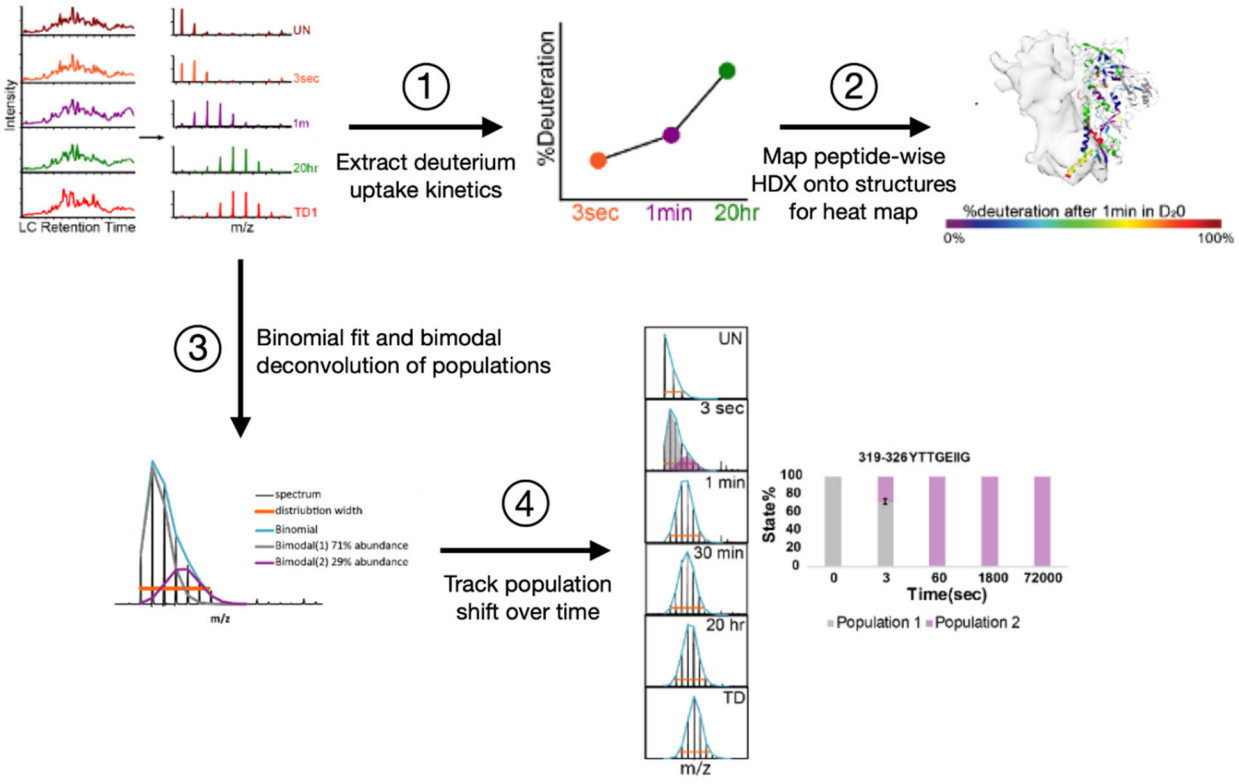

Figure S2.1. HDX analysis workflow, related to Figures 2.1-2.7

Initially after data collection each peptide's m/z, charge state, unique retention time and drift time are uploaded into HDExaminer, which extracts each peptide's mass spectra at each time point (1) and plots the % deuteration with time based on centroid fitting. The percent deuteration of each peptide at the 1minute timepoint is then color coded and mapped onto the structure of a SOSIP (2) to generate an HDX heatmap for each individual isolate. Next the HDExaminer centroid fit data is exported into HX-Expressv2 for binomial fitting (3). The analysis in HX-Express takes into account the mass envelope distribution

width. Anything unusually broad is flagged as bimodal, and bimodal deconvolution allows for the identification of EX1 kinetics that are indicative of conformational switching. The percent abundance of the two populations (colored gray and purple respectively) across time are then converted into a bar plot (4) to determine the rate of the conformational transition from the protected to the exposed populations.

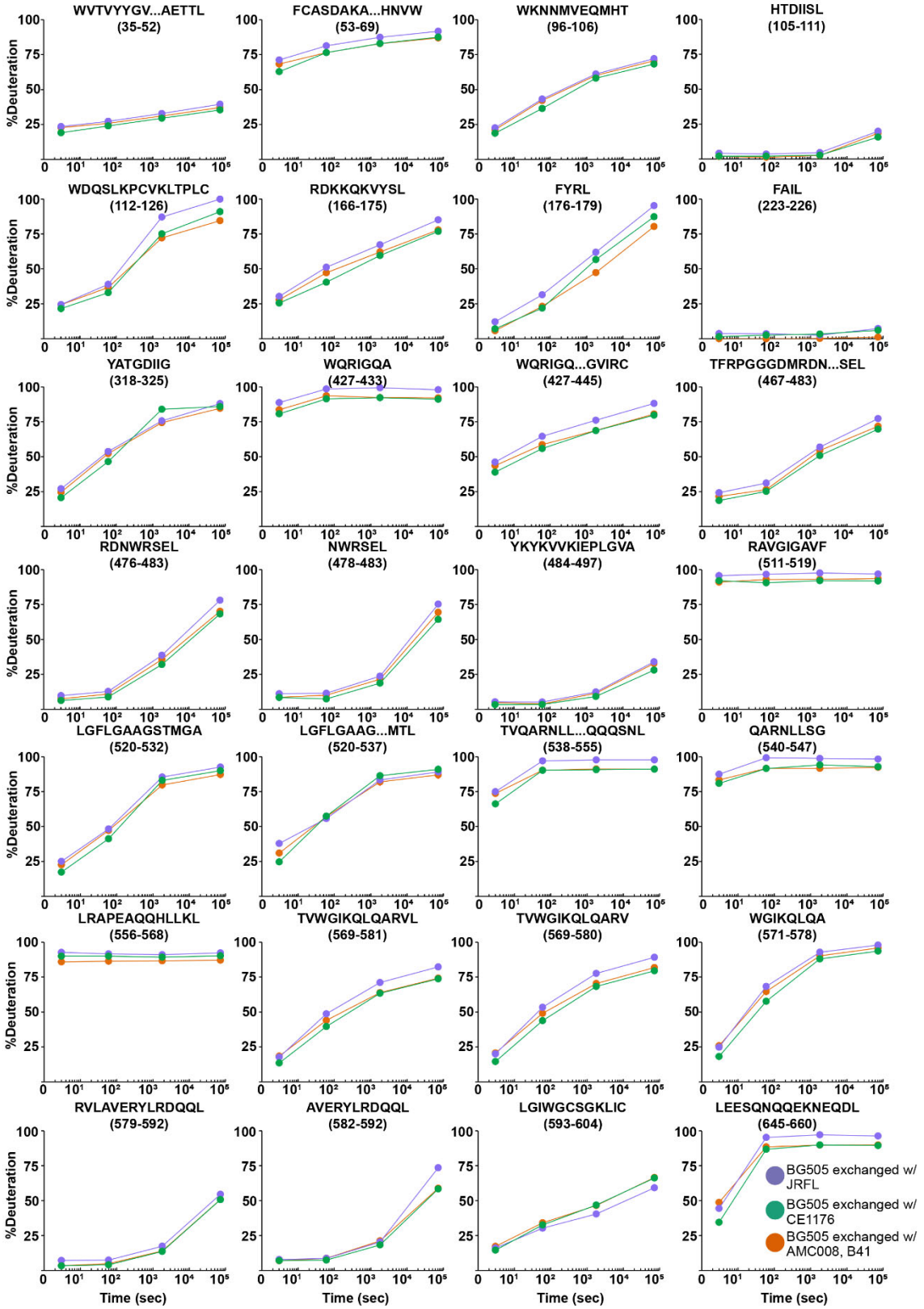
WVTVYYGV...AETTL
(35-52)
FCASDAKA...HNVW
(53-69)
WKNNMVEQMHT
(96-106)
HTDIISL
(105-111)
WDQSLKPCVKLTPLC
(112-126)
RDKKQKVYSL
(166-175)
FYRL
(176-179)
FAIL
(223-226)
YATGDIIG
(318-325)
WQRIGQA
(427-433)
WQRIGQ...GVIRC
(427-445)
TFRPGGGDMRDN...SEL
(467-483)
RDNWRSEL
(476-483)
NWRSEL
(478-483)
YKYKVVKIEPLGVA
(484-497)
RAVGIGAVF
(511-519)
LGFLGAAGSTMGA
(520-532)
LGFLGAAG...MTL
(520-537)
TVQARNLL...QQQSNL
(538-555)
QARNLLSG
(540-547)
LRAPEAQQHLLKL
(556-568)
TVWGIKQLQARVL
(569-581)
TVWGIKQLQARV
(569-580)
WGIKQLQA
(571-578)
RVLAVERYLRDQQL
(579-592)
AVERYLRDQQL
(582-592)
LGIWGCSGKLIC
(593-604)
LEESQNQQEKNEQDL
(645-660)
%Deuteration
Time (sec)
BG505 exchanged w/ JRFL
BG505 exchanged w/ CE1176
BG505 exchanged w/ AMC008, B41

Figure S2.2. BG505 HDX reference controls, related to Figures 2.3-2.4

Percent deuteration of commonly found homologous peptides across different isolates from BG505 biological replicates that were exchanged alongside other isolates as an HDX control standard. Purple uptake curves represent BG505 exchanged alongside JRFL, green was BG505 exchanged in tandem with CE1176, and orange indicates BG505 exchanged in tandem with AMC008 and B41 constructs. Each time point is the average of duplicate measurements with error bars displaying standard deviation.

A

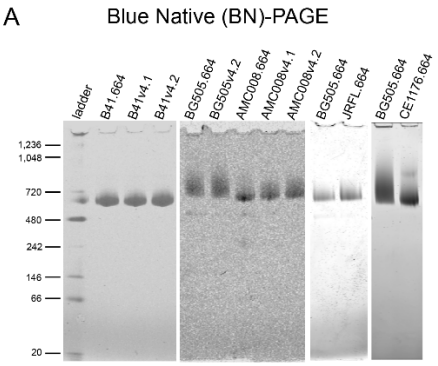

B

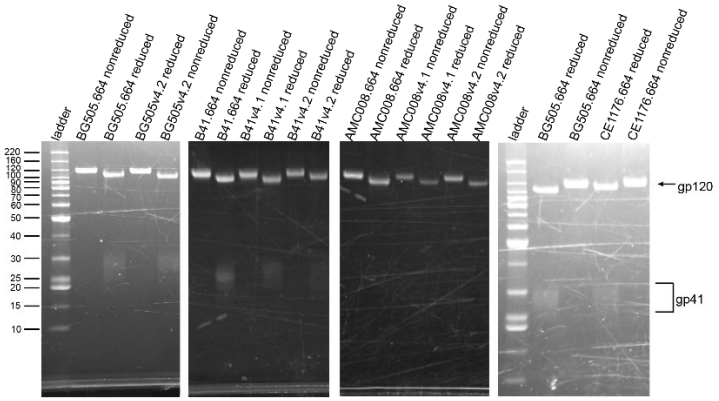

C

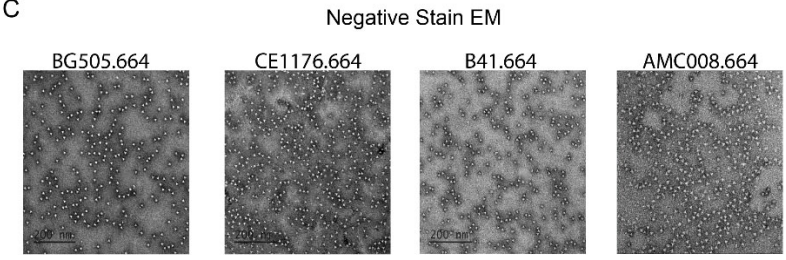

D

SOSIP	Avg radius (nm)	Radius std dev	Avg %polydispersity	Avg %abundance
BG505.664	6.7	0.10	9.0	100
BG505v4.2	6.9	0.11	11.4	100
B41.664	6.8	0.21	12.9	100
B41v4.1	7.0	0.12	14.5	100
B41v4.2	6.8	0.1	15.8	100
AMC008.664	7.0	0.1	10.6	100
AMC008v4.1	7.0	0	13.7	100
AMC008v4.2	7.0	0	16.6	100
JRFL.664	7.0	0.06	12.9	100
CE1176.664	7.0	0.07	13.1	100

Figure S2.3. SOSIP characterization by blue native (BN)-PAGE, SDS-PAGE, and dynamic light scattering (DLS).

To assess trimer purity each SOSIP was characterized by BN-PAGE (A), SDS-PAGE (B), negative stain EM (C), and DLS (D) after purification and prior to HDX and BLI experiments. On the SDS-PAGE each sample was run non-reduced and reduced via addition of DTT. The single band in the non-reduced lane runs at a slightly higher MW due to the presence of an additional inter-subunit disulfide bond linking gp120 and gp41. The weakly visible gp41 bands in the reduced lane are smeared likely due to glycan heterogeneity.

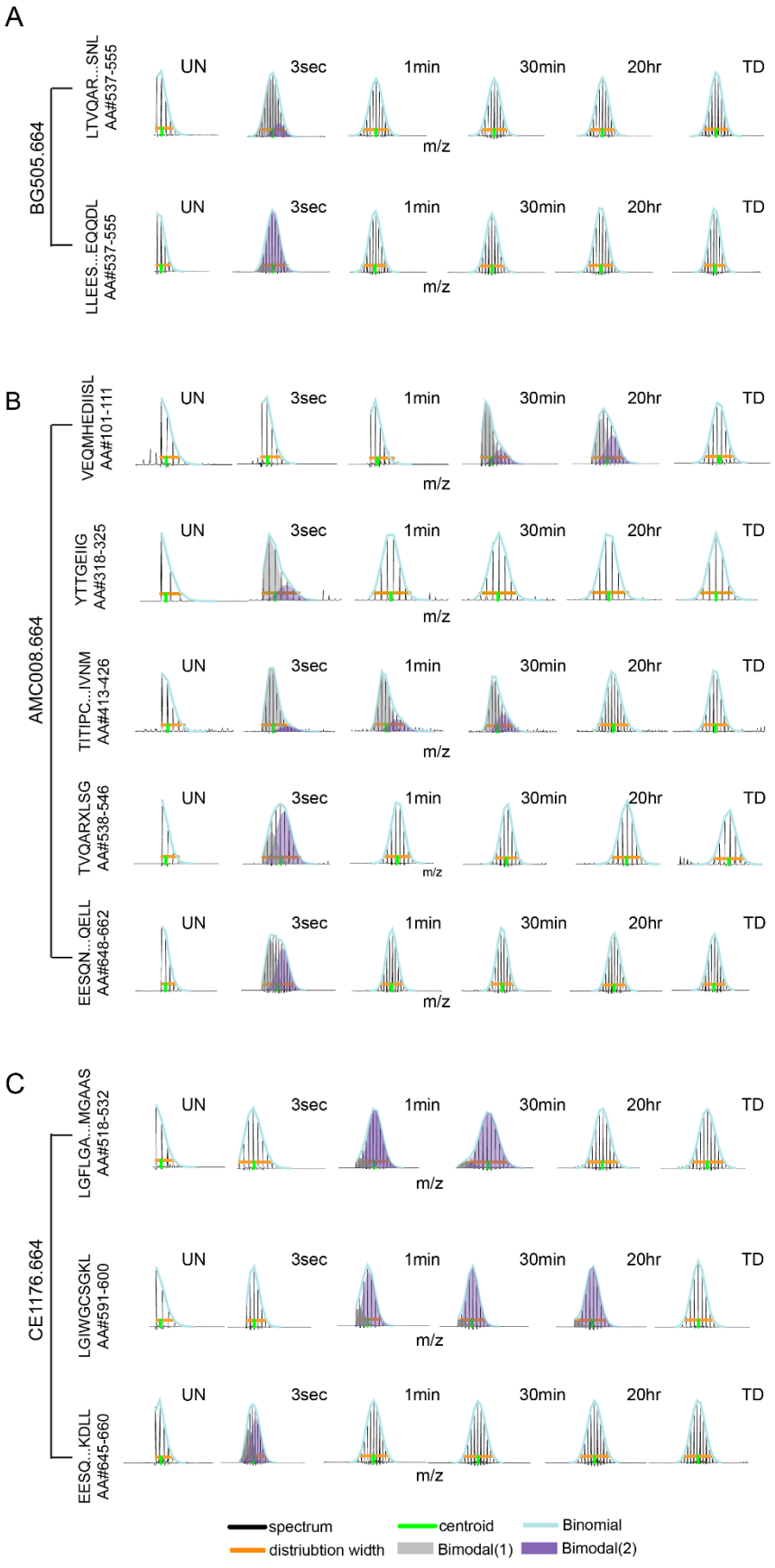
A
BG505.664
LTVQAR...SNL
AA#537-555
LLEES...EQQDL
AA#537-555
UN
3sec
1min
30min
20hr
TD
m/z
B
AMC008.664
VEQMHEDIISL
AA#101-111
YTTGEIIG
AA#318-325
TITIPC...IVNM
AA#413-426
TVQARXLSG
AA#538-546
EESQN...QELL
AA#648-662
C
CE1176.664
LGFLGA...MGAAS
AA#518-532
LGIWGCSGKL
AA#591-600
EESQ...KDLL
AA#645-660
spectrum
centroid
Binomial
distriubtion width
Bimodal(1)
Bimodal(2)

Figure S2.4. Bimodal spectra suggestive of conformational switching across strains, related to Figure 2.6.

Two peptides in BG505.664, five peptides in AMC008.664, and three peptides in CE1176.664 exhibited unusually broad isotopic distributions that were binomially fit to two populations (Figures A-C respectively). Each panel displays the spectra from each respective time point. The lighter in mass/more protected population is shaded in gray, and the heavier in mass/faster exchanging population is shaded in purple. The legend describing the centroid, peak envelope, and binomial fit are displayed in the bottom center of the Figure.

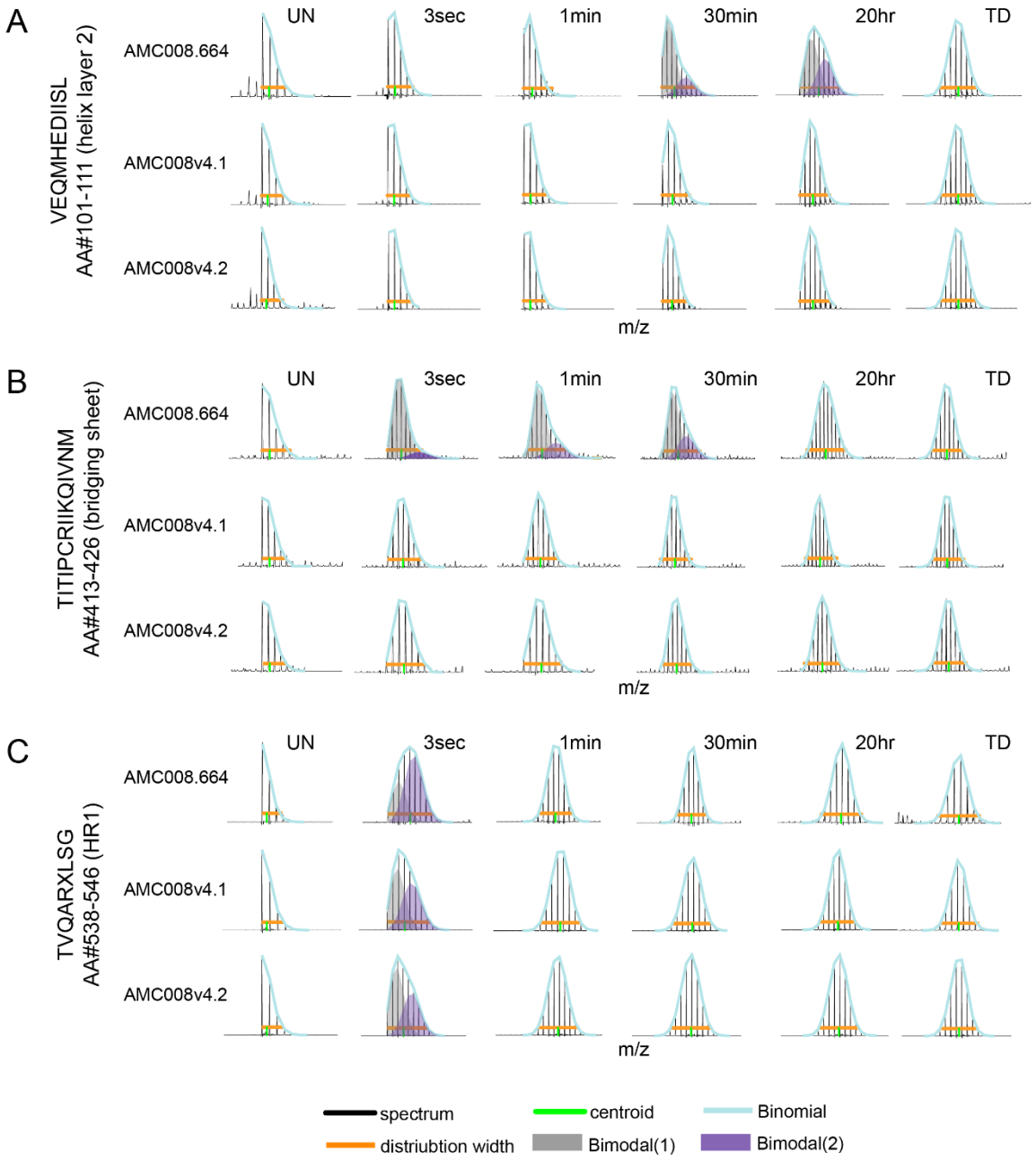

Figure S2.5. Additional stabilizing mutations quench conformational sampling observed in the dynamic AMC008.664 trimer, related to Figure 2.7.

Mass spectra at each HDX time point of the AMC008 SOSIP constructs (.664, v4.1, and v4.2) are aligned. Spectra with a mass envelope width that was unusually broad were binomially fit to two populations. The lighter in mass/more protected population is shaded in gray, and the heavier in mass/more exposed population is shaded in purple. Peptides are highlighted spanning the gp120 inner domain helix 2 **(A)**, the bridging sheet **(B),** and HR1 in gp41 **(C).** Two of the three peptides displayed bimodal spectra only in the

minimally engineered SOSIP.664 trimers, however the peptide 538-546 in gp41, where an X is used for the L543N mutation site in the v4 constructs, displayed bimodal spectra at the earliest time point in all three constructs.

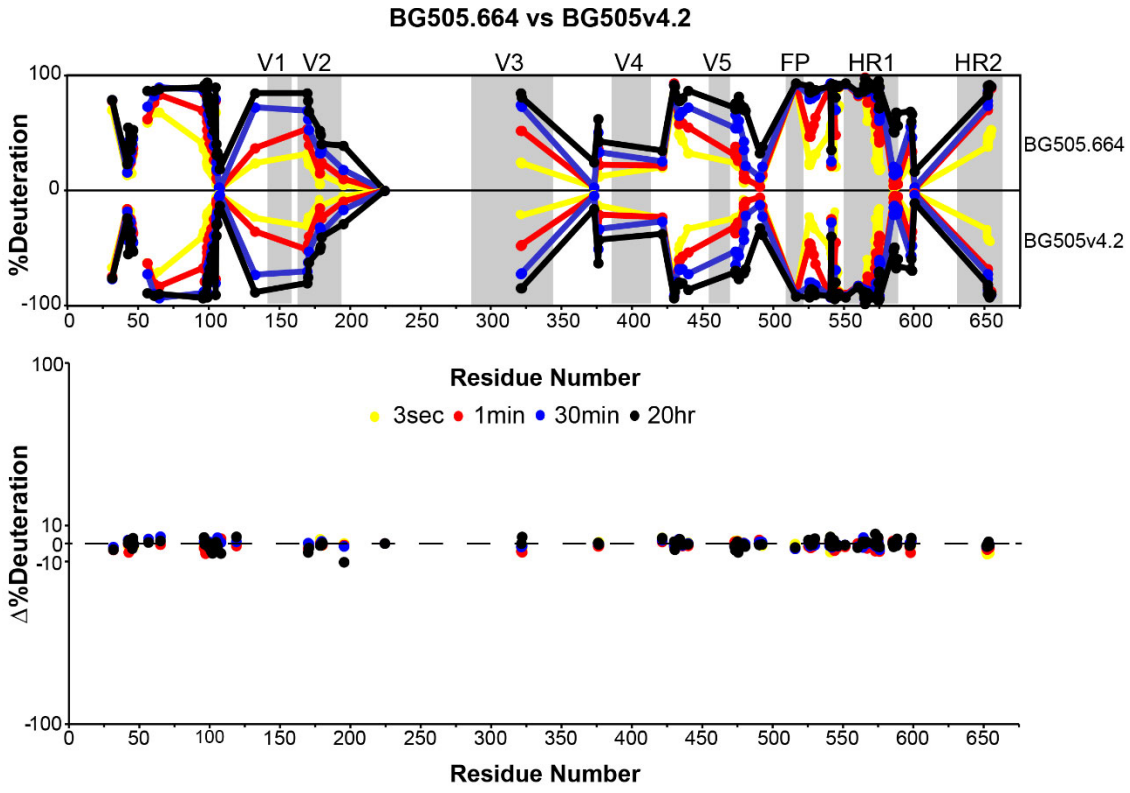

Figure S2.6 BG505.664 and BG505v4.2 butterfly and differential plots, related to Figure 2.7

The top Figure is a butterfly plot. The mid-point of each homologous peptide found in BG505.664 (top half) and BG505v4.2 (bottom half) is plotted to show deuterium uptake with time (3 second time point in yellow, 1 minute time point in red, 30 minute time point in blue, and 20 hour time point in black). The bottom Figure is a differential plot where the %difference in exchange between BG505.664 and v4.2 is plotted. Peptides falling below the 0 dashed line are regions more protected from exchange in the v4.2 construct, and peptides falling above the dashed line are regions that became less protected from exchange in the v4.2 construct.

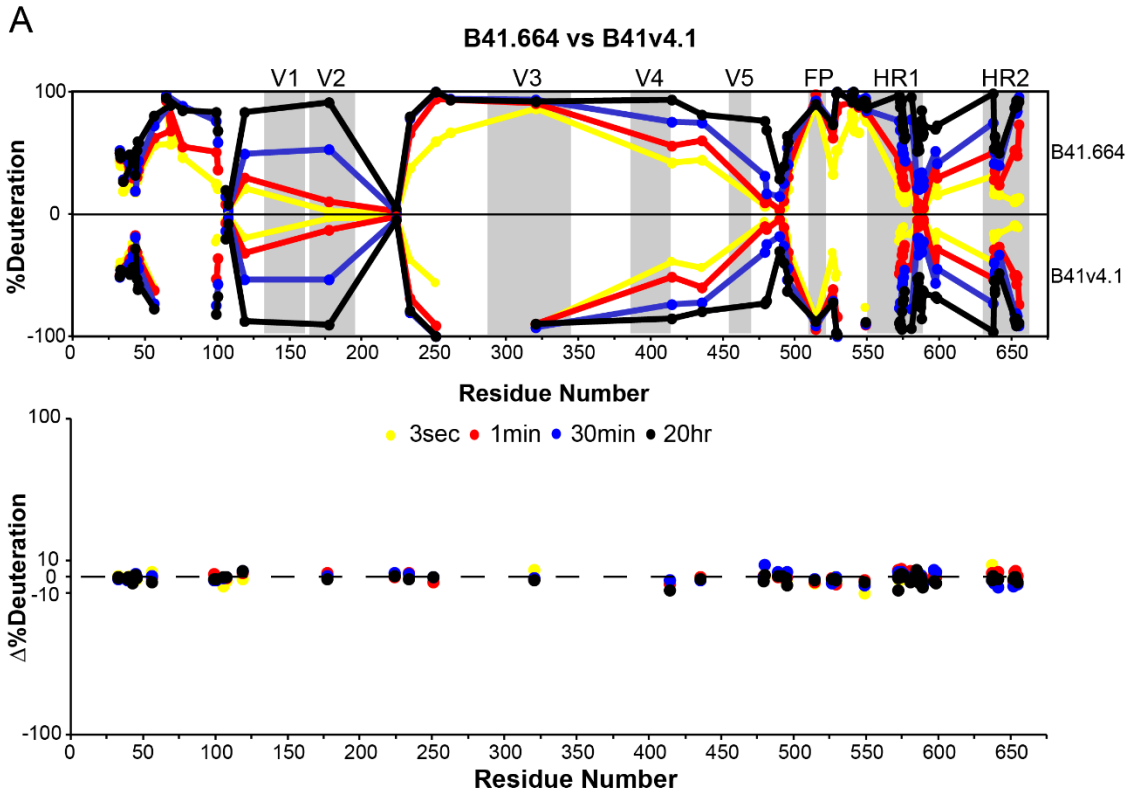
A
B41.664 vs B41v4.1
V1 V2
V3
V4
V5
FP
HR1
HR2
%Deuteration
B41.664
B41v4.1
Residue Number
3sec 1min 30min 20hr
Δ%Deuteration
Residue Number

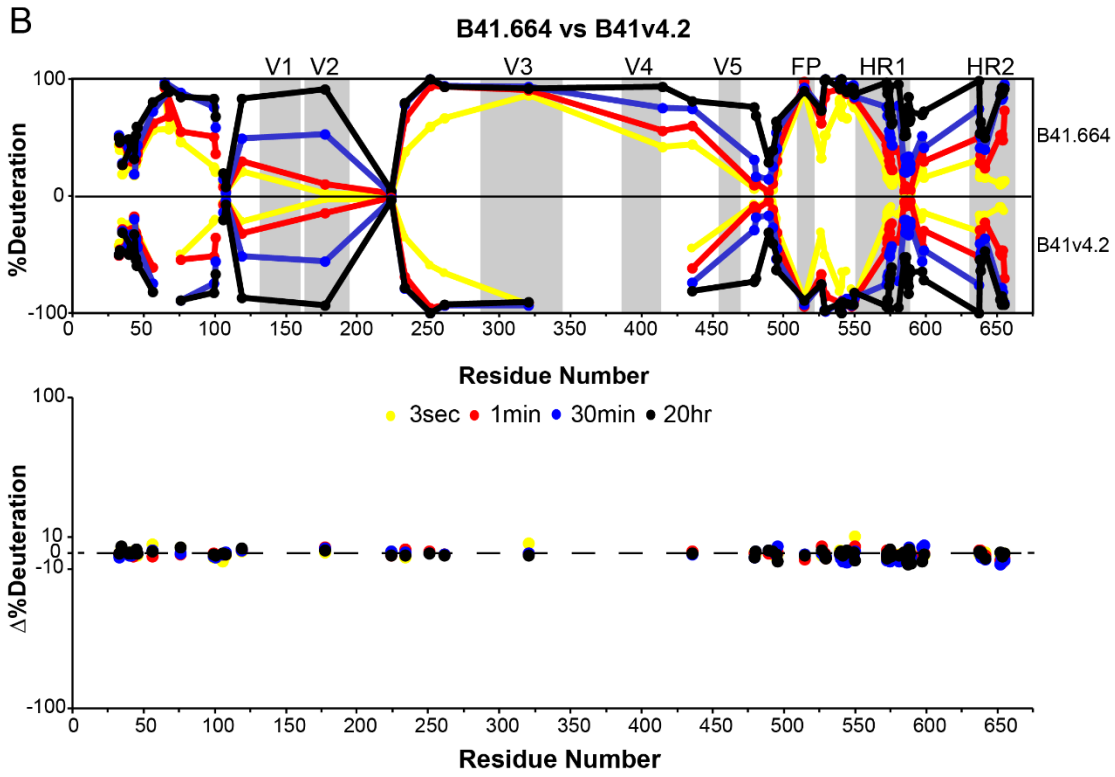
B
B41.664 vs B41v4.2
V1 V2
V3
V4
V5
FP
HR1
HR2
%Deuteration
B41.664
B41v4.2
Residue Number
3sec 1min 30min 20hr
Δ%Deuteration
Residue Number

Figure S2.7 B41.664, B41v4.1, and B41v4.2 butterfly plots, and differential plots, related to Figure 2.7

(A) The top panel is a butterfly plot. The mid-point of each homologous peptide found in B41.664 (top half) and B41v4.1 (bottom half) is plotted to show deuterium uptake with time (3 second time point in yellow, 1 minute time point in red, 30 minute time point in blue, and 20 hour time point in black). The bottom panel is a differential plot where the %difference in exchange between B41.664 and v4.1 is plotted. Peptides falling below the 0 dashed line are regions more protected from exchange in the v4.1 construct, and peptides falling above the dashed line are regions that became less protected from exchange in the v4.1 construct. Figure (B) is similar to Figure (A), but compares B41.664 to B41v4.2.

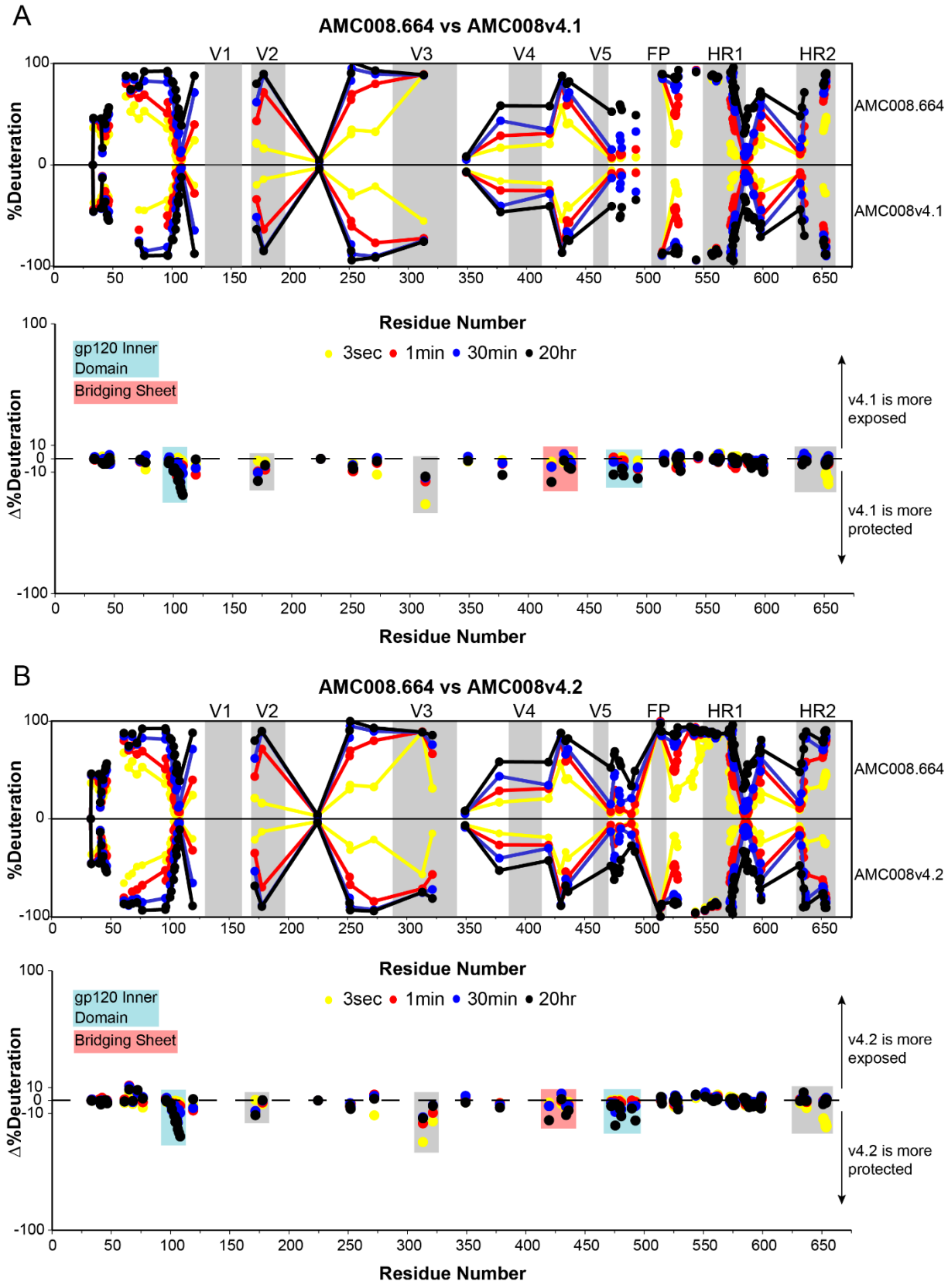
A
AMC008.664 vs AMC008v4.1
V1
V2
V3
V4
V5
FP
HR1
HR2
%Deuteration
AMC008.664
AMC008v4.1
Residue Number
gp120 Inner Domain
Bridging Sheet
3sec 1min 30min 20hr
Δ%Deuteration
v4.1 is more exposed
v4.1 is more protected
Residue Number
B
AMC008.664 vs AMC008v4.2
V1
V2
V3
V4
V5
FP
HR1
HR2
%Deuteration
AMC008.664
AMC008v4.2
Residue Number
gp120 Inner Domain
Bridging Sheet
3sec 1min 30min 20hr
Δ%Deuteration
v4.2 is more exposed
v4.2 is more protected
Residue Number

Figure S2.8 AMC008.664, AMC008v4.1, and AMC008v4.2 butterfly plots, differential plots, and deuterium uptake plots, related to Figure 2.7.

(A) The top panel is a butterfly plot. The mid-point of each homologous peptide found in AMC008.664 (top half) and AMC008v4.1 (bottom half) is plotted to show deuterium uptake with time (3 second time point in yellow, 1 minute time point in red, 30 minute time point in blue, and 20 hour time point in black). The bottom panel is a differential plot where the %difference in exchange between AMC008.664 and v4.1 is plotted. Peptides falling below the 0 dashed line are regions more protected from exchange in the v4.1 construct, and peptides falling above the dashed line are regions that became less protected from exchange in the v4.1 construct. Figure (B) is similar to Figure (A), but compares ACM008.664 to AMC008v4.2.

Dataset	**BG505.664**	**BG505v4.2**	
HDX reaction details	85% D2O buffer, pH* 7.457, labeled at RT (23.4°C), Quenched at pH 2.51 in 200mM TCEP, 8M urea, 0.2%FA	85% D2O buffer, pH* 7.457, labeled at RT (23.4°C), Quenched at pH 2.51 in 200mM TCEP, 8M urea, 0.2%FA	
HDX time course	3 sec, 1 min, 30 min, 20 hrs	3 sec, 1 min, 30 min, 20 hrs	
HDX controls	PPPI, PPPF	PPPI, PPPF	
Back-exchange	10.2 +/- 7.4%	11.5 +/- 11.4%	
Number of peptides	154	154	
Sequence coverage	58.70%	58.70%	
Average peptide length/redundancy	12.1 residue length/ 2.8 redundancy	12.1 residue length/2.8 redundancy	
Replicates (biological or technical)	two technical replicates, 3 biological replicates	two technical replicates	
Repeatability	stddev of 1.1% across technical replicates	stddev of 1.5% across technical replicates	
Dataset	**AMC008.664**	**AMC008v4.1**	**AMC008v4.2**
HDX reaction details	85% D2O buffer, pH* 7.457, labeled at RT (23.4°C), Quenched at pH 2.51 in 200mM TCEP, 8M urea, 0.2%FA	85% D2O buffer, pH* 7.457, labeled at RT (23.4°C), Quenched at pH 2.51 in 200mM TCEP, 8M urea, 0.2%FA	85% D2O buffer, pH* 7.457, labeled at RT (23.4°C), Quenched at pH 2.51 in 200mM TCEP, 8M urea, 0.2%FA
HDX time course	3 sec, 1 min, 30 min, 20 hrs	3 sec, 1 min, 30 min, 20 hrs	3 sec, 1 min, 30 min, 20 hrs
HDX controls	BG505.664, PPPI, PPPF	BG505.664, PPPI, PPPF	BG505.664, PPPI, PPPF
Back-exchange	12.8 +/- 8.0%	12.1 +/- 7.9%	12.3 +/- 7.3%
Number of peptides	135	135	135

Sequence coverage	61.10%	61.10%	61.10%
Average peptide length/redundancy	13.0 residues/2.6 redundancy	13.0 residues/2.6 redundancy	13.0 residues/2.6 redundancy
Replicates (biological or technical)	two technical replicates	two technical replicates	two technical replicates
Repeatability	stddev of 0.90% across technical replicates	stddev of 1.1% across technical replicates	stddev of 0.96% across technical replicates
Dataset	**B41.664**	**B41v4.1**	**B41v4.2**
HDX reaction details	85% D2O buffer, pH* 7.457, labeled at RT (23.4°C), Quenched at pH 2.51 in 200mM TCEP, 8M urea, 0.2%FA	85% D2O buffer, pH* 7.457, labeled at RT (23.4°C), Quenched at pH 2.51 in 200mM TCEP, 8M urea, 0.2%FA	85% D2O buffer, pH* 7.457, labeled at RT (23.4°C), Quenched at pH 2.51 in 200mM TCEP, 8M urea, 0.2%FA
HDX time course	3 sec, 1 min, 30 min, 20 hrs	3 sec, 1 min, 30 min, 20 hrs	3 sec, 1 min, 30 min, 20 hrs
HDX controls	BG505.664, PPPI, PPPF	BG505.664, PPPI, PPPF	BG505.664, PPPI, PPPF
Back-exchange	11.5 +/- 13.1%	13.2 +/- 13.4%	10.5 +/- 6.8%
Number of peptides	89	89	89
Sequence coverage	60.60%	60.60%	60.60%
Average peptide length/redundancy	12.0 residues/1.7 redundancy	12.0 residues/1.7 redundancy	12.0 residues/1.7 redundancy
Replicates (biological or technical)	two technical replicates	two technical replicates	two technical replicates
Repeatability	stddev of 1.8% across technical replicates	stddev of 1.7% across technical replicates	stddev of 0.93% across two technical replicates
Dataset	**JRFL.664**	**CE1176.664**	
HDX reaction details	85% D2O buffer, pH* 7.514, labeled at RT (22.1°C), Quenched at pH 2.509 in 200mM TCEP, 8M urea, 0.2%FA	85% D2O buffer, pH* 7.514, labeled at RT (23.3°C), Quenched at pH 2.511 in 200mM TCEP, 8M urea, 0.2%FA	
HDX time course	3 sec, 1 min, 30 min, 20 hrs	3 sec, 1 min, 30 min, 20 hrs	
HDX controls	BG505.664, PPPI, PPPF	BG505.664, PPPI, PPPF	
Back-exchange	8.4 +/- 7.9%	8.2 +/- 7.3%	
Number of peptides	98	80	
Sequence coverage	60.40%	61.00%	
Average peptide length/redundancy	13.0 residues/2.0 redundancy	13.7 residues/1.3 redundancy	
Replicates (biological or technical)	two technical replicates	three technical replicates	
Repeatability	stddev of 1.6%	stddev of 0.87%	

Table S2.1, related to Figure 2.2.

HDX reaction details and coverage information across each SOSIP construct.

			Open/Closed Conformation specific				CD4 bs	V3 N332	V3 tip specific			V2i		gp120-41
Tier	Clade	SOSIP	PGT145 K_D	PG16 K_D	b12 K_D	17b K_D	VRC01 K_D	PGT121 K_D	447-52D K_D	3074 K_D	3869 K_D	830A K_D	2158 K_D	35022 K_D
1B	B	AMC008.664	735.4+/-246.9	ND	20.2 +/- 2.1	135.2 +/- 4.0	24.5 +/- 7.9	8.7 +/- 3.9	27.8 +/- 3.3	48.9 +/- 3.7	13.5 +/- 0.6	ND	ND	72.6 +/- 19.3
1B	B	AMC008v4.2	265.5 +/- 152.0	ND	ND	ND	6.5 +/- 3.9	2.4 +/- 1.4	ND	ND	ND	ND	ND	41.5 +/- 8.7
2	B	B41.664	23.4 +/- 0.9	419 +/- 110.3	102.5 +/- 19.0	ND	90.3 +/- 10.3	115.5 +/- 2.1	125.5 +/- 21.9	662.5 +/- 95.5	97.1 +/- 22.6	145.0 +/- 31.1	ND	160.5 +/- 16.3
2	B	B41v4.2	15.4 +/- 7.9	346.5 +/- 10.6	151.0 +/- 36.8	ND	108.9 +/- 38.4	91.5 +/- 38.9	184.2 +/- 139.8	ND	220.5 +/- 105.4	276.5 +/- 232.6	ND	119.0 +/- 19.7
2	A	BG505.664	15.6 +/- 4.6	86.8 +/- 8.5	1114.4 +/- 315.7	ND	8.1 +/- 1.7	15.8 +/- 5.4	33.0 +/- 12.4	62.8 +/- 1.6	257.5 +/- 191.7	ND	ND	78.1 +/- 28.1
2	A	BG505v4.2	13.2 +/- 5.6	67.4 +/- 21.0	120.8 +/- 20.2	ND	11.2 +/- 6.5	15.3 +/- 4.7	ND	6542 +/- 5412	1036.0 +/- 444.2	ND	ND	28.0 +/- 3.5

	K_D nM
	0-10
	11-50
	50-250
	250-500
	500-1000

Table S2.2: Isolate specific differences in binding affinities of Abs specific for different regions on Env, related to Figure 2.8. The BLI determined average binding affinities from at least two independent experiments of each of the five isolates for a panel of Abs specific different conformations or localized regions of interest. Affinities and binding rates are colored as indicated above to highlight differences in binding affinity (K_D).

	k_{on} 1/Ms
	>1.0E+05
	1.0E+04 - 1.0E+05
	1.0E+03 - 1.0E+04
	1.0E+02 - 1.0E+03
	<1.0E+02

Table S2.3: Isolate specific differences in association rates of Abs specific for different regions on Env, related to Figure 2.8. The BLI determined average association rates from at least two independent experiments of each of the five isolates for a panel of Abs specific different conformations or localized regions of interest. Binding rates are colored as indicated above to highlight differences in binding association rates (k_{on}) across strains.

			Open/Closed Conformation specific				CD4 bs	V3 N332	V3 tip specific			V2i		gp120-41
Tier	Clade	SOSIP	PGT145 k_{off} (1/s)	PGT16 k_{off} (1/s)	b12 k_{off} (1/s)	17b k_{off} (1/s)	VRC01 k_{off} (1/s)	PGT121 k_{off} (1/s)	447-52D k_{off} (1/s)	3074 k_{off} (1/s)	3869 k_{off} (1/s)	830A k_{off} (1/s)	2158 k_{off} (1/s)	35022 k_{off} (1/s)
1B	B	AMC008.664	1.63E-03	ND	5.47E-04	5.43E-04	2.89E-04	3.43E-04	1.18E-03	1.85E-03	4.86E-04	no off rate	ND	4.80E-04
1B	B	AMC008v4.2	1.44E-03	ND	ND	ND	7.36E-05	1.21E-04	ND	ND	ND	ND	ND	3.18E-04
2	B	B41.664	5.60E-04	3.62E-03	1.11E-03	ND	3.54E-04	5.57E-04	8.57E-04	2.89E-03	5.35E-04	8.27E-04	ND	1.10E-03
2	B	B41v4.2	5.57E-04	2.71E-03	1.08E-03	ND	5.92E-04	8.09E-05	1.17E-03	ND	9.05E-04	ND	ND	8.01E-04
2	A	BG505.664	1.85E-03	2.72E-03	2.17E-03	ND	1.14E-04	3.53E-04	6.35E-05	2.10E-04	2.98E-04	ND	ND	4.52E-04
2	A	BG505v4.2	1.68E-03	3.37E-03	5.67E-04	ND	1.95E-04	3.14E-04	ND	6.10E-04	3.81E-04	ND	ND	2.30E-04

	k_{off} (1/s)
	>1.0E-03
	1.0E-04 - 1.0E-03
	<1.0E-04

Table S2.4: Isolate specific differences in dissociation rates of Abs specific for different regions on Env, related to Figure 2.8. The BLI determined average dissociation rates from at least two independent experiments of each of the five isolates for a panel of Abs specific different conformations or localized regions of interest. Dissociation rates are colored as indicated above to highlight differences dissociation rates (k_{off}) across strains.

Chapter 3. A Broadly Neutralizing HIV Env Antibody Overcomes Structural and Dynamic Variation through Focused Targeting with a Minimal Epitope Footprint

3.1 Introduction

The Env glycoprotein on HIV mediates the essential processes of receptor binding and membrane fusion to initiate infection of a host cell. Env is the sole target for neutralizing antibodies and due to intense immune selection pressures, has diversified to become the most variable, rapidly evolving part of HIV, with sequences differing by more than 30% in some cases [1]. While we have long been aware of the astounding sequence variation in the HIV-1 envelope glycoprotein (Env) gene, the structural and functional implications of this diversity are only beginning to be examined and grasped. Structural variation in Env impacts its interactions with all key drivers of viral fitness and replication, and this is not captured solely by variation in sequence. These differences underlie viral phenotypic traits such as neutralization sensitivity, tropism, infectivity, and transmissibility. Recent studies have provided detailed structural information for trimeric Env ectodomains from a small set of viral isolates usually complexed with stabilizing antibodies. However, these structures represent static, platonic ideals of Env assemblies. Under native conditions, HIV Env is a dynamic fusion protein complex that can flicker between antigenically and functionally distinct conformational states, even in the absence of receptor. This propensity to undergo large-scale dynamic movements is highly isolate-specific in nature [2-5].

We recently reported the use of a powerful structural mass spectrometry approach, Hydrogen/Deuterium-exchange Mass Spectrometry (HDX-MS) to investigate differences in Env structure and organization in a small set of HIV Env native-like trimers [2, 6]. The Envs in that initial set, like most under examination in the field, had been selected for study due to their

robust expression in cell culture and ability to form native-like trimers with high yields [7, 8]. Despite those common traits, our analysis revealed that many of the regions on Env showed significant differences in structural dynamics that map to conformational epitopes that are targeted by bnAbs. We hypothesized that the intrinsic dynamic traits of local epitope dynamics and large-scale conformational switching are key determinants of neutralization phenotypes, impacting the ability of antibodies to bind [9].

Remarkably broadly neutralizing antibodies (bnAbs) capable of neutralizing over 90% of circulating HIV isolates have been identified in 15-20% of infected individuals [10]. Structures of bnAb Fabs bound often to native-like Env trimers derived from the well-studied clade A BG505 isolate [11] have demonstrated the 3-dimensional organization of bnAbs and the trimer antigen locked into its “closed” prefusion configuration. It is also necessary to understand how such bnAbs are able to cope with a target as varied and divergent as Env by examining their engagement with diverse Envs that may not be well-represented by the rather unique BG505 isolate. To assess antigenic variation across isolates representative of global HIV-1 diversity, we now have examined native-like Env trimers based upon isolates identified in the global panel of Tier 2 neuralization resistant isolates [1, 12] with additional trimers from well-characterized reference isolates such as BG505, JR-FL, B41, and AMC008 [7]. Using HDX-MS, we document a dramatic degree of variation in local epitope dynamics across this expanded panel of diverse isolates. We use bio-layer interferometry to measure antibody binding kinetics and observe a clear, inverse correlation of association rates and local epitope dynamics. These results demonstrate that local epitope dynamics embody a cryptic determinant of Env antigenicity that is not readily evident from protein sequence or from high resolution, static structures.

To complement the dynamic characterization of unbound Env trimers, we performed HDX-MS analysis and obtained cryo-EM structures of a bnAb-Env complex for two isolates with trimers at opposing ends of the dynamics spectrum. We focused here on the extent of structural

variation in the V1/V2 trimer apex and its impact on antibody recognition for the bnAb PGT145 that targets this important epitope [13, 14]. These results underscore the exquisitely focused targeting of the epitope by this bnAb and also reveals a more complete picture of how the conserved N160 and N156 glycans are coordinated by the key residues that undergo somatic hypermutation resulting in the mature PGT145 bnAb.

3.2 Materials and Methods

3.2.1 Protein expression and purification

SOSIPs were produced and purified as previously described by Verkerke et al and briefly below. Briefly, Expi293F cells (ThermoFisher Scientific) were transiently transfected at a density of roughly 3 million cells/mL using polyethylenimine (PEI) with plasmids encoding each SOSIP isolate co-transfected with furin in pcDNA.3.1 at a ratio of three SOSIPs to one furin to ensure proteolytic cleavage between gp120 and gp41 subunits during production. After roughly six days the cell supernatants were cleared by centrifugation and filtered through a 0.2-micron vacuum filtration unit and supplemented with protease inhibitors (Roche) and sodium azide to prevent microbial growth. Glycosylated trimers were extracted using Galanthus nivalis lectin (GNL) coupled to agarose beads overnight at 4°C and washed with 20 mM Tris (pH 7.4), 1 mM EDTA, 1 mM EGTA, 0.02% azide, and 120 mM NaCl; glycoproteins were eluted with 7 to 10 column volumes of 1 M alphamethyl-mannopyrannoside dissolved in 20 mM Tris (pH 7.4), 1 mM EDTA, 1 mM EGTA, 0.02% azide, and 120 mM NaCl. GNL eluates were concentrated using Amicon ultrafiltration units (nominal molecular mass cutoff of 100 kDa) and buffer exchanged into DEAE low-salt buffer (20 mM Tris [pH 8.0], 100 mM NaCl) before anion-exchange chromatography using a DEAE column. Following 10 min of isocratic flow in 100 mM NaCl, a gradient to 1 M NaCl was initiated and fractions were collected through-out to remove protein aggregates. The DEAE flowthrough was buffer exchanged into 2 M ammonium sulfate– 0.1 M phosphate (pH

7.4) via dialysis and loaded onto a 5mL HIC HiTrap Phenyl HP column. A step-wise gradient of 2M to 0M ammonium sulfate in 0.1 M phosphate (pH 7.4) over 90 min was used to separate trimers from dimers and monomers. The early-eluting fractions (containing native-like trimers) were concentrated, and if enough protein was available loaded onto a Superdex S200PG size exclusion chromatography (SEC) column in PBS (20mM sodium phosphate [pH 7.4], 150 mM sodium chloride, 0.02% sodium azide). Peak fractions were concentrated and characterized by DLS, SDS, BN-PAGE, and negative stain EM (Figure S3.4) to ensure homogenous, pure trimer populations immediately prior to HDX and BLI experiments.

PGT145 IgG was produced by transient co-transfection of plasmids containing heavy and light chain fragments at a 1:1 ratio in HEK293F cells. Cultures were allowed to grow for approximately 6 days before harvesting. Secreted IgG was isolated and purified by affinity chromatography using a Hi-Trap Protein A column and eluted using 100mM Glycine pH2.0 and neutralized by addition of 1M Tris pH8.0. Purity was assessed by SDS-PAGE

3.2.2 SDS-PAGE and BN-PAGE

SDS denaturing PAGE and blue native PAGE (BN-PAGE) analyses with precast gels (Novex) were performed to assess the oligomeric species present throughout purification and immediately prior to experiments. 10µg of protein was loaded per lane for BN-PAGE analysis and 5µg per lane was loaded for SDS-PAGE analysis.

3.2.3 Dynamic light scattering (DLS)

Dynamic light scattering (DLS) measurements were performed on a Dynapro Nanostar (Wyatt Technologies). Trimer samples were diluted to 1 mg/ml in PBS and centrifuged at 15,000xg for 20 min prior to loading of 10µl into a low-volume quartz cuvette. The mean estimated hydrodynamic radius, and polydispersity were generated from 30 acquisitions of 5 s at 20°C.

3.2.4 Hydrogen/Deuterium exchange mass spectrometry

5 µgs (42 pmol) per timepoint of each protein were incubated in deuterated buffer (20mM PBS, 85% D2O, pH*7.52) for 3s, 1min, 30min, and 20hrs at room temperature. The reaction was stopped via diluting 1:1 in ice-cold quench buffer (200 mM tris(2-chlorethyl) phosphate (TCEP), 8 M urea, 0.2% formic acid) to a final pH of 2.5 and flash frozen in liquid nitrogen followed by storage in -80°C prior to analysis. Online pepsin digestion was performed and analyzed by LC-MS-IMS utilizing a Waters Synapt G2-Si Q-TOF mass spectrometer as described previously utilizing a 15 minute gradient and a home-made HDX cold box that maintains the pepsin digestion at 4°C and the LC plumbing at 0°C [15, 16]. Pepsin digest eluates from undeuterated sample LC-MS runs were collected, dried by speed vac, incubated in deuteration buffer for 1 hour at 65°C, and quenched as described above to prepare fully deuterated controls. Pepsin digest eluates from undeuterated sample LC-MS runs were also collected, dried by speed vac, resuspended in mobile buffer for peptide identification using nano LC-MS on an Orbitrap Fusion mass spectrometer. A 2 cm trapping column and a 35 cm analytical column were freshly prepared in fused silica (100 µm ID) with 5 µM ReproSil-Pur C18 AQ beads (Dr. Maisch). 8 µL of sample was injected and run using a 60-minute linear gradient from 2% to 30% acetonitrile in 0.1% FA, followed by 10 minutes of 80% acetonitrile. An EThcD method was optimized as follows: ion source: 2.1 kV for positive mode; ion transfer tube temperature: 350 °C; resolution: MS1 = 120000, MS2 = 30000; AGC target: MS1 = 2e5, MS2 = 1e5; and injection time: MS1 = 50 ms, MS2 = 60 ms. Orbitrap Fusion data was processed using Byonic (Version 3.8, Protein Metrics Inc.) to obtain a peptide reference list and identify peptic glycopeptides and glycosylation sites. Deuterium uptake analysis was performed with HD-Examiner (Version 2.5, Sierra Analytics) followed by HX-Express v2 for binomial fitting [17, 18]. The percent exchange was normalized to the fully deuterated samples. The well characterized BG505 SOSIP was exchanged alongside each new construct as a positive control sample and Internal exchange

standards (Pro-Pro-Pro-Ile [PPPI] and Pro-Pro-Pro-Phe [PPPF]) were included in each reaction to control for variations in ambient temperature during the labeling reactions. HDX reaction details, sequence coverage, and repeatability are shown in figure S3.5 and table S3.5.

3.2.5 Biolayer interferometry

The binding kinetics of the SOSIP constructs against a panel of IgG's were determined via BLI on an Octet Red system (FortèBio). Anti-human IgG Fc capture biosensors were presoaked in binding buffer (phosphate-buffered saline (PBS pH 7.4) supplemented with 0.1% BSA, 0.005% Tween 20, and 0.02% NaN3) for 10 minutes. The hydrated tips were then loaded with purified IgG prepared at 8µg/mL in binding buffer for 80 seconds. After reaching a stable baseline, antibody-immobilized biosensors were moved into wells containing a 2-fold dilution series of SOSIP trimer to monitor association for 3 mins, then biosensors were moved back into wells containing binding buffer to monitor dissociation for 3 mins. Responses were calculated and double referenced against the buffer reference signal and non-specific binding of analyte to biosensor in absence of IgG. Kinetic data were analyzed by using FortéBio Data Analysis 11.0 software and were smoothed by Savitzky-Golay filtering prior to fitting using a 1:1 binding model. Reported values are averages of data repeated in at least two independent experiments.

3.2.6 Glycan profiling

To identify the presence of glycans at each glycosite in the V2 loop and assess the relative heterogeneity of glycoforms bottom-up mass spectrometry (MS) was utilized. SOSIPs (0.02mgs) were denatured in a solution containing 25 mM Tris (pH 8.0), 7 M guanidinium chloride (GdnHCl) and 50 mM dithiothreitol (DTT) at 90°C for 30 min. Reduced cysteines were alkylated by adding fresh iodoacetamide (IAA) to 100 mM and incubating at room temperature for 1 h in the dark. 50 mM excess DTT was then added to quench the remaining IAA. The GndHCl concentration was reduced to 0.6 M by diluting the samples 11-fold with a 10 mM Tris

(pH 8.0), 2 mM calcium chloride solution. Samples were then digested using trypsin, and chymotrypsin separately at a ratio of 1:30 (w/w) for 4 h at 37°C, or a combination of Lys-C and Glu-C at a ratio of 1:30 (w/w). Each SOSIP was digested first by Lys-C for 4 h at 37°C followed by an overnight digestion of Glu-C 37°C. All proteases were MS grade (Promega) and the digestion reactions were quenched by the addition of 0.02% formic acid. The digested samples were desalted by Sep-Pak C18 cartridges (Waters) following the manufacturer's suggested protocol. Glycoform determination was performed via nano LC-MS using an Orbitrap Fusion mass spectrometer (Thermo Fisher) as described above in the HDX-MS method section using EThcD and the processing software Byonic (Version 3.8, Protein Metrics Inc.) using a 6 ppm precursor and 10 ppm fragment mass tolerance. Glycopeptides were searched using the N-glycan 309 mammalian database in Protein Metrics PMI-Suite and scored based on the assignment of correct c- and z- fragment ions. The true-positive entities were further validated by the presence of glycan oxonium ions m/z at 204 (HexNAc ions) and 366 (HexNAcHex ions). Glycoforms were categorized as either high mannose: HexNAc(2)Hex(9-5); Hybrid: HexNAc(3)Hex(5-6); or complex (Table S3.2).

3.3 Results

3.3.1 Env trimers across the global panel of neutralization resistant isolates exhibit significant dynamic variation in the V1/V2 apex

The apex of the HIV Env trimer is composed of V1 and V2 loops layered on top of the V3 loop (Fig 3.1A). While certain elements of these so-called "hypervariable loops", notably at turns in the loops that project from the trimer exhibit high sequence variability, the core structural elements are relatively conserved as they serve important roles in mediating contacts

between protomers and packing interactions with the rest of the trimer that are necessary to maintain the prefusion conformation.

We used HDX-MS to probe the local structural dynamics of the V1/V2 apex across a panel of highly diverse Env and examined whether this localized region exhibits differences in structural ordering and stability that can impact antibody recognition. These native-like trimers were purified and characterized using a range of biophysical techniques to high sample homogeneity (see Methods, Figure S3.4) across a global panel of HIV isolates that best represents the global diversity of HIV across all genetic subtypes and major circulating recombinant forms, and spans a broad range of neutralization sensitivities to pooled polyclonal antibodies [1, 12]. We observed dramatic differences in dynamics across many homologous peptides, particularly in regions important for bnAb and receptor binding (see Ch.4), but here we primarily focus on the highly dynamic V2 loop that is the target of some of the most potent bnAbs (overall details on HDX coverage and reproducibility are highlighted in S3.5 and table S3.5).

One of the conserved, V2 loop homologous peptides that is identifiable in the mass spectra across isolates contains residues 176-179 (peptide FYR/KL; Figure 3.1A, B). This peptide exhibits similar profiles of deuterium exchange protection after 3 s in deuterated buffer across the panel of native-like Env trimers, which suggests this motif exists in a similar ground state conformation in these trimers. After 20 h in deuterated buffer most isolates reach a similarly exchanged endpoint. CNE8, however, stands out as an outlier after 20 h where it is still considerably more protected than the other isolates, suggesting this region less frequently samples an exchange accessible conformation, while in the other Envs over time the peptide segment frequently samples a more exposed configuration.

Another key region in V2 is the peptide segment containing residues 166-175 (peptide RDKKQKVYSL; Figure 3.1A, B). Residues in this region are part of V2 loop C strand and part of the epitope for both PGT145 and the VRC26 lineage antibodies [19]. In this region we find fewer isolates with peptides that can be directly compared bearing the same number of residues, however, we clearly observe that CNE8 and BG505 possess C beta strands with reduced kinetics of deuterium uptake compared to TRO11 and BJOX2000, suggesting greater loop ordering in these viral isolates.

3.3.2 The Impact of V2 epitope dynamics on bnAb recognition and binding kinetics

Given the large differences in dynamics we observed in the V2 loops across diverse isolates, we next sought to determine whether local epitope dynamics influence antibody binding. From structures of antibody Fabs bound to the well-characterized clade A BG505 SOSIP trimer, it has been recognized that the epitope for bnAbs such as PGT145, PG9/16, and others bind to a quaternary epitope involving a basic residue charge “sink” as well as the conserved N160 glycans from more than one gp120 subunit [20, 21]. Likewise the glycan at N156 has been implicated in playing an important role in binding of many of these apex antibodies, but in structures this glycan chain is frequently not resolved, thus it has been inferred to play an indirect role in positioning and stabilizing adjacent features that themselves are directly recognized by the antibodies [22].

Our observation of the highly variable V2 loop ordering in the Env apex and the conformational nature of the epitope targeted by apex antibodies led us to hypothesize that V2 epitope dynamics would impact an antibody’s ability to bind and form a stable complex. Indeed, both homologous V2 loop peptides described above either contain residues that are direct binding contacts to the conformation specific antibody PGT145 (peptide 166-175) or are adjacent to the epitope (peptide 176-179 Figure 3.1A). PGT145 IgG binding kinetics were

measured using BLI (Figure 3.1C, Figure S3.1, Table S3.1). For PGT145 the large differences in binding affinities were mainly driven by large differences in association rates. We observed an inverse correlation between binding association rates and V2 loop dynamics at the epitope using the sum of the exchange of peptides spanning residues 166-179 (Figures 3.1D, E). The general trend was that isolates with a more ordered, exchange-protected epitope, such as BG505, CNE8, CNE55 exhibited faster PGT145 IgG association rates in comparison to isolates with more flexible, dynamic epitopes, such as in TRO11, CH119 and CE1176. Outlier isolates B41 and JRFL both contain differences in sequence at residues that directly contact PGT145 or have been shown to abrogate neutralization potency (168E and 169I respectively, Figure 3.2) [23]. We note that there was no apparent trend between epitope dynamics and dissociation rates. Indeed, the PGT145 dissociation rates were fairly similar across all trimer constructs (Figure 3.1C, Figure S3.1, Table S3.1).

In contrast to the observed correlation between local V2 dynamics and antibody binding, no clear correlation was identifiable between binding kinetics and V2 loop length or net charge, but they are properties that can in some circumstances correlate with apex bnAb neutralization sensitivities, and should be considered (Figure 3.2) [24]. Similarly, glycan occupancy at N156 and N160 can influence PGT145-mediated neutralization [22]. In our panel of Env trimers, all were occupied with predominantly high mannose glycoforms at N156 and N160; in CH119, we were unable to determine the glycoprofile for position N156 due noisy MS/MS spectra. In B41, only nonglycosylated and a complex glycoform was detected at N156 (Figure 3.2B, Table S3.2). Coverage in this region in JRFL was lacking, however, we note that other labs have glycoprofiled different JRFL constructs that displayed predominantly high mannose sugars at N156 and complex or high mannose at N160 depending on the construct and purification method used to isolate the JRFL trimers [25]. Thus differences in the predominate glycoforms

and glycosite occupancies at these key apex positions does not seem to explain the differences in PGT145 antibody binding trends.

3.3.3 The bnAb PGT145 binding footprint is highly focused across diverse trimers, despite differences in epitope flexibility

We sought to analyze how the antibody engages with divergent Env trimers such as those with highly dynamic apexes and those that are more conformationally constrained. We thus applied HDX-MS and single particle cryo-EM analysis to examine the bnAb Fab engaging with a highly dynamic Env trimer, isolate BJOX2000, and a highly ordered trimer, isolate CNE55. These experiments provide insight into recognition of conserved epitope motifs in the midst of highly variable contexts, a key aspect underlying an antibody's ability to exhibit broad cross-reactivity and neutralization.

By quantitatively comparing the deuterium-exchange profiles across the CNE55 and BJOX2000 Env sequences in bound and unbound states, we could identify sites that changed in response to PGT145 binding. The differential HDX-MS results clearly demonstrate that the PGT145 binding footprint is highly localized to the V2 loop (Figure 3.3). In agreement with BG505 and AMC011 PGT145 bound structures, the peptides with the largest increase in backbone amide protection contained R166 and K169 (Figure 3.3C, D).

Previously we had observed HDX bimodal spectra indicative of conformational sampling throughout localized regions in the Env trimer apex and base in an isolate dependent context [2]. As a result, here we hypothesized that PGT145 binding may shift the conformational equilibrium of Env towards a closed conformational state and eliminate bimodal spectra that may be present in the unbound trimer.

Two regions in the unbound BJOX2000 trimers in particular, the CD4 binding loop in gp120 and HR1 in gp41, exhibit isotopic distributions that are unusually broad, which is indicative of conformational sampling between two or more states with different degrees of backbone amide protection [26, 27] (Figure S3.2). CNE55, on the other hand, appears more conformationally rigid and exhibited only unimodal spectra. The width of each peptide's mass envelopes were measured in both the unbound and bound BJOX2000 states [17, 18]. Surprisingly, PGT145 binding did not alter the profile of bimodal spectra throughout the BJOX2000 trimer structure (figure S3.2), suggesting there was minimal long-range allosteric effects on stabilizing the trimer. In both the highly dynamic BJOX2000 trimer as well as the ordered, conformationally inert CNE55 trimer, PGT145's impact was strictly local and confined to the immediate peptide segment in V2 highlighted in the differential HDX-MS plots (Figure 3.3).

3.3.4 Single-particle cryo-EM structures of PGT145 with divergent Env trimers reveal antibody engagement of all N160 glycans across all three protomers

To further ascertain the nature of PGT145 recognition of diverse antigens, we obtained single particle cryo-EM structures of the same complexes used in the HDX-MS epitope footprinting analysis: BJOX2000+PGT145 Fab and CNE55+PGT145 Fab. The cryo-EM structures, without any symmetry imposed, were calculated to a global resolution of 4.9 Å for the BJOX2000+PGT145 Fab complex and 5.14 Å for the CNE55+PGT145 complex according to the 0.143 FSC gold standard criterion (Figure S3.3). The atomic model of BG505 Env in complex with PGT145 (PDB: 5V8L) was used for initial rigid body fitting into the cryo-EM maps and real space refinement was carried out to optimize map occupancy. The atomic model of BG505+PGT145 Fab exhibited a good global fit to the cryoEM maps of both BJOX2000 and

CNE55 complexes. PGT145 Fab nestles into the apex ~4Å lower in the structure of the BJOX2000 complex when compared to the BG505 complex, however the contacts between Env and the Fab, especially for the Env contacting HCDR3 loop of PGT145, are the same.

Clear density was observed for the N160 glycan in both the BJOX2000 and CNE55 complex maps, with glycan densities in the BJOX+PGT145 Fab complex being more defined due to better local resolution at the Env-Fab interface (Figure 3.4). Notably, in both of the maps, N160 glycan density from each gp120 subunit within an Env trimer can be seen interacting with the Fab. This differs from the BG505+PGT145 structure where only two of the three N160 glycans were reported to be making strong contacts with the Fab [20]. In our structures, the density corresponding to N160 glycan in chain A interacts with the tip of the Fab's HCDR2 region (residues G53, D54, K55). In chain C, the N160 glycan density shows interaction with the tip of LCDR1 loop of the Fab with potential interactions with tip of LCDR3. In chain D, the N160 glycan density is expansive and interacts with HCDR1 near N31 residue and HCDR3 near K97-R99. The sites of interaction between the Fab and Env regions are similar between BJOX2000 and CNE55 confirming that the Fab binds its target epitope on Env in a conserved manner that is considerably more dependent on glycan contacts from all three subunits than had been previously appreciated.

The C chain N160 glycan forms contacts both with CDRH3 as well as CDRH2. In our structures N160 from the third subunit chain A, likewise, contacts CDRH2. We also resolve contacts with framework region 3 that undergo somatic hypermutation. The PGT145 paratope thus appears to include residues outside the long CDR3 loop and include regions in the CDR1 and CDR2 loops. Previously somatic hypermutations (comparing the inferred germline gene sequence and mature PGT145 sequence) in the CDR1 and 2 regions had been thought to primarily act to stabilize the CDR3 loop, but not directly contact the trimer surface [20, 23].

3.4 Discussion

V2 apex targeting antibodies, including PGT145 and VRC26.25, are some of the most potent bnAbs against HIV [19]. Remarkably, they achieve this while targeting an epitope that is highly structurally variable. PGT145 has a long CDR3 loop that reaches past the dense glycan shield at the trimer apex to interact with a positively charged cationic sink formed by all three Env protomers. This charged feature is composed of R166 residues from the three converging V2 loops [23, 28]. Additionally, mutational scanning has been used to demonstrate the requirement of having positive charges at residues 168 and 169 for effective PGT145 binding [23]. PGT145's CDR3 loop includes two sulfated tyrosines that engage in electrostatic interactions with K169 and K121 [19, 20].

In order to understand the structural and physical basis for how bnAbs recognize diverse antigenic targets and recognize conserved features in the midst of variation, it is necessary to examine a given antibody with multiple targets. Here, cryo-EM and HDX-MS revealed a common mode of interaction and set of contacts with two highly divergent— both in overall sequence and dynamic behavior— Env trimers. BJOX2000 tends to be more flexible across much of the trimer structure, and exhibits local regions with bimodal spectra indicative of transitions between conformations with differences in backbone amide protection. As the cryoEM structures demonstrate, for both the relatively static CNE55 trimer as well as the more dynamic BJOX2000 trimer, PGT145 was able to engage N160 across all three protomers, as well as to insert its CDRH3 deep into the apex to reach the basic residue sink. There, in BJOX2000, the loop nestled several Å deeper into the apex, likely reflecting the more labile, dynamic apex found in this case. Remarkably even after binding this dynamic target, PGT145 had negligible dynamic impact on, even nearby sites that maintained their high level of conformational dynamics. In recent work examining other highly dynamic Env trimers, we identified isolate specific regions throughout Env that sample conformational states on

drastically different time scales. Those data indicated that there were various structural elements throughout the trimer that were not tightly coupled [2]. This may likewise explain why PGT145-induced stabilization of the V1V2 apex was not observed to propagate throughout the rest of the trimer. In CNE55, a far more ordered trimer, where one might anticipate the assembly behaves in a unitary cooperative fashion, the antibody binding likewise had only a local, targeted effect. These findings underscore the exquisitely focused nature of apex antibodies such as PGT145.

Even though PGT145 binding did not appear to make regions outside the V2 loop more conformationally rigid, we hypothesized that isolate specific differences in V2 loop dynamics could influence PGT145 IgG binding. Indeed, across native-like Env trimers derived from diverse isolates of HIV some of the largest differences in dynamics we measured using HDX-MS map to the V2 loop. This region in the apex exhibits significant conformational diversity, which has been captured in static high-resolution structures (Figure S3.4). These V1V2 structures, observed when presented as the excised V1/V2 loop displayed on a scaffold protein and bound by different Fabs, range from four-stranded beta barrel conformations to more disorded loop, helical conformations [13, 29-32]. The increased PGT145 binding rate we observed in isolates with a more ordered apex suggests that dynamic motions in the V2 loop may be disrupting the 3D conformational epitope this antibody recognizes; there likely also is an entropic cost when binding to a highly flexible epitope [33, 34]. We did not observe a correlation between dynamics and the PGT145 IgG dissociation rates. Indeed, the dissociation rates of the PGT145-SOSIP complexes were similar across most of the isolates we evaluated (Figure S3.1, Table S3.1, Figure 3.1C). In neutralization assays, PGT145 exhibits notable breadth and potency across a wide range of primary HIV isolates; 64% neutralization breadth and 0.042ug/mL median IC_{50} across a 77 pseudovirus panel [35]. It thus clearly has evolved to overcome substantial variability in epitope contexts.

How is a bnAb able to bind tightly while having such a minimal footprint on the underlying protein substrate? The interactions with conserved glycans, all three from N160 and one from N156 are essential for PGT145 binding. The majority of the contact surface between PGT145 and Env involves the conserved N160 glycans. Our new cryo-EM structures reveal that glycans from all three gp120 subunits are engaged by PGT145. This includes chain A, which we find interacts with CDRH2, including forming contacts with residues that undergo somatic hypermutation to produce mature PGT145 [20, 23]. Loss of a glycan at N156 has been shown to reduce the neutralization potency of PGT145 as well, suggesting a role in the epitope. Cryo-EM and glycan modeling have suggested that the N156 and N160 glycans interact to help stabilize the Env trimer [36]. In our PGT45-bound structures, apparent density connecting N156 on chain A and PGT145 Fab is seen and appears to contact with CDRH1 where again, sites of somatic hypermutation have been identified, but to date had not been associated with antibody contacts [23]. In total these new structures provide a considerably more complete portrait of the antibody's epitope and help to explain the changes that emerged in PGT145 during affinity maturation that provide its neutralization breadth and potency.

We speculate that by incorporating glycans into the cognate epitope, bnAbs against HIV-1 Env avoid being as reliant on interactions with protein residues, which can vary in accessibility, and mutate significantly. While some degree of glycoform heterogeneity is not uncommon, the core portions of most N-linked glycans are largely maintained, and it is these that tend to be recognized by bnAbs [37]. Additionally, inherently more flexible and dynamic in nature than ordered, globular proteins, glycans may offer some degree of "give" that dampens underlying protein motions and dynamics.

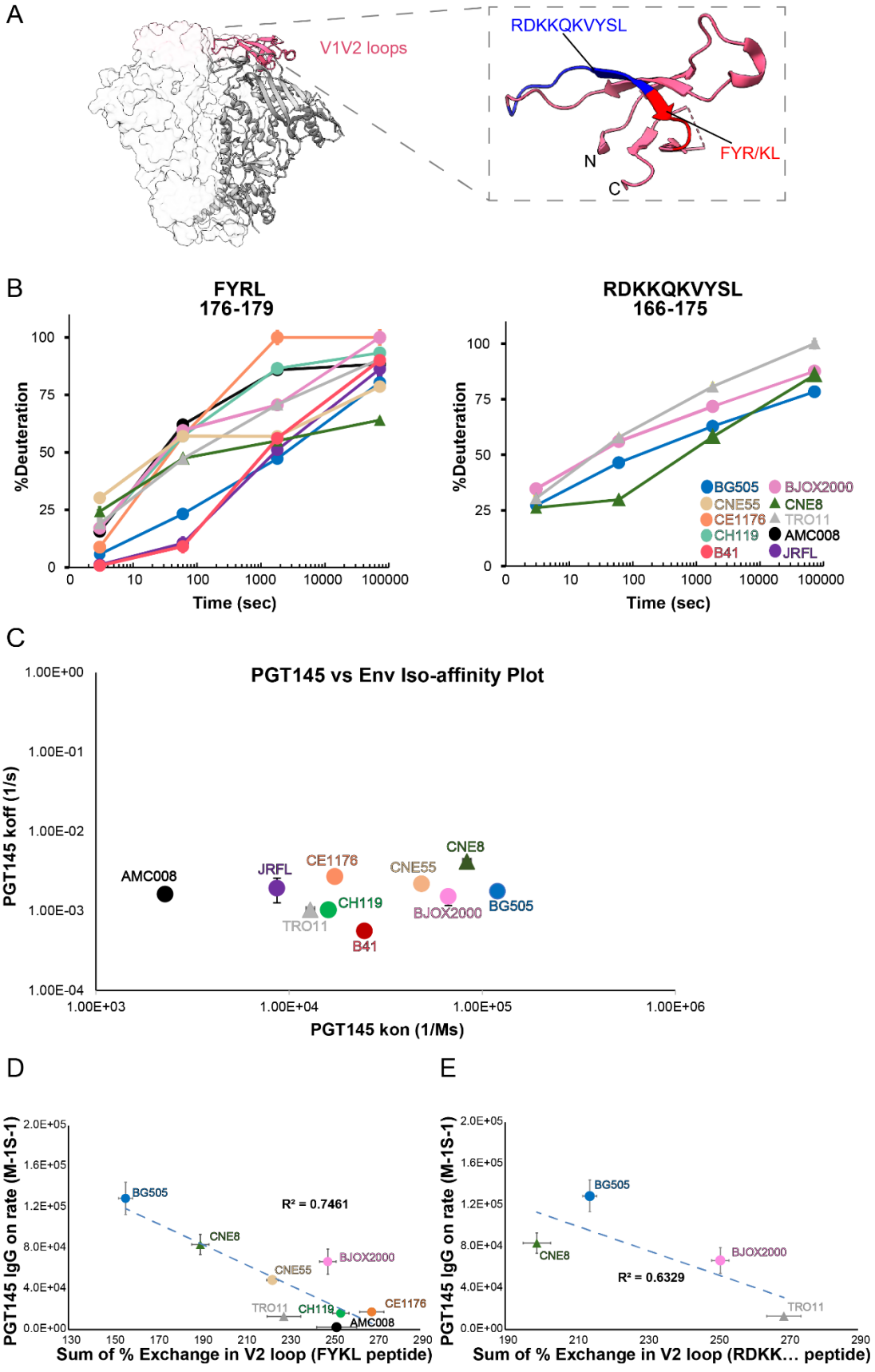
A
V1V2 loops
RDKKQKVYSL
FYR/KL
N
C
B
FYRL
176-179
%Deuteration
Time (sec)
RDKKQKVYSL
166-175
BG505
BJOX2000
CNE55
CNE8
CE1176
TRO11
CH119
AMC008
B41
JRFL
C
PGT145 vs Env Iso-affinity Plot
PGT145 koff (1/s)
PGT145 kon (1/Ms)
D
PGT145 IgG on rate (M-1S-1)
R² = 0.7461
Sum of % Exchange in V2 loop (FYKL peptide)
E
R² = 0.6329
Sum of % Exchange in V2 loop (RDKK… peptide)

Figure 3. 1. The V1V2 apex is known to be conformationally flexible and HDX signatures across V2 loop peptides suggest differences in V2 bnAb epitope dynamics that are correlated with PGT145 IgG association rates. The V1V2 loops rest at the trimer apex in prefusion closed Env structures and they are highlighted in maroon (PDB 5V8L with 2/3 protomers displayed in surface representation and 1 protomer displayed in ribbon) (A). Two homologous V2 loop peptides with the same number of exchangeable backbone amide residues that can be found across many HIV isolates are shown and highlighted in red and blue on the zoomed in V1V2 loops (A). Deuterium uptake plots in (B) demonstrate dramatic differences in V2 loop dynamics across diverse HIV trimers (BG505 depicted as blue circles, tan circles for CNE55, orange circles for CE1176, lime circles for CH119, red circles for B41, BJOX2000 in pink circles, green triangles for CNE8, gray triangles for TRO11, black circles for AMC008, and purple circles for JRFL). Each HDX uptake plot consists of the average percent deuteration of at least two replicates after 3 seconds, 1 minute, 30 minutes, and 20 hours of exchange normalized to a fully deuterated control with standard deviation error bars. The bnAb PGT145 binds this localized region in the V2 loop and we used BLI to measure the PGT145 IgG association and dissociation rates across the diverse Env trimers (C). Average association and dissociation rates are the averages of at least two independent experiments with error bars reporting the percent standard deviation. Differences in the average PGT145 association rates and epitope flexibilities across diverse trimers are correlated in (D) and (E). The x-axis is the sum of the %exchange in the V2 loop peptide FYKL spanning residues 176-179 (E) or RDKKQKVYSL spanning residues 166-175 (D) and the y-axis is the average PGT145 association rate for each SOSIP-derived from different HIV isolates (blue circle for BG505, pink circle for BJOX2000, tan circle for CNE55, lime circle for CH119, orange circle for CE1176, black circle for AMC008, gray triangle for TRO11, and green triangle for CNE8). Error bars report the summed standard deviation across time for HDX and the standard deviation from at

least two independent BLI experiments for the association rates. Related to table S3.1 and figure S3.1.

Isolate	V2 length	Net charge	N156 glycan	N160 glycan
BG505	46	+3	H	H
CE1176	38	+2	H	H
B41	45	+3	C	H
AMC008	40	-1	H	H
JRFL	38	-2	NC	NC
CNE55	40	+2	H	H
BJOX	38	+2	H	H
TRO11	41	+2	H	H
CH119	43	+3	ND	H
CNE8	37	+1	H	H

Figure 3. 2. Other variables, besides dynamics, impact bnAb recognition of the V2 region of trimers. The PGT145 antibody target the V2 loop trimer apex hole and the positively charged C-strand of Env across diverse HIV isolates. The sequences of the V2 loops across diverse isolates of HIV are aligned in figure A. Residues that directly interact with PGT145 (residues 166 and 169) are colored red, residue 168 that has been shown to influence

neutralization sensitivity is colored blue, and glycans at N156 and N160 are highlighted in green. The table in figure B displays the V2 loop length, net charge, and predominate glycoform at N156 and N160. The structure of the V1V2 4 stranded beta-barrel (from BG505 structure PDB 4VTP) is shown in ribbon representation in figure C. Antibody binding contacts are colored as in figure A, and the base two HexNAc sugars at N156 and N160 are shown in stick representation. Related to table S3.2.

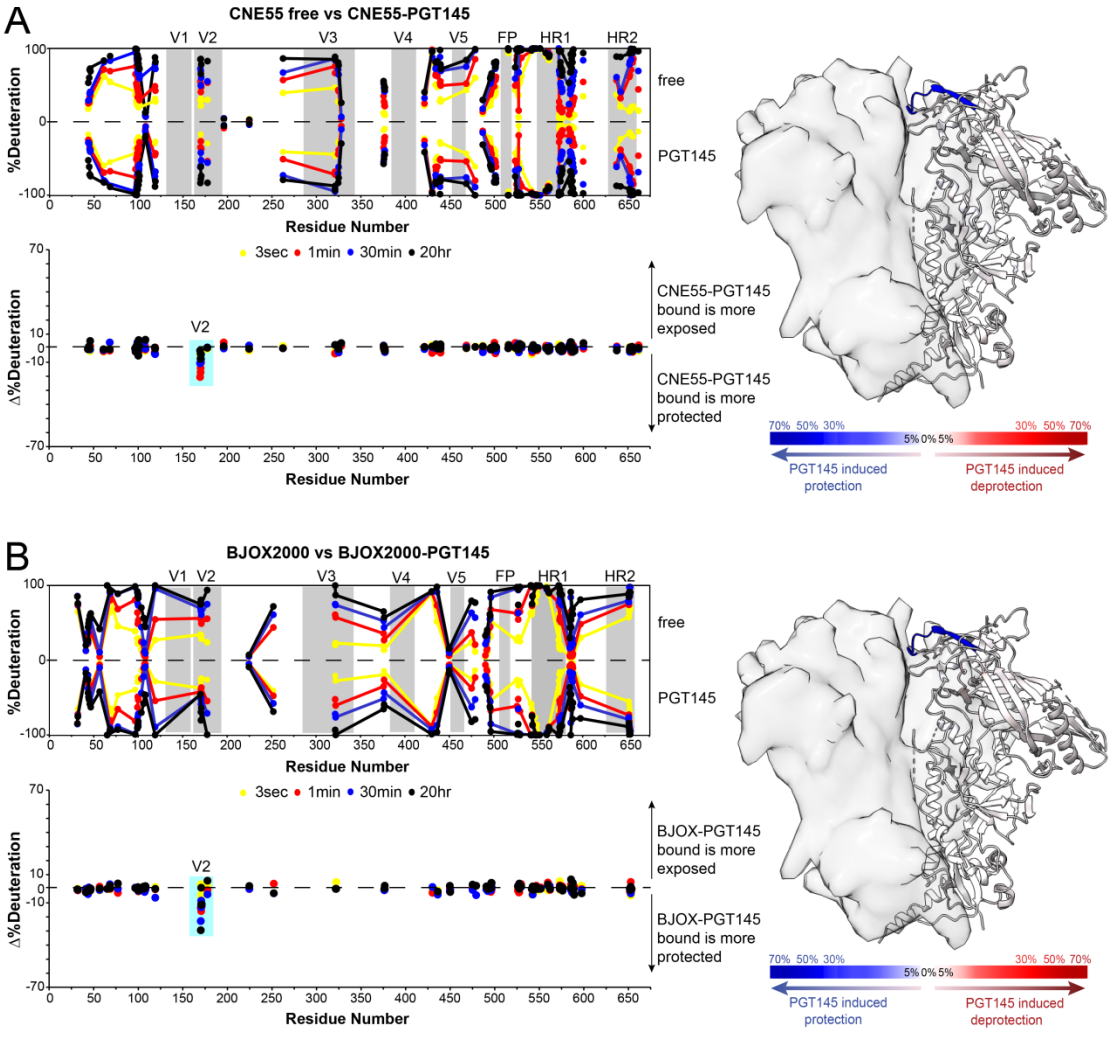
A
CNE55 free vs CNE55-PGT145
V1 V2
V3
V4
V5
FP
HR1
HR2
%Deuteration
free
PGT145
Residue Number
3sec 1min 30min 20hr
Δ%Deuteration
CNE55-PGT145 bound is more exposed
CNE55-PGT145 bound is more protected
70% 50% 30%
5% 0% 5%
30% 50% 70%
PGT145 induced protection
PGT145 induced deprotection
B
BJOX2000 vs BJOX2000-PGT145
BJOX-PGT145 bound is more exposed
BJOX-PGT145 bound is more protected

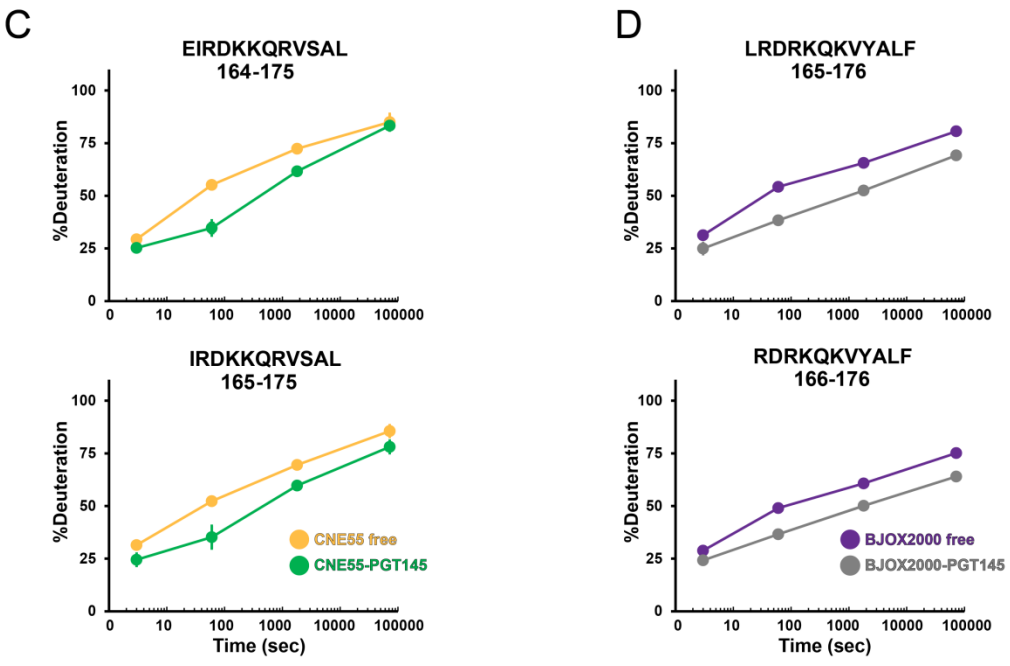
C
EIRDKKQRVSAL
164-175
IRDKKQRVSAL
165-175
%Deuteration
Time (sec)
CNE55 free
CNE55-PGT145
D
LRDRKQKVYALF
165-176
RDRKQKVYALF
166-176
BJOX2000 free
BJOX2000-PGT145

Figure 3. 3. PGT145 binding induces localized protection in the V2 loop and does not reduce localized dynamics throughout the rest of the trimer structure in two isolates

The top left figure is a butterfly plot (A). The mid-point of each homologous peptide found in CNE55.664 unbound (top half) and CNE55.664 bound to PGT145 (bottom half) is plotted to show deuterium uptake with time (3-second time point in yellow, 1-minute time point in red, 30-minute time point in blue, and 20-hour time point in black). Underneath the butterfly plot is a differential plot where the %difference in exchange between the free and PGT145 bound states is plotted. Peptides falling below the 0 dashed lines are regions more protected from exchange when PGT145 is bound, and peptides falling above the dashed line are regions that became less protected from exchange in the PGT145 bound state. To the right of the plots is a BG505 structure (PDB 5ACO) where the sum of %difference in deuterium exchange across time are mapped onto the structure. Regions that became more protected after PGT145 binding are colored blue, and regions that became less protected are colored red. Figure B is the same as figure A, except it compares the isolate BJOX2000.664 unliganded with BJOX2000.664 complexed with PGT145. The deuterium uptake plots of four peptides that are part of the PGT145 epitope in the V2 loop are shown in figure C for the isolate CNE55 (the unbound state uptake curve is colored blue, the PGT145 bound state is colored green) and in figure D for the isolate BJOX2000 (the unbound state uptake curve is colored blue, the PGT145 bound state is colored red).

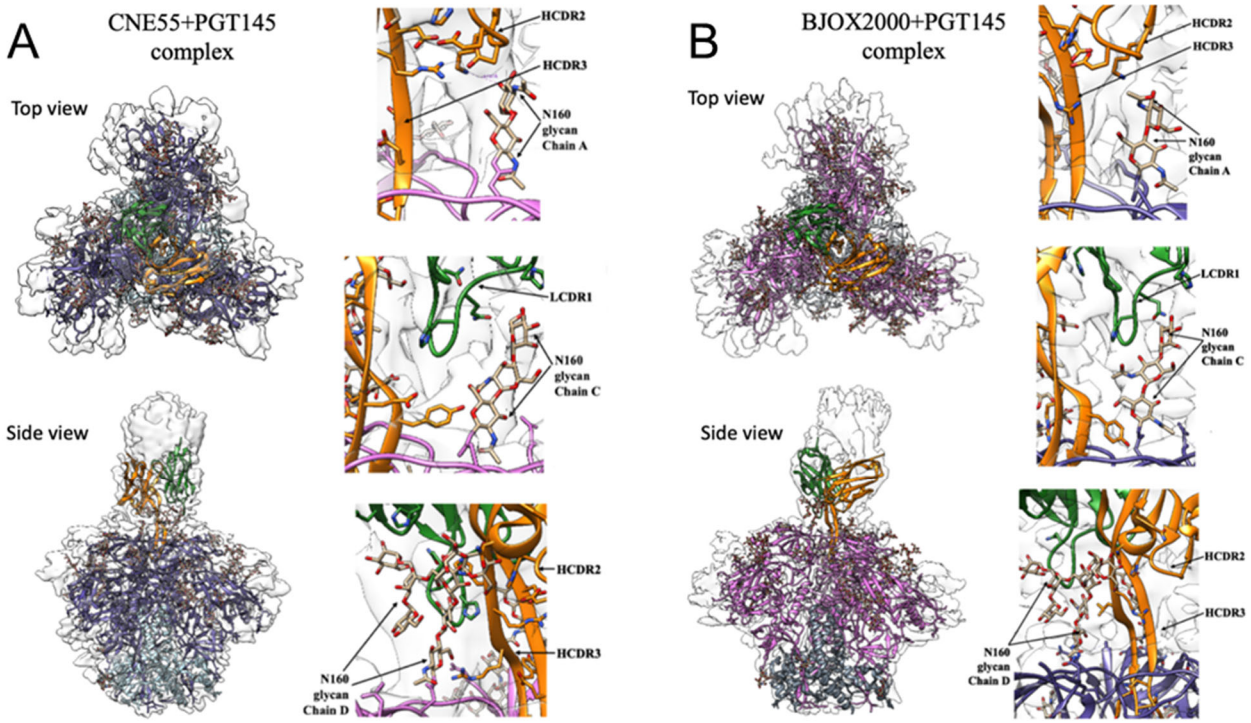

Figure 3. 4. PGT145-CNE55 and PGT145-BJOX2000 cryo-EM structures. A) Top (above) and side (below) views of the cryo-EM reconstruction and structural model of the CNE55 SOSIP trimer bound to the PGT145 Fab. The three gp120 subunits are colored in dark blue, the base gp41 fusion subunits are colored in light blue, the PGT145 variable heavy chain is colored in orange, and the PGT145 variable light chain in green. The three zoomed in panels on the right reveal densities corresponding to the N160 glycans across all three protomers, and their contacts with the HCDR2, and LCDR1.Similarly figure B is identical to figure A, however, cryo-EM reconstructions of the BJOX2000 SOSIP trimer bound to the PGT145 Fab are shown. Cryo-EM reconstructions and figures were provided by Vidya Prasad and Ananya Chatterjee.

References

1. Seaman, M.S., et al., *Tiered Categorization of a Diverse Panel of HIV-1 Env Pseudoviruses for Assessment of Neutralizing Antibodies.* Journal of Virology, 2010. **84**(3): p. 1439-1452.

2. Hodge, E.A., et al., *Structural dynamics reveal isolate-specific differences at neutralization epitopes on HIV Env.* iScience, 2022. **25**(6): p. 104449.
3. Munro, J.B., et al., *Conformational dynamics of single HIV-1 envelope trimers on the surface of native virions.* Science, 2014. **346**(6210): p. 759-763.
4. Guttman, M., et al., *CD4-Induced Activation in a Soluble HIV-1 Env Trimer.* Structure, 2014. **22**(7): p. 974-984.
5. Stadtmueller, B.M., et al., *DEER Spectroscopy Measurements Reveal Multiple Conformations of HIV-1 SOSIP Envelopes that Show Similarities with Envelopes on Native Virions.* Immunity, 2018. **49**(2): p. 235-2460000.
6. Guttman, M., et al., *Antibody potency relates to the ability to recognize the closed, pre-fusion form of HIV Env.* Nature Communications, 2015. **6**(1): p. 6144.
7. de Taeye, S.W., et al., *Immunogenicity of Stabilized HIV-1 Envelope Trimers with Reduced Exposure of Non-neutralizing Epitopes.* Cell, 2015. **163**(7): p. 1702-1715.
8. Torrents de la Pena, A. and R.W. Sanders, *Stabilizing HIV-1 envelope glycoprotein trimers to induce neutralizing antibodies.* Retrovirology, 2018. **15**(1): p. 63.
9. Montefiori, D.C., et al., *Neutralization tiers of HIV-1.* Current Opinion in HIV and AIDS, 2018. **13**(2): p. 128.
10. McGuire, A.T., et al., *HIV antibodies. Antigen modification regulates competition of broad and narrow neutralizing HIV antibodies.* Science (New York, N.Y.), 2014. **346**(6215): p. 1380-1383.
11. Sanders, R.W., et al., *A next-generation cleaved, soluble HIV-1 Env trimer, BG505 SOSIP. 664 gp140, expresses multiple epitopes for broadly neutralizing but not non-neutralizing ….* A next-generation cleaved, soluble HIV-1 Env trimer, BG505 SOSIP. 664 gp140, expresses multiple epitopes for broadly neutralizing but not non-neutralizing …, 2013.
12. deCamp, A., et al., *Global panel of HIV-1 Env reference strains for standardized assessments of vaccine-elicited neutralizing antibodies.* Journal of virology, 2014. **88**(5): p. 2489-2507.
13. Duerr, R. and M.K. Gorny, *V2-Specific Antibodies in HIV-1 Vaccine Research and Natural Infection: Controllers or Surrogate Markers.* Vaccines, 2019. **7**(3): p. 82.
14. Powell, R.L.R.L.R., et al., *Plasticity and Epitope Exposure of the HIV-1 Envelope Trimer.* Journal of virology, 2017. **91**(17).
15. Verkerke, H.P., et al., *Epitope-Independent Purification of Native-Like Envelope Trimers from Diverse HIV-1 Isolates.* Journal of Virology, 2016. **90**(20): p. 9471-9482.
16. Watson, M.J., et al., *Simple Platform for Automating Decoupled LC-MS Analysis of Hydrogen/Deuterium Exchange Samples.* J Am Soc Mass Spectrom, 2021. **32**(2): p. 597-600.
17. Guttman, M., et al., *Analysis of Overlapped and Noisy Hydrogen/Deuterium Exchange Mass Spectra.* Journal of The American Society for Mass Spectrometry, 2013. **24**(12): p. 1906-1912.
18. Weis, D.D., et al., *Identification and characterization of EX1 kinetics in H/D exchange mass spectrometry by peak width analysis.* Journal of The American Society for Mass Spectrometry, 2006. **17**(11): p. 1498-1509.
19. Gorman, J., et al., *Structure of Super-Potent Antibody CAP256-VRC26.25 in Complex with HIV-1 Envelope Reveals a Combined Mode of Trimer-Apex Recognition.* Cell Rep, 2020. **31**(1): p. 107488.
20. Lee, J.H., et al., *A broadly neutralizing antibody targets the dynamic HIV envelope trimer apex via a long, rigidified, and anionic β-hairpin structure.* A broadly neutralizing antibody targets the dynamic HIV envelope trimer apex via a long, rigidified, and anionic β-hairpin structure, 2017.

21. Amin, M.N., et al., *Synthetic glycopeptides reveal the glycan specificity of HIV-neutralizing antibodies.* Nat Chem Biol, 2013. **9**(8): p. 521-6.
22. Behrens, A.J., et al., *Composition and Antigenic Effects of Individual Glycan Sites of a Trimeric HIV-1 Envelope Glycoprotein.* Cell Rep, 2016. **14**(11): p. 2695-706.
23. Andrabi, R., et al., *Identification of Common Features in Prototype Broadly Neutralizing Antibodies to HIV Envelope V2 Apex to Facilitate Vaccine Design.* Immunity, 2015. **43**(5): p. 959-973.
24. Bricault, C.A., et al., *HIV-1 Neutralizing Antibody Signatures and Application to Epitope-Targeted Vaccine Design.* Cell Host Microbe, 2019. **25**(1): p. 59-72 e8.
25. Go, E.P., et al., *Glycosylation Benchmark Profile for HIV-1 Envelope Glycoprotein Production Based on Eleven Env Trimers.* Journal of Virology, 2017. **91**(9): p. 16.
26. Hodge, E.A., M.A. Benhaim, and K.K. Lee, *Bridging protein structure, dynamics, and function using hydrogen/deuterium-exchange mass spectrometry.* Protein Sci, 2020. **29**(4): p. 843-855.
27. Benhaim, M.A., et al., *Structural monitoring of a transient intermediate in the hemagglutinin fusion machinery on influenza virions.* Sci Adv, 2020. **6**(18): p. eaaz8822.
28. Lee, J.H., et al., *A Broadly Neutralizing Antibody Targets the Dynamic HIV Envelope Trimer Apex via a Long, Rigidified, and Anionic beta-Hairpin Structure.* Immunity, 2017. **46**(4): p. 690-702.
29. Pan, R., et al., *The V1V2 Region of HIV-1 gp120 Forms a Five-Stranded Beta Barrel.* Journal of virology, 2015. **89**(15): p. 8003-8010.
30. Zolla-Pazner, S., et al., *Vaccine-induced IgG antibodies to V1V2 regions of multiple HIV-1 subtypes correlate with decreased risk of HIV-1 infection.* PloS one, 2014. **9**(2).
31. Wibmer, C., et al., *Common helical V1V2 conformations of HIV-1 Envelope expose the α4β7 binding site on intact virions.* Nature Communications, 2018. **9**(1): p. 4489.
32. Spurrier, B., et al., *Functional Implications of the Binding Mode of a Human Conformation-Dependent V2 Monoclonal Antibody against HIV.* Journal of Virology, 2014. **88**(8): p. 4100-4112.
33. Brady, G.P. and K.A. Sharp, *Entropy in protein folding and in protein-protein interactions.* Curr Opin Struct Biol, 1997. **7**(2): p. 215-21.
34. Kwong, P.D., et al., *HIV-1 evades antibody-mediated neutralization through conformational masking of receptor-binding sites.* Nature, 2002. **420**(6916): p. 678-682.
35. Sok, D., et al., *Recombinant HIV envelope trimer selects for quaternary-dependent antibodies targeting the trimer apex.* Proceedings of the National Academy of Sciences of the United States of America, 2014. **111**(49): p. 17624-17629.
36. Antanasijevic, A., et al., *Structural and functional evaluation of de novo-designed, two-component nanoparticle carriers for HIV Env trimer immunogens.* PLOS Pathogens, 2020. **16**(8).
37. Nguyen, D.N., et al., *Oligomannose Glycopeptide Conjugates Elicit Antibodies Targeting the Glycan Core Rather than Its Extremities.* ACS Cent Sci, 2019. **5**(2): p. 237-249.

Supplemental Figures

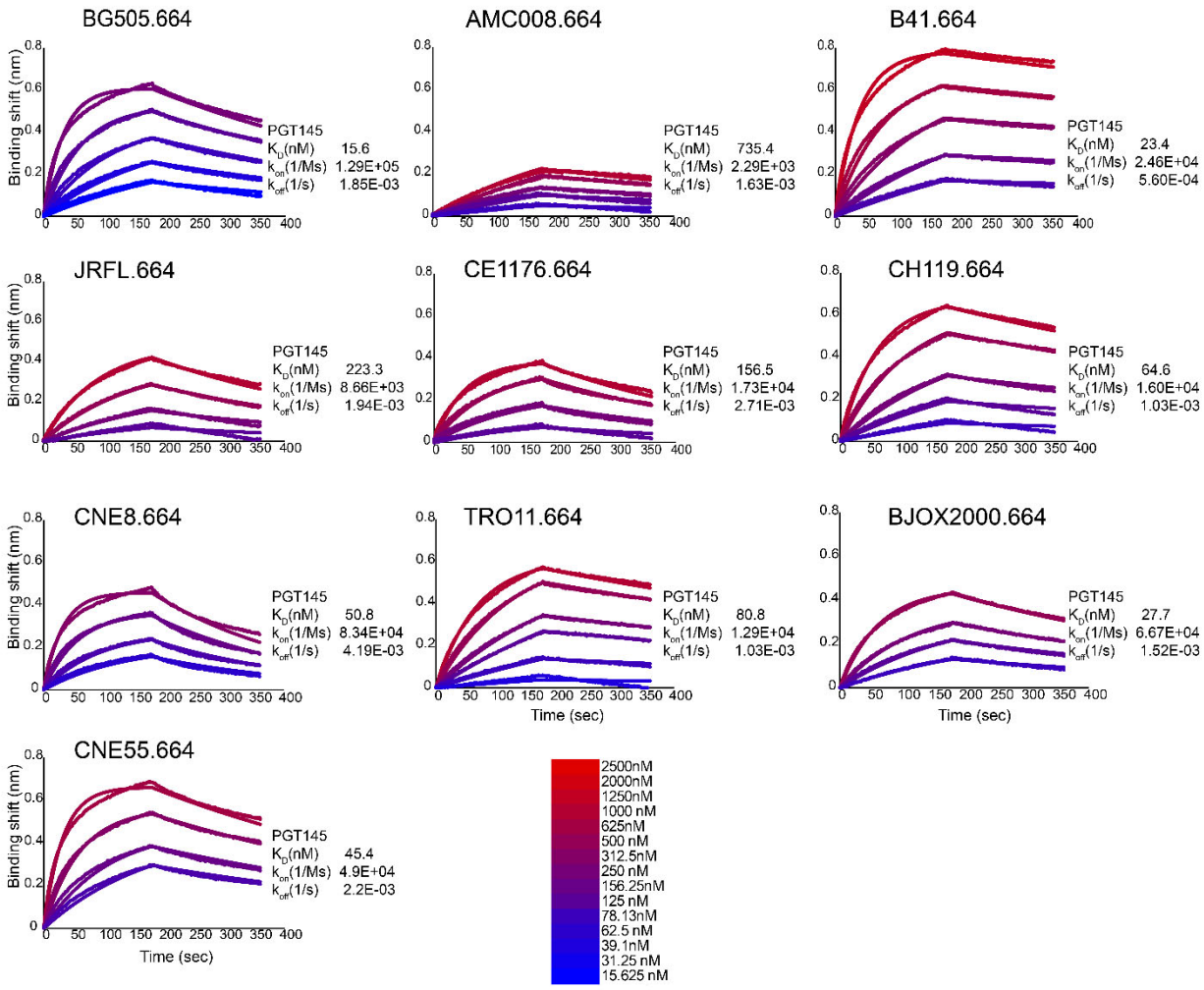

Figure S3.1. PGT145 IgG binding kinetics to Env trimers derived from different HIV isolates. Representative BLI sensorgrams of PGT145 binding to serially diluted SOSIPs derived from different HIV isolates are shown. SOSIP concentrations are shown according to the legend using a red to blue color gradient.

A

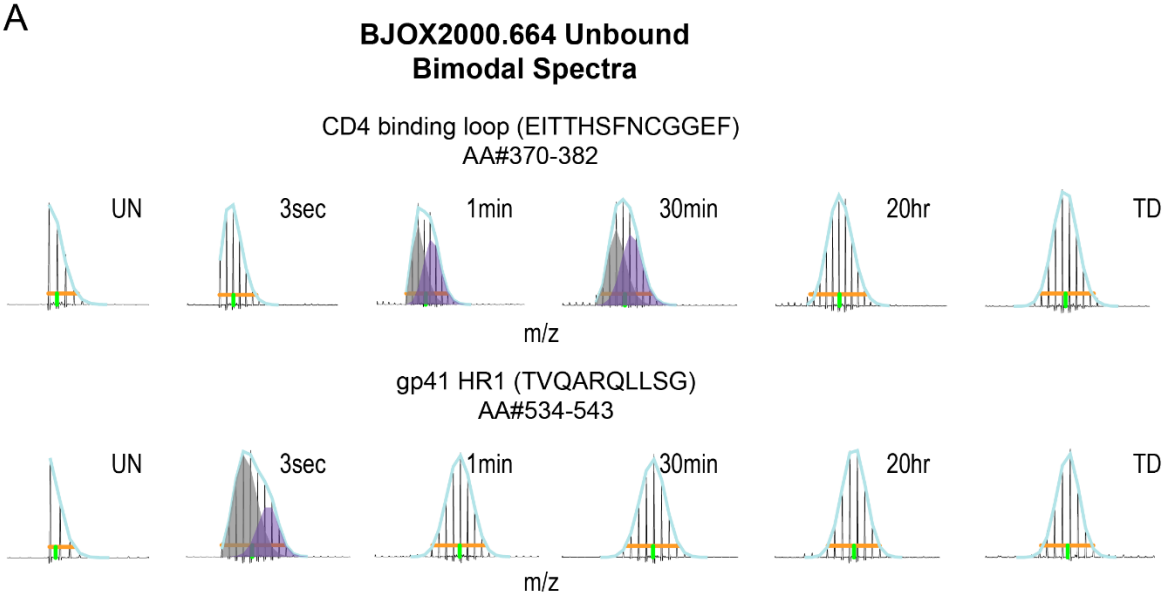
BJOX2000.664 Unbound
Bimodal Spectra
CD4 binding loop (EITTHSFNCGGEF)
AA#370-382
UN
3sec
1min
30min
20hr
TD
m/z
gp41 HR1 (TVQARQLLSG)
AA#534-543
UN
3sec
1min
30min
20hr
TD
m/z

B

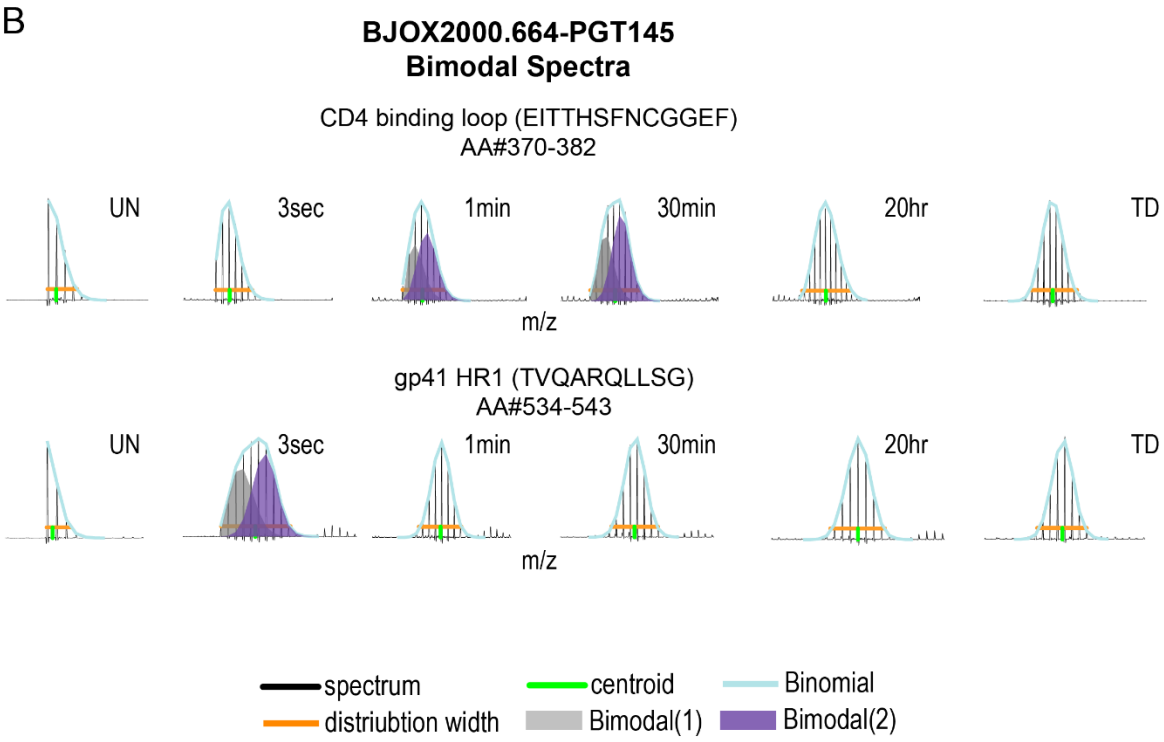
BJOX2000.664-PGT145
Bimodal Spectra
CD4 binding loop (EITTHSFNCGGEF)
AA#370-382
UN
3sec
1min
30min
20hr
TD
m/z
gp41 HR1 (TVQARQLLSG)
AA#534-543
UN
3sec
1min
30min
20hr
TD
m/z
spectrum
centroid
Binomial
distriubtion width
Bimodal(1)
Bimodal(2)

Figure S3.2. PGT145 binding does not abrogate conformational sampling throughout the BJOX2000 trimer structure. Two peptides in BJOX2000.664 unbound and BJOX2000 bound to PGT145 exhibited unusually broad isotopic distributions that were binomially fit to two populations (figures A and B respectively). Each panel displays the spectra from each respective time point. The lighter in mass/more protected population is shaded in gray, and the heavier in mass/faster exchanging population is shaded in purple. The legend describing the centroid, peak envelope, and binomial fit are displayed in the bottom center of the figure.

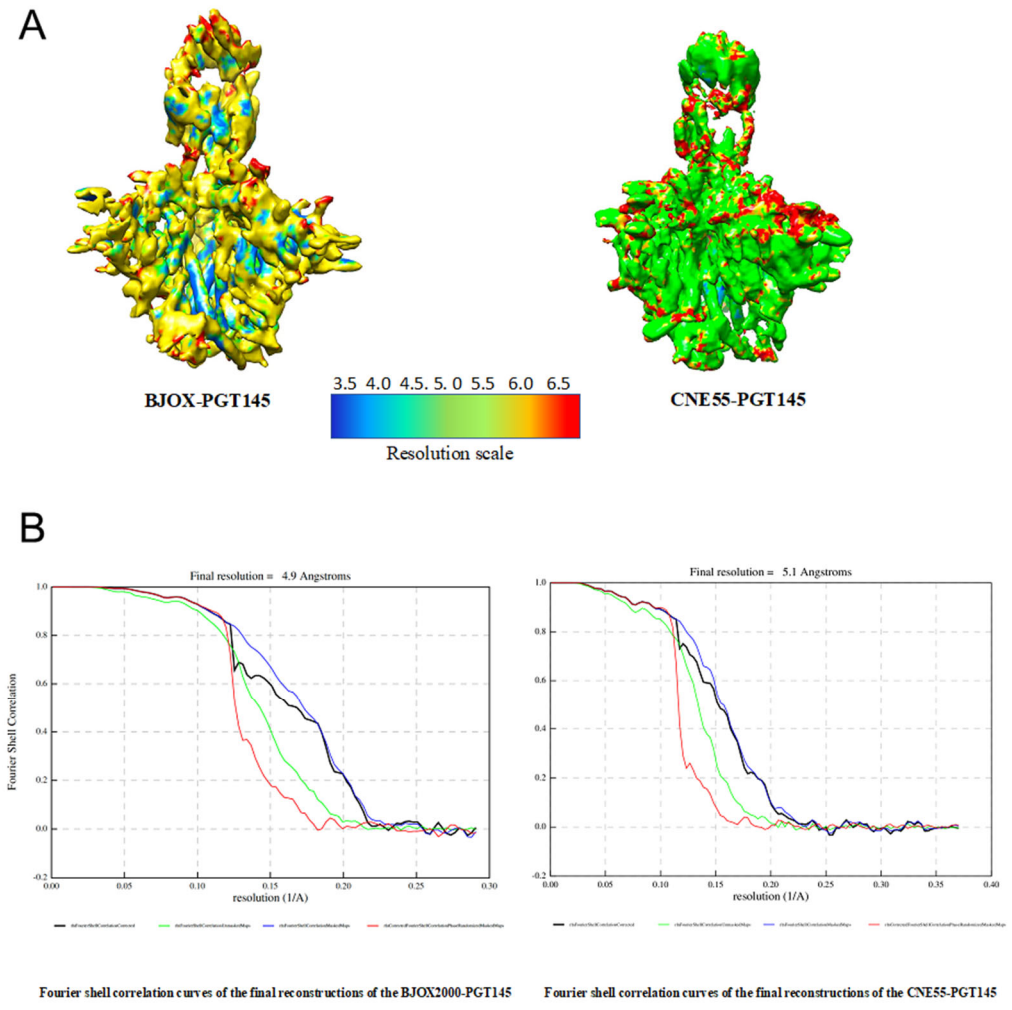

Figure S3.3. Local resolution maps of BJOX2000-PGT145 & CNE55-PGT145. A) Local resolution analysis of the BJOX2000-PGT145 and CNE55-PGT145 structures. The color key shown indicates local resolution in Å. Figure B shows the fourier-shell correlation curves for correlation corrected (black), unmasked (green), masked (blue), and phase randomized (red). Resolution maps and fourier-shell correlation curves were provided by Vidya Prasad and Ananya Chatterjee.

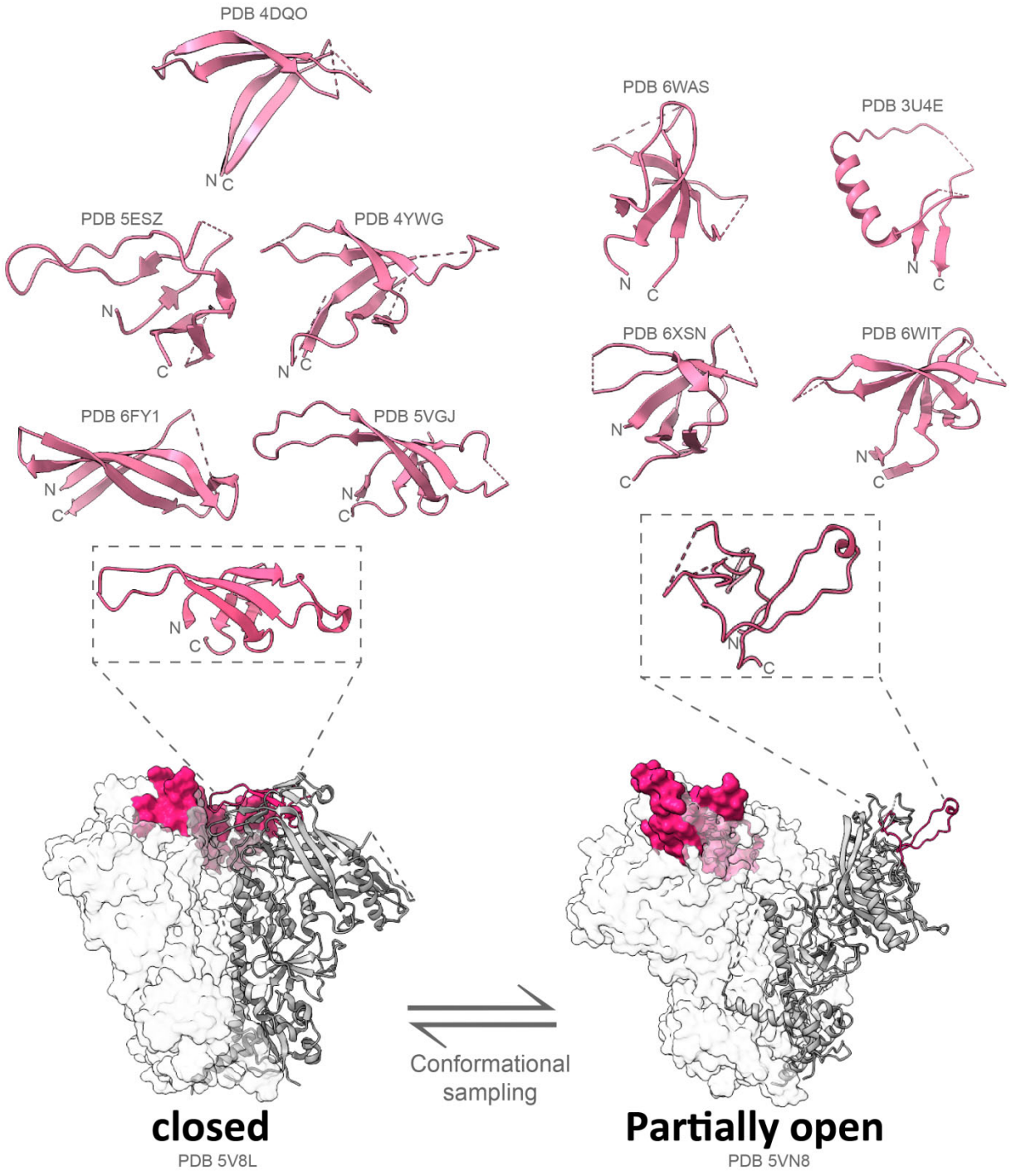

Figure S3.4. V1V2 conformations on native-like Env trimers and presented on scaffold proteins. The V1V2 apex is known to sample a wide range of conformations. On the bottom are Fab bound EM structures of SOSIP trimers in the closed conformation (PDB 5V8L) and a partially open conformation (PDB 5VN8) with 2 protomers displayed in white surface

representation, and 1 protomer displayed in gray ribbon representation with residues 126-196 spanning the V1V2 region highlighted in red. Above the SOSIP trimers are V1V2 crystal structures (residues 126-196) presented on scaffold protein and Fab bound to increase resolution and highlight the conformational plasticity of this region (PDB 4DQO, 5ESZ, 4YWG, 6FY1, 5VGJ, 6WAS, 3U4E, 6XSN, and 6WIT).

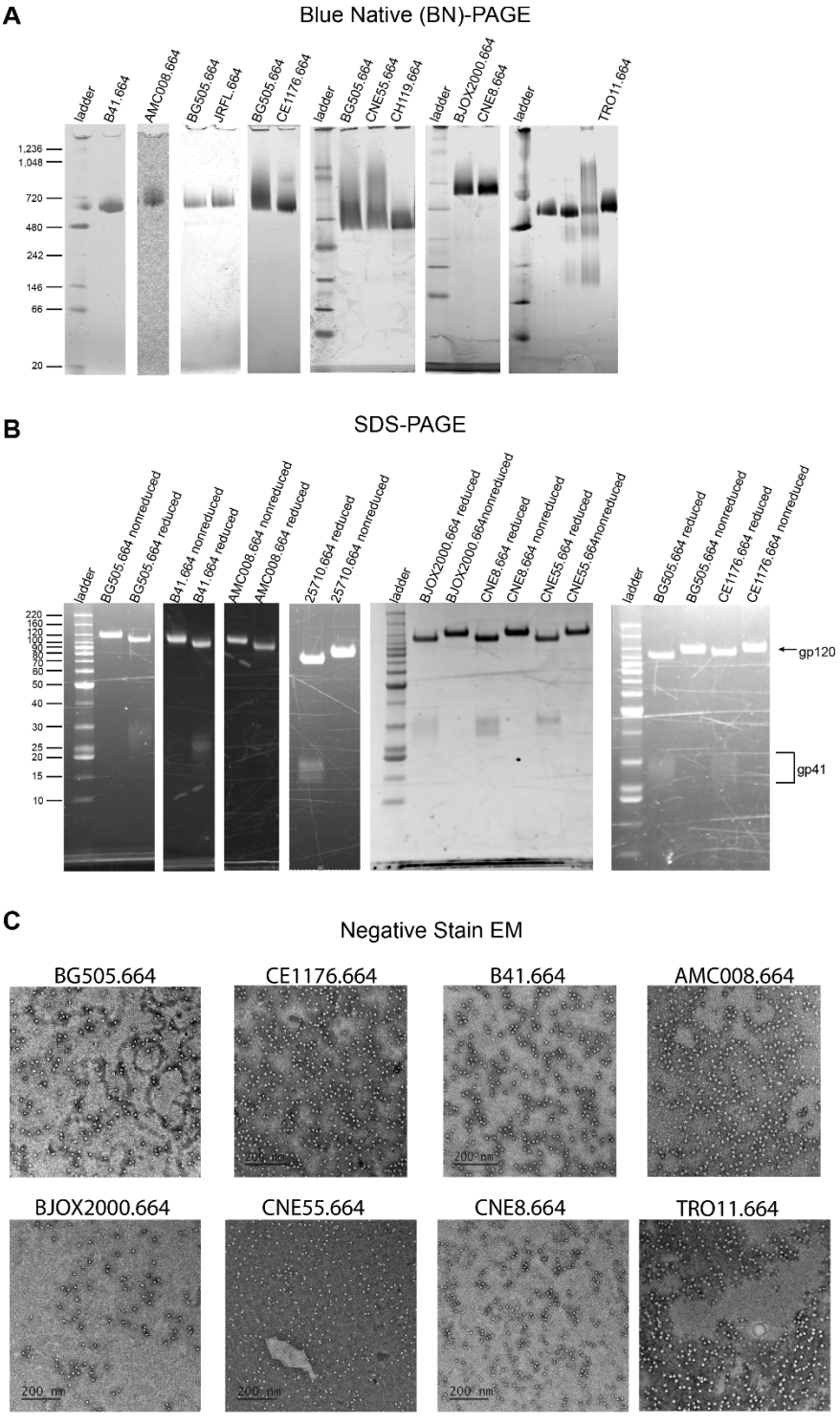
A
Blue Native (BN)-PAGE
ladder
B41.664
AMC008.664
BG505.664
JRFL.664
BG505.664
CE1176.664
ladder
BG505.664
CNE55.664
CH119.664
ladder
BJOX2000.664
CNE8.664
ladder
TRO11.664
1,236
1,048
720
480
242
146
66
20
B
SDS-PAGE
ladder
BG505.664 nonreduced
BG505.664 reduced
B41.664 nonreduced
B41.664 reduced
AMC008.664 nonreduced
AMC008.664 reduced
25710.664 reduced
25710.664 nonreduced
ladder
BJOX2000.664 reduced
BJOX2000.664nonreduced
CNE8.664 reduced
CNE8.664 nonreduced
CNE55.664 reduced
CNE55.664nonreduced
ladder
BG505.664 reduced
BG505.664 nonreduced
CE1176.664 reduced
CE1176.664 nonreduced
220
160
120
100
90
80
70
60
50
40
30
25
20
15
10
gp120
gp41
C
Negative Stain EM
BG505.664
CE1176.664
B41.664
AMC008.664
BJOX2000.664
CNE55.664
CNE8.664
TRO11.664
200 nm

Figure S3.4. SOSIP characterization by blue native (BN)-PAGE, SDS-PAGE, and Negative Stain EM (NS-EM). Each SOSIP was characterized by BN-PAGE (A), SDS-PAGE (B), and negative stain EM (C) after purification and prior to HDX and BLI experiments. On the SDS-PAGE each sample was run non-reduced and reduced via addition of DTT. The single band in the non-reduced lane runs at a slightly higher MW due to the presence of an additional inter-subunit disulfide bond linking gp120 and gp41.

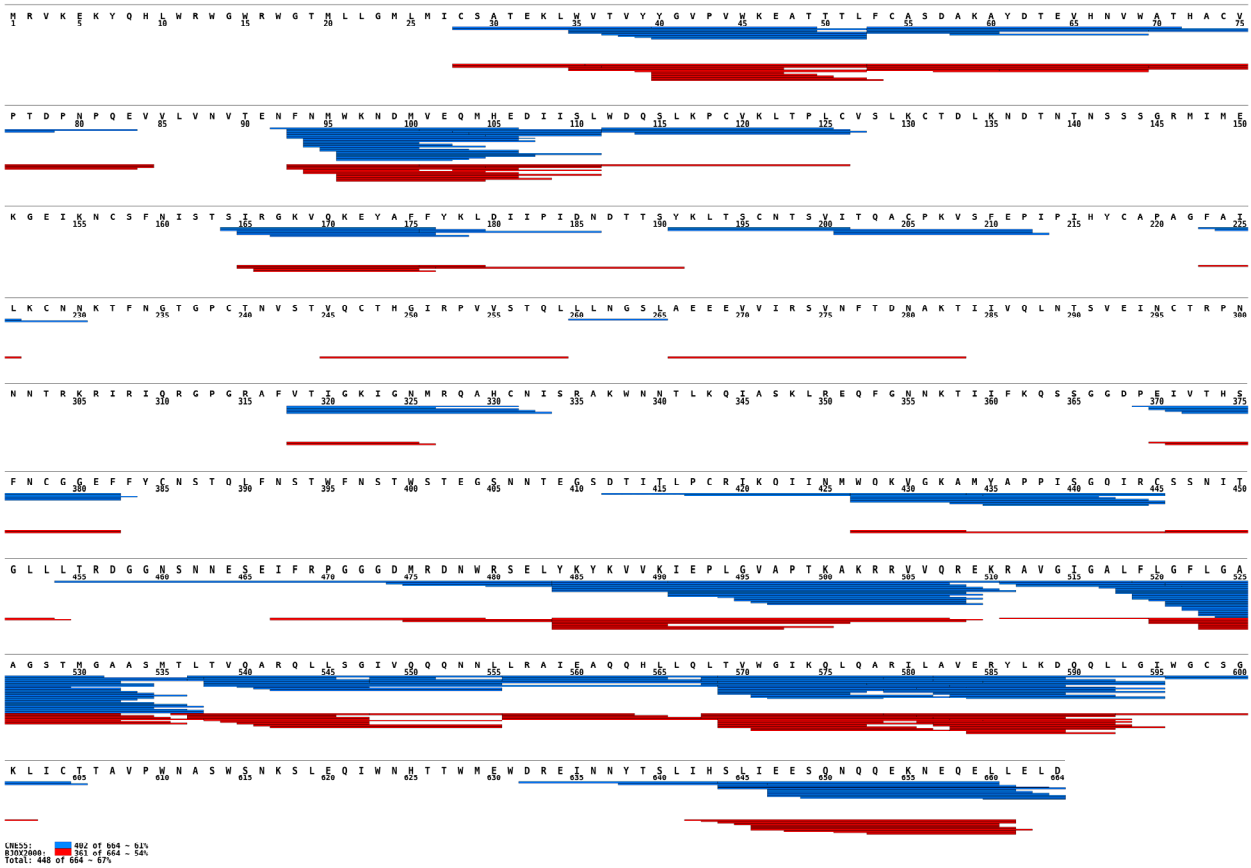

Figure S5. CNE55 & BJOX2000 SOSIP HDX-MS coverage map. CNE55 (red) and BJOX2000 (blue) SOSIP trimer peptic peptides are shown as bars in the coverage map created using MSTools. HXB2 sequence and numbering are used. Missing coverage at the N-terminus is likely due to signal peptide cleavage of Env trimers post-translation.

PGT145 Binding Kinetics			
SOSIP	**PGT145 K_D (nM)**	**PGT145 K_{on} (1/Ms)**	**PGT145 k_{off} (1/s)**
AMC008	**735.4 +/- 246.9**	**2.29E+03 +/- 4.41E+02**	**1.63E-03 +/- 2.42E-04**
B41	**23.4 +/- 0.9**	**2.46E+04 +/- 2.47E+03**	**5.60E-04 +/- 3.35E-05**
CNE8	**50.8 +/- 9.9**	**8.34E+04 +/- 9.86E+03**	**4.19E-03 +/- 3.27E-04**
TRO11	**80.75 +/- 14.4**	**1.29E+04 +/- 1.21E+03**	**1.03E-03 +/- 8.75E-05**
BJOX	**27.7 +/- 9.3**	**6.67E+04 +/- 1.24E+04**	**1.52E-03 +/- 3.43E-04**
BG505	**16.0 +/- 3.9**	**1.20E+05 +/- 4.07E+04**	**1.77E-03 +/- 1.54E-04**
CE1176	**156.5 +/- 19.1**	**1.73E+04 +/- 2.47E+02**	**2.71E-03 +/- 3.80E-04**
CNE55	**45.35 +/- 1.1**	**4.86E+04 +/- 7.78E+02**	**2.20E-03 +/- 8.98E-05**
JRFL	**223.33 +/- 71.5**	**8.66E+03 +/- 1.15E+03**	**1.94E-03 +/- 6.69E-04**
CH119	**64.55 +/- 6.2**	**1.60E+04 +/- 3.68E+02**	**1.03E-03 +/- 7.45E-05**

Table S3.1. Isolate-specific differences in binding Kinetics of PGT145 IgG. BLI determined binding affinities (K_D), binding association rates (k_{on}), and dissociation rates (k_{off}) for PGT145 IgG are shown. Values reported are the average of at least two independent experiments with standard deviations shown.

	BG505		**CE1176**		**B41**	
Asn (N) Residue number	**156**	**160**	**156**	**160**	**156**	**160**
	HexNAc(2)Hex(9)	HexNAc(2) Hex(9)	HexNAc (2) Hex(9)	HexNAc(2) Hex(7)	nonglycosylated	nonglycosylated
	HexNAc(2)Hex(8)	HexNAc(2) Hex(8)	HexNAc (2) Hex(7)	HexNAc(2) Hex(5)	HexNAc(5) Hex(6) Fuc(2)NeuAc(3	HexNAc(4)Hex(5) Fuc(2)NeuAc(2)
	HexNAc(2)Hex(7)	HexNAc(2) Hex(7)		HexNAc(2) Hex(4)		HexNAc(2)Hex(6)
	HexNAc(2)Hex(6)	HexNAc(2) Hex(6)		HexNAc(2) Hex(3)		HexNAc(2)Hex(7)
	HexNAc(3)Hex(3) Fuc(1)	HexNAc(2) Hex(5)				HexNAc(2)Hex(8)
	HexNAc(5)Hex(3) Fuc(1)					HexNAc(2)Hex(5)
	HexNAc(4)Hex(3) Fuc(1)					HexNAc(2)Hex(9)
	AMC008		**JRFL**		**CNE55**	
Asn (N)	**156**	**160**	**156**	**160**	**156**	**160**

Residue number						
	HexNAc(2) Hex(9)	nonglycosylated	NC	NC	HexNAc(2) Hex(9)	non-glycosylated
	HexNAc(2) Hex(8)	HexNAc(2) Hex(9)			HexNAc(2) Hex(8)	HexNAc(2)Hex(6)
		HexNAc(2) Hex(8)				HexNAc(2)Hex(5)
		HexNAc(2) Hex(7)				HexNAc(2)Hex(7)
		HexNAc(2) Hex(6)				
		HexNAc(2) Hex(5)				
		HexNAc(2) Hex(4)				
		HexNAc(5) Hex(6)				
		HexNAc(3) Hex(3)Fuc(1)				
		HexNAc(3) Hex(4)Fuc(1)				

	BJOX2000		TRO11		CH119	
Asn (N) Residue number	156	160	156	160	156	160
	non-glycosylated	non-glycosylated	non-glycosylated	non-glycosylated	nonglycosylated	HexNAc(2)Hex(8)
	HexNAc(2)Hex(7)	HexNAc(2) Hex(8)	HexNAc(9)	HexNAc(2)	not determined	HexNAc(2)Hex(5)
		HexNAc(2) Hex(7)	HexNAc(7)	HexNAc(8)		HexNAc(5)Hex(3) Fuc(1)
		HexNAc(2) Hex(6)		HexNAc(9)		
		HexNAc(2) Hex(5)				

	CNE8	
Asn (N) Residue number	156	160
	nonglycosylated	HexNAc(2) Hex(9)
	HexNAc(2)Hex(8)	HexNAc(2) Hex(8)
	HexNAc(2)Hex(7)	HexNAc(2) Hex(7)
	HexNAc(2)Hex(6)	HexNAc(2) Hex(5)
	HexNAc(6) Hex(6)NeuAc(3)	HexNAc(5)Hex(5) Fuc(1)NeuAc(1)
		HexNAc(6)Hex(7) Fuc(1)
		HexNAc(5)Hex(5) Fuc(2)NeuAc(2)

Table S3.2. N156 and N160 Glycoprofiles. Each Asn (N) residue at residues 156 and 160 in the V2 loop with the NxS/T motif indicating a glycosite is in a column with a list of the glycoforms identified via MS/MS using EThcD. Regions with no coverage are listed as NC, and ND indicates areas where the glycoform was not determined (for example low quality/scoring

MS/MS spectra). Glycoforms were categorized as either high mannose: HexNAc(2)Hex(9-5) (green) or complex (red). Abbreviations and glycan classifications used are according to Essentials of Glycobiology, 3rd ed. HexNAc: N-acetylhexosamines; Hex: Hexose; Fuc: L-Fucose; NeuAc: N-acetyl neuraminic acid.

A	Total trimer SA (Å^2)	Total trimer SA w/o N160 glycans (Å^2)	Total complex SA (Å^2)	Total complex SA w/o N160 glycans (Å^2)	Total SA for Fab (Å^2)
BJOX2000	94113.4	92603.4	104784	104377	14307.2
CNE55	88857.2	87264.4	100022	99489.4	14307.2

B	Total contact area (Å^2)	Contact area w/o N160 glycan (Å^2)	Contact area of N160 glycan (Å^2)
BJOX2000	1818.3	1266.8	551.5
CNE55	1571.2	1041.1	530.1

Table S3.3. EM structure contact area calculation. The contact area between Fab and the trimer were calculated using the solvent accessible area (SA) from the PDB of both BJOX and CNE55. The total SA of the trimer, trimer without N160 glycan, env-Fab complex, env-Fab complex without glycans and only Fab is calculated and provided in the above table.

For calculating the contact area:

[(Total SA of trimer + Total SA of Fab) – Total SA for complex] / 2

The same calculation was repeated for the PDB without N160 glycan in table B.

Table and calcs were provided by Vidya Prasad and Ananya Chatterjee.

	Single particle Cryo-EM map of BJOX	Single particle Cryo-EM map of CNE55
Data collection and processing		
Magnification		105000
Voltage (KV)	300	300
Electron exposure ((e–/Å2)	1.44	0.88
Defocus range (μm)	0.75-3 μm	0.75-3 μm
Pixel size (Å)	0.86	1.35
Symmetry imposed	C1	C1
Initial particle images (no.)	4860777(untilted), 1526177(tilted)	238605(untilted) , 1602666(tilted)
Final particle images (no.)	667012	527385
FSC threshold Map resolution range (Å)	4.9	5.14
Refinement		
Initial model used (PDB code)	5V8L	5V8L

Table S3.4. Cryo-EM data collection

Dataset	**CNE55.664**	**CNE55-PGT145**
HDX reaction details	85% D2O buffer, pH* 7.466, labeled at RT (22.0°C), Quenched at pH 2.502 in 200mM TCEP, 8M urea, 0.2%FA	85% D2O buffer, pH* 7.466, labeled at RT (22.0°C), Quenched at pH 2.502 in 200mM TCEP, 8M urea, 0.2%FA
HDX time course	3 sec, 1 min, 30 min, 20 hrs	3 sec, 1 min, 30 min, 20 hrs
HDX controls	PPPI, PPPF	PPPI, PPPF
Avg Back-exchange	12.7%	13.4%
Number of peptides	184	184
Sequence coverage	61.5%	61.5%
Average peptide length/redundancy	13.4 residue length/ 3.8 redundancy	13.4 residue length/ 3.8 redundancy
Replicates (biological or technical)	two technical replicates	two technical replicates
Repeatability	5.0	5.0
Dataset	**BJOX2000.664**	**BJOX2000-PGT145**
HDX reaction details	85% D2O buffer, pH* 7.466, labeled at RT (22.0°C), Quenched at pH 2.502 in 200mM TCEP, 8M urea, 0.2%FA	85% D2O buffer, pH* 7.466, labeled at RT (22.0°C), Quenched at pH 2.502 in 200mM TCEP, 8M urea, 0.2%FA
HDX time course	3 sec, 1 min, 30 min, 20 hrs	3 sec, 1 min, 30 min, 20 hrs

HDX controls	PPPI, PPPF	PPPI, PPPF
Back-exchange	9.0	9.0
Number of peptides	127	127
Sequence coverage	57.8	57.8
Average peptide length/redundancy	12.8 residue length/ 2.6 redundancy	12.8 residue length/ 2.6 redundancy
Replicates (biological or technical)	two technical replicates	two technical replicates
Repeatability	Stddev of 6.3%	Stddev of 6.3

Table S3.5. HDX reaction details

Chapter 4. Bridging HIV neutralization sensitivities and Env dynamic phenotypes across genetically diverse variants

4.1 Introduction

Extreme genetic diversity among HIV-1 isolates poses a major challenge to development of effective vaccines and use of antibodies for passive immunization or therapeutic control of an established infection. While recent years have seen significant strides made in our understanding of the architecture of the HIV-1 Env glycoprotein (Env) and identification of the sites of vulnerability on Env targeted by neutralizing antibodies, our understanding of HIV Env structural variation and the impact of variation on antibody recognition remain poorly characterized.

HIV-1 isolates are classified into genetic subtypes and circulating recombinant forms (CRF's), where the genetic sequences of different subtypes can differ by 17-35%.[1] In an effort to codify HIV-1 Env diversity based on phenotypic traits such as neutralization profile, a number of recent studies have examined large panels of Env pseudotyped on a common HIV backbone and determined that circulating isolates can be classified into 4 "tiers" based upon their sensitivity to pooled sera from HIV infected individuals (Figure 4.1A) [2]. The lowest tier in this scheme, so-called Tier 1a viruses, correspond to HIV-1 isolates that are readily neutralized by sera, while Tier 1b viruses are somewhat more resistant, and Tier 2 viruses, which comprise the majority of typical circulating isolates are generally neutralization resistant. A small proportion of isolates exhibit very high neutralization resistance and are classified as Tier 3 viruses. As Tier 2 isolates appear to reflect the most common phenotype, major efforts have been devoted to identifying panels of isolates that recapitulate the antigenic diversity of viruses found world-wide [2-5].

Despite the usefulness of these panels in determining the breadth of an antibody or individual serum in regards to neutralizing genetically diverse variants, there is a lot of variability within each tier, and a structure-based explanation for differences in antigenicity across the viruses in such panels on a molecular level is missing [6]. For example, a particular serum is sometimes able to neutralize viruses scattered across the different tiers, and the polyclonal nature of serum often leaves Env-IgG interactions that contribute to neutralization enigmatic [7, 8].

Given that Env is the only target for antibodies on the surface of the virus, its structure has been intensely studied. Env is a trimer of heterodimers, consisting of three gp120 receptor binding subunits noncovalently bound to three base gp41 subunits that harbor the hydrophobic fusion peptide [9, 10]. Functionally Env undergoes dramatic structural rearrangements to drive fusion of the virus and target cell membrane allowing virus entry and infection [11, 12]. Preceding the post fusion state (where gp41 exists as a rigid 6-helix bundle after the membranes have been merged), high-resolution static structures have provided atomic details of multiple pre-fusion conformations derived from Env bound to Fabs specific for different conformations that occur along the fusion pathway. Notably these static images only report on conformational endpoints, and not the mechanisms or motions that lead to those endpoints. In prefusion closed trimer structures variable loops 1 and 2 (V1V2) shield the co-receptor binding site and V3 loops [13, 14]. Env complexed to CD4 receptor and antibodies specific for the open state have revealed structural differences between the closed and open states that include: displacement of the V1V2 apex to the trimer sides, a rotation of the gp120 subunits outward, formation of the bridging sheet and α0 helix, exposure of the V3 loops, and repositioning of the gp41 helices [15]. Env trimers bound to Fabs specific for partially open states, suggest that Env can undergo some of these changes observed in the open state while maintaining features of a closed conformation, such as a conformation that includes rotation of gp120 outwards without

formation of the bridging sheet as observed in b12 Fab bound EM structures [14]. Antibodies prevent infection by inhibiting such structural rearrangements or by blocking interactions with the CD4 receptor or co-receptor (CXCR4 or CCR5). After a few years of infection, many infected individuals are able to produce antibodies with at least some level of neutralization breadth [16, 17]. Sites of vulnerability across the trimer structure that are targets of antibodies capable of neutralizing genetically diverse strains (bnAbs) have been identified. These include the CD4 binding site, the base of the V3 loop, a conformational epitope at the apex of the V2 loops, the gp120-gp41 interface, the fusion peptide, and the membrane proximal external region (MPER) that is absent on native-like trimer constructs [18-22]. But subsets of viruses are still able to escape neutralization by even some of the most potent broadly neutralizing antibodies.

Factors contributing to differences in neutralization sensitivities include differential glycosylation, variations in epitope residues, variations in hypervariable loop lengths, and differences in Env conformational dynamics [8, 23, 24]. Dynamics play a considerably significant role in modulating antigenicity. It has been demonstrated that Env reversibly samples multiple pre-fusion conformations even in the absence of receptor, where dynamic motions can disrupt conformational epitopes and alter which binding sites are exposed to antibodies [25].Single molecule techniques like smFRET that monitor the kinetics of Env conformational transitions revealed that native Env on viral particles transiently sample at least three distinct states [25]. From a limited comparison of a few Env variants, notable isolate-specific differences were observed for the relative population distributions among the conformational states. A highly neutralization sensitive lab-adapted Env, NL4-3, was observed to more readily sample and populate states interpreted to reflect a more open trimer. However the spatial information provided by smFRET is limited to deducing the relative separation of inserted fluorophores, with numerous caveats associated with the derived distances. Studies using DEER spectroscopy have also hinted at conformational heterogeneity, without providing a means to assess

dynamics and transitions due to the requirement that the samples be frozen [26].The current prevailing hypothesis is that neutralization sensitivity is predominantly determined by how frequently the surface Env proteins on a virus samples an open conformational state in which certain immunodominant epitopes such as the V3 loop and co-receptor binding site are accessible [6, 27]. Tier 2 and 3 viruses are thought to display Env that predominantly populates a closed conformation where many epitopes for non- or weakly protective antibodies are hidden. The open conformation can be sampled spontaneously or triggered by binding CD4, and displays many epitopes that antibodies with poor breadth bind, such as the co-receptor binding site or the tip of the third variable loop (V3) [13, 28]. smFRET has been used to examine conformational switching in Env from a limited number of isolates including a lab adapted tier 1 isolate, NL4-3, which sampled an open conformation more readily than the harder to neutralize tier 2 isolates such as JR-FL and BG505, providing support for this hypothesis [25, 29, 30]. However, smFRET only reports on the relative positions of inserted fluorophores on Env that spans the distance of many epitopes, and currently the assignment of smFRET states to specific conformations of Env is a subject of debate [31].

Highlighting the impact epitope dynamics have on antibody binding, our lab previously observed a correlation between epitope flexibility and conformation dependent antibodies' association rates using soluble gp120 constructs [32]. Previously we used HDX-MS to compare native-like Env trimers derived from five well-studied isolates and observed that some of the largest differences in local structural dynamics mapped to regions targeted by bnAbs against HIV-1 [33]. Additionally, we observed correlated H/D exchange indicative of conformational switching in regions that largely aligned with areas known to undergo the CD4 inducible transition from the closed to the open state across a broad range of timescales (from seconds to hours), and this was largely isolate dependent [15].

However, five isolates largely skewed towards genetic subtype B is not representative of the global diversity of HIV, including 3 subtype B and one each from subtype A and C. HIV-1 group M has been divided into nine genetic subtypes with an ever-growing list of over one hundred recognized genetic recombinants [34]. Statistical methods have been used by deCamp et al to select a panel of 12 HIV variants across all major subtypes and CRFs that captures the global antigenic diversity of HIV [2]. Additionally, the neutralization sensitivity of this panel has been determined using pooled human serum. Here we expressed soluble, pre-fusion stabilized native-like Env trimers (known as SOSIPs) across variants from this global panel to address how extreme sequence diversity impacts dynamics, and to test if differences in dynamics might help explain their neutralization tier assignment. We utilized hydrogen/deuterium exchange mass spectrometry (HDX-MS) to characterize each isolates' dynamic phenotype with peptide level resolution across many key epitopes in order to test the hypothesis that the isolate dependent dynamic phenotype of Env can mechanistically explain its neutralization sensitivity.

We found substantial variability across each trimers' dynamic phenotype ranging from differences in faster structural fluctuations to differences in larger subdomain rearrangements that happen on slower timescales. These differences existed within the tier 1 isolates, as well as within the diverse tier 2 isolates. Even though the tier 2 isolates exhibit a broad range of neutralization sensitivities to pooled serum, we did not observe any clear trends between local dynamics and neutralization resistance across trimers derived from the tier 2 viruses. However, in a comparison between the tier 1 and tier 2 trimers, we observed multiple regions where the SOSIP trimers from tier 1 isolates exhibited a significantly different dynamic phenotype compared to the tier 2 trimers that likely explains their neutralization sensitivity. Furthermore, we observe significant differences in dynamics in our comparison of trimers derived from tier 1a and tier 1b viruses, where our tier 1a trimer displayed the greatest number of regions that sampled two distinct conformational states.

4.2 Materials and Methods

4.2.1 Cell lines for antibody production

HEK293F cells (ThermoFisher Scientific) used for expression of antibodies were grown at 37°C, 8% CO2, with shaking at 125 rpm in Freestyle 293 media (ThermoFisher Scientific) without additives. The cell lines were not authenticated within our lab, but a certificate of analysis from the manufacturer is available. The sex of the 293F cell line is female.

4.2.2 Cell lines for SOSIP production

Expi293 cells (ThermoFisher Scientific) used for expression of SOSIP Env glycoproteins were grown at 37°C, 8% CO2, with shaking at 125 rpm in Expi293 expression media (ThermoFisher Scientific) without additives. The cell lines were not authenticated within our lab, but a certificate of analysis from the manufacturer is available.

4.2.3 Design of SOSIPs from multiple diverse HIV-1 Env sequences

The Env sequences from isolates selected for the global HIV panel chosen in deCamp et al were used as the template to insert the stabilizing SOSIP mutations (Env sequences are linked via the accession numbers in the reagent table) [2, 35]. Mutations include a disulfide bridge between cysteines at positions 501 and 605 (SOS), an Ile-to-Pro mutation in the HR1 domain of gp41 (IP), modification of the proteolytic cleavage site $_{508}$REKR$_{511}$ to a hexa-arginine motif to enhance furin cleavage, and replacement of the native leader sequence with that of the tissue plasminogen activator (tPA) to enhance secretion. New SOSIP genes were synthesized by

ThermoFisher Life Technologies with flanking PST1/NOT1 restriction sites and subsequently cloned into the pcDNA3.1 mammalian expression vector.

4.2.4 Protein expression and purification

SOSIPs were produced and purified as previously described by Verkerke et al and briefly below. Briefly, Expi293 cells were transiently transfected at a density of roughly 3 million cells/mL using polyethylenimine (PEI) with plasmids encoding each SOSIP from each respective isolate co-transfected with the furin encoding gene in pcDNA3.1 at a ratio of three SOSIPs to one furin to ensure proteolytic cleavage between gp120 and gp41 subunits during production. After roughly six days (or until ~90% of cells were non-viable) the cell supernatants were cleared by centrifugation and filtered through a 0.2-micron vacuum filtration unit and supplemented with protease inhibitors (Roche) and sodium azide to prevent microbial growth. Glycosylated trimers were extracted using *Galanthus nivalis* lectin (GNL) coupled to agarose beads overnight at 4°C and washed with 20 mM Tris (pH 7.4), 1 mMEDTA, 1 mM EGTA, 0.02% azide, and 120 mM NaCl; glycoproteins were eluted with 7 to 10 column volumes of 1 M alphamethyl-mannopyrannoside dissolved in 20 mM Tris (pH 7.4), 1 mM EDTA, 1 mM EGTA,0.02% azide, and 120 mM NaCl. GNL eluates were concentrated using Amicon ultrafiltration units (nominal molecular mass cutoff of 100 kDa) and buffer exchanged into DEAE low-salt buffer (20 mM Tris [pH 8.0], 100 mM NaCl) before anion-exchange chromatography using a DEAE column. Following 10 min of isocratic flow in 100 mM NaCl, a gradient to 1 M NaCl was initiated and fractions were collected throughout to remove protein aggregates. The DEAE flowthrough was buffer exchanged into 2 M ammonium sulfate– 0.1 M phosphate (pH 7.4) via dialysis and loaded onto a 5mL HIC HiTrap Phenyl HP column. A step-wise gradient of 2M to 0M ammonium sulfate in 0.1 M phosphate (pH 7.4) was used to separate trimers from dimers and monomers. The early-eluting fractions (containing native-like trimers) were concentrated prior to being loaded onto a Superdex S200PG size exclusion chromatography (SEC) column in PBS (20mM sodium

phosphate [pH 7.4], 150 mM sodium chloride, 0.02% sodium azide). Peak fractions were concentrated and characterized by DLS, SDS, BN-PAGE, and negative stain EM (Figure S4.1) to ensure homogenous, pure trimer populations immediately prior to HDX and BLI experiments.

Antibodies purified in house were produced by transient co-transfection of plasmids containing heavy and light chain fragments at a 1:1 ratio in HEK293F cells. Cultures were allowed to grow for approximately 6 days before harvesting. Secreted IgG was isolated and purified by affinity chromatography using a Hi-Trap Protein A column and eluted using 100mM Glycine pH 2.0 and neutralized by addition of 1M Tris pH8.0. Purity was assessed by SDS-PAGE

4.2.5 SDS-PAGE and BN-PAGE

SDS denaturing PAGE and blue native PAGE (BN-PAGE) analyses with precast gels (Novex) were performed to assess the oligomeric species present throughout purification and immediately prior to experiments. Typically, between 10 and 15µg of protein was loaded per lane for BN-PAGE analysis and 5µg per lane was loaded for SDS-PAGE analysis.

4.2.6 Dynamic light scattering (DLS)

Dynamic light scattering (DLS) measurements were performed on a Dynapro Nanostar (Wyatt Technologies). Trimer samples were diluted to 1 mg/ml in PBS and centrifuged at 15,000xg for 20 min prior to loading of 10µl into a low-volume quartz cuvette. The mean estimated hydrodynamic radius, and polydispersity were generated from 30 acquisitions of 5 s at 20°C.

4.2.7 Hydrogen/Deuterium exchange mass spectrometry

HDX-MS was performed as described previously in Hodge et al [33]. Briefly, 5 µgs (42 pmol) per timepoint of each protein were incubated in deuterated buffer (20mM PBS, 85% D2O, pH*7.52) for 3s, 1min, 30min, and 20hrs at room temperature. The reaction was stopped via diluting 1:1 in ice-cold quench buffer (200 mM tris(2-chlorethyl) phosphate (TCEP), 8 M urea, 0.2% formic acid) to a final pH of 2.5 and flash frozen in liquid nitrogen followed by storage in -80°C prior to analysis. Online pepsin digestion was performed and analyzed by LC-MS-IMS utilizing a Waters Synapt G2-Si Q-TOF mass spectrometer as described previously utilizing a 15 minute gradient and a home-made HDX cold box that maintains the pepsin digestion at 4°C and the LC plumbing at 0°C[33, 36]. Pepsin digest eluates from undeuterated sample LC-MS runs were collected, dried by speed vac, incubated in deuteration buffer for 1 hour at 65°C, and quenched as described above to prepare fully deuterated controls. Pepsin digest eluates from undeuterated sample LC-MS runs were also collected, dried by speed vac, resuspended in mobile buffer for peptide identification using nano LC-MS on an Orbitrap Fusion mass spectrometer. A 2 cm trapping column and a 35 cm analytical column were freshly prepared in fused silica (100 µm ID) with 5 µM ReproSil-Pur C18 AQ beads (Dr. Maisch). 8 µL of sample was injected and run using a 60-minute linear gradient from 2% to 30% acetonitrile in 0.1% FA, followed by 10 minutes of 80% acetonitrile. An EThcD method was optimized as follows: ion source: 2.1 kV for positive mode; ion transfer tube temperature: 350 °C; resolution: MS1 = 120000, MS2 = 30000; AGC target: MS1 = 2e5, MS2 = 1e5; and injection time: MS1 = 50 ms, MS2 = 60 ms. Orbitrap Fusion data was processed using Byonic (Version 3.8, Protein Metrics Inc.) to obtain a peptide reference list and identify peptic glycopeptides and glycosylation sites. Deuterium uptake analysis was performed with HD-Examiner (Version 2.5, Sierra Analytics) followed by HX-Express v2 for binomial fitting[37]. The percent exchange was normalized to the fully deuterated samples. The well characterized BG505 SOSIP was exchanged alongside each new construct as a positive control sample and internal exchange standards (Pro-Pro-Pro-Ile

[PPPI] and Pro-Pro-Pro-Phe [PPPF]) were included in each reaction to control for variations in ambient temperature during the labeling reactions.

4.2.8 Biolayer interferometry

The binding kinetics of the SOSIP constructs against a panel of IgG's were determined via BLI on an Octet Red system (FortèBio). Anti-human IgG Fc capture biosensors were presoaked in binding buffer (phosphate-buffered saline (PBS pH 7.4) supplemented with 0.1% BSA, 0.005% Tween 20, and 0.02% NaN3) for 10 minutes. The hydrated tips were then loaded with purified IgG prepared at 8μg/mL in binding buffer for 80 seconds. After reaching a stable baseline, antibody-immobilized biosensors were moved into wells containing a 2-fold dilution series of SOSIP trimer to monitor association for 3 mins, then biosensors were moved back into wells containing binding buffer to monitor dissociation for 3 mins. Responses were calculated and double referenced against the buffer reference signal and non-specific binding of analyte to biosensor in absence of IgG. Kinetic data were analyzed by using FortéBio Data Analysis 11.0 software and were processed by Savitzky-Golay filtering prior to fitting using a 1:1 binding model. Reported values are averages of data repeated in at least two independent experiments.

4.3 Results

4.3.1 Dynamic differences among Env trimers derived from viruses across the neutralization resistance spectrum

In order to generate native-like HIV-1 Env trimers spanning the spectrum of neutralization resistance, we engineered the minimal SOSIP.664 modifications into Env from the global panel of tier 2 neutralization isolates [2], as well as from the widely used Tier 1a SF162 reference isolate and the Tier 1b BX08 isolate. The minimal SOSIP changes include truncation

at residue 664, an I559P point mutation in HR1, and the addition of a disulfide bridge between A501C and T605C that help maintain trimers in a native-like prefusion conformation [35, 38]. Additionally, the trimers are fully cleaved into gp120 and gp41 subunits due to inclusion of an R_6 cleavage motif between gp120 and gp41 and co-expression of furin protease.

Trimers were expressed using purification methods that purify SOSIPs based on their biophysical properties without relying upon antibody affinity purification, in order to avoid selecting for sub-populations of glycoforms [39]. For example, Colins et al have shown that PGT145 and 2G12 Env based purifications can alter trimer antigenicity [40]. Post purification trimer population homogeneity was assessed by Blue Native-PAGE (BN-PAGE), SDS-PAGE, DLS, and negative stain EM (ns-EM) (Figure S4.1). By these assays, all preparations contained trimers consistent with a well-folded, native-like prefusion form. Freshly purified trimers were used for HDX-MS and biolayer interferometry (BLI) experiments, without subjecting the delicate trimers to any freeze/thaw cycles. Of the 12 Envs in the global panel, we were able to obtain sufficient preparations of trimers for isolates 25710 (subtype C), CNE8 (CRF01), TRO11 (subtype B), BJOX2000 (CRF07), CE1176 (subtype C), CH119 (CRF07), and CNE55 (CRF01) that expressed pure, homogenous populations of trimers [41-44]. Additionally, trimers from two tier 1 isolates, SF162 tier 1A (subtype B) and BX08 tier 1B (subtype B), were successfully purified (Figure 4.1A). And the well-characterized BG505 trimer (subtype A) was included as a positive control [45, 46].

In order to directly compare differences in Env dynamics across the panel variants, only homologous peptides with the same number of exchangeable backbone amides can be compared (Figures 4.1C, 4.2 and 4.3). Due to large differences in amino acid sequence that alters proteolytic cleavage sites across these diverse isolates, regions that could be quantitatively compared were limited to about 90 peptides (some peptides were more common in some isolates than others) across the structure. From our analysis of the panel of global tier 2

neutralization isolates, we observed significant structural dynamic variation throughout the trimer structure including at most neutralizing antibody epitopes. A heatmap highlighting sequence conservation and variation across the panel isolates mapped onto a trimer structure is shown in Figure 4.1B. Indeed, we observed significant differences in trimer dynamics (Figure 4.1C), even in regions with high sequence homology (magenta color, Figure 4.1B), such as the bridging sheet, CD4 binding loop, and V3 loop. Figure 4.1C maps the regions with the largest differences in dynamics, as well as regions where dynamics were highly conserved across the tier 2 isolates. For a direct quantitative comparison only homologous peptides with the same number of exchangeable amides were included in figure 4.1C. However, Figure S4.3 shows trimer heatmaps that include non-homologous peptides for a relative comparison with more detailed coverage.

Comparing the eight isolates categorized as neutralization resistant (tier 2), some regions exhibited conserved dynamics, in which there was little variation in inter-strain behavior. These regions include the gp120/gp41 interface, the fusion peptide, and the region in between HR1 and HR2 in the gp41 subunit (colored blue in Figures 4.1C, 4.2). Regions with large differences in dynamics across tier 2 isolates are colored red on the trimer structure.

The largest differences in dynamics map to a region that is one of the most immunodominant regions on the structure, the V3 loop (Figure 4.1C, Figure 4.2) [47, 48]. The sequence of this localized region in the V3 loop was fairly well conserved (Figure S4.2, Figure 4.1B) across isolates, and it likely has sequence constraints in order to maintain functionality as part of the binding site for co-receptor. Isolates 25710 and CE1176 had the most protected V3 loops, while CNE55 and BJOX2000 had the most dynamic V3 loops across the tier 2 isolates. All of the isolates started with a similarly protected V3 loop after 3 seconds of deuteration, which suggests a starting conformation with similar solvent accessibility and secondary structure. Some isolates however, such as BJOX2000, more frequently samples an exchange competent

conformation and became deuterated more quickly with time. CNE55, a highly neutralization resistant isolate, was an outlier, where it was the only tier 2 isolate with a V3 loop that was significantly more deuterated at the earliest timepoint, which suggests either a more solvent exposed ground state conformation, or a V3 loop that is engaged in fewer protective H-bonds.

The V2 loop, which sits above the V3 loop in the closed trimer conformation also displayed large differences in tier 2 inter-isolate variation (Figure 4.1C, 4.2). CE1176, CH119, 25710, and BJOX2000 exhibited more flexible V2 loops in comparison to CNE8, CNE55, and the BG505 positive control. Differences in the shape of the uptake curves also reveal differences in the propensity of this region in the V2 loop to sample a more exposed, exchange competent conformation. The base of the first variable loop (V1) which forms an integral part of the bridging sheet (co-receptor binding site in the open state) also exhibited a high degree of variation in dynamics across the tier 2 isolates, despite high sequence homology of this peptide (residues 112-127) across the panel of isolates. All tier 2 isolates in this region of the bridging sheet started off similarly protected after 3 seconds in deuterated buffer, but the rate at which this region's backbone amides sample an exchange competent conformation is different across isolates; CNE55 remained relatively more protected across time, while CH119, 25710, and BJOX2000 have a higher propensity to sample conformations where backbone amides are more exposed.

Peptides including residues involved in CD4 binding contacts (this also includes many CD4 binding site targeting bnAbs, such as VRC01) are labeled in Figure 4.2 and Figure S4.4. CNE8 and BJOX2000 tend to have a more flexible CD4 binding site across all these peptides. The CD4 binding site is discontinuous in sequence and CH119 has the most flexible CD4 binding site in the localized region spanning residues 374-386, however, CH119 has the most protected CD4 binding site in the localized region spanning residues 427-445.

Regions in the base gp41 fusion subunit also exhibited large differences in dynamics. The largest differences in the base of tier 2 isolate trimers were located in the N and C termini of HR1 (Figure 2, Figure S4). For instance, CE1176 has a considerably more rigid HR1 at the N-terminus (peptide 9) than the other tier 2 isolates, especially in contrast to CNE8, which has an N-terminal HR1 that is maximally deuterated after only 3 seconds. The C-terminus of HR1 predominately exists as a helix in static high-resolution structures [49, 50]. Our data suggests significant differences in the stability of this helix, since backbone amides engaged in stabilizing H-bonds need to be disrupted through protein motions in order to take up deuterium. At the C-terminus of HR1 25710 and CH119 have more rigid helices in comparison to the more flexible helices observed in CNE8 and CNE55. As we have observed previously, the region that includes the helix disrupting I559P SOSIP mutation in HR1, was likely very disordered in agreement with static SOSIP structures and HDX profiles that were fully, or nearly fully, deuterated at early timepoints (Figure S4.4, residues 556-568) [33].

4.3.2 A structural dynamics-based explanation for neutralization resistance between tier 1 and tier 2 isolates

Structural studies by cryo-EM and X-ray crystallography have focused primarily on trimers from the relatively resistant Tier 2 viruses, and the majority have used the well-studied BG505 Env trimer. However, Env from Tier 1a strains, especially SF162, are frequently used as a reference isolate in assessing the activity of monoclonal antibodies and sera [6]. To date, structural studies elucidating the characteristics of Env from Tier 1 viruses have been lacking, though it has been hypothesized based upon antibody binding profiles, that Tier 1 viruses expose V3 and co-receptor binding sites and preferentially adopt conformations more consistent with CD4-induced open states [1, 6, 27].

HDX-MS analysis of SF162 (tier 1A) and BX08 (tier 1B) native-like trimers revealed substantially different structural ordering relative to the Tier 2 isolates. We note that by NS-EM

and other biophysical and biochemical assays, the Tier 1a and 1b trimers were purified to comparable homogeneity and appeared similar in biochemical properties and low-resolution structures to those derived from the neutralization resistant Tier 2 isolates. Regions of greatest divergence in local structural ordering and dynamics between Tier 1 vs Tier 2 isolates are highlighted in red on the trimer structure in Figure 4.3.

Both SF162 and BX08 exhibited substantially more dynamic gp120/gp41 interfaces relative to Tier 2 Envs (Figure 4.3). While the SF162 and BX08 interface peptides were similarly protected at early time points as the Tier 2 isolates, they took on deuterium more rapidly, reflecting a dynamic interface with transient local exposure to solvent. The N-terminal end of the gp120 inner domain helix was also more flexible in BX08 and SF162. Additionally, the Tier 1a and 1b isolates exhibited the most solvent-exposed V3 loops among all of the Envs we tested (Figure 4.3). Likewise, SF162 and BX08 exhibited unusually dynamic HR1 helices in comparison to Env from the Tier 2 isolates.

In analyzing the mass spectra for individual peptides, we frequently observed bimodal or broadened spectral envelopes. Such signatures can be indicative of a peptide adopting more than one conformational environment, for example a conformation with protected backbone amides and a more exposed, solvent accessible conformation [51, 52]. We fit our HDX data to binomial functions and tested for spectral broadening and signs of bimodal envelopes that would result from a peptide sampling states of varying degrees of backbone solvent exposure [37, 53]. For proteins undergoing dynamic motions, often the rate at which backbone amides interconvert between a protected and a deuterium exchange facile state is much faster than the deuterium labeling rate, and thus backbone amides must undergo multiple opening and closing events in order for any individual amide to take up deuterium (uncorrelated exchange or EX2 kinetics). Less commonly, protein motions can be slower than the labeling rate. In this exchange regime (EX1 kinetics), as soon as a localized region samples an exchange competent

conformation, multiple backbone amides are deuterated in tandem before they return to an exchange incompetent conformation. This manifests in the MS data as broadened or bimodal spectra with sub-populations shifting towards the more deuterium-exchanged state over time, reporting on the propensity of that region to undergo conformational switching [51, 54].

In the case of SF162, the Env where we observed the most abundant number of bimodal spectra, we assessed the contribution of any non-native sub-populations to be at most <9%. By all biochemical and ns-EM assays, this material was indistinguishable in purity and homogeneity from the other trimer preparations in our study. HDX-MS, however, is much more sensitive to conformational heterogeneity. In order to distinguish between static conformational heterogeneity such as might exist due to the presence of a misfolded species, and conformational dynamics that may involve the Env trimer switching between conformational states, we quantify the relative abundance of the populations over time. Bimodal spectra where the protected population does not change in percent abundance with time is indicative of sample impurity [37]. We observed a minor subpopulation of misfolded trimers or aggregate (5-10%) at peptides that are part of the gp120/gp41 interface, which we have shown previously to be a good marker for well folded trimers (Figure S4.5) [55]. Sample heterogeneity can easily be visualized and distinguished from EX1 or mixed EX1/EX2 kinetics using bubble plots. The majority of bimodal spectra across the SF162 trimer are suggestive of conformational switching, however, in regions where 5-10% of the protected population has not transitioned to the exposed state after 20 hours, we cannot rule out the contribution of sample aggregate or some non-native conformation.

Indeed, among the entire panel of Env trimers, SF162, had the most abundant number of bimodal spectra (Figure 4.4, Figure S4.5). The majority of bimodal spectra across the SF162 trimer are indicative of conformational transitions between two states. Regions in the SF162 trimer that showed signs of conformational switching include the gp120 inner domain helix

(peptide 1, Figure 4.4) and the bridging sheet at the base of V1, which forms part of the binding site for co-receptor when Env samples an open conformation (peptide 2, figure 4.4). Bimodal spectra in the gp120 inner domain layer 1 (peptide 2 Figure S5) suggests frequent transitions from a protected to an exposed conformation. Both the V2 and V3 loops exhibit bimodal spectra suggestive of conformational switching (Figure 4, Figure S4.5) [56]. Similar regions, including residues that form part of the CD4 binding site (Figure S4.5), interconvert between at least two distinct conformations. In gp41, the fusion peptide is typically very exposed and disordered on most static structures, with few exceptions [57, 58]. SF162, however, has a fusion peptide that is protected and gradually takes on deuterium (Figure 4.3). The adjacent fusion peptide proximal region (FPPR, Figure S4.5) also samples two distinct conformations, but over a slower timescale. In the base, gp41 subunit both HR1 and HR2 helices predominantly exist in a more protected conformation, but transiently sample a significantly more exposed conformational state. SF162 thus appears to be a highly dynamic, labile Env trimer, with transient exposure of interfaces and epitope motifs that often are more ordered and protected in neutralization resistant Envs.

Surprisingly, and in contrast to the hypothesis that associates neutralization resistance with an Env always adopting a closed, prefusion organization, conformational switching and bimodal mass spectra were also observed in some harder to neutralize tier 2 isolates, though in a more localized fashion than seen in the Tier 1a SF162 trimer. Three of the tier 2 isolates contain regions that appear to sample at least two distinct conformational states; BJOX2000, CE1176, and CH119. CE1176 only appears to undergo detectable conformational transitions in the base gp41 subunit (Figure S4.6) similar to what we have observed previously, though its V1/V2 apex also appears to exhibit a relatively high level of dynamics without showing clear bimodal spectra, suggesting rapid, transient local structural fluctuations in V2 in this case (Figure 2, peptide 4.5) [33]. Similarly, bimodal spectra are observed in BJOX2000 Env, which

interconverts between a protected and more exposed conformation in the base HR1 and HR2 helices, but also undergoes a conformational transition in the gp120 apex in an area that is part of the CD4 binding site.

Unexpectedly, the harder to neutralize tier 2 isolate, CH119, exhibits multiple regions across the apex and base that undergo conformational switching over a range of timescales (Figure 4.5). These regions include the gp120 inner domain helix, the base of V1/bridging sheet, the V3 loop, the CD4 binding site, and HR1 and HR2 at the trimer base. Many of these regions in CH119 sampling distinct conformations are in similar regions as SF162 and a tier 1B neutralization sensitive isolate we previously characterized, AMC008 (Figure 4.5) [33].

These data indicate that neutralization resistant HIV-1 isolates do not necessarily bear Env trimers that stably maintain an inert, closed prefusion conformation, as has been previously hypothesized [2, 6].

4.3.3 Dynamic profiles of Tier 1 versus Tier 2 isolates correlate with neutralization sensitivity to antibodies

In order to assess the linkage between antibody neutralization activity and the structural dynamic properties we identified, neutralization assays using monoclonal IgGs targeting epitopes throughout Env were performed (Table 4.1). Comparing trends in diverse trimer dynamics against antibody-mediated neutralization using individual mAbs is more straightforward and removes many of the confounding variables present in interpreting neutralization resistance assigned using pooled polyclonal serum from infected donors.

Tier 1 and Tier 2 pseudoviruses exhibited markedly different neutralization profiles. The Tier 1 viruses, SF162 and BXO8, were highly susceptible to antibody-mediated neutralization using most bnAbs, as well as antibodies typically considered weakly or non-neutralizing; including antibodies specific for the tip of the V3 loop (447-52D, 3074, 3869), antibodies specific

for a part of the V2 loop that overlaps a posited integrin binding site (V2i epitope; 2158, 830A), an antibody specific for the co-receptor binding site that is formed in the open state (17b), and an antibody specific for a partially open state (b12) [59-63]. Peptides comprising these epitopes exhibited a high degree of structural dynamics by HDX-MS, consistent with substantial exposure and accessibility to solvent and as a result, to antibodies.

By contrast, the antibodies that are specific for the open and partially open states were unable to neutralize Tier 2 pseudovirus, even those that exhibited elevated structural dynamics, such as CH119 and CE1176. V3 tip targeting antibodies, generally were unable to neutralize most Tier 2 viruses, although the 25710 virus was an exception, exhibiting measurable neutralization by 3074 IgG, which is consistent with previous neutralization studies, though at higher concentrations compared to the tier 1 isolates [8].

4.3.4 Native-like trimers derived from diverse isolates with a range of neutralization sensitivities tend to bind more mAbs than can neutralize the corresponding psuedovirus

While SOSIPs are widely regarded as structurally and antigenically similar to native Env, the engineered modifications, though somewhat limited, and absence of presentation on a membrane could potentially influence their conformational and antigenic profiles. Sanders et al demonstrated a correlation between the BG505 SOSIP-antibody binding via ELISA (EC_{50}) and virus neutralization (IC_{50}) and de la Pena et al demonstrated a similar correlation between the SOSIP antigenicity and virus neutralization for the neutralization sensitive AMC011 isolate (though some antibodies were outliers) [64, 65]. We compared antigenicity in terms of equilibrium dissociation affinity constants (K_Ds) as determined by BLI for the present panel of native-like trimers with their corresponding antibody-mediated neutralization IC50's determined using pseudovirus neutralization assays (Figure 4.6, tables 4.1 and 4.2, Figure S4.7). bnAbs (such as VRC01, PGT145, PG16, and PGT121) generally were able to bind the SOSIP and

neutralize the corresponding virus showing expected congruence of SOSIP antigenicity and neutralization of pseudotyped HIV-1 viruses-bearing native Envs.

Unexpectedly, a number of instances were identified where an antibody was able to bind the SOSIP construct but not neutralize the corresponding virus. The majority of these antibodies were non- or weakly neutralizing and targeted sites such as the tip of the V3 loop, the V2i epitope, or were specific for a partially open or fully open state (b12 or 17b) (Tables 4.1 and 4.2). Likewise, the gp120/gp41 interface-specific bnAb 35022, was able to bind most SOSIPs, but not neutralize the corresponding pseudoviruses.

These data demonstrate that while SOSIPs generally are relatively close mimics of the native Env proteins, they can exhibit differences in antigenic profile, which are important to consider when approaching the use of such constructs as possible vaccine immunogens, for example.

4.4 Discussion

4.4.1 Coming to grips with HIV-1 Env structural variation

HIV-1 Env variation poses one of the defining challenges to the immune system that has confounded efforts to develop an HIV-1 vaccine. It is widely thought that an effective vaccine would need to elicit neutralizing antibodies that are active against a broad swath of Env variants found on diverse HIV-1 isolates. We posit that to understand how broadly neutralizing antibodies perform their remarkable functions, it is necessary to understand how they cope with variation manifested in their cognate target, either through recognition of conserved features in the midst of variable contexts or through plasticity and tolerance of variation in paratope-epitope interactions. To date however, our understanding of HIV Env structural variation has been

lacking, despite significant advances in high-resolution structural analysis of a limited set of well-behaved Env trimers [13, 14, 66].

Structures of Env determined by cryo-EM and X-ray crystallography have elucidated a subset of conformational states of the Env glycoprotein trimer, however, the majority of structures are based on the subtype A BG505 isolate, and these predominantly have examined Env in its prefusion, closed state [13]. Many studies have used engineered trimers that often are hyperstabilized to quench structural dynamics and completely lock in a prefusion closed conformation [66-68]. Additionally, the majority of available structures are determined with tightly bound antibody Fabs, resulting in the normally dynamic assembly being further constrained in a static conformational state [13]. Here we applied structural mass spectrometry to a diverse panel of native-like Env trimers representative of global HIV diversity with the aims of: 1) investigating the range of conformational and structural dynamic variation across Env sequence diversity space, thus providing new insights into the extent of structural variation among antigenically diverse Env, 2) structurally characterizing the nature of Tier 1 HIV-1 isolates, which are frequently used as references strains in assessing nAb and serum neutralization activity, but have lacked structural characterization, 3) testing the hypothesis that neutralization sensitivity is linked to an Env trimer's dynamic phenotype, and 4) increasing our mechanistic understanding of how differences in epitope structural ordering and dynamic variation impact antibody binding.

From HDX-MS analysis of a large panel of native-like HIV-1 Env trimers, we identified dramatic differences in structural ordering throughout the Env trimers including in regions targeted by bnAbs as well as what are typically thought of as non-neutralizing, less desirable epitopes. These differences were especially pronounced between Tier 1a/1b and Tier 2 viruses, but importantly, notable variation was also clearly evident among Tier 2 Envs as well. Unexpectedly, the regions with the largest differences in dynamics across our diverse panel of trimers were regions where the sequence is fairly conserved. This highlights the role that a

conserved peptide segment's tertiary and quaternary context plays in modulating its specific structural dynamics and local stability.

4.4.2 The structural profile of neutralization-sensitive Tier 1 Envs

We first sought to determine if these large differences in dynamics across trimers correlates with neutralization phenotypes as they suggest that epitope stability and accessibility may be dramatically different across different isolates. Indeed, drastic differences in dynamic phenotypes were observed between trimers derived from the Tier 1 and Tier 2 viruses indicating structure-based properties that underlie their high degree of sensitivity to antibody-mediated neutralization. Both SF162 (Tier 1A) and BX08 (Tier 1B) Env trimers exhibited a measurably more dynamic phenotype in key regions relative to Env from Tier 2 isolates (Figure 4.3). The HR1 helix exhibited elevated dynamics relative to the Tier 2 trimers. Likewise, the N and C termini of gp120, which are held by the gp41 base that wraps around these segments in the prefusion trimer, were considerably more dynamic in SF162 and BX08 Env, indicating that these trimers are likely more labile and may be more prone to shedding of the gp120 subunits. Wang et al have pointed out that the gp120 N and C termini regions likely undergo a pivoting motion to get from the static closed trimer state to the outwardly rotated gp120 conformations observed in open and partially open trimers [14], thus we speculate the increased dynamics in the tier 1 isolates could suggest more frequent pivoting motions around the β4 and β26 strands. Additionally, the gp120 inner domain helix and V3 loop exhibited elevated dynamics in the Tier 1a and 1b isolates. We observed a similarly dynamic phenotype in the tier 1B AMC008 trimer we previously characterized using HDX-MS [33]. This correlates well with the observations that Tier 1 isolates are highly susceptible to neutralization by HIV patient serum that is generally rich in antibodies against the immunodominant V3 epitope [6-8].

The most neutralization sensitive SF162 trimer was found to bear the greatest abundance of regions across the trimer structure that sample two distinct conformations on a slow time scale (in comparison to the labeling rate) as indicated by bimodal spectra. Interestingly, these regions exist in distinct conformations in open and closed trimer structures (Figure S4.5), suggesting that SF162 trimers undergo conformational sampling between a closed prefusion state and a state that is reminiscent of CD4-induced, open conformations. This is in agreement with the high affinities measured here using BLI for antibodies specific for open conformations (table 4.2). For example, the gp120 inner domain bimodal spectra suggest a relatively fast timescale transition from the closed to the exposed state (bimodal spectra only present at the 3 sec timepoint in peptide residues 53-69) suggesting frequent conformational switching events. This region (residues 53-69) is disordered in pre-fusion closed trimers, but has been shown to exist as a stable helix (α0 helix) in CD4 bound open trimer structures and is a region targeted by SOSIP hyperstabilizing mutations designed to suppress dynamics described elsewhere [14, 33, 66]. Parts of the bridging sheet (peptides 112-126 and 423-433) that are more disordered in closed trimers, but become a 4-stranded beta sheet in open trimers, undergoes a slow timescale transition from a protected to an exposed conformation where bimodal spectra are observed from 3 seconds up to 20 hours, which suggests infrequent conformational switching. Both the V2 and V3 loops are regions that have been captured via EM and X-ray crystallography in distinct conformations, and both these regions exhibit bimodal spectra in SF162 suggesting a moderate to slow timescale transition from a protected to a more exposed conformations (Figure 4.4, Figure S4.5) [56, 69].The vast majority of prefusion closed structures reveal the fusion peptide to be highly disordered and solvent accessible, with a few exceptions [57, 58]. SF162 however exhibits a trimer with a fusion peptide and FPPR that samples a more protected conformation in solution (peptides 511-519 and 520-536). Static structures of partially open trimers suggest the fusion peptide can take on more helical conformations [14]. Additionally, we observe the interconversion between two conformations in

peptides that are part of the HR1 and HR2 helices across a slow timescale indicative of infrequent conformational switching events. In the comparison of closed and open trimer structures the HR1 helix is more extended and adopts a more helical structure in the open trimer structures [14].

Notably the other more neutralization resistant tier 1 isolate, BX08, did not show any indication of localized conformational switching on the range of timescales we probed, though as noted above, elevated solvent accessibility in several regions were observed. This indicates either that those regions are persistently more exposed or if conformational switching between a closed prefusion and open state is occurring in BX08, it is on a time scale faster than the time scale of intrinsic deuteration for the given peptide sequence [37, 51]. These differences between SF162 and BX08 trimer behaviors underscores variant specific idiosyncracies of Envs among Tier 1 isolates. We previously characterized the tier 1B AMC008 trimer, which did exhibit numerous regions in the trimer apex and base that exhibited signs of conformational switching that explained this trimer's affinities for antibodies specific for the open and partially open conformational states. Thus from a structural dynamics and antigenicity perspective, AMC008 trimers seem more similar to SF162 trimers than BX08. These dynamic differences between tier 1 virus trimers highlights intra-tier 1 diversity that may help explain differences in neutralization sensitivities and soluble trimer antigenicities between tier 1a SF162 and tier 1b BX08 isolates.

4.4.3 Neutralization resistant isolates do not universally maintain a closed, prefusion structure

Next, we asked whether the diverse Tier 2 isolates show convergence of their dynamic phenotypes. In the global panel, these isolates are generally more resistant to neutralization by pooled human serum from infected donors in comparison to the tier 1 isolates, and it was hypothesized that tier 2 native-like trimers would preferentially adopt a closed, prefusion state [6, 27]. Surprisingly, significant structural dynamic variation was observed throughout Tier 2 Env

trimers. Some of the regions with substantial dynamic variation overlapped with regions that differed substantially between Tier 1 and Tier 2 trimers. These regions included the V3 loop, the V2 loop (reported by residues 176-179), and the CD4 binding site. Indeed, both the V3 loop and CD4 binding loop are functionally essential due to their role in receptor binding, and thus constrained in ability to mutate. These regions have also been shown to exist in multiple conformations in open and closed structures [70, 71]. It has been suggested from MD simulations that the V3 loop can flicker out from under the V1/V2 trimer apex independently of V1/V2 [56, 72]. Similarly, The V2 loop has been shown to be capable of adopting a range of conformations seen in cryo-EM and crystal structures of the V1/V2 loops, often in complex with antibody Fabs, presented on native like trimers or scaffold proteins [69, 72, 73]. The base of V1, which is also part of the bridging sheet, and the conformational CD4 binding site peptides also exhibited considerable dynamic variation across tier 2 trimers. Likewise, in the functionally essential fusion machinery at the trimer base, the core HR1 helix showed dramatic differences in stability across the diverse HIV isolates, despite high sequence conservation. Thus significant structural variation is observed among Tier 2 Env, suggesting that the hypothesis that they uniformly adopt, stable trimers that maintain a relatively similar, dynamically inert closed, prefusion state is somewhat of an over-simplification.

4.4.4 Dynamics of Env trimers from neutralization resistant tier 2 viruses do not explain differences in their neutralization phenotypes

We next wanted to see if the differences in dynamics across tier 2 isolates might correlate with the broad range of neutralization sensitivities assigned to the tier 2 isolates in the global panel using pooled serum from infected donors. The most obvious place to look seemed to be the V3 loop, because it is the most highly immunodominant region on the trimer, and it has been shown that polyclonal sera is often rich in anti-V3 loop antibodies [6-8]. Additionally there

is antigenic evidence from Han et al that V3 Abs specific for open conformations can neutralize subsets of tier 2 ranked viruses [8]. We hypothesized that neutralization sensitivities would correlate with V3 loop accessibility. However, across the tier 2 isolates, there did not seem to be a clear correlation between neutralization sensitivity and V3 loop flexibility as measured by HDX-MS applied to the native-like trimers. The most neutralization resistant tier 2 isolate, CNE55, had the most exposed V3 loop, while the most neutralization sensitive tier 2 isolate, 25710, had the most protected V3 loop, and other trimers did not follow any clear trends in tier 2 assignment. We checked other antigenic sites across the trimer structure for trends between epitope dynamics and neutralization resistance. Similarly there were no clear trends focusing on V2 loop dynamics, where roughly 20% of infected individuals that generate bnAb responses have V2 apex directed antibodies in their serum [74]. Checking for similar trends between local dynamics including antigenic sites across the rest of the trimer structure, such as the bridging sheet, and the CD4 binding site for example, also did not suggest any clear correlations that could explain differences in rank order of tier 2 virus neutralization sensitivities. Indeed, other factors including glycosylation, differences in epitope sequence and charge, length of the variable loops make neutralization susceptibility multi-factorial and complex. Additionally we measured dynamics using soluble native-like Env trimers and not membrane-bound Env, where differences such as glycosylation and the presence of the cytoplasmic domain could lead to subtle differences in conformation or antigenicity [75, 76]. Further complicating matters is the fact that the neutralization phenotypes across the panel isolates were assigned using pooled polyclonal serum, where many antibodies binding to multiple distinct regions on Env may have synergistic or antagonistic effects depending on the structural context.

4.4.5 Env structural dynamics and antibody binding

Data presented here also provides novel insights into how trimer dynamics influence IgG recognition. The antibody 17b is specific for the exposed co-receptor binding site only present

when Env samples an open conformation. 17b was only able to bind to soluble trimers that exhibited signs of conformational switching in the gp120 inner domain helix, the bridging sheet, or the CD4 binding site, including SF162, CH119, and BJOX2000. This is consistent with our previous structural study that included the AMC008 trimer, which exhibited signs of conformational switching in the trimer bridging sheet and also bound 17b IgG [33]. Env trimers with bimodal spectra in the V3 loop were able to bind much more tightly (low nM affinities) to antibodies specific for the tip of V3 (3869, 3074, and 447-52d IgG), which likely is due to this region frequently sampling a more IgG accessible conformation. Reinforcing the idea that epitope dynamics can impact antibody recognition, we have observed a correlation between apex trimer dynamics in the V2 loop with antibody association rates using the conformation specific bnAb, PGT145 (chapter 3). However, in other regions of interest across trimers with differences in local dynamics, such as the CD4 binding site, a clear correlation was not observed between trimer epitope dynamics and antibody recognition. We speculate this may be because bnAbs have already evolved to better be able to cope with large differences in epitope presentation and context including in terms of local structural dynamics. By definition, they are antibodies that are capable of managing Env diversity.

We observed a number of instances where antibodies were able to bind our SOSIP trimers, but they were unable to neutralize the corresponding pseudovirus (Figure 6, Figure S7, tables 1-2). Other groups have made similar observations, for example Landais et al. noted instances where binding of the SOSIP trimer did not match neutralization of the corresponding Env clone presented on the virus [77]. This appears to be the case for V3 tip targeting and other non- or weakly neutralizing antibodies. The second most neutralization resistant isolate CH119 in particular had a salient mismatch between soluble trimer antigenicity and pseudovirus neutralization profile. The CH119 trimer exhibited multiple regions in the apex that transition between two distinct conformational states, as reflected by the observed bimodal spectra, and

that explains this trimer's affinity for Abs specific for the open and partially open states. The recombinant trimers may embody a difference relative to CH119 trimers presented on a pseudovirus since the neutralization sensitivity of the pseudotyped CH119 isolate against a panel of nAbs was rather different compared to the recombinant, soluble CH119 trimer antigenicity measured by BLI. Previous studies have noted differences between SOSIPs and native Env on membranes. smFRET studies of a limited set of Envs have indicated that the two forms of trimer exhibit different population distributions among conformational states at equilibrium [30, 78]. Alternatively, differential glycoforms on the trimers may underlie differences in antigenicity of SOSIP trimers and neutralization profiles of pseudotyped virus. In some cases, SOSIPs have been shown to harbor a higher percent abundance of high mannose glycans than Env presented on a membrane [79-81], which may influence binding of some antibodies that are selective for specific glycoforms in their epitopes. Lastly, the length of time of the antibody-Env incubation may be an important factor. Here, and in general, the viruses were incubated with IgG for 30 minutes in neutralization assays used for this study, but it has been noted by other groups that some HIV antibodies need to be incubated for over 12 hours in order to see any antibody-mediated neutralization [82]. Indeed in previous work using HDX-MS to examine a subtype B SOSIP trimer, we observed that some epitopes in Env sample distinct conformational states on a slow timescale on the order of several hours [33]. For our BLI experiments using immobilized weakly or non-neutralizing nAbs, we often had to start our Env dilutions at very high concentrations (up to 2,000nM) to observe measurable binding signal. Conversely, there is likely considerably less Env present on the surface of psuedotyped virus in neutralization assays. The larger amount of Env trimer present in the BLI experiments may increase the probability that a subpopulation of trimers in solution have sampled an IgG accessible conformational state, especially in regard to some of the slow timescale conformational transitions we have observed using HDX-MS.

That being said, SOSIPs are currently the best mimic of native Env trimers on the virus surface to date, and SOSIPs derived from numerous isolates have been shown to generally match their corresponding Env structure and antigenicity [38, 65]. A recent study that included data from HDX-MS experiments of soluble Env BG505 trimers and Env presented on a VLP suggests key regions share similar structural dynamics across the trimer structure especially in the gp120 subunit [9]. Even in cases where antibody-SOSIP binding does not match membrane Env neutralization, from a broader perspective, comparing soluble SOSIP antigen epitope dynamics against antibody binding kinetics could still be useful to gain a more fundamental understanding of how epitope dynamics influence IgG recognition.

Interestingly we observed a strong correlation between the soluble SF162 trimer (SOSIP) antigenicity and membrane bound SF162 Env neutralization IC50's (Figure S4.7). A correlation between tier 2 soluble trimer antigenicity and pseudovirus neutralization by the corresponding antibodies was harder to determine, because the majority of the non- or weakly neutralizing antibodies did not neutralize the virus within the concentrations and incubation times used in this study so there are too few data points to determine a trend.

4.4.6 Env structural diversity and implications for Env as an antigenic target

In summary, our HDX-MS data presented here further our mechanistic understanding of the idiosyncratic nature of trimers across genetically diverse HIV viruses. Some isolates have trimers that are more flexible than others, but this is largely regional specific on the trimer structure in an isolate dependent manner. Some trimers like SF162 and BX08 tend to have a more dynamic phenotype in key regions, and SF162 exhibits many regions that sample distinct conformations. Increased exposure of regions like the gp120-gp41 interface, the tip of V3, or the bridging sheet that is part of the co-receptor binding site in the open state may help explain their tier 1/neutralization sensitive phenotypes in comparison to trimers derived from the harder to

neutralize tier 2 isolates. It has also been hypothesized that Tier 2, neutralization resistant Envs preferentially maintain a closed, prefusion state with conserved epitopes, such as the V3 crown and co-receptor binding site, conformationally masked from antibodies. Here, we find that trimers from Tier 2 viruses are considerably more structurally and dynamically variable than the previously proposed model would suggest. Instead, some Env such as those from CE1176 and CH119, both relatively far into the neutralization resistant spectrum, are highly dynamic and capable of exhibiting dynamic switching similar to, if not as widespread and dramatic as SF162 tier 1a trimers.

It is interesting that trimers derived from the harder to neutralize viruses can also be highly dynamic in many regions targeted by antibodies, and also show signs of conformational switching, such as CE1176, BJOX2000, and CH119 trimers. However, within the tier 2 isolates we did not observe any clear trends linking local trimer dynamics to the broad spectrum of neutralization sensitivities assigned to the diverse tier 2 isolates. Clearly other factors play an important role in determining an isolate's neutralization phenotype, such as glycosylation, variable loop length, epitope sequence, charge interactions, and these myriad viral signatures have been well studied elsewhere [8, 23].

This study is unique in that it presents isolate specific differences in dynamics with high sequence resolution using trimers from isolates that are representative of the global diversity of HIV. The impact of large sequence diversity on fusion protein dynamics is likely applicable to other viral fusion proteins with high mutation rates, such influenza and SARS-CoV-2. Indeed, biophysical studies have demonstrated strain specific differences in fusion protein dynamics in both influenza and SARS-CoV-2 [54, 83, 84]. These data may help inform selection of Envs for use as immunogens for example.

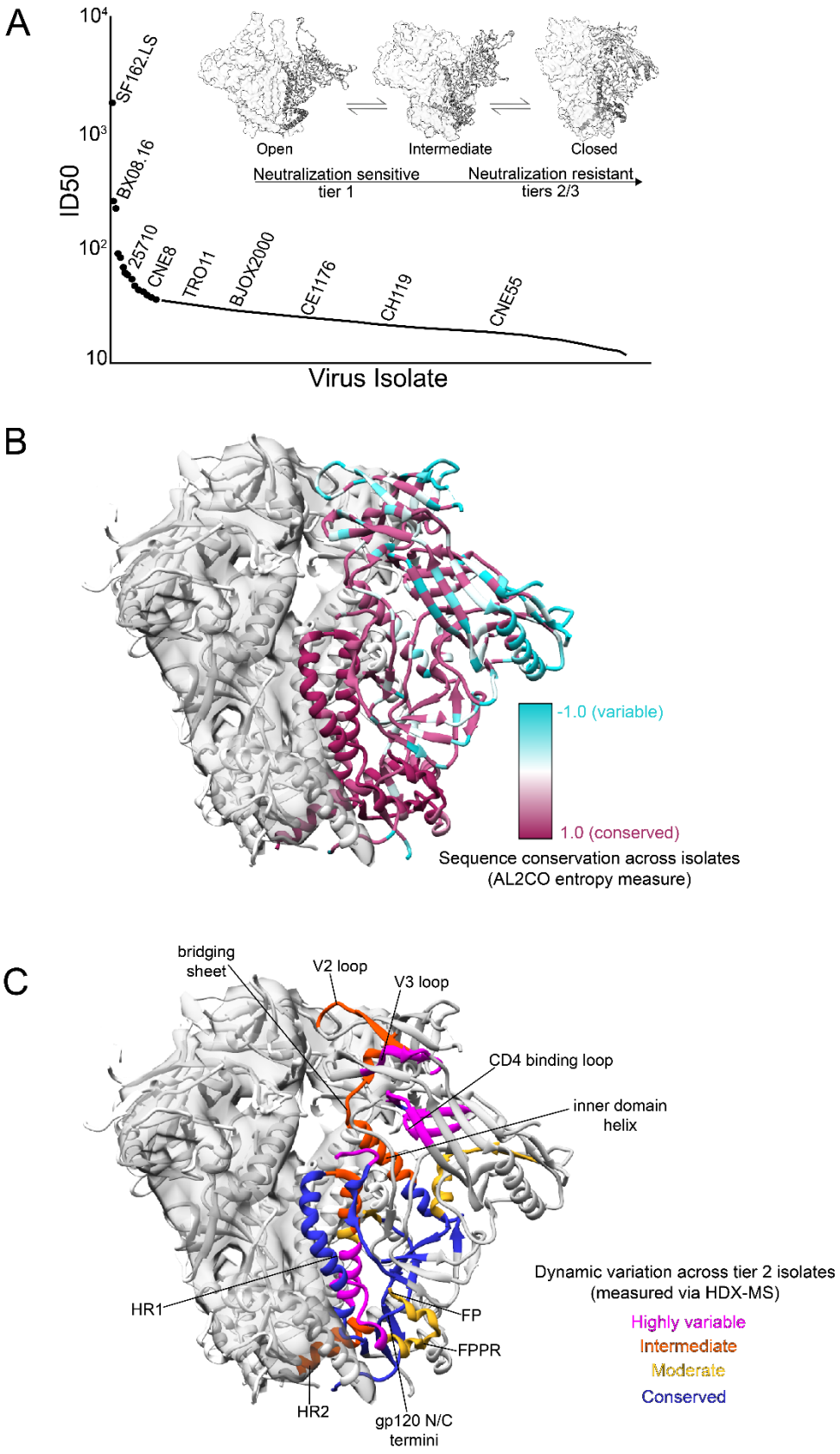
A
ID50
Virus Isolate
SF162.LS
BX08.16
25710
CNE8
TRO11
BJOX2000
CE1176
CH119
CNE55
Open
Intermediate
Closed
Neutralization sensitive
tier 1
Neutralization resistant
tiers 2/3
B
-1.0 (variable)
1.0 (conserved)
Sequence conservation across isolates
(AL2CO entropy measure)
C
bridging sheet
V2 loop
V3 loop
CD4 binding loop
inner domain helix
HR1
FP
FPPR
HR2
gp120 N/C termini
Dynamic variation across tier 2 isolates
(measured via HDX-MS)
Highly variable
Intermediate
Moderate
Conserved

Figure 4. 1. Env trimers from genetically diverse isolates with a range of neutralization sensitivities exhibit dramatic differences in dynamics, even in regions with conserved sequence homology. Figure A is adapted from deCamp et al and indicates the neutralization phenotype of isolates that we were able to purify Env trimers from for subsequent analysis [2]. The current hypothesis is that more neutralization sensitive isolates more frequently sample an open state (PDB 3J70) or partially open state (PDB 5V8L) compared to harder to neutralize tier 2 and 3 viruses, which spend more time in a closed conformation (PDB 5ACO). Figure B maps the amino acid sequence homology onto the trimer structure (PDB 5FUU, 2/3 protomers displayed in gray ribbon and surface, and 1 protomer displayed in colored ribbon) using an AL2CO entropy measure in Chimera [85]. Cyan indicates regions with large differences in sequence frequencies across the Env panel, and areas colored magenta indicate conserved sequence homology (related to the sequence alignment in figure S4.2). In figure C the pooled variation in dynamics (the sum of the average %standard deviation for each isolate at each HDX timepoint) measured at the peptide level using HDX-MS is mapped onto the trimer structure (PDB 5FUU) revealing which regions exhibited similar dynamics across the tier 2 isolates (blue and yellow), and which regions exhibited large differences in dynamics (pink and orange).

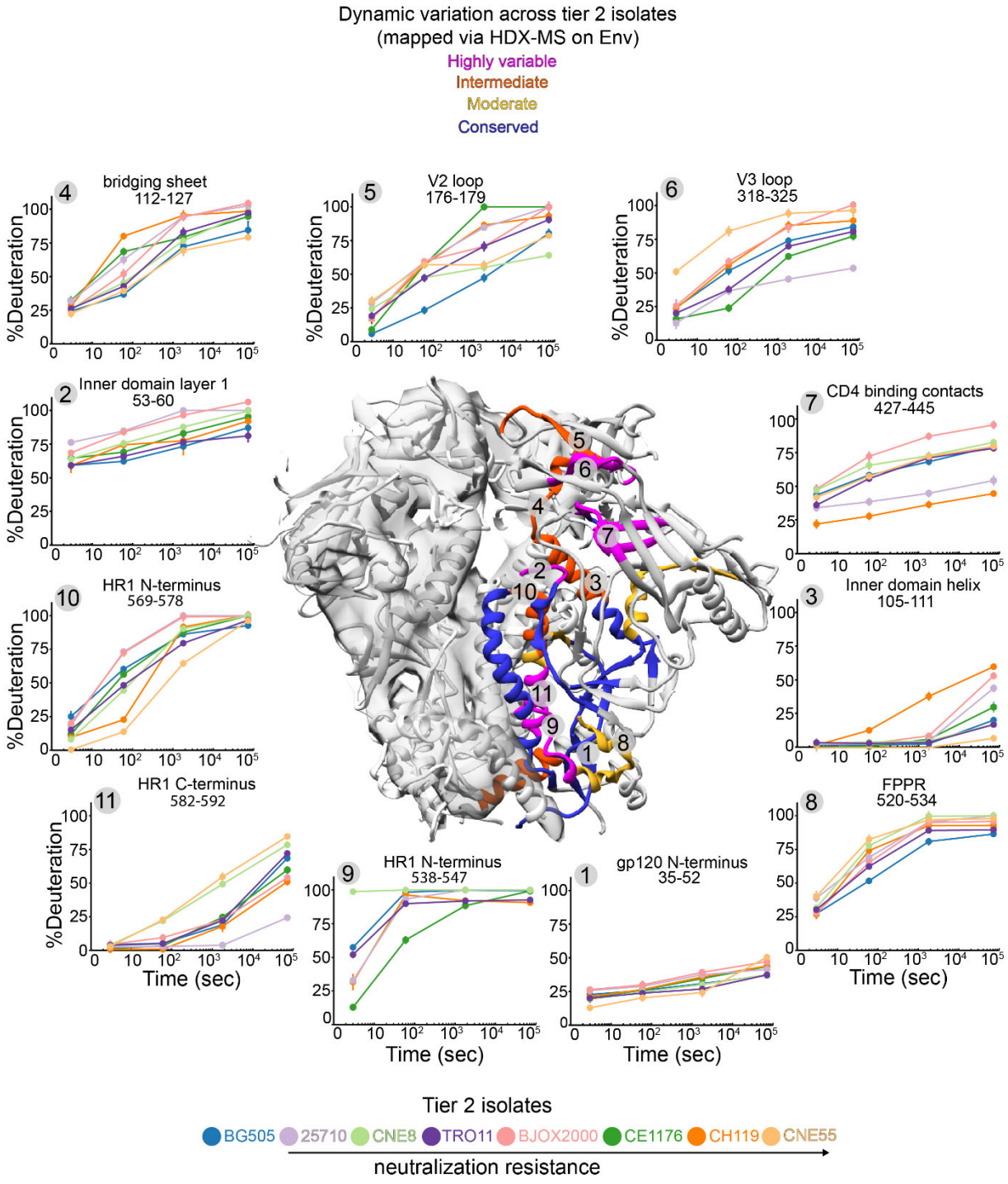
Dynamic variation across tier 2 isolates
(mapped via HDX-MS on Env)
Highly variable
Intermediate
Moderate
Conserved
4 bridging sheet 112-127
5 V2 loop 176-179
6 V3 loop 318-325
2 Inner domain layer 1 53-60
7 CD4 binding contacts 427-445
10 HR1 N-terminus 569-578
3 Inner domain helix 105-111
11 HR1 C-terminus 582-592
9 HR1 N-terminus 538-547
1 gp120 N-terminus 35-52
8 FPPR 520-534
%Deuteration
Time (sec)
Tier 2 isolates
BG505 25710 CNE8 TRO11 BJOX2000 CE1176 CH119 CNE55
neutralization resistance

Figure 4. 2. Isolate-specific variation in dynamics across Env trimers derived from a global panel. Deuterium uptake plots of homologous peptides from trimers across the global panel are shown. Each HDX uptake plot consists of the average percent deuteration of at least two replicates after 3 seconds, 1 minute, 30 minutes, and 20 hours of exchange normalized to a fully deuterated control with error bars reporting average percent standard deviation. All homologous peptides contain the same number of exchangeable backbone amides across the eight tier 2 isolates. Isolates are indicated by a circle and solid line (BG505 dark blue, 25710 light purple, CNE8 light green, TRO11 dark purple, BJOX2000 pink, CE1176 dark green, CH119 dark orange, CNE55 light orange). In each uptake plot, the homologous peptide sequence is based on HXB2 numbering and the sequences are aligned in figure S4.2.

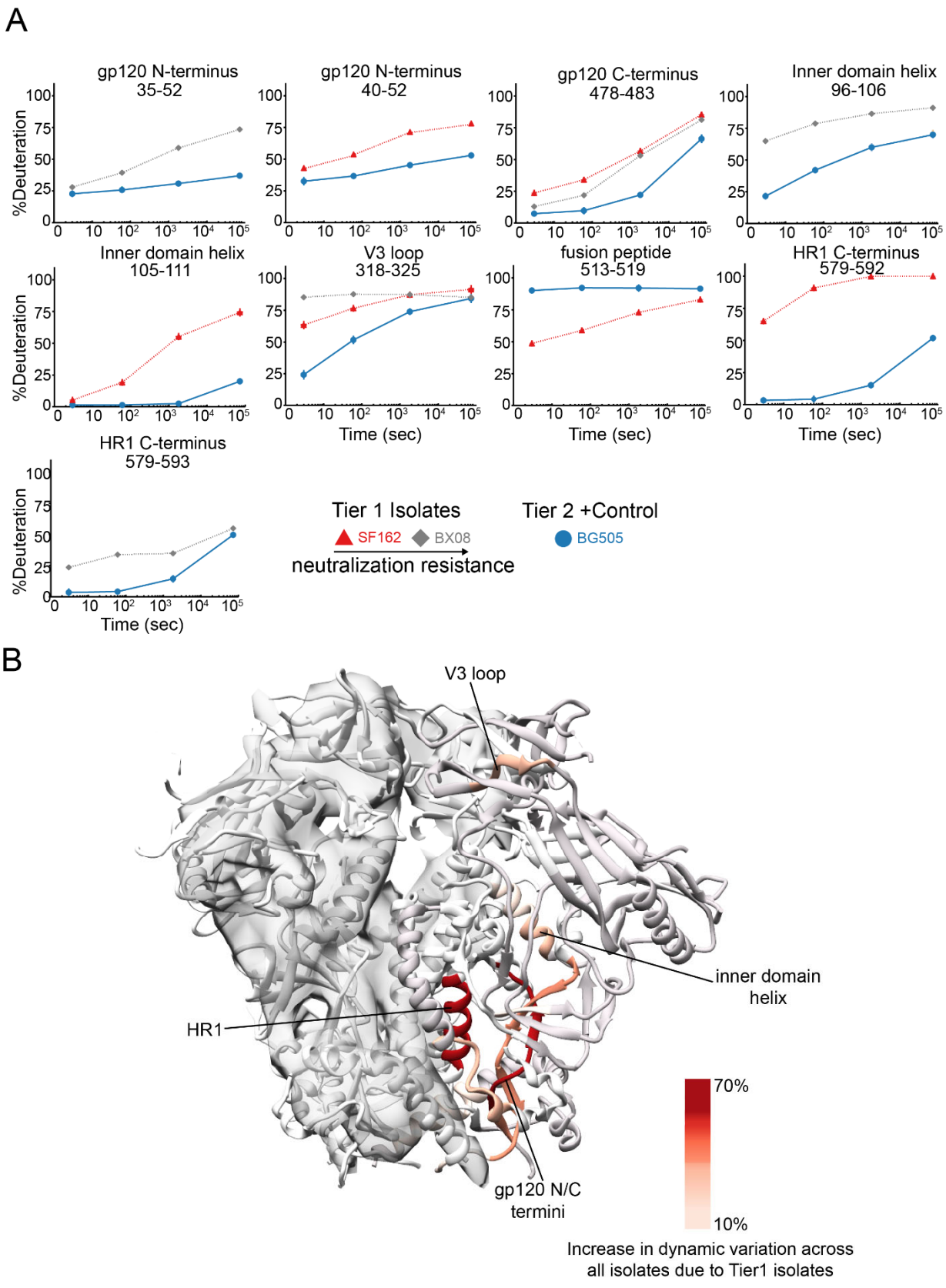
A
gp120 N-terminus 35-52
gp120 N-terminus 40-52
gp120 C-terminus 478-483
Inner domain helix 96-106
Inner domain helix 105-111
V3 loop 318-325
fusion peptide 513-519
HR1 C-terminus 579-592
HR1 C-terminus 579-593
%Deuteration
Time (sec)
Tier 1 Isolates
SF162
BX08
Tier 2 +Control
BG505
neutralization resistance
B
V3 loop
inner domain helix
HR1
gp120 N/C termini
70%
10%
Increase in dynamic variation across all isolates due to Tier1 isolates

Figure 4. 3. Tier 1 isolates exhibit increased dynamics compared to the tier 2 isolates in some key regions. A) Deuterium uptake plots of homologous peptides comparing the tier 1 isolates SF162 (red triangle), BX08 (gray diamond) and the tier 2 positive control BG505 (blue circle). Each HDX uptake plot consists of the average percent deuteration of at least two replicates after 3 seconds, 1 minute, 30 minutes, and 20 hours of exchange normalized to a fully deuterated control with error bars reporting average percent standard deviation. B) The differential heatmap indicates the difference between the variation (pooled HDX standard deviation) of all isolates (tiers 1 and 2) subtracted from the variation measured in only the tier 2 isolates to highlight regions where the tier 1 isolates significantly increase variation in dynamic behavior mapped onto the trimer structure (PDB 5FUU, 2 protomers displayed in surface and 1 protomer displayed in ribbon).

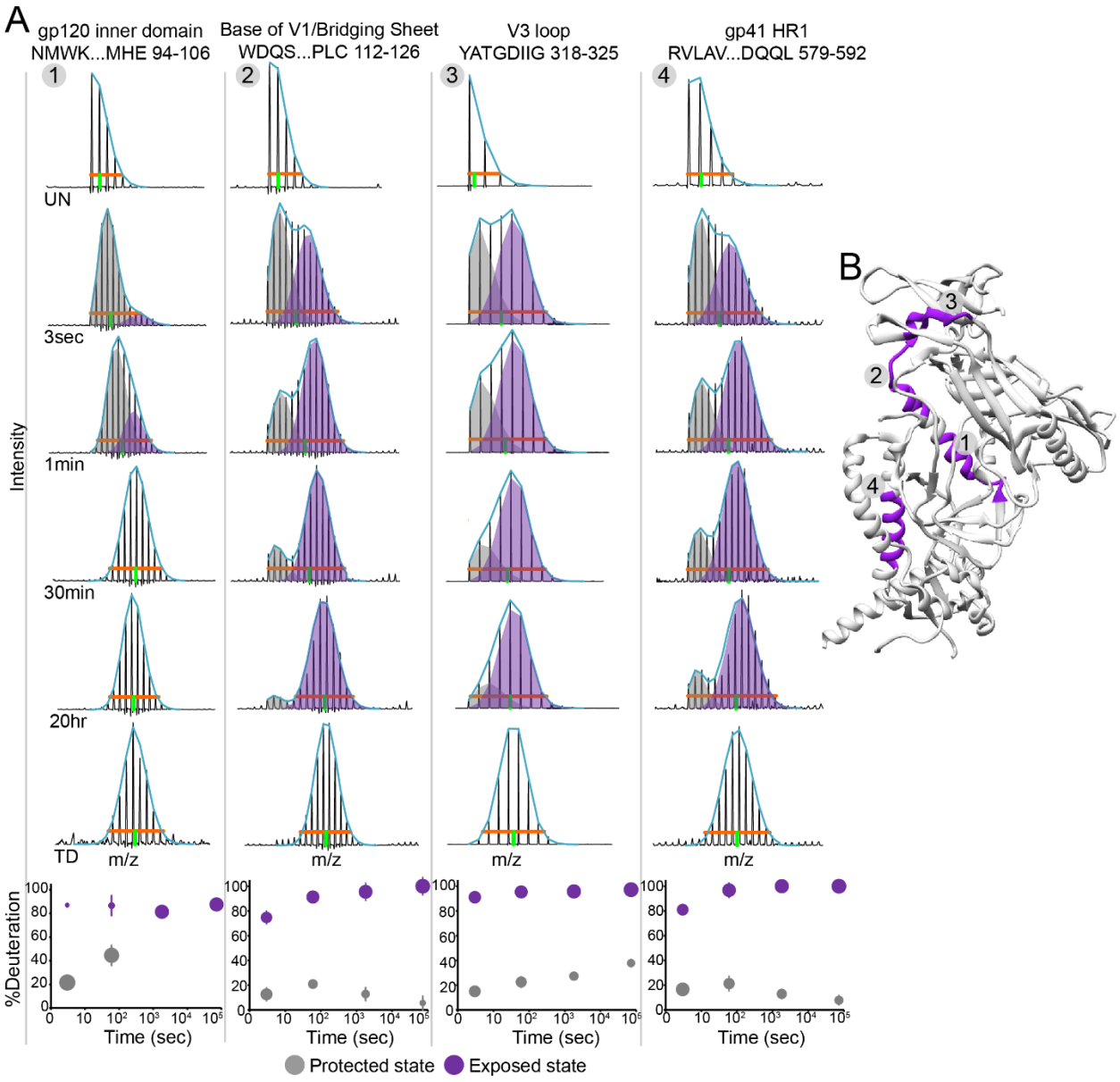

Figure 4. 4. The most neutralization sensitive isolate trimer (tier 1A SF162) exhibits the largest number of regions with bimodal spectra indicative of the interconversion between two distinct conformations. Related to figure S4.5. **(A)** Bimodal spectra in peptides across the SF162 trimer reveal localized conformational switching. The mass envelopes at each deuteration time point are shown, as well as the undeuterated (UN) and totally deuterated controls (TD). The width of each isotopic distribution is displayed as a horizontal orange line and each centroid is the vertical green line. Unusually broad spectra were binomially fit to two

populations; a protected state in gray, and an exposed state in purple. The cyan curve above each spectrum is the summation of each binomial fit. At the bottom of the spectra of each peptide are bubble plots that better characterize the transition from the protected (gray) to the exposed state (purple) across time. The size of the bubble corresponds to the percent abundance of the population at that point in time. **(B)** The location of the regions undergoing conformational switching are highlighted on the structure in purple (one protomer in ribbon diagram PDB 5FUU).

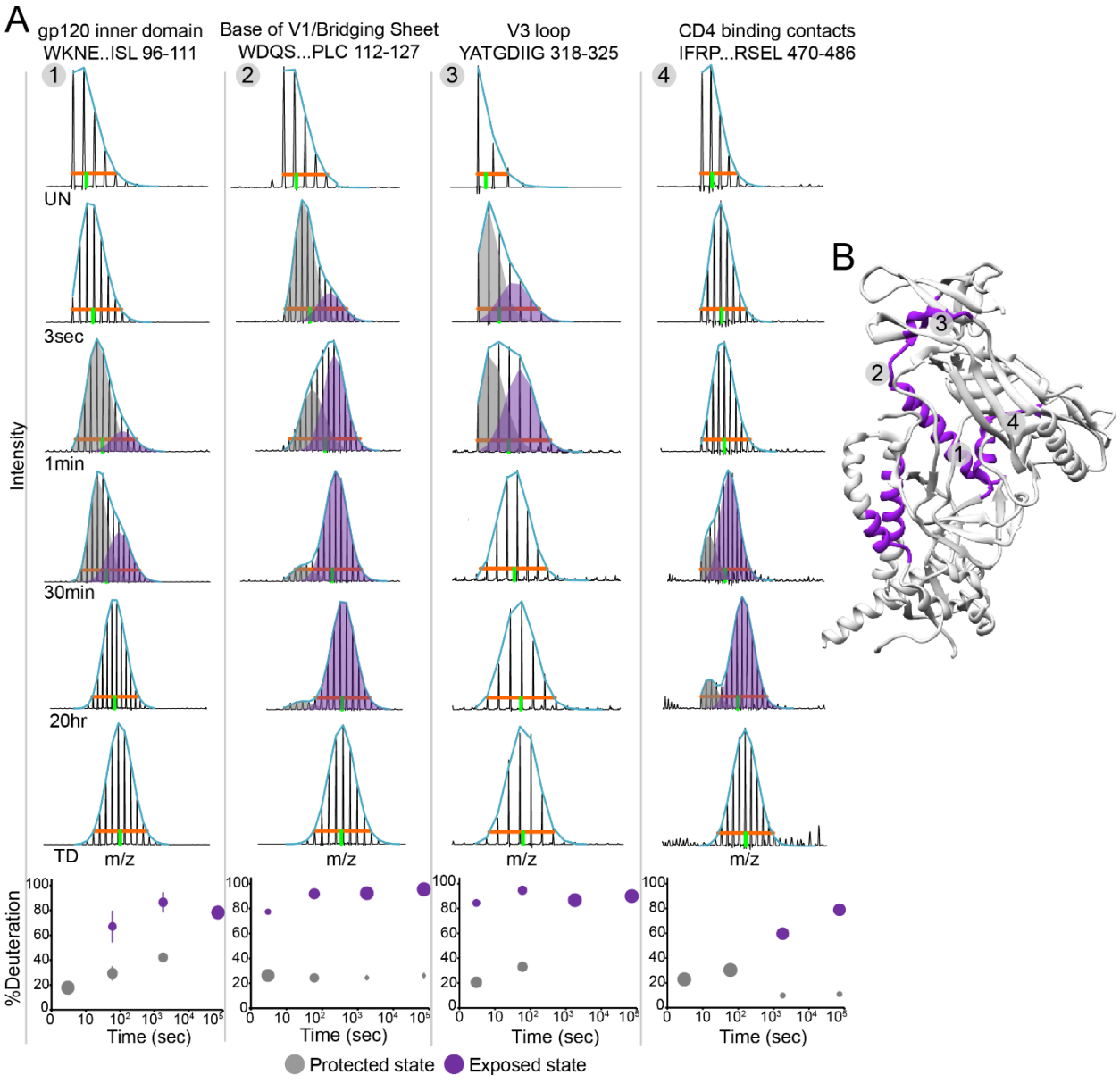

Figure 4. 5. The 2nd most neutralization resistant isolate trimer (tier 2 CH119) also exhibits many regions with bimodal spectra indicative of the interconversion between distinct conformations similar to SF162. (A) Bimodal spectra in peptides across the CH119 trimer reveal localized conformational switching. The mass envelopes at each deuteration time point are shown, as well as the undeuterated (UN) and totally deuterated controls (TD). The width of each isotopic distribution is displayed as a horizontal orange line and each centroid is the vertical green line. Unusually broad spectra were binomially fit to two populations; a protected state in gray, and an exposed state in purple. The cyan curve above each spectrum is the summation of each binomial fit. At the bottom of the spectra of each peptide are bubble plots that better characterize the transition from the protected (gray) to the exposed state (purple) across time. The size of the bubble corresponds to the percent abundance of the population at that point in time. **(B)** The location of the regions undergoing conformational switching are highlighted on the structure in purple (one protomer in ribbon diagram PDB 5FUU).

		IC50 (ug/ml) in TZM-bl Cells									
		SF162	BX08	BG505	25710	CNE8	TRO.11	BJOX	Ce1176	CNE55	CH119
Sample ID	Epitope	Tier 1A	Tier 1B	Tier 2	Tier 2	Tier 2	Tier 2	Tier 2	Tier 2	Tier 2	Tier 2
PGT145	V2 apex	>5	0.009	0.021	0.004	0.45	0.048	2.53	>5	0.005	0.196
PG16	V2-glycan	>5	0.033	0.014	0.023	1.36	>5	0.03	0.006	>5	0.926
b12	CD4bs	0.027	0.374	>5	>5	>5	>5	>5	>5	>5	>5
VRC01	CD4bs	0.331	0.702	0.106	0.688	2.01	0.744	>5	3.947	0.69	1.86
17b	co-receptor bs	0.86	0.503	>5	>5	>5	>5	>5	>5	>5	>5
PGT121	V3-glycan	0.003	0.004	0.016	0.018	>5	0.014	0.02	0.014	>5	0.032
VRC34.01	FP	0.053	0.532	0.064	3.859	>5	>5	0.22	0.136	>5	0.089
447-52D	V3 crown	0.083	0.082	>25	>25	>25	>25	>25	>25	>25	>25
3074	V3 crown	0.035	0.397	>25	4.594	>25	>25	>25	>25	>25	>25
3869	V3 crown	0.005	0.375	>25	>25	>25	>25	>25	>25	>25	>25
830A	V2i	1.237	>25	>25	>25	>25	>25	>25	>25	>25	>25

2158	V2i	5.224	4.786	>25	>25	>25	>25	>25	>25	>25	>25
35022	gp120-gp41	>25	0.018	>25	>25	>25	>25	>25	0.006	>25	>25

Table 4.1. Trimers derived from Tier 2 isolates presented on pseudovirus were resistant to neutralization by most mAbs targeting the tip of the V3 loop, the V2i epitope, the co-receptor binding site, and the gp120/gp41 interface targeted by the bnAb 35022. Trimers derived from Tier 1 isolates presented on pseudovirus were highly sensitive to neutralization by most mAbs. The IC50's from TZM-bl neutralization assays using a panel of mAbs specific for different epitopes are reported in the table. Data was collected and provided by Hongmei Gao.

		BLI measured K_D (nM)									
		SF162	**BX08**	**BG505**	**25710**	**CNE8**	**TRO.11**	**BJOX**	**CE1176**	**CNE55**	**CH119**
Sample ID	**Epitope**	**Tier 1A**	**Tier 1B**	**Tier 2**	**Tier 2**	**Tier 2**	**Tier 2**	**Tier 2**	**Tier 2**	**Tier 2**	**Tier 2**
PGT145	V2 apex	51.9	44.3	16	23.7	50.8	80.8	27.7	156.5	45.4	64.6
PG16	V2-glycan	ND	877	86.8	158.9	1,844	ND	84.6	37.4	337	109.5
b12	CD4bs	19.9	331.5	1,114	203.7	372	ND	14.4	212	3065	10.9
VRC01	CD4bs	27.3	212.7	8.1	97.9	230	228	40.9	495.5	139.5	12.9
17b	co-receptor bs	11.8	ND	ND	ND	ND	ND	50.5	1125.1	ND	50.9
PGT121	V3-glycan	9.3	740.7	15.8	39.7	ND	14.6	10.1	2.4	ND	27.3
VRC34	FP	52.6	1.7		0.1	2.7	27.6	0.3	0.36	12	0.552
447-52D	V3 crown	<1.0	197.5	33	136.1	512	43.7	392	29.8	ND	47.6

3074	V3 crown	<1.0	50.6	62.8	45.5	29.9	297.8	27.1	48	430.3	2.4
3869	V3 crown	<1.0	1930	257.5	171.7	1449	567.2	23.8	43.4	1860	3.9
830A	V2i	25	181	ND	848	146	ND	171	102.3	1244	14.3
2158	V2i	65.6	170.5	ND	ND	134	ND	266	214	ND	41.1
35022	gp120-gp41	341	ND	78.1	186	183	45.9	110.9	35.7	283.5	61.6

Table 4.2: SOSIP trimers derived from the global panel isolates exhibit a range of binding affinities to a panel of antibodies specific for different regions on the trimer structure.

The average binding affinities (K_Ds) determined using BLI and serially diluted SOSIP trimers from duplicate experiments are reported. ND indicates a binding affinity was not determined using the concentration range in the experiment, and a blank cell indicates the antibody-trimer complex was not evaluated.

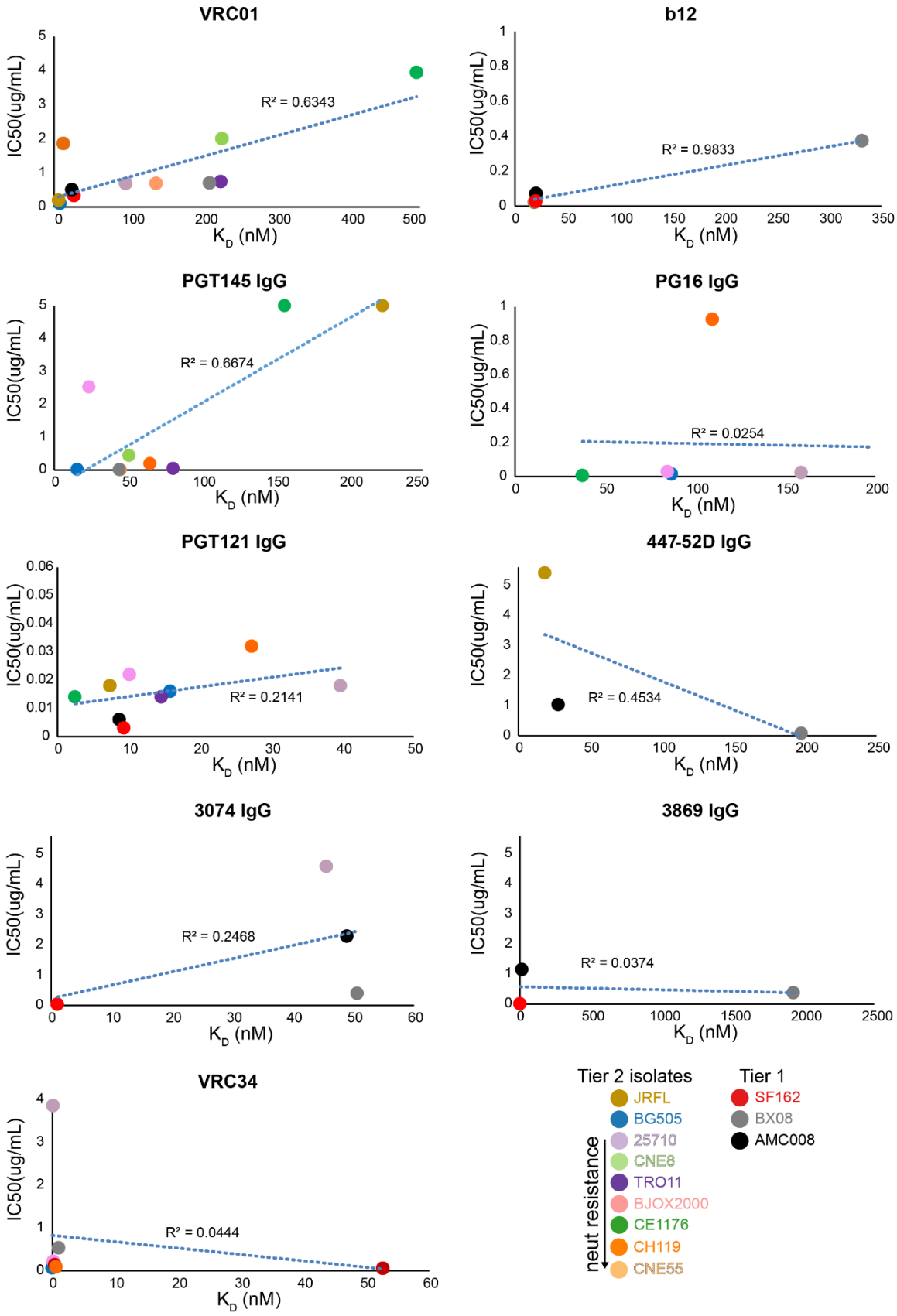
VRC01
R² = 0.6343
IC50(ug/mL)
K_D (nM)
b12
R² = 0.9833
PGT145 IgG
R² = 0.6674
PG16 IgG
R² = 0.0254
PGT121 IgG
R² = 0.2141
447-52D IgG
R² = 0.4534
3074 IgG
R² = 0.2468
3869 IgG
R² = 0.0374
VRC34
R² = 0.0444
Tier 2 isolates
JRFL
BG505
25710
CNE8
TRO11
BJOX2000
CE1176
CH119
CNE55
neut resistance
Tier 1
SF162
BX08
AMC008

Figure 4. 6: Env psuedovirus neutralization sensitivities (IC50's) do not always correlate with their corresponding SOSIP binding affinity (K_DS). BLI measured binding affinities of each respective SOSIP against a panel of antibodies are plotted on the x-axis and the neutralization assay determined IC50's using Env presented on a pseudovirus against the same panel of antibodies are on the y-axis. Isolates are colored red for SF162, gray for BX08, black for AMC008, blue for BG505, lavender for 25710, lime for CNE8, purple for TRO11, pink for BJOX2000, green for CE1176, peach for CNE55, orange for CH119, and gold for JRFL.

References

1. Seaman, M.S., et al., *Tiered Categorization of a Diverse Panel of HIV-1 Env Pseudoviruses for Assessment of Neutralizing Antibodies.* Journal of Virology, 2010. **84**(3): p. 1439-1452.
2. deCamp, A., et al., *Global panel of HIV-1 Env reference strains for standardized assessments of vaccine-elicited neutralizing antibodies.* Journal of virology, 2014. **88**(5): p. 2489-2507.
3. Hraber, P., et al., *Impact of clade, geography, and age of the epidemic on HIV-1 neutralization by antibodies.* J Virol, 2014. **88**(21): p. 12623-43.
4. Hraber, P., et al., *Panels of HIV-1 Subtype C Env Reference Strains for Standardized Neutralization Assessments.* J Virol, 2017. **91**(19).
5. Rademeyer, C., et al., *Features of Recently Transmitted HIV-1 Clade C Viruses that Impact Antibody Recognition: Implications for Active and Passive Immunization.* PLoS Pathog, 2016. **12**(7): p. e1005742.
6. Montefiori, D.C., et al., *Neutralization tiers of HIV-1.* Current Opinion in HIV and AIDS, 2018. **13**(2): p. 128.
7. Hraber, P., et al., *A single, continuous metric to define tiered serum neutralization potency against HIV.* eLife, 2018. **7**.
8. Han, Q., et al., *Difficult-to-neutralize global HIV-1 isolates are neutralized by antibodies targeting open envelope conformations.* Nature Communications, 2019. **10**(1): p. 2898.
9. Mangala Prasad, V., et al., *Cryo-ET of Env on intact HIV virions reveals structural variation and positioning on the Gag lattice.* Cell, 2022. **185**(4): p. 641-653 e17.
10. Li, Z., et al., *Subnanometer structures of HIV-1 envelope trimers on aldrithiol-2-inactivated virus particles.* Nat Struct Mol Biol, 2020. **27**(8): p. 726-734.
11. Ward, A.B. and I.A. Wilson, *The HIV-1 envelope glycoprotein structure: nailing down a moving target.* Immunological Reviews, 2017. **275**(1): p. 21-32.
12. Wang, H., et al., *Partially Open HIV-1 Envelope Structures Exhibit Conformational Changes Relevant for Coreceptor Binding and Fusion.* Cell Host & Microbe, 2018. **24**(4): p. 579-5920000.
13. Bricault, C.A., et al., *HIV-1 Neutralizing Antibody Signatures and Application to Epitope-Targeted Vaccine Design.* Cell Host Microbe, 2019. **25**(1): p. 59-72 e8.
14. Kwong, P.D., et al., *HIV-1 evades antibody-mediated neutralization through conformational masking of receptor-binding sites.* Nature, 2002. **420**(6916): p. 678-682.

15. Munro, J.B., et al., *Conformational dynamics of single HIV-1 envelope trimers on the surface of native virions.* Science, 2014. **346**(6210): p. 759-763.
16. Stadtmueller, B.M., et al., *DEER Spectroscopy Measurements Reveal Multiple Conformations of HIV-1 SOSIP Envelopes that Show Similarities with Envelopes on Native Virions.* Immunity, 2018. **49**(2): p. 235-2460000.
17. Guttman, M., et al., *Antibody potency relates to the ability to recognize the closed, pre-fusion form of HIV Env.* Nature Communications, 2015. **6**(1): p. 6144.
18. Chuang, G.-Y., et al., *Structure-Based Design of a Soluble Prefusion-Closed HIV-1-Env Trimer with Reduced CD4 Affinity and Improved Immunogenicity.* Journal of Virology, 2017: p. 16.
19. Ma, X., et al., *Single-Molecule FRET Delineates Asymmetric Trimer Conformations during HIV-1 Entry.* Biophysical Journal, 2017. **112**(3).
20. Ma, X., et al., *HIV-1 Env trimer opens through an asymmetric intermediate in which individual protomers adopt distinct conformations.* eLife, 2018. **7**.
21. Liang, Y., et al., *Probing the Impact of Local Structural Dynamics of Conformational Epitopes on Antibody Recognition.* Biochemistry, 2016. **55**(15): p. 2197-2213.
22. Hodge, E.A., et al., *Structural dynamics reveal isolate-specific differences at neutralization epitopes on HIV Env.* iScience, 2022. **25**(6): p. 104449.
23. Guttman, M., et al., *CD4-Induced Activation in a Soluble HIV-1 Env Trimer.* Structure, 2014. **22**(7): p. 974-984.
24. Rawson, J.M.O., et al., *Recombination is required for efficient HIV-1 replication and the maintenance of viral genome integrity.* Nucleic Acids Res, 2018. **46**(20): p. 10535-10545.
25. Julien, J.-P., et al., *Crystal Structure of a Soluble Cleaved HIV-1 Envelope Trimer.* Science, 2013. **342**(6165): p. 1477-1483.
26. Verkerke, H.P., et al., *Epitope-Independent Purification of Native-Like Envelope Trimers from Diverse HIV-1 Isolates.* Journal of virology, 2016. **90**(20): p. 9471-9482.
27. Colin, P., et al., *Conformational antigenic heterogeneity as a cause of the persistent fraction in HIV-1 neutralization.* Res Sq, 2023.
28. Abrahams, M.R., et al., *Quantitating the multiplicity of infection with human immunodeficiency virus type 1 subtype C reveals a non-poisson distribution of transmitted variants.* J Virol, 2009. **83**(8): p. 3556-67.
29. Gnanakaran, S., et al., *Genetic signatures in the envelope glycoproteins of HIV-1 that associate with broadly neutralizing antibodies.* PLoS Comput Biol, 2010. **6**(10): p. e1000955.
30. Kulkarni, S.S., et al., *Highly complex neutralization determinants on a monophyletic lineage of newly transmitted subtype C HIV-1 Env clones from India.* Virology, 2009. **385**(2): p. 505-20.
31. Li, M., et al., *Human immunodeficiency virus type 1 env clones from acute and early subtype B infections for standardized assessments of vaccine-elicited neutralizing antibodies.* J Virol, 2005. **79**(16): p. 10108-25.
32. Cheng-Mayer, C., et al., *Macrophage tropism of human immunodeficiency virus type 1 and utilization of the CC-CKR5 coreceptor.* J Virol, 1997. **71**(2): p. 1657-61.
33. Binley, J.M., et al., *Comprehensive cross-clade neutralization analysis of a panel of anti-human immunodeficiency virus type 1 monoclonal antibodies.* J Virol, 2004. **78**(23): p. 13232-52.
34. D'Souza, M.P., et al., *Engineering immunity for next generation HIV vaccines: The intersection of bioengineering and immunology.* Vaccine, 2020. **38**(2): p. 187-193.
35. Derking, R. and R.W. Sanders, *Structure-guided envelope trimer design in HIV-1 vaccine development: a narrative review.* J Int AIDS Soc, 2021. **24 Suppl 7**: p. e25797.

36. Guttman, M., et al., *Analysis of Overlapped and Noisy Hydrogen/Deuterium Exchange Mass Spectra.* Journal of The American Society for Mass Spectrometry, 2013. **24**(12): p. 1906-1912.
37. Weis, D.D., et al., *Identification and characterization of EX1 kinetics in H/D exchange mass spectrometry by peak width analysis.* Journal of The American Society for Mass Spectrometry, 2006. **17**(11): p. 1498-1509.
38. Hodge, E.A., M.A. Benhaim, and K.K. Lee, *Bridging protein structure, dynamics, and function using hydrogen/deuterium-exchange mass spectrometry.* Protein Sci, 2020. **29**(4): p. 843-855.
39. Benhaim, M.A., et al., *Structural monitoring of a transient intermediate in the hemagglutinin fusion machinery on influenza virions.* Sci Adv, 2020. **6**(18): p. eaaz8822.
40. Guttman, M. and K.K. Lee, *A functional interaction between gp41 and gp120 is observed for monomeric but not oligomeric, uncleaved HIV-1 Env gp140.* J Virol, 2013. **87**(21): p. 11462-75.
41. Powell, R.L.R.L.R., et al., *Plasticity and Epitope Exposure of the HIV-1 Envelope Trimer.* Journal of virology, 2017. **91**(17).
42. Kumar, S., et al., *Capturing the inherent structural dynamics of the HIV-1 envelope glycoprotein fusion peptide.* Nature Communications, 2019. **10**(1): p. 763.
43. Ananthaswamy, N., et al., *A sequestered fusion peptide in the structure of an HIV-1 transmitted founder envelope trimer.* Nature Communications, 2019. **10**(1): p. 873.
44. Mayr, L.M., et al., *Epitope mapping of conformational V2-specific anti-HIV human monoclonal antibodies reveals an immunodominant site in V2.* PloS one, 2013. **8**(7).
45. McLellan, J.S., et al., *Structure of HIV-1 gp120 V1/V2 domain with broadly neutralizing antibody PG9.* Nature, 2011. **480**(7377): p. 336-43.
46. Zhou, T., et al., *Structural definition of a conserved neutralization epitope on HIV-1 gp120.* Nature, 2007. **445**(7129): p. 732-737.
47. Kwong, P.D., et al., *Structure of an HIV gp120 envelope glycoprotein in complex with the CD4 receptor and a neutralizing human antibody.* Nature, 1998. **393**(6686): p. 648-59.
48. Hioe, C.E., et al., *Anti-V3 Monoclonal Antibodies Display Broad Neutralizing Activities against Multiple HIV-1 Subtypes.* PLoS ONE, 2010. **5**(4).
49. Sanders, R.W., et al., *A Next-Generation Cleaved, Soluble HIV-1 Env Trimer, BG505 SOSIP.664 gp140, Expresses Multiple Epitopes for Broadly Neutralizing but Not Non-Neutralizing Antibodies.* PLoS Pathogens, 2013.
50. de la Peña, A., et al., *Similarities and differences between native HIV-1 envelope glycoprotein trimers and stabilized soluble trimer mimetics.* PLoS pathogens, 2019. **15**(7).
51. de Taeye, S.W., et al., *Immunogenicity of Stabilized HIV-1 Envelope Trimers with Reduced Exposure of Non-neutralizing Epitopes.* Cell, 2015. **163**(7): p. 1702-1715.
52. Torrents de la Pena, A. and R.W. Sanders, *Stabilizing HIV-1 envelope glycoprotein trimers to induce neutralizing antibodies.* Retrovirology, 2018. **15**(1): p. 63.
53. Torrents de la Pena, A., et al., *Similarities and differences between native HIV-1 envelope glycoprotein trimers and stabilized soluble trimer mimetics.* PLoS Pathog, 2019. **15**(7): p. e1007920.
54. Rasheed, M., R. Bettadapura, and C. Bajaj, *Computational Refinement and Validation Protocol for Proteins with Large Variable Regions Applied to Model HIV Env Spike in CD4 and 17b Bound State.* Structure, 2015. **23**(6): p. 1138-49.
55. Ozorowski, G., et al., *Open and closed structures reveal allostery and pliability in the HIV-1 envelope spike.* Nature, 2017. **547**(7663): p. 360.
56. Pan, R., et al., *The V1V2 Region of HIV-1 gp120 Forms a Five-Stranded Beta Barrel.* Journal of virology, 2015. **89**(15): p. 8003-8010.

57. Sahoo, A., et al., *Structure-guided changes at the V2 apex of HIV-1 clade C trimer enhance elicitation of autologous neutralizing and broad V1V2-scaffold antibodies.* Cell Rep, 2022. **38**(9): p. 110436.
58. Duerr, R. and M.K. Gorny, *V2-Specific Antibodies in HIV-1 Vaccine Research and Natural Infection: Controllers or Surrogate Markers.* Vaccines, 2019. **7**(3): p. 82.
59. MacLeod, D.T., et al., *Early Antibody Lineage Diversification and Independent Limb Maturation Lead to Broad HIV-1 Neutralization Targeting the Env High-Mannose Patch.* Immunity, 2016. **44**(5): p. 1215-26.
60. Landais, E., et al., *HIV Envelope Glycoform Heterogeneity and Localized Diversity Govern the Initiation and Maturation of a V2 Apex Broadly Neutralizing Antibody Lineage.* Immunity, 2017. **47**(5): p. 990-1003 e9.
61. Lu, M., et al., *Associating HIV-1 envelope glycoprotein structures with states on the virus observed by smFRET.* Nature, 2019. **568**(7752): p. 415-419.
62. Cao, L., et al., *Global site-specific N-glycosylation analysis of HIV envelope glycoprotein.* Nature Communications, 2017. **8**: p. 14954.
63. Upadhyay, C., et al., *Signal peptide of HIV-1 envelope modulates glycosylation impacting exposure of V1V2 and other epitopes.* PLoS Pathog, 2020. **16**(12): p. e1009185.
64. Sanders, R.W., et al., *A next-generation cleaved, soluble HIV-1 Env trimer, BG505 SOSIP. 664 gp140, expresses multiple epitopes for broadly neutralizing but not non-neutralizing ….* A next-generation cleaved, soluble HIV-1 Env trimer, BG505 SOSIP. 664 gp140, expresses multiple epitopes for broadly neutralizing but not non-neutralizing …, 2013.
65. Garcia, N.K., et al., *Dynamic Changes during Acid-Induced Activation of Influenza Hemagglutinin.* Structure, 2015: p. 665-676.
66. Costello, S.M., et al., *The SARS-CoV-2 spike reversibly samples an open-trimer conformation exposing novel epitopes.* Nat Struct Mol Biol, 2022. **29**(3): p. 229-238.
67. Stavenhagen, K., et al., *Quantitative mapping of glycoprotein micro-heterogeneity and macro-heterogeneity: an evaluation of mass spectrometry signal strengths using synthetic peptides and glycopeptides.* J Mass Spectrom, 2013. **48**(6): p. 627-39.
68. Pei, J. and N.V. Grishin, *AL2CO: calculation of positional conservation in a protein sequence alignment.* Bioinformatics, 2001. **17**(8): p. 700-12.
69. Schneider, C.A., W.S. Rasband, and K.W. Eliceiri, *NIH Image to ImageJ: 25 years of image analysis.* Nat Methods, 2012. **9**(7): p. 671-5.
70. Watson, M.J., et al., *Simple Platform for Automating Decoupled LC-MS Analysis of Hydrogen/Deuterium Exchange Samples.* J Am Soc Mass Spectrom, 2021. **32**(2): p. 597-600.

Supplemental Figures

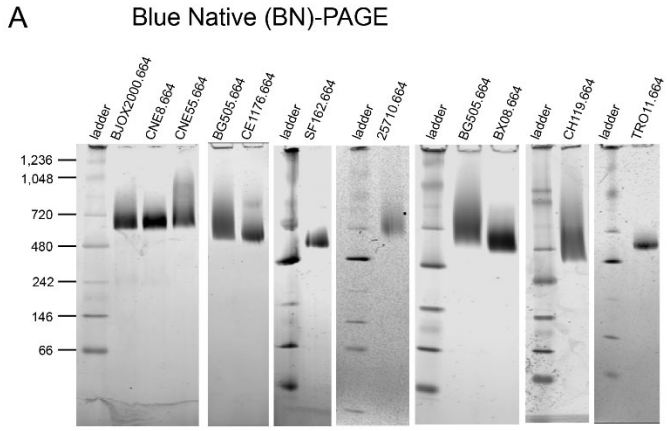

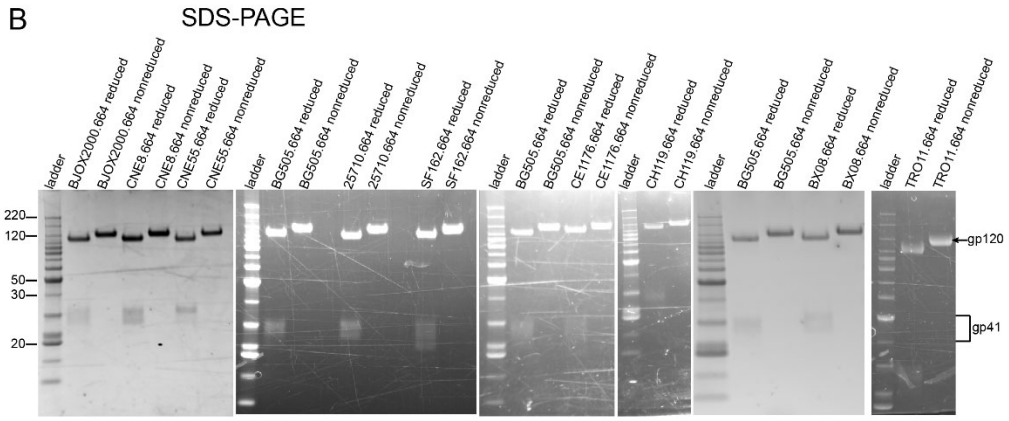

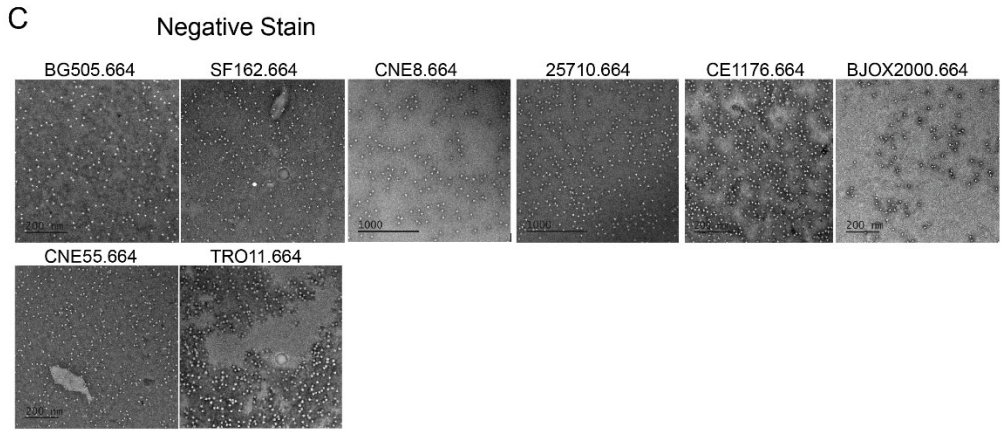

D

SOSIP construct	Radius (nm)	% polydispersity	% abundance
BG505	7.0	12.8	100

SF162	7.0	13.0	100
BX08	6.7	9.5	100
25710	7.4	21	100
CNE8	6.8	12.5	100
CE1176	7.0	13.1	100
BJOX2000	7.0	15.8	100
CH119	7.1	14.4	100
TRO11	6.8	12.2	100
CNE55	6.7	9.7	100

Figure S4.1. SOSIP characterization by blue native (BN)-PAGE, SDS-PAGE, NS-EM, and dynamic light scattering (DLS). Trimer purity was characterized by BN-PAGE (A), SDS-PAGE (B), negative stain EM (C), and DLS (D) after purification and prior to HDX and BLI experiments. On the SDS-PAGE each sample was run non-reduced and reduced via addition of DTT. The single band in the non-reduced lane runs at a slightly higher MW due to the presence of an additional inter-subunit disulfide bond linking gp120 and gp41. The weakly visible gp41 bands in the reduced lane are smeared likely due to glycan heterogeneity.

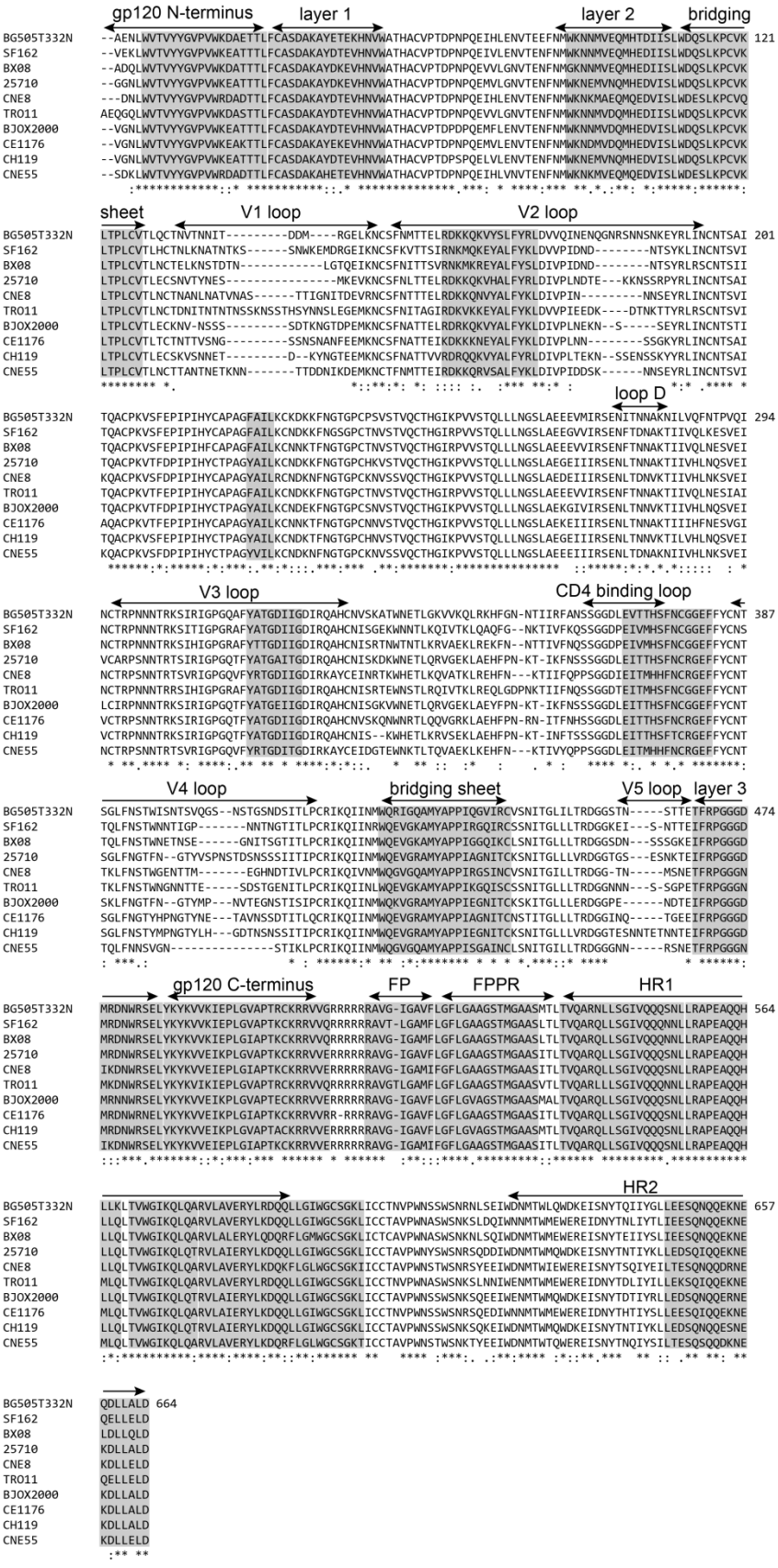
gp120 N-terminus
layer 1
layer 2
bridging
sheet
V1 loop
V2 loop
loop D
V3 loop
CD4 binding loop
V4 loop
bridging sheet
V5 loop
layer 3
gp120 C-terminus
FP
FPPR
HR1
HR2
BG505T332N
SF162
BX08
25710
CNE8
TRO11
BJOX2000
CE1176
CH119
CNE55

Figure S4.2. Sequence alignment. Sequences were aligned using clustal omega and are numbered according to HXB2 numbering. Regions where homologous peptides with the same number of exchangeable amides could be found across the ten isolates used in figures 2-3 are highlighted in gray. Asterisks indicate a fully conserved residue and colons indicate conservation between residues with similar properties.

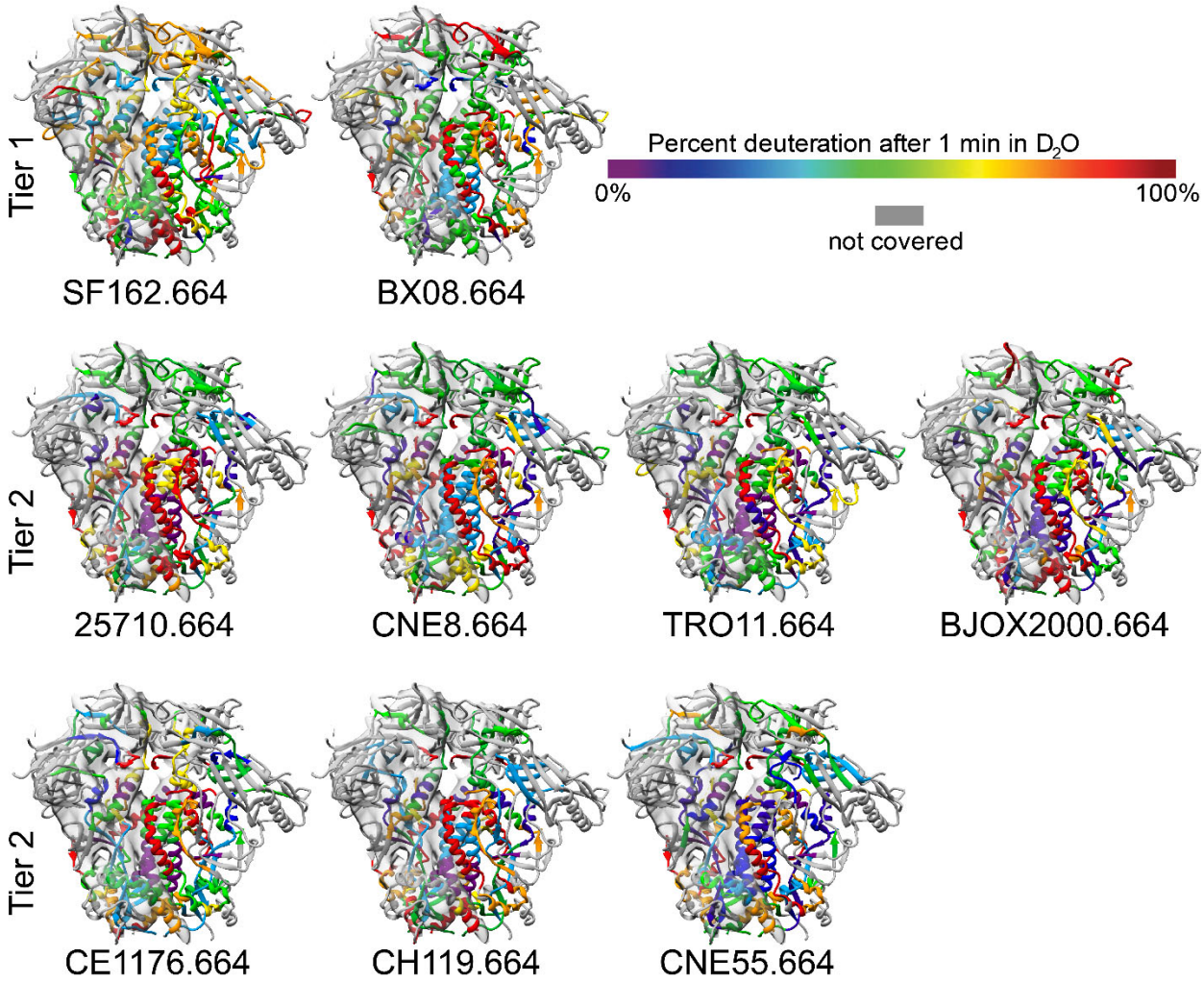

Figure S4.3. HDX heatmaps reveal localized differences in Env dynamic phenotype across trimers derived from the Env panel isolates. The percent deuteration after 1 minute in deuterated buffer of each peptide for each trimer isolate is mapped onto the trimer structure (PDB

5FUU, two protomers displayed in surface and one protomer displayed in ribbon). These heatmaps include non-homologous peptides with differences in the number of exchangeable amides, and thus are a relative comparison of localized dynamics.

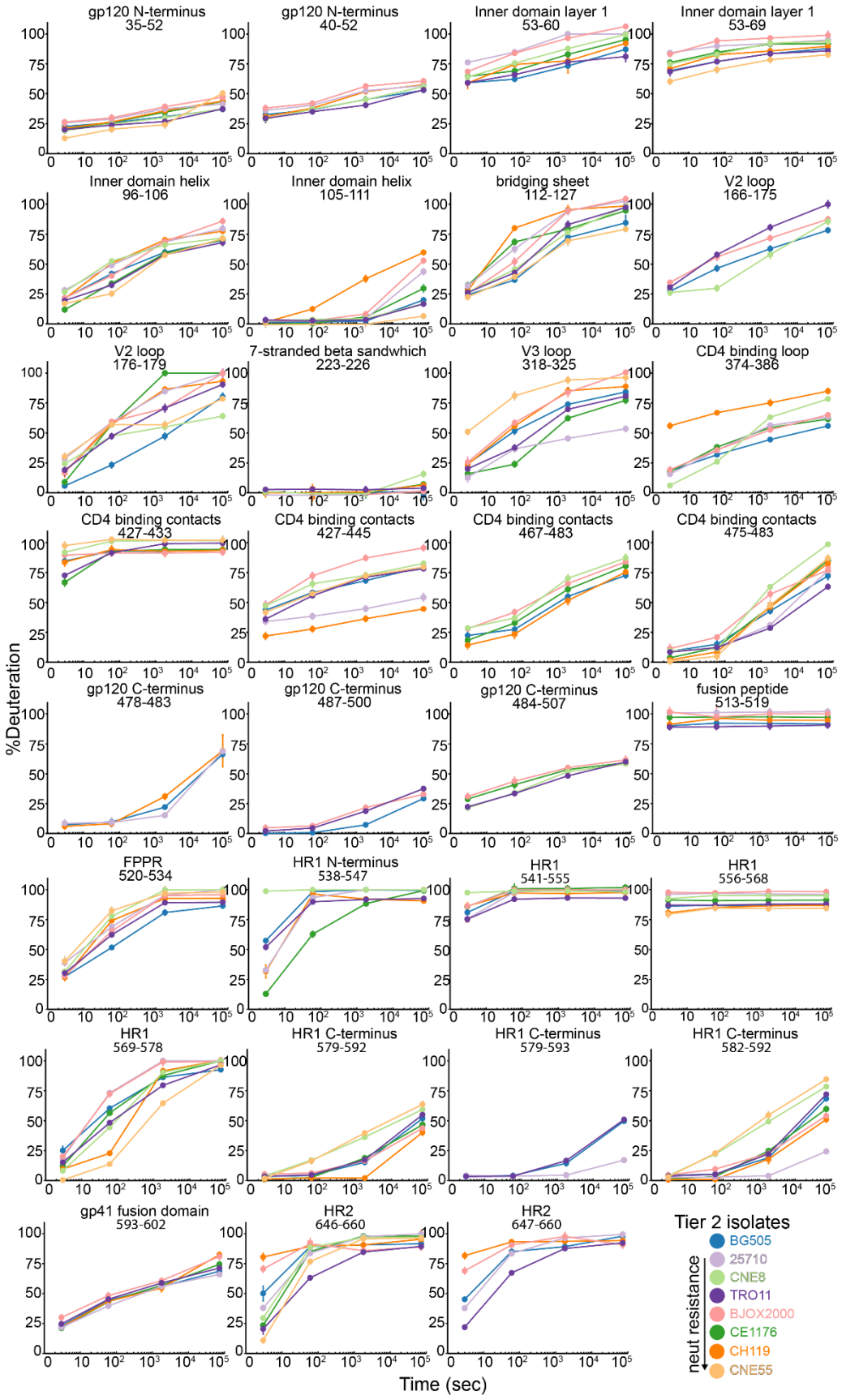
gp120 N-terminus 35-52
gp120 N-terminus 40-52
Inner domain layer 1 53-60
Inner domain layer 1 53-69
Inner domain helix 96-106
Inner domain helix 105-111
bridging sheet 112-127
V2 loop 166-175
V2 loop 176-179
7-stranded beta sandwhich 223-226
V3 loop 318-325
CD4 binding loop 374-386
CD4 binding contacts 427-433
CD4 binding contacts 427-445
CD4 binding contacts 467-483
CD4 binding contacts 475-483
gp120 C-terminus 478-483
gp120 C-terminus 487-500
gp120 C-terminus 484-507
fusion peptide 513-519
FPPR 520-534
HR1 N-terminus 538-547
HR1 541-555
HR1 556-568
HR1 569-578
HR1 C-terminus 579-592
HR1 C-terminus 579-593
HR1 C-terminus 582-592
gp41 fusion domain 593-602
HR2 646-660
HR2 647-660
%Deuteration
Time (sec)
Tier 2 isolates
BG505
25710
CNE8
TRO11
BJOX2000
CE1176
CH119
CNE55
neut resistance

Figure S4.4. Isolate-specific variation in dynamics across tier 2 Env trimers derived from a global panel. Deuterium uptake plots of homologous peptides from trimers across the global panel are shown. Each HDX uptake plot consists of the average percent deuteration of at least two replicates after 3 seconds, 1 minute, 30 minutes, and 20 hours of exchange normalized to a fully deuterated control with error bars reporting average percent standard deviation. All homologous peptides contain the same number of exchangeable backbone amides across the eight tier 2 isolates. Isolates are indicated by a circle and solid line (BG505 dark blue, 25710 light purple, CNE8 light green, TRO11 dark purple, BJOX2000 pink, CE1176 dark green, CH119 dark orange, CNE55 light orange). In each uptake plot, the homologous peptide sequence is based on HXB2 numbering and the sequences are aligned in figure S4.2.

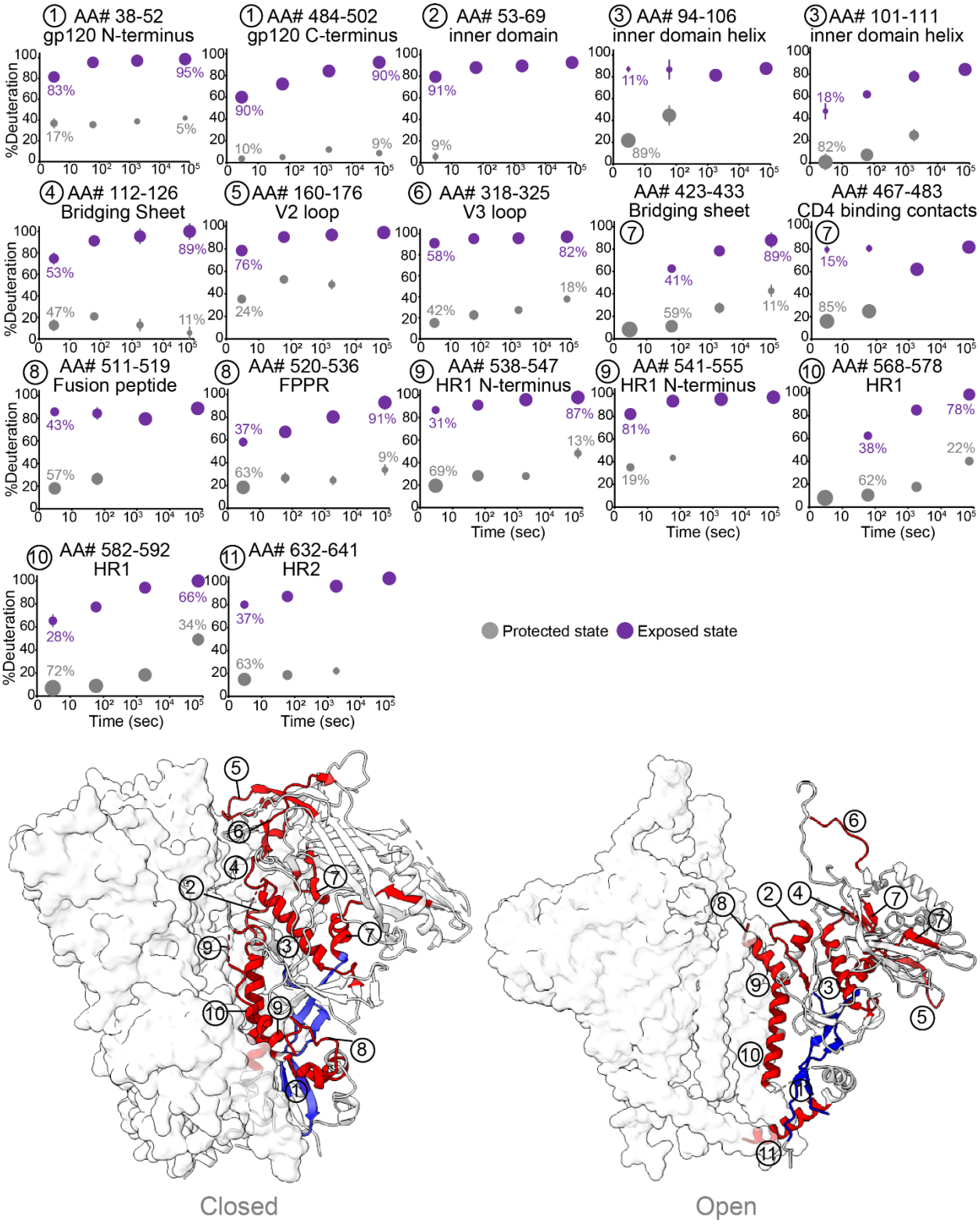
① AA# 38-52
gp120 N-terminus
① AA# 484-502
gp120 C-terminus
② AA# 53-69
inner domain
③ AA# 94-106
inner domain helix
③ AA# 101-111
inner domain helix
④ AA# 112-126
Bridging Sheet
⑤ AA# 160-176
V2 loop
⑥ AA# 318-325
V3 loop
AA# 423-433
Bridging sheet
AA# 467-483
CD4 binding contacts
⑧ AA# 511-519
Fusion peptide
⑧ AA# 520-536
FPPR
⑨ AA# 538-547
HR1 N-terminus
⑨ AA# 541-555
HR1 N-terminus
⑩ AA# 568-578
HR1
⑩ AA# 582-592
HR1
⑪ AA# 632-641
HR2
%Deuteration
Time (sec)
Protected state
Exposed state
Closed
Open

Figure S4.5. Many peptides across the SF162 trimer exhibit bimodal spectra suggestive of conformational switching. (A) Bimodal spectra in peptides across the SF162 trimer reveal localized conformational switching. Unusually broad spectra were binomially fit to two populations; a protected state in gray, and an exposed state in purple. Each peptide with bimodal spectra are displayed as bubble plots that characterize the transition from the protected (gray) to the exposed state (purple) across time. The size of the bubble represents the percent abundance of the population at that point in time. The peptides are numbered and highlighted on the structure at the bottom (PDB 5ACO: 2 protomers displayed in white surface, and one protomer displayed in ribbon). From the bubble plots of the two Peptides at the gp120 N and C termini (blue on the structure) it is apparent that roughly 5-10% of trimers in solution may be misfolded or aggregated from the protected/gray population that does not change in percent abundance or take up deuterium with time. The other peptide bubble plots are highlighted in red on the structure and reveal either EX1 or mixed EX1/EX2 uptake kinetics.

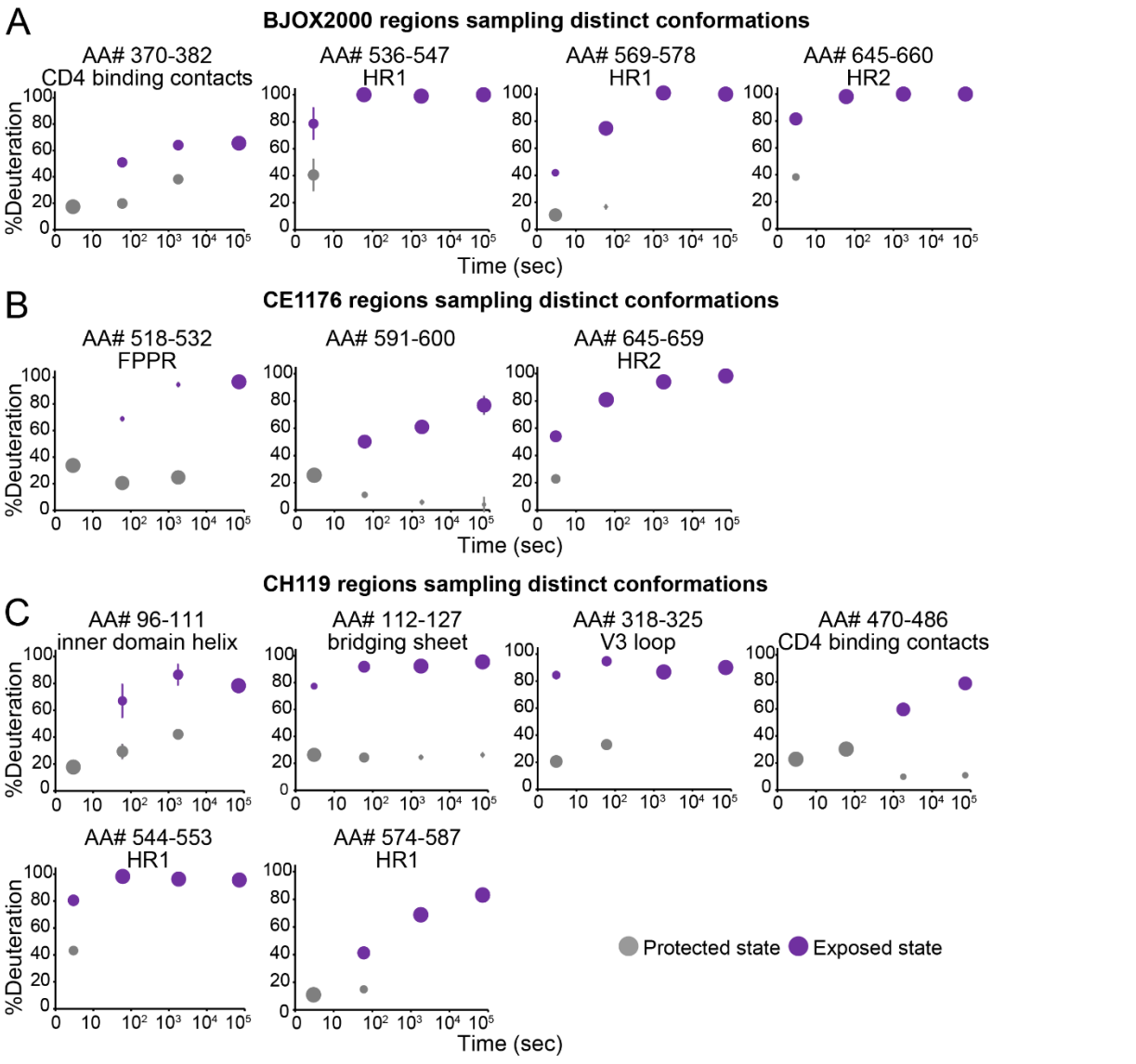
A
BJOX2000 regions sampling distinct conformations
AA# 370-382
CD4 binding contacts
AA# 536-547
HR1
AA# 569-578
HR1
AA# 645-660
HR2
%Deuteration
Time (sec)
B
CE1176 regions sampling distinct conformations
AA# 518-532
FPPR
AA# 591-600
AA# 645-659
HR2
%Deuteration
Time (sec)
C
CH119 regions sampling distinct conformations
AA# 96-111
inner domain helix
AA# 112-127
bridging sheet
AA# 318-325
V3 loop
AA# 470-486
CD4 binding contacts
AA# 544-553
HR1
AA# 574-587
HR1
%Deuteration
Time (sec)
Protected state
Exposed state
D
BJOX2000
CE1176
CH119

Figure S4.6. Trimers derived from tier 2 isolates also exhibit localized conformational switching in a strain dependent manner. (A) Bimodal spectra in peptides across the tier 2 isolates BJOX2000, CE1176, and CH119 trimers reveal localized conformational switching. Unusually broad spectra were binomially fit to two populations; a protected state in gray, and an exposed state in purple. Each peptide with bimodal spectra are displayed as bubble plots that characterize the transition from the protected (gray) to the exposed state (purple) across time. The size of the bubble represents the percent abundance of the population at that point in time. The peptides are numbered and highlighted on the structures at the bottom (PDB 5FUU: 2 protomers displayed in gray surface, and one protomer displayed in ribbon).

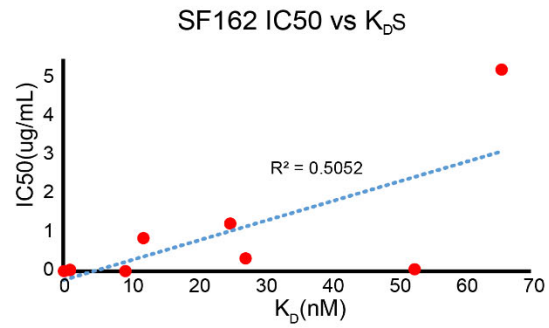
SF162 IC50 vs K$_D$S
IC50(ug/mL)
R² = 0.5052
K$_D$(nM)

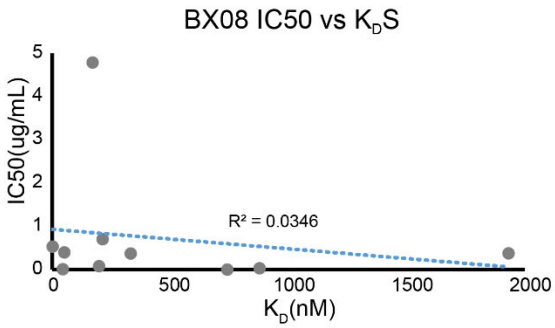
BX08 IC50 vs K$_D$S
IC50(ug/mL)
R² = 0.0346
K$_D$(nM)

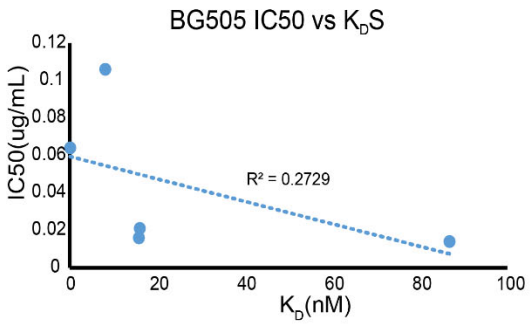
BG505 IC50 vs K$_D$S
IC50(ug/mL)
R² = 0.2729
K$_D$(nM)

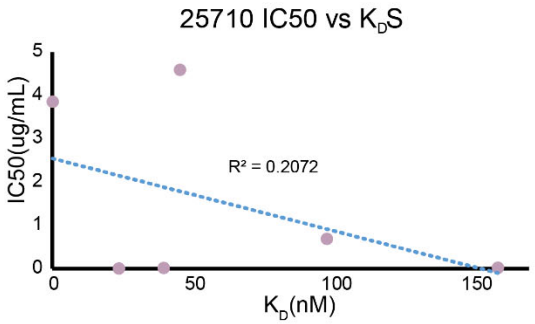
25710 IC50 vs K$_D$S
IC50(ug/mL)
R² = 0.2072
K$_D$(nM)

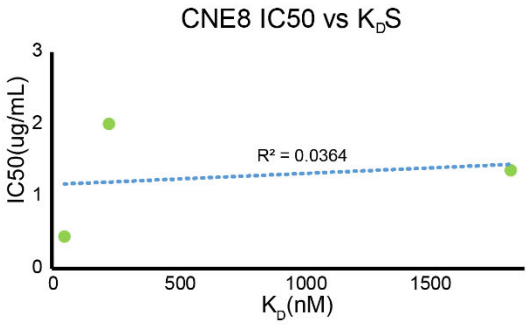
CNE8 IC50 vs K$_D$S
IC50(ug/mL)
R² = 0.0364
K$_D$(nM)

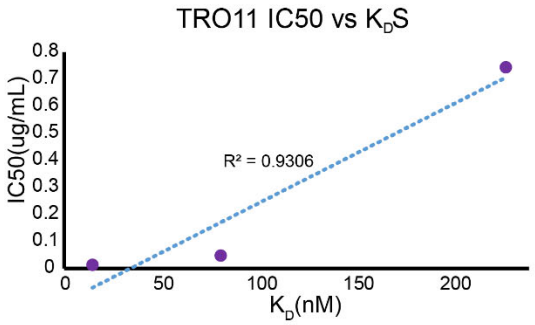
TRO11 IC50 vs K$_D$S
IC50(ug/mL)
R² = 0.9306
K$_D$(nM)

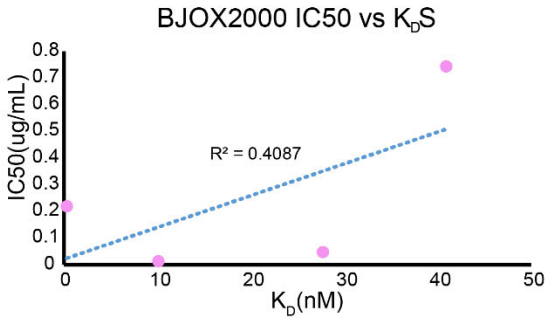
BJOX2000 IC50 vs K$_D$S
IC50(ug/mL)
R² = 0.4087
K$_D$(nM)

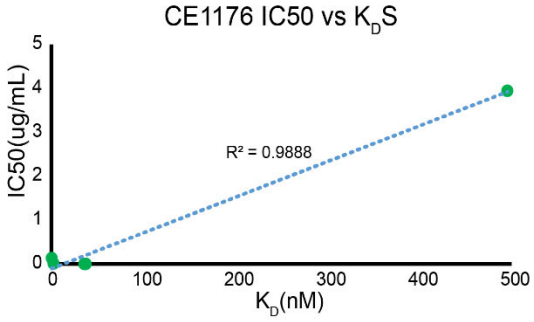
CE1176 IC50 vs K$_D$S
IC50(ug/mL)
R² = 0.9888
K$_D$(nM)

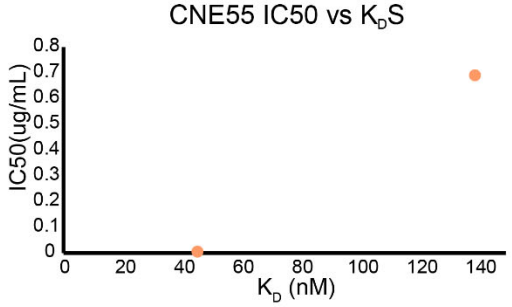
CNE55 IC50 vs K$_D$S
IC50(ug/mL)
K$_D$ (nM)

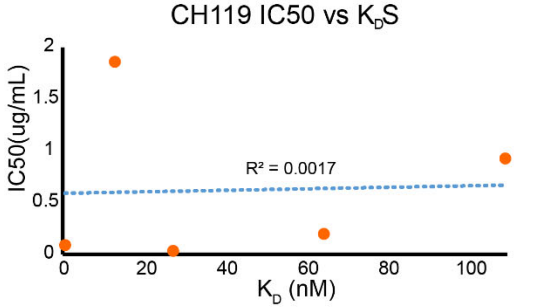
CH119 IC50 vs K$_D$S
IC50(ug/mL)
R² = 0.0017
K$_D$ (nM)

Figure S4.7. SOSIP Trimers' IgG antigenicity does not always correlate with IgG neutralization potency. The average binding affinities (K_DS) determined using BLI from duplicate experiments are plotted against the neutralization IC50's for each corresponding IgG. Many of the weakly or non-neutralizing antibodies that were able to bind the SOSIP were not able to neutralize the corresponding trimer presented on a pseudovirus membrane. Thus some plots have few data points making it hard to determine trends.

Chapter 5. Perspectives and Future Directions

5.1 Introduction

The HIV Env fusion protein is required for cellular entry and infection. Despite over 40 years of intense research, and despite Env being the only available viral target on the virus surface, scientists have been unable to generate antibodies in humans capable of surmounting Env's immune evasion strategies and protecting against infection from diverse variants—a requirement for any successful vaccine. The most challenging evasion strategy is HIV's large and ever-growing genetic diversity focused in the Env gene. The objective of this dissertation was to probe the effects of HIV's remarkable genetic diversity on Env fusion protein dynamics and test the supposed connection between Env dynamic phenotype, antigenicity, and antibody-mediated neutralization.

In chapter 1 I briefly introduce the HIV Env fusion protein and lay a strong foundation for the reader's understanding of HDX-MS as a biophysical tool that is used throughout this dissertation to build evidence of the dynamic variation that I have observed across Env variants. Subsequently HDX-MS is used in chapter 2 to characterize the dynamics of Env trimers derived from five isolates. I highlight interesting differences in dynamics and conformational sampling across these variants along with differences in antigenicity using BLI and a panel of IgG's specific for different regions across the trimer structure. After the insertion of stabilizing mutations into three Env trimers, I identified a structure-based explanation for the improved antigenicity of the neutralization sensitive/ tier 1 AMC008 trimer.

Next in chapter 3 I focus on the apex V2 loop, which is targeted by some of the most potent anti-HIV bnAbs. I point out the extreme variability in dynamics of this antigenic region across diverse trimers using HDX-MS. The correlation between V2 epitope flexibility and

PGT145 association rates suggests dynamic motions may be disrupting this bnAb's quaternary epitope. In collaboration with others we used cryo EM to map the PGT145 binding site across two dynamically diverse trimers and observe that the binding footprint of PGT145 is heavily dependent on glycans across all three Env protomers, which had not been observed in previously published structures using the AMC011 or BG505 isolates [1, 2]. A complementary epitope mapping technique, differential HDX-MS, was used to further characterize the BJOX2000 and CNE55 trimer PGT145 epitopes. Trimer protection and stabilization was surprisingly localized to the V2 loop, and no distal allosteric stabilization was observed.

Chapter 4 extends my characterization of Env dynamic variation using a larger and more diverse HIV isolate panel previously selected to best recapitulate the genetic diversity of HIV circulating around the globe. Similar to chapter 2 I use a panel of antibodies specific for different regions across the trimer structure to correlate differences in epitope flexibility with differences in antigenicity. In collaboration with others we also look at pseudotyped virus neutralization data using the same isolates and antibodies. Collectively the works presented here deepen our understanding of the immense impact extreme sequence diversity has on trimer dynamics. While we show epitope dynamics can likely influence IgG recognition, such as in the case of PGT145, we see that many other bnAbs are able to bind their target tightly even in the presence of variability in epitope dynamics. During affinity maturation, along the path to development of breadth, it is interesting to speculate if variability in epitope dynamics among HIV mutants helps to drive breadth and select for early ancestor B-cells able to overcome dynamic variation. Additionally, we test a structure-dynamic hypotheses that has been proposed and suggests the neutralization sensitivity of viruses to pooled human serum in a 12-virus global panel is primarily determined based on differences in the propensity of each viruses' surface Env to sample more open conformational states. In support of this hypothesis I found localized regions where trimers derived from the most neutralization sensitive tier 1 viruses do have a more dynamic phenotype

across their structure in comparison to harder to neutralize tier 2 viruses that may explain differences in neutralization sensitivities. Focusing solely on trimers derived from the harder to neutralize tier 2 viruses that also exhibit a wide range of neutralization sensitivities, there were no clear trends linking differences in local dynamics to neutralization resistance. This lack of a correlation between dynamics and neutralization tier assignment observed across tier 2 trimers supports the contribution that other Env properties, like differences in glycans, lengths of variable loops, epitope charge and sequence play in regard to neutralization by pooled serum. Additionally work presented in chapter 4 underscores dynamic variation in dynamics across the tier 2 trimers and suggests not all trimers derived from harder to neutralize viruses maintain a closed, prefusion conformation.

5.2 Future directions

5.2.1 Epitope focusing during affinity maturation of a V2-targeting bnAb

In order to test whether germline antibodies are more impacted by dynamic variation at an epitope and test whether the correlation between V2 dynamics and antibody binding kinetics was more generally applicable to other apex V2 bnAbs besides PGT145, I measured the binding kinetics against another potent bnAb that binds a very similar region on the V2 loop; VRC26. The binding mode of VRC26 is similar to PGT145, but also distinct; VRC26 forms parallel β strand H-bonds along the V2 loop C-strand more similar to PG9 than PGT145, and likely penetrates the trimer apex hole less deeply than PGT145, and is less impacted by loss of glycans at N160 and N156 [3, 4]. I selected multiple antibodies from the VRC26 lineage that had underwent different degrees of affinity maturation and thus had differences in breadth and potencies (Table 5.1), including six antibodies isolated from an HIV superinfected patient across increasing time points and five early ancestor antibodies whose sequences were inferred from phylogenetics data, the inferred unmutated common ancestor (VRC26.UCA) and inferred

pathway intermediates (VRC26.I1, I2, I5, and I6) [5]. I selected four SOSIPs with differences in V2 loop dynamics (BG505, CNE8, BJOX2000, and CE1176) that I thought would bind these VRC26 antibodies from published virus neutralization and mutagenesis experiments [4, 5]. The binding kinetics of the VRC26 lineage antibodies to these SOSIPs are presented in Table 5.2 and Figures 5.1-5.4. As expected, the binding affinities of the lineage for each SOSIP generally increased with affinity maturation. The increase in binding affinities with affinity maturation across isolates was driven by both an increase in the association rates and a decrease in dissociation rates (Figure 5.5). The decrease in the dissociation rates were larger than the increase in association rates across the VRC26 lineage for all isolates, except BJOX2000 (based on the fold change comparing VRC26.25 to the least affinity mature ancestor that bound each respective trimer).

Similar to PGT145, I looked for correlations between V2 peptide dynamics and antibody binding kinetics. Unlike PGT145, across the VRC26 lineage antibodies, the association rates for each Env trimer were fairly similar, and differences in overall affinity were mainly due to differences in dissociation rates. More data points are needed to make sense of trends in the data, and some other trimers tested did not have measurable binding rates to some of these early lineage VRC26 antibodies. However, from this limited data set, a more dynamic epitope correlated with a slower antibody off rate and an overall tighter binding affinity (Figure 5.6). This trend between dynamics and K_D's and K_{off}'s existed for VRC26.25, VRC26.08, VRC26.05, and VRC26.03, but only using a homologous peptide (peptide 166-175, Figure 5.6) that contained residues that were direct antibody binding contacts. Slightly C-terminal this localized region there was no correlation using the adjacent region (peptide FYKL). On the other hand, the two least affinity mature antibodies, (VRC26.01 and the inferred developmental intermediate VRC26.I2) that were able to bind to at least ¾ of the trimer constructs were potentially impacted by V2 loop dynamics across a larger surface area (Figure 5.6, both peptides spanning residues

166-175 and 176-179). For VRC26.01 a more dynamic epitope correlated with a slower association rate and a slower dissociation rate, which suggests this less affinity matured antibody from the VRC26 lineage may be more impacted by V2 loop dynamics. Similarly VRC26.I2 dissociation rates were impacted by both regions in the V2 loop, however, the association rates for VRC26.I2 were similar across all trimer constructs. While it's hard to mechanistically make sense of how a more dynamic epitope could impact antibody dissociation rates, and more data points are needed, the trends observed between V2 dynamics and antibody binding across a larger surface area for the two least affinity mature antibodies may highlight a benefit of affinity maturation when it comes to epitope refinement in regard to binding a highly dynamic target and warrants further investigation. I speculate that focusing the VRC26 epitope to a smaller region in the V2 loop during affinity maturation could be a mechanism early lineage B-cells use to overcome some of the large differences in dynamics in the upstream FYKL region of the V2 loop.

5.2.2 VRC26.25 and a novel VRC26J3LS bispecific IgG target the V2 loop

In order to test how similar the VRC26.25 binding footprint is to that of PGT145, I used differential HDX-MS comparing HDX of the unbound BG505 trimer against the BG505 trimer bound to VRC26.25 Fab (Figure 5.7A & 5.8A, Figure S5.1). Similar to PGT145 the VRC26.25 epitope is highly focused to the C strand of the V2 loop, with no signs of distal allosteric stabilization. Only peptides with residues previously shown via EM to directly contact the IgG paratope (residues 166-170) showed any increase in backbone amide protection [4]. The C-terminal adjacent region (FYRL, residues 176-179) showed no signs of an increase in protection. Additionally in a collaboration with the Vaccine Research Center (VRC), I mapped the epitope of a novel bispecific antibody, CAP256J3L, which is a version of the VRC26.25 IgG with a flexible linker attaching the Fab light chain to a CD4-binding site directed llama nanobody (J3) to improve the antibodies breadth [6]. These data highlight the sensitivity of HDX when it

comes to epitope mapping. In agreement with the EM structure of the Fab bound BG505 trimer, peptides that were both part of the V2 loop VRC26.25 epitope, as well as peptides that are part of the CD4 binding site showed an increase in protection. Interestingly, a slight increase in the stability of the HR1 helix (residues 569-578) was observed, suggesting the bispecific antibody has some allosteric effects that stabilize the fusion subunit.

A natural future direction of this work would be to test the hypothesis that the VRC26 epitope becomes more refined during affinity maturation. This could be done by comparing the binding footprint of the affinity mature bnAb VRC26.25 against the VRC26.I2 binding footprint across a few different trimers that bind both antibodies. BG505, CNE8, and BJOX2000 trimers would be a good selection from my BLI data (Figure 5.1-5.4). I hypothesize that the FYR/KL region in the V2 loop may be impacted by the immature developmental intermediate VRC26.I2 binding, but not the affinity mature VRC26.25, like we see in BG505. That would suggest affinity maturation drives the epitope to become more focused and less reliant on the highly dynamic FYR/KL region in the V2 loop.

5.2.3 Hyperstabilizing mutations that suppress trimer dynamics

Another natural extension of this work would be to apply some of the hyperstabilizing SOSIP mutations described in chapter 2 to other trimers that show signs of conformational switching across the trimer structure. Notably mutations designed to lock the V3 loop under the apex (A316W) and mutations designed to stabilize the closed conformation (E64K or H66R) worked well to suppress dynamics in the neutralization sensitive AMC008 trimer [7]. These same mutations had little to no effect in the less flexible tier 2 BG505 and B41 trimers. Additionally, I tried inserting the A316W and E64K mutations into the more dynamic CE1176 trimer, but yields of this v4.1SOSIP construct were too low for HDX and BLI experiments. It is possible that adding additional stabilizing mutations into CE1176, such as L543N or inserting an

additional disulfide bridge in the gp120 bridging sheet could help boost yields and suppress dynamics in the CE1176 trimer [8-12]. Other groups have similarly noted that stabilizing mutations that work in trimers derived from one isolate may not work in trimers derived from other isolates [8, 13]. CH119 (tier 2) and SF162 (tier 1) in particular show signs of localized conformational switching and could make good targets to see whether stabilizing mutations can suppress dynamics and abrogate binding of 17b, V2i Abs, and V3 tip targeting Abs.

5.2.4 Dynamic characterization of Env on a membrane

SOSIPs are currently the best mimic of native Env trimers, but there are important differences. Soluble, non-membrane bound native-like trimers have been shown to have a higher percent abundance of high mannose glycans compared to Env on a membrane [14]. Upadhyay et al have demonstrated that switching the signal peptide on Env constructs can lead to differences in trimer antigenicity using V2 apex targeting antibodies, likely by altering trimer glycosylation or conformational dynamics. Biophysical studies using smFRET across a few trimers has suggested that membrane bound Env and native-like trimers differ in the amount of time they spend sampling distinct fret states [15]. These differences could be due, for instance, to lack of the transmembrane region and cytoplasmic tails. It is likely that some of these differences explain the mismatch I, and others, have sometimes observed between SOSIP antigenicity and the corresponding pseudotyped virus neutralization sensitivity to antibodies described in more details in chapter 4 [13]. Thus it will be important to compare native-like trimers, such as SOSIPs, to the dynamics and conformation of their isolate matched full length Env dynamics on a membrane using a technique like HDX-MS. Some work in our lab has already characterized the dynamics of Env displayed on a VLP and compared it to the soluble BG505 SOSIP [16]. However, the two constructs were derived from different HIV isolates, and VLP-Env peptides tended to suffer from low signal intensity that led to overall low coverage across the trimer structure. As recent advancements in HDX-MS make rapid lipid membrane

removal more facile and mass spectrometers continue to become more sensitive, probing full length Env in more native environments will become more feasible.

5.3 Concluding remarks

In summary, these works emphasize the impact of the large genetic diversity across HIV isolates on the dynamic variation in the Env fusion protein, and highlight the idiosyncratic nature of native-like trimers. Stabilizing mutations capable of suppressing dynamics in one isolate, such as AMC008, may have little to no impact in trimers derived from other isolates. Additionally, these works investigate the supposed link between trimer dynamics and neutralization sensitivities. Neutralization sensitive, tier 1 isolates such as AMC008, BX08, and SF162, had markedly different dynamic phenotypes compared to more neutralization resistant tier 2 isolates. Regions of note included the gp120-gp41 interface, the V3 loop, the bridging sheet, gp120 inner domain helix, and HR1 in the base fusion machinery. These differences in conformation and dynamics help support the hypothesis suggesting that tier 1 isolates are more dynamic and spend more time sampling open conformations. However, I also observe significant dynamic variation across trimers derived from tier 2 isolates, including slow timescale conformational transitions as evidenced by bimodal spectra. Thus an isolate's susceptibility to neutralization by pooled human sera, which is used to determine an isolate's neutralization tier, is multi-factorial and complex. As is well documented in the literature, isolate dependent differences in glycosylation, epitope sequence variation, charge variation, length of variable loops and other factors can influence neutralization sensitivities [17]. One clear caveat in these data are potential differences between SOSIPs and full length Env presented on a membrane. However, from a more fundamental perspective, these works still help us better understand some basic outstanding science questions; 1) the effects of extreme sequence variation on protein dynamics and 2) how differences in local epitope dynamics impact antibody recognition. In the case of PGT145 we see a clear correlation between V2 apex dynamics and IgG

association rates. Other bnAbs appear to have overcome isolate dependent differences in epitope flexibility. More work needs to be done to investigate the impact of epitope dynamics on less affinity mature antibodies, such as some preliminary work I've shown in this chapter looking at the VRC26 lineage antibodies. Taken together these finding expand our understanding of Env dynamic variation and have translational importance in regard to structure-based vaccine design.

Antibody	% mutation from inferred UCA VH AA sequence	% mutation from inferred UCA VL AA sequence	CDRH3 length (# of amino acids)	Presence of disulfide bridge in CDR H3	%neutralization breadth (46 isolates)	Median IC_{50} (μg/mL) (46 isolates)
VRC26.01	20.8	8.1	35	no	20	3.32
VRC26.03	20.8	14.4	35	yes	35	0.06
VRC26.05	23.4	13.5	35	yes	22	0.02
VRC26.08	28.8	14.4	37	yes	46	0.08
VRC26.11	26.4	20.7	35	yes	26	1.04
VRC26.25	22.8	16.2	36	yes	63	0.003

Table 5.1. VRC26 antibody lineage characteristics

A table adapted from Doria-Rose et al [4, 5] indicating differences in VRC26 lineage antibody neutralization breadth, potencies, and mutations in amino acid sequence from antibodies isolated in a superinfected individual across time.

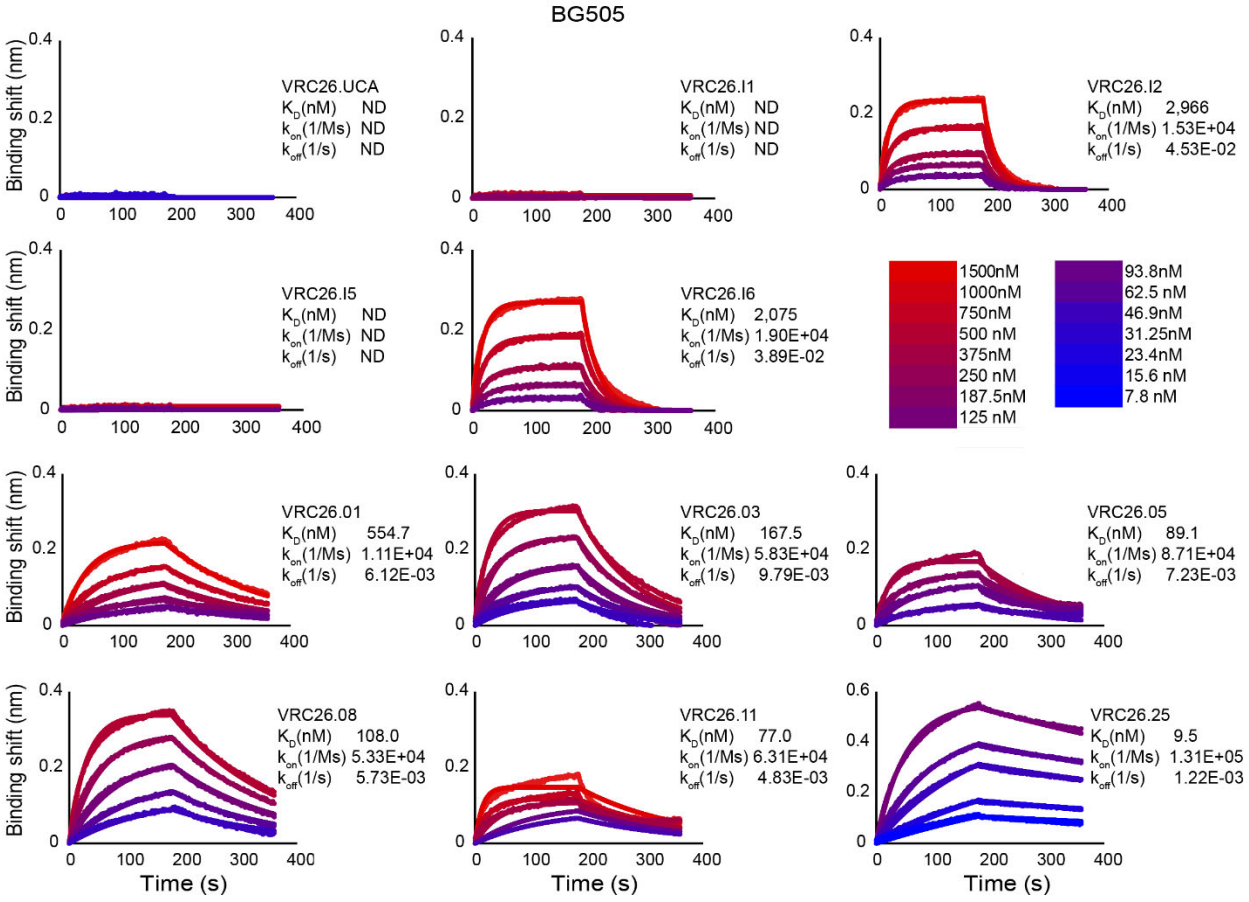

Figure 5. 1. VRC26 lineage IgG binding kinetics to BG505 Env trimers. Representative BLI sensorgrams of VRC26 lineage IgG binding to serially diluted BG505 SOSIP is shown. SOSIP concentrations are shown according to the legend using a red to blue color gradient.

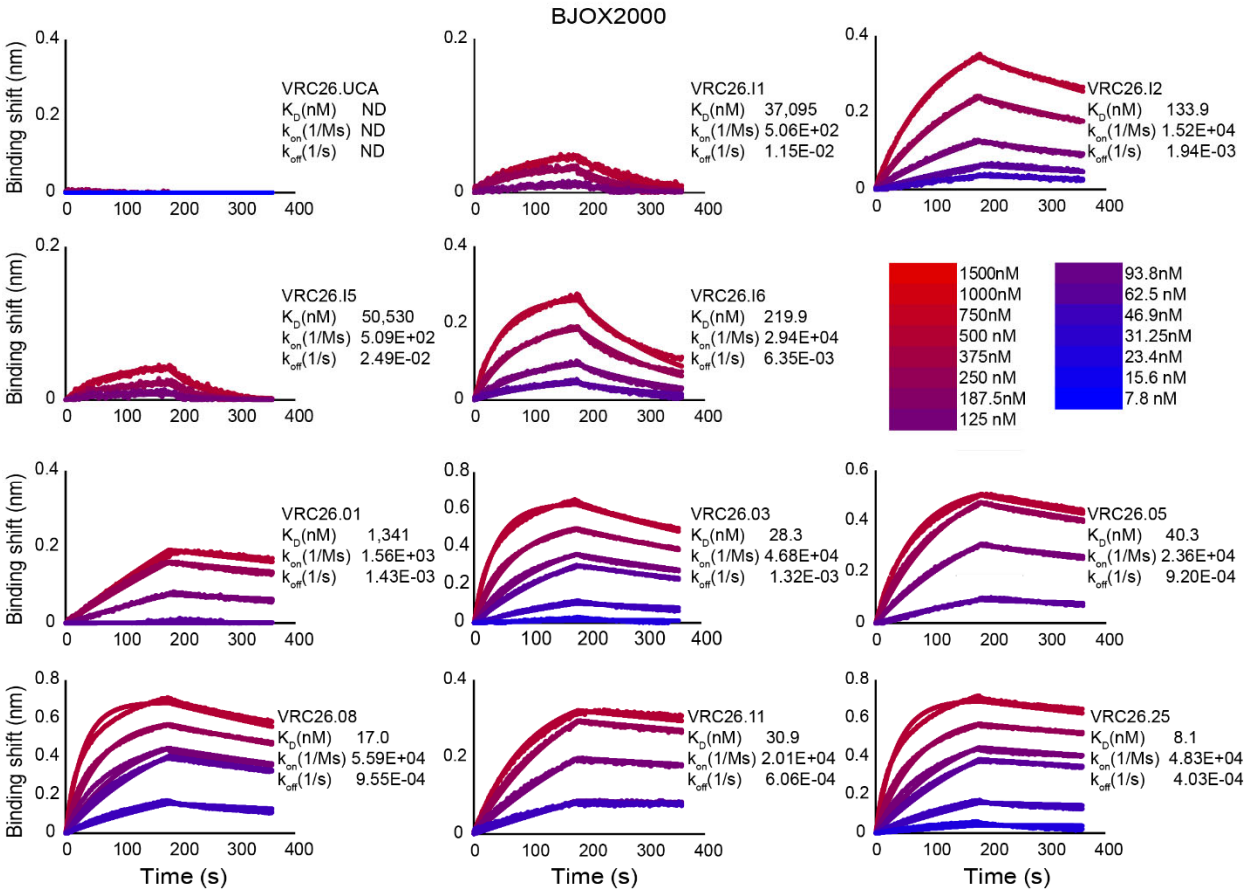

Figure 5. 2. VRC26 lineage IgG binding kinetics to BJOX2000 Env trimers. Representative BLI sensorgrams of VRC26 lineage IgG binding to serially diluted BJOX2000 SOSIP is shown. SOSIP concentrations are shown according to the legend using a red to blue color gradient.

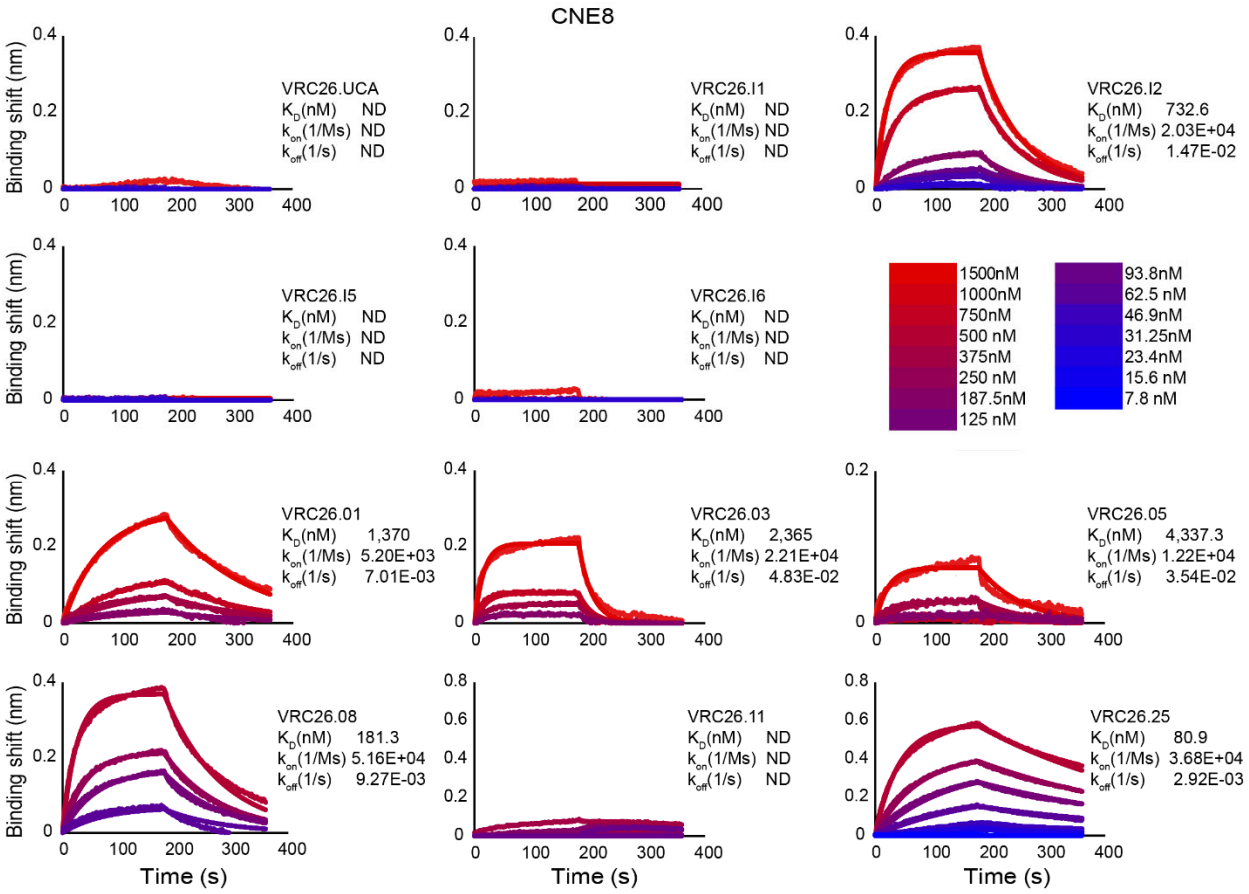

Figure 5. 3. VRC26 lineage IgG binding kinetics to CNE8 Env trimers. Representative BLI sensorgrams of VRC26 lineage IgG binding to serially diluted CNE8 SOSIP is shown. SOSIP concentrations are shown according to the legend using a red to blue color gradient.

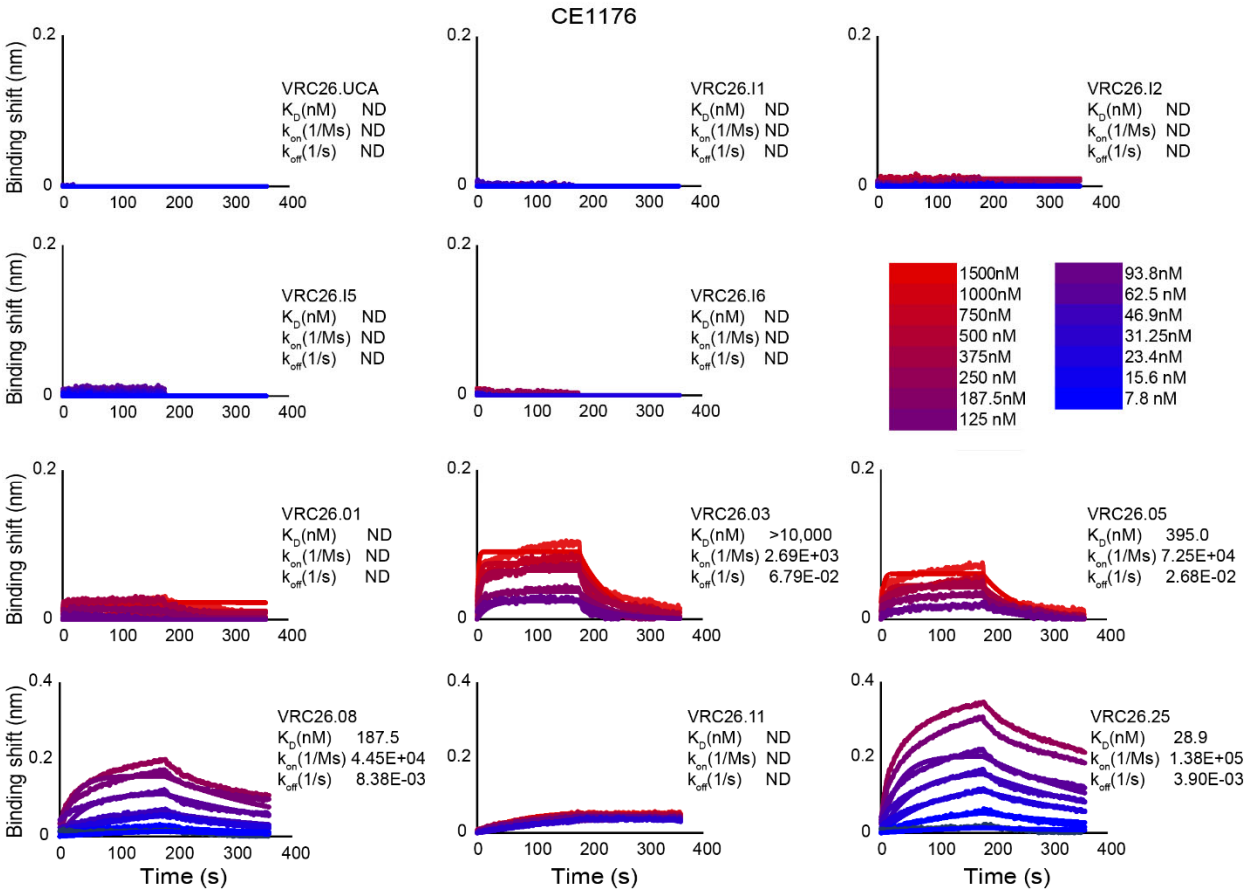

Figure 5. 4. VRC26 lineage IgG binding kinetics to CE1176 Env trimers. Representative BLI sensorgrams of VRC26 lineage IgG binding to serially diluted CE1176 SOSIP is shown. SOSIP concentrations are shown according to the legend using a red to blue color gradient.

A

SOSIP	VRC26.UCA K_D(nM)	VRC26.I1 K_D(nM)	VRC26.I2 K_D(nM)	VRC26.I5 K_D(nM)	VRC26.I6 K_D(nM)	VRC26.01 K_D(nM)	VRC26.03 K_D(nM)	VRC26.05 K_D(nM)	VRC26.08 K_D(nM)	VRC26.11 K_D(nM)	VRC26.25 K_D(nM)
BG505	ND	ND	2965.5 +/- 190.2	ND	2,075 +/- 417.2	554.17 +/- 113.2	167.5 +/- 12.0	89.1 +/- 33.9	108.0 +/- 11.3	77.0 +/- 10.5	9.5 +/- 2.2
CE1176	ND	ND	ND	ND	ND	ND	> 10,000	395.0 +/- 171.1	187.5 +/- 17.7	ND	28.9 +/- 5.7
CNE8	ND	ND	732.6 +/- 150.5	ND	ND	1,370 +/- 144.2	2,365.0 +/- 728.3	4337.3 +/- 3454	181.3 +/- 18.6	ND	80.9 +/- 14.5
BJOX	ND	> 10,000	133.9 +/- 55.5	> 10,000	219.9 +/- 48	1,341.3 +/- 1084	28.3 +/- 0.8	40.3 +/- 9.9	17.0 +/- 1.0	30.9 +/- 9.3	8.1 +/- 2.2

B

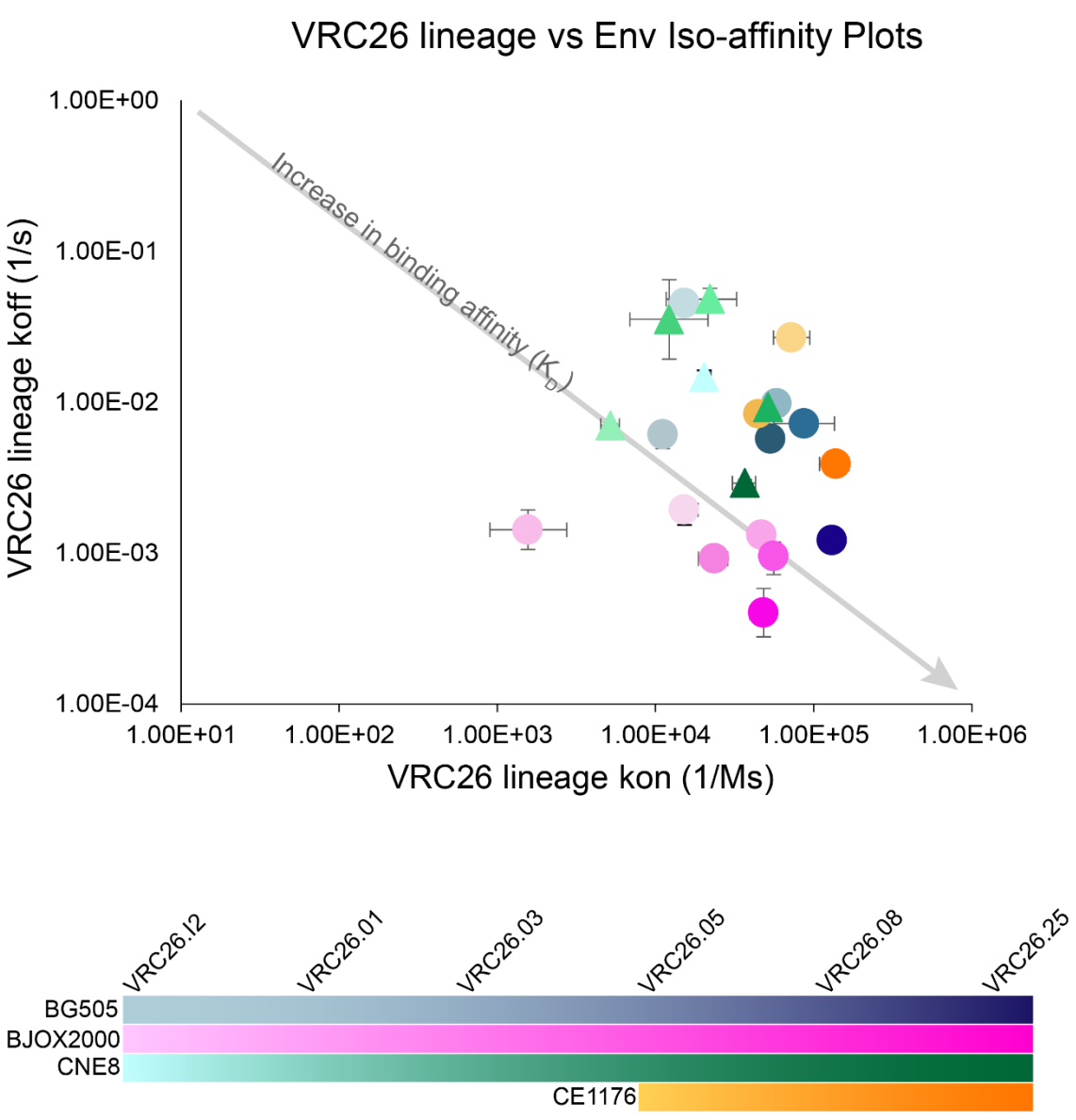

Figure 5. 5. Differences in VRC26 lineage IgG binding affinities to four diverse Env trimers are often driven by differences in off rates for each respective antibody. A table reports the average binding affinity (K_D) of each VRC26 lineage IgG for each respective Env trimer across at least two duplicate experiments +/- the percent standard deviation. An iso-affinity plot is shown (B) including antibodies that bound at least 3 of the 4 Env trimers with the average dissociation rate on the y-axis and the average association rate on the x-axis. Each trimer is colored differently; BG505 in blue, CE1176 in orange, BJOX2000 in pink, and CNE8 in green triangles. The shades of the color indicate the VRC26 lineage antibody the binding data corresponds to. The lighter shades are the less affinity mature versions of the VRC26 lineage antibodies, and the shades become darker with the more affinity mature constructs. Binding kinetics values are the average from at least two independent experiments with percent standard deviation error bars.

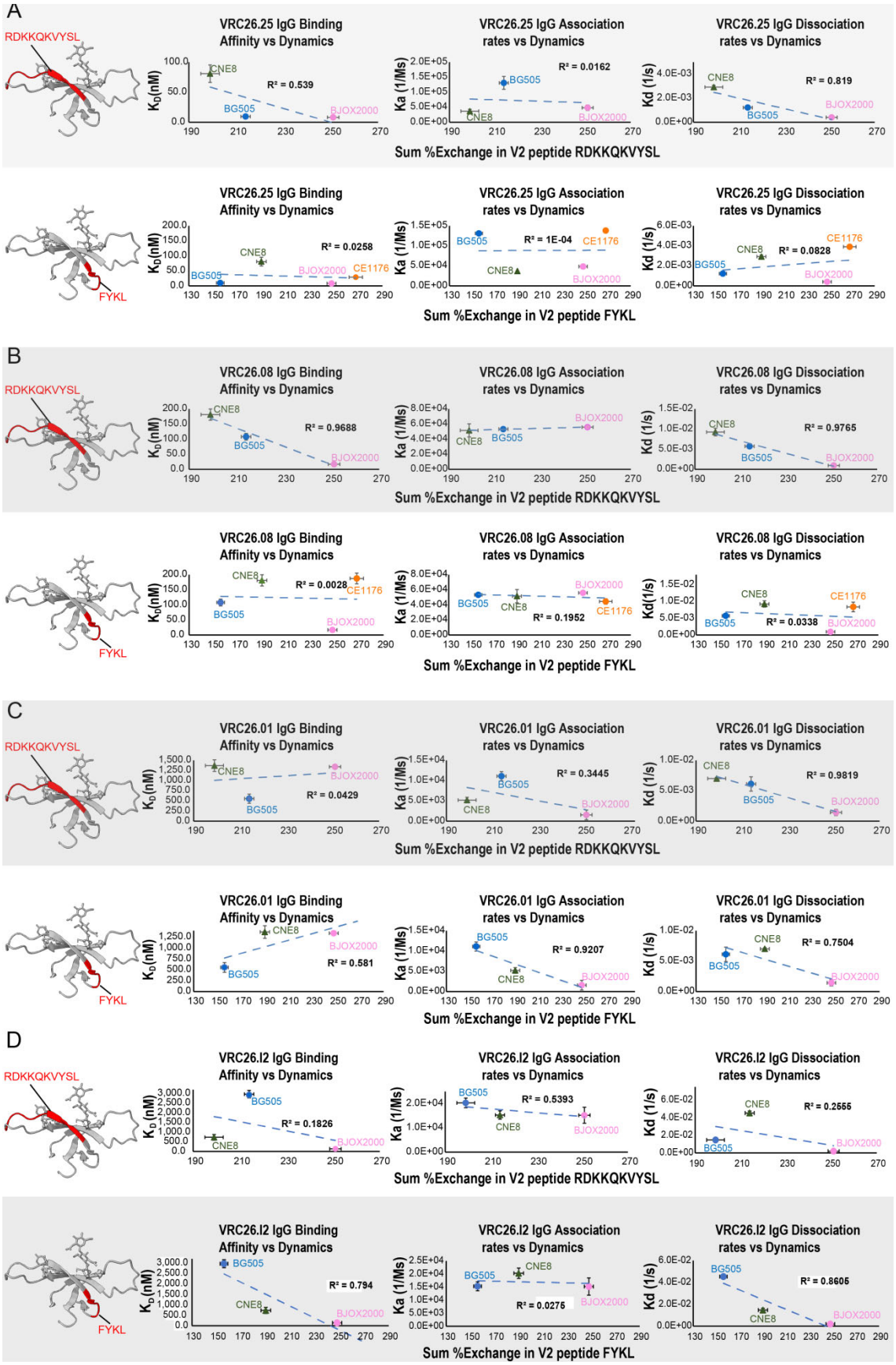
A
RDKKQKVYSL
VRC26.25 IgG Binding Affinity vs Dynamics
VRC26.25 IgG Association rates vs Dynamics
VRC26.25 IgG Dissociation rates vs Dynamics
KD(nM)
Ka (1/Ms)
Kd (1/s)
CNE8
BG505
BJOX2000
R² = 0.539
R² = 0.0162
R² = 0.819
Sum %Exchange in V2 peptide RDKKQKVYSL
FYKL
R² = 0.0258
R² = 1E-04
R² = 0.0828
CE1176
Sum %Exchange in V2 peptide FYKL
B
VRC26.08 IgG Binding Affinity vs Dynamics
VRC26.08 IgG Association rates vs Dynamics
VRC26.08 IgG Dissociation rates vs Dynamics
R² = 0.9688
R² = 0.9765
R² = 0.0028
R² = 0.1952
R² = 0.0338
C
VRC26.01 IgG Binding Affinity vs Dynamics
VRC26.01 IgG Association rates vs Dynamics
VRC26.01 IgG Dissociation rates vs Dynamics
R² = 0.0429
R² = 0.3445
R² = 0.9819
R² = 0.581
R² = 0.9207
R² = 0.7504
D
VRC26.I2 IgG Binding Affinity vs Dynamics
VRC26.I2 IgG Association rates vs Dynamics
VRC26.I2 IgG Dissociation rates vs Dynamics
R² = 0.1826
R² = 0.5393
R² = 0.2655
R² = 0.794
R² = 0.0275
R² = 0.8605

Figure 5. 6. VRC26 lineage antibody dissociation rates moderately correlate with V2 loop epitope dynamics, and less affinity mature antibodies are impacted by V2 loop dynamics across a larger surface area. The sum of the %exchange in the V2 loop peptide RDKKQKVYSL spanning residues 166-175 and FYKL spanning residues 176-179 (highlighted in red on the PDB 4VTP structure) are plotted against the average VRC26 antibody binding affinity, association rate, and dissociation rate for each SOSIP derived from different HIV isolates (blue circle for BG505, pink circle for BJOX2000, green circle for CE1176, and green triangle for CNE8). The most affinity mature antibody from the VRC26 lineage (VRC26.25) is shown in (A), VRC26.08 is shown in (B), VRC26.01 is shown in (C), and VRC26.I2 in (D).

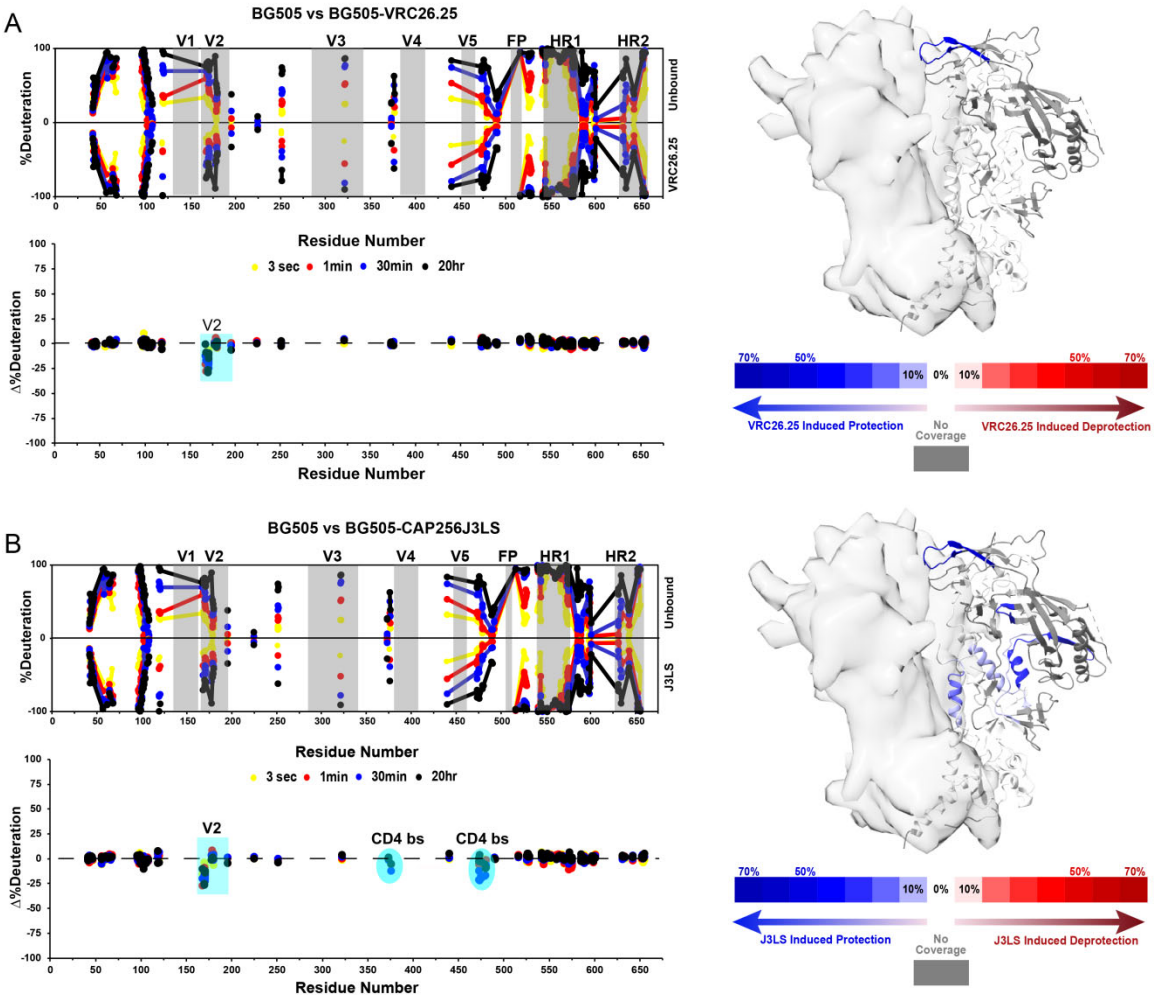

Figure 5. 7. HDX differential plots map the VRC26.25 and CAP256J3LS binding site on the BG505 trimer. A butterfly plot showing the profile of dynamics for free BG505 SOSIP (top) and the VRC26.25 fAb bound state (A) or the CAP256J3LS bound state (B) on the bottom. The mid-point of each homologous peptide found in BG505 unbound (top half) and BG505 bound to VRC26.25 (bottom half in A) or CAP256J3LS (bottom half in B) is plotted to show deuterium uptake with time (3-second time point in yellow, 1-minute time point in red, 30-minute time point in blue, and 20-hour time point in black). Underneath each butterfly plot is a differential plot showing the percent difference in exchange between the free BG505 state and the BG505 bound to VRC26.25 fAb (A) or CAP256J3LS state (B). Peptides falling below the 0 dashed lines are regions more protected from exchange when VRC26.25 (A) or CAP256J3LS (B) is bound, and peptides falling above the dashed line are regions that became less protected from exchange. To the right the sum of the differences in backbone amide dynamics comparing BG505 unbound and VRC26.25 bound (A) or CAP256J3LS bound (B) across time are mapped onto the BG505 SOSIP structure (PDB 5ACO). Regions colored blue are more protected from exchange in the bound state, and regions colored red are regions that are more exposed.

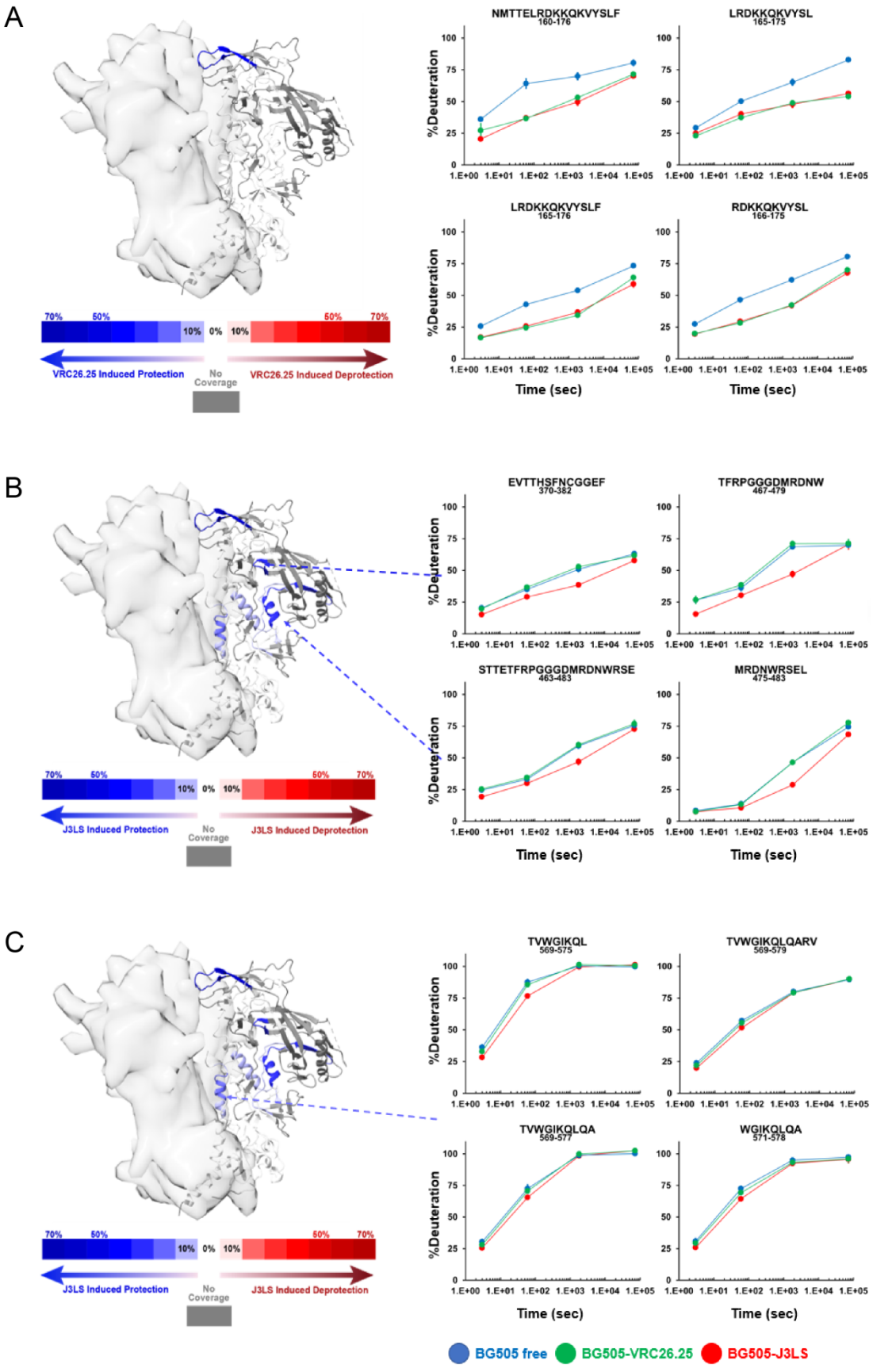
A
NMTTELRDKKQKVYSLF
160-176
LRDKKQKVYSL
165-175
LRDKKQKVYSLF
165-176
RDKKQKVYSL
166-175
%Deuteration
Time (sec)
70% 50% 10% 0% 10% 50% 70%
VRC26.25 Induced Protection
No Coverage
VRC26.25 Induced Deprotection
B
EVTTHSFNCGGEF
370-382
TFRPGGGDMRDNW
467-479
STTETFRPGGGDMRDNWRSE
463-483
MRDNWRSEL
475-483
J3LS Induced Protection
J3LS Induced Deprotection
C
TVWGIKQL
569-575
TVWGIKQLQARV
569-579
TVWGIKQLQA
569-577
WGIKQLQA
571-578
BG505 free
BG505-VRC26.25
BG505-J3LS

Figure 5. 8. The VRC26.25 epitope is focused in the V2 loop C strand, while the bispecific CAP256J3LS binding site includes the V2 loop and CD4 binding site, as well as allosteric stabilization in HR1. The sum of the differences in backbone amide dynamics between the free BG505 trimer and the BG505-VRC26.25 Fab bound state across time are mapped onto the BG505 SOSIP structure (PDB 5ACO) in figure A. Regions colored blue are more protected from exchange in the VRC26.25 bound state, and regions colored red are regions that are more exposed. Similarly the sum of the differences in backbone amide dynamics between the free BG505 trimer and the BG505-CAP25J3LS bound state across time are mapped onto the BG505 SOSIP structure (PDB 5ACO) in figure B and C. Deuterium uptake plots are to the right comparing differences in backbone amide protection across time (3secs, 1min, 30min, 20hr) in free BG505, BG505-VRC26.25, and BG505-J3LS (blue, green, and red circles respectively). Each point on the plot is the average percent deuteration of two replicates normalized to a fully deuterated control with standard deviation bars.

References

1. Andrabi, R., et al., *Identification of Common Features in Prototype Broadly Neutralizing Antibodies to HIV Envelope V2 Apex to Facilitate Vaccine Design.* Immunity, 2015. **43**(5): p. 959-973.
2. Lee, J.H., et al., *A broadly neutralizing antibody targets the dynamic HIV envelope trimer apex via a long, rigidified, and anionic β-hairpin structure.* A broadly neutralizing antibody targets the dynamic HIV envelope trimer apex via a long, rigidified, and anionic β-hairpin structure, 2017.
3. Gorman, J., et al., *Structure of Super-Potent Antibody CAP256-VRC26.25 in Complex with HIV-1 Envelope Reveals a Combined Mode of Trimer-Apex Recognition.* Cell Rep, 2020. **31**(1): p. 107488.
4. Doria-Rose, N.A., et al., *New Member of the V1V2-Directed CAP256-VRC26 Lineage That Shows Increased Breadth and Exceptional Potency.* J Virol, 2016. **90**(1): p. 76-91.
5. Doria-Rose, N.A., et al., *Developmental pathway for potent V1V2-directed HIV-neutralizing antibodies.* Nature, 2014. **509**(7498): p. 55-62.
6. Zhang, B., et al., *Bispecific antibody CAP256.J3LS targets V2-apex and CD4-binding sites with high breadth and potency.* MAbs, 2023. **15**(1): p. 2165390.
7. Hodge, E.A., et al., *Structural dynamics reveal isolate-specific differences at neutralization epitopes on HIV Env.* iScience, 2022. **25**(6): p. 104449.

8. Wrapp, D., et al., *Structure-Based Stabilization of SOSIP Env Enhances Recombinant Ectodomain Durability and Yield.* J Virol, 2023. **97**(1): p. e0167322.
9. de Taeye, S.W., et al., *Immunogenicity of Stabilized HIV-1 Envelope Trimers with Reduced Exposure of Non-neutralizing Epitopes.* Cell, 2015. **163**(7): p. 1702-1715.
10. de la Peña, A., et al., *Improving the Immunogenicity of Native-like HIV-1 Envelope Trimers by Hyperstabilization.* Cell Reports, 2017. **20**(8): p. 1805-1817.
11. de Taeye, S.W., et al., *Stabilization of the V2 loop improves the presentation of V2 loop-associated broadly neutralizing antibody epitopes on HIV-1 envelope trimers.* The Journal of biological chemistry, 2019. **294**(14): p. 5616-5631.
12. Rawi, R., et al., *Automated Design by Structure-Based Stabilization and Consensus Repair to Achieve Prefusion-Closed Envelope Trimers in a Wide Variety of HIV Strains.* Cell Rep, 2020. **33**(8): p. 108432.
13. Landais, E., et al., *HIV Envelope Glycoform Heterogeneity and Localized Diversity Govern the Initiation and Maturation of a V2 Apex Broadly Neutralizing Antibody Lineage.* Immunity, 2017. **47**(5): p. 990-1003 e9.
14. Cao, L., et al., *Global site-specific N-glycosylation analysis of HIV envelope glycoprotein.* Nature Communications, 2017. **8**: p. 14954.
15. Lu, M., et al., *Associating HIV-1 envelope glycoprotein structures with states on the virus observed by smFRET.* Nature, 2019. **568**(7752): p. 415-419.
16. Mangala Prasad, V., et al., *Cryo-ET of Env on intact HIV virions reveals structural variation and positioning on the Gag lattice.* Cell, 2022. **185**(4): p. 641-653 e17.
17. Bricault, C.A., et al., *HIV-1 Neutralizing Antibody Signatures and Application to Epitope-Targeted Vaccine Design.* Cell Host Microbe, 2019. **25**(1): p. 59-72 e8.

Supplementary Figures

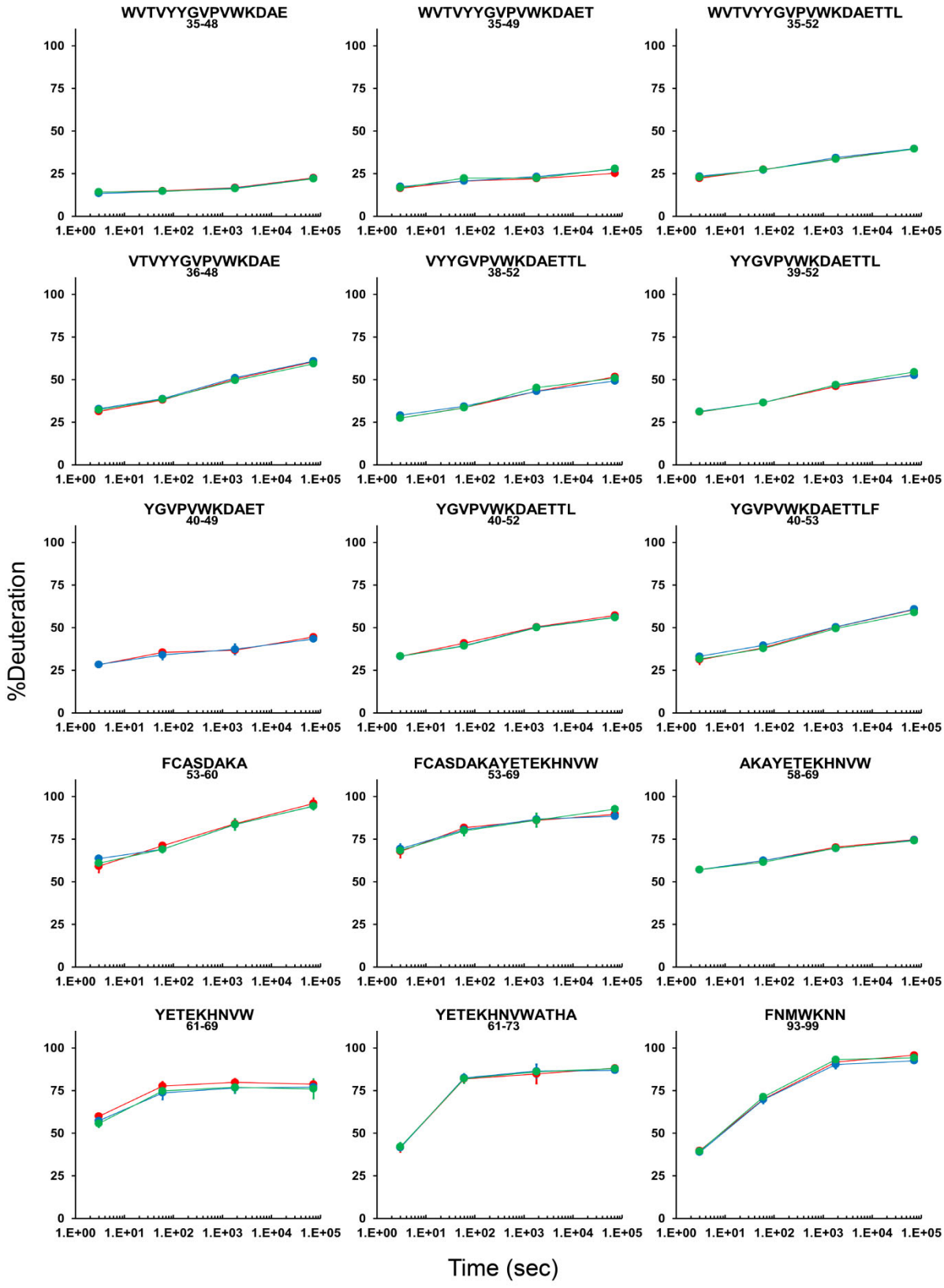
WVTVYYGVPVWKDAE
35-48
WVTVYYGVPVWKDAET
35-49
WVTVYYGVPVWKDAETTL
35-52
VTVYYGVPVWKDAE
36-48
VYYGVPVWKDAETTL
38-52
YYGVPVWKDAETTL
39-52
YGVPVWKDAET
40-49
YGVPVWKDAETTL
40-52
YGVPVWKDAETTLF
40-53
FCASDAKA
53-60
FCASDAKAYETEKHNVW
53-69
AKAYETEKHNVW
58-69
YETEKHNVW
61-69
YETEKHNVWATHA
61-73
FNMWKNN
93-99
%Deuteration
Time (sec)
0
25
50
75
100
1.E+00
1.E+01
1.E+02
1.E+03
1.E+04
1.E+05

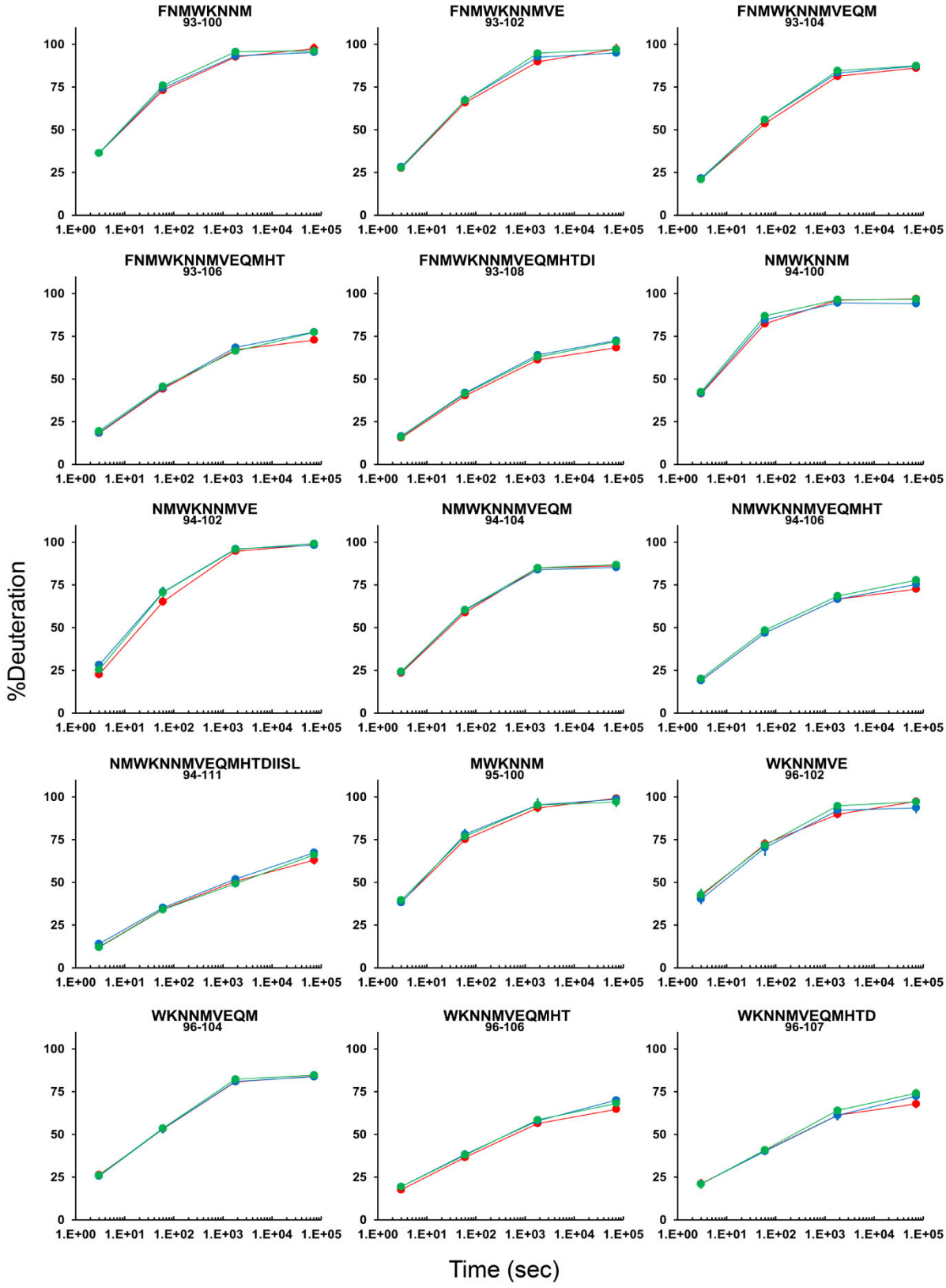
FNMWKNNM
93-100
FNMWKNNMVE
93-102
FNMWKNNMVEQM
93-104
FNMWKNNMVEQMHT
93-106
FNMWKNNMVEQMHTDI
93-108
NMWKNNM
94-100
NMWKNNMVE
94-102
NMWKNNMVEQM
94-104
NMWKNNMVEQMHT
94-106
NMWKNNMVEQMHTDIISL
94-111
MWKNNM
95-100
WKNNMVE
96-102
WKNNMVEQM
96-104
WKNNMVEQMHT
96-106
WKNNMVEQMHTD
96-107
100
75
50
25
0
1.E+00
1.E+01
1.E+02
1.E+03
1.E+04
1.E+05
%Deuteration
Time (sec)

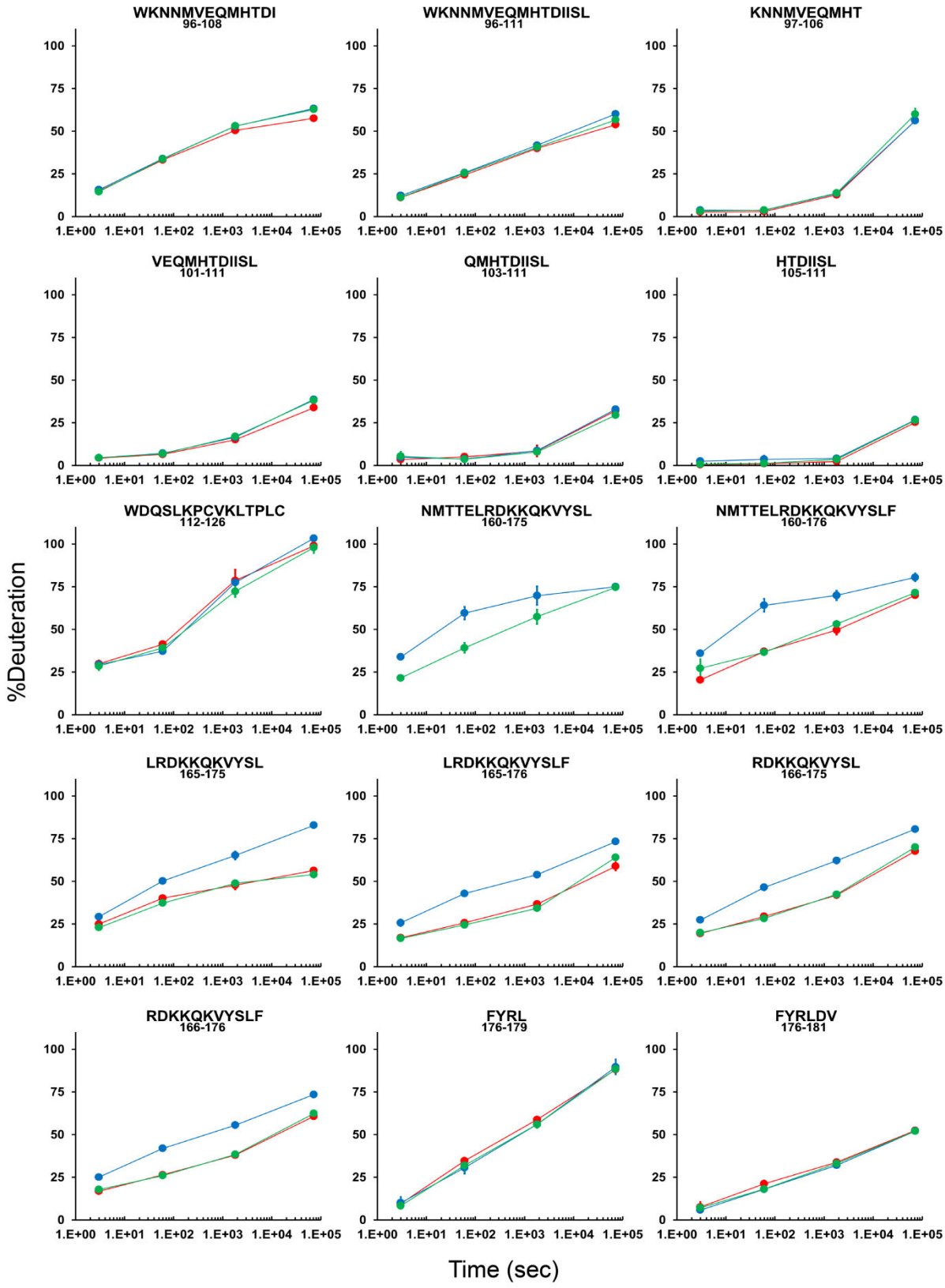
WKNNMVEQMHTDI
96-108
WKNNMVEQMHTDIISL
96-111
KNNMVEQMHT
97-106
VEQMHTDIISL
101-111
QMHTDIISL
103-111
HTDIISL
105-111
WDQSLKPCVKLTPLC
112-126
NMTTELRDKKQKVYSL
160-175
NMTTELRDKKQKVYSLF
160-176
LRDKKQKVYSL
165-175
LRDKKQKVYSLF
165-176
RDKKQKVYSL
166-175
RDKKQKVYSLF
166-176
FYRL
176-179
FYRLDV
176-181
%Deuteration
Time (sec)

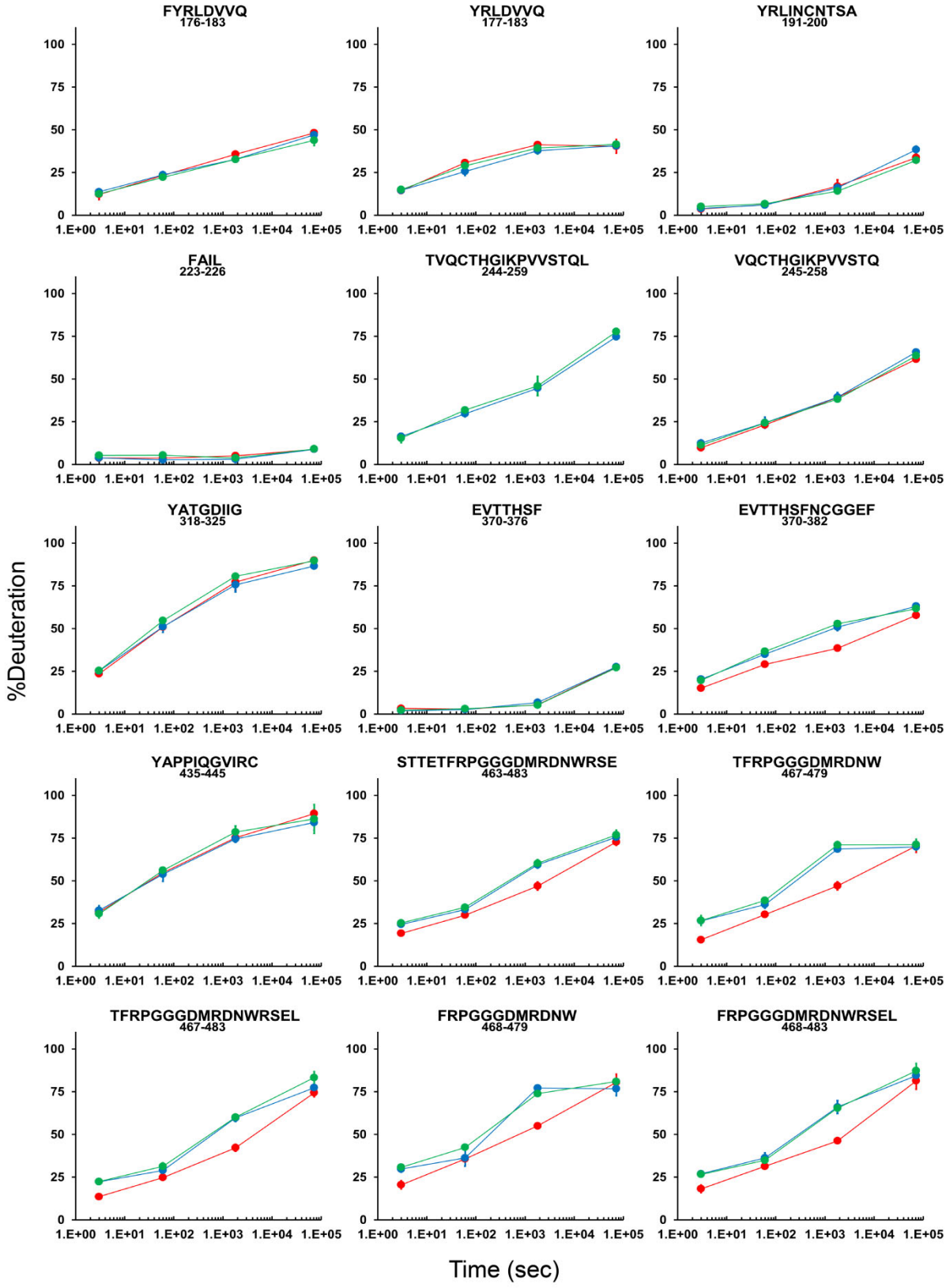
FYRLDVVQ
176-183
YRLDVVQ
177-183
YRLINCNTSA
191-200
FAIL
223-226
TVQCTHGIKPVVSTQL
244-259
VQCTHGIKPVVSTQ
245-258
YATGDIIG
318-325
EVTTHSF
370-376
EVTTHSFNCGGEF
370-382
YAPPIQGVIRC
435-445
STTETFRPGGGDMRDNWRSE
463-483
TFRPGGGDMRDNW
467-479
TFRPGGGDMRDNWRSEL
467-483
FRPGGGDMRDNW
468-479
FRPGGGDMRDNWRSEL
468-483
%Deuteration
Time (sec)

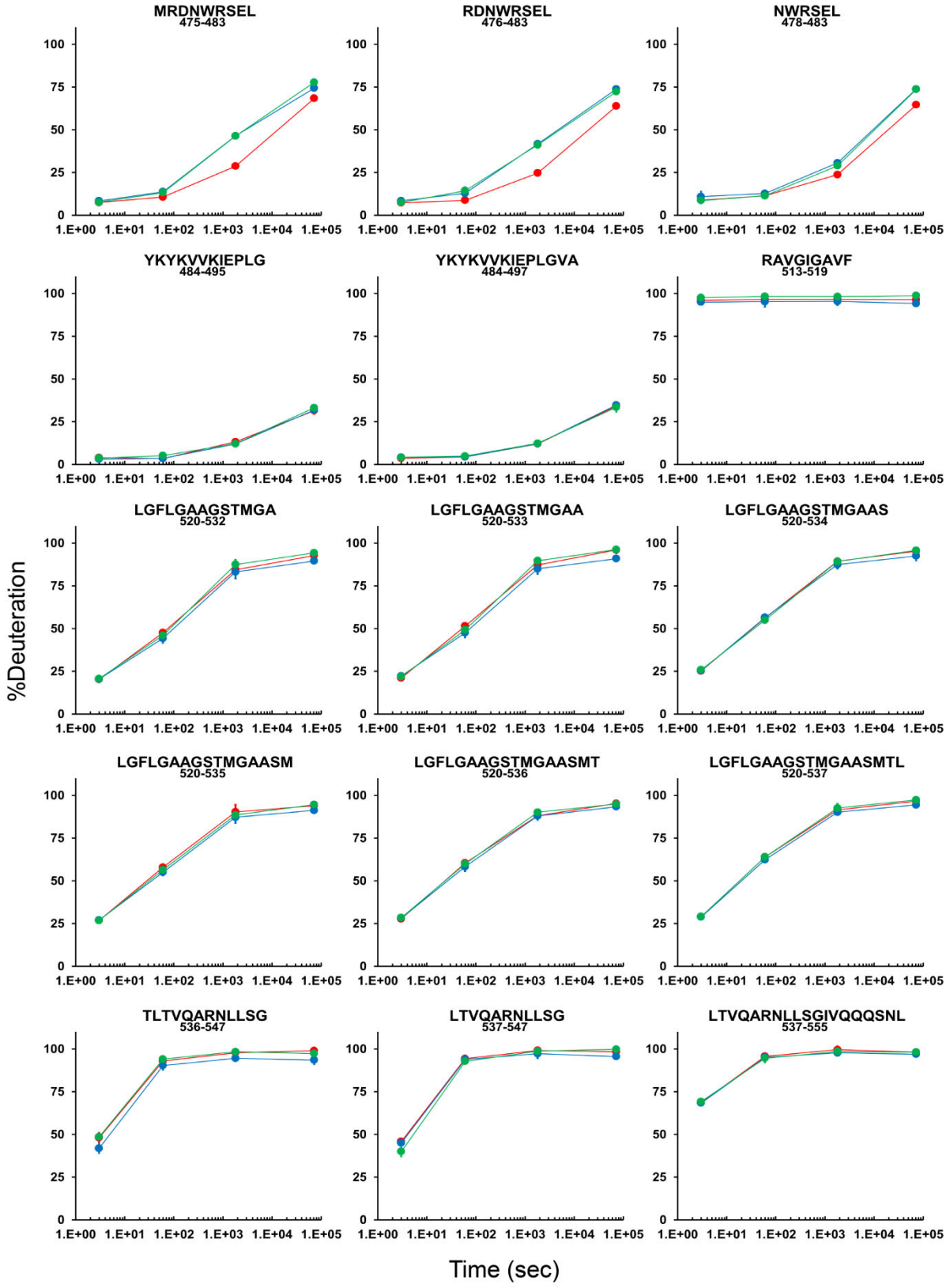
MRDNWRSEL
475-483
RDNWRSEL
476-483
NWRSEL
478-483
YKYKVVKIEPLG
484-495
YKYKVVKIEPLGVA
484-497
RAVGIGAVF
513-519
LGFLGAAGSTMGA
520-532
LGFLGAAGSTMGAA
520-533
LGFLGAAGSTMGAAS
520-534
LGFLGAAGSTMGAASM
520-535
LGFLGAAGSTMGAASMT
520-536
LGFLGAAGSTMGAASMTL
520-537
TLTVQARNLLSG
536-547
LTVQARNLLSG
537-547
LTVQARNLLSGIVQQQSNL
537-555
%Deuteration
Time (sec)

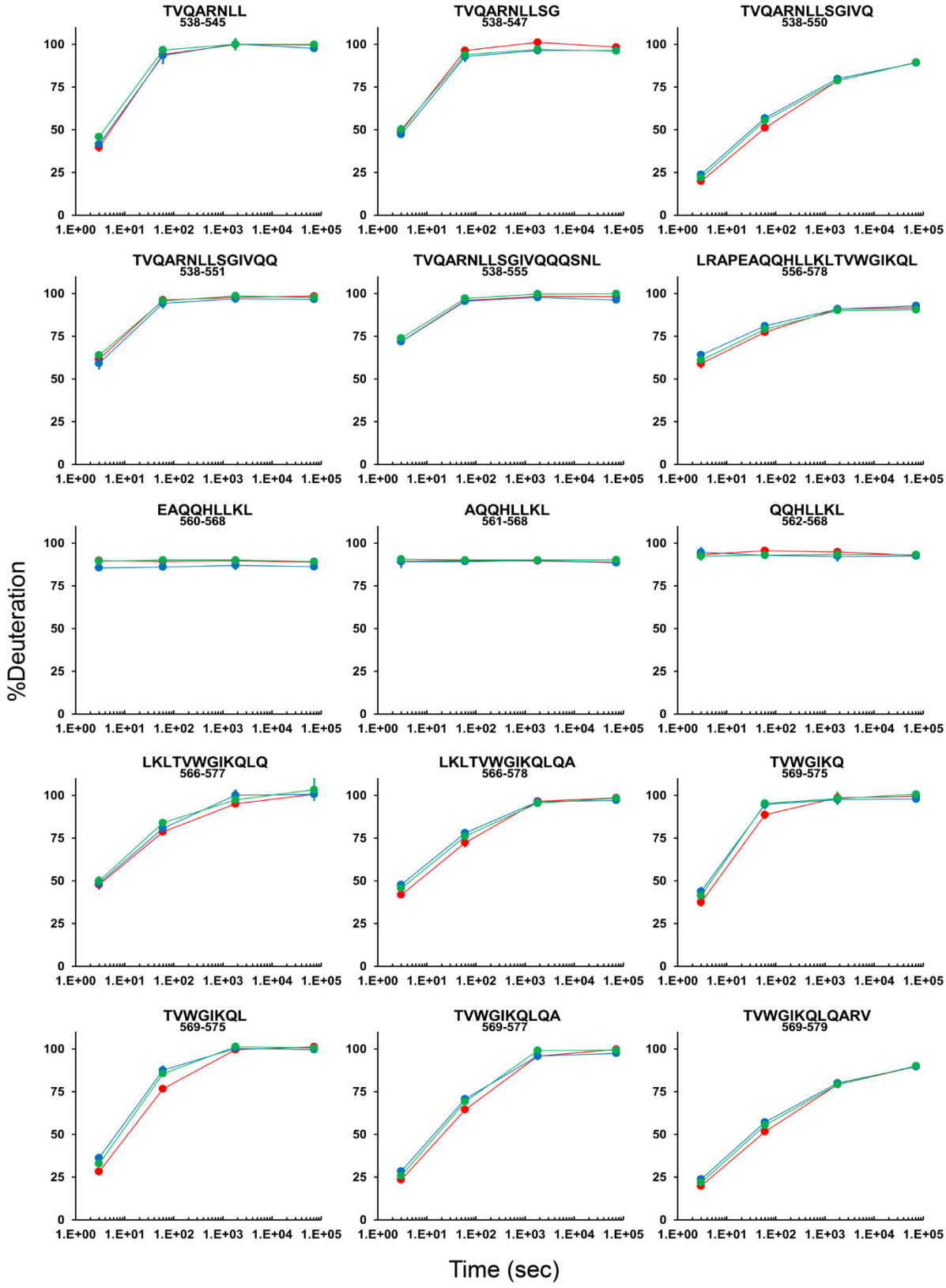
TVQARNLL
538-545
TVQARNLLSG
538-547
TVQARNLLSGIVQ
538-550
TVQARNLLSGIVQQ
538-551
TVQARNLLSGIVQQQSNL
538-555
LRAPEAQQHLLKLTVWGIKQL
556-578
EAQQHLLKL
560-568
AQQHLLKL
561-568
QQHLLKL
562-568
LKLTVWGIKQLQ
566-577
LKLTVWGIKQLQA
566-578
TVWGIKQ
569-575
TVWGIKQL
569-575
TVWGIKQLQA
569-577
TVWGIKQLQARV
569-579
%Deuteration
Time (sec)
0
25
50
75
100
1.E+00
1.E+01
1.E+02
1.E+03
1.E+04
1.E+05

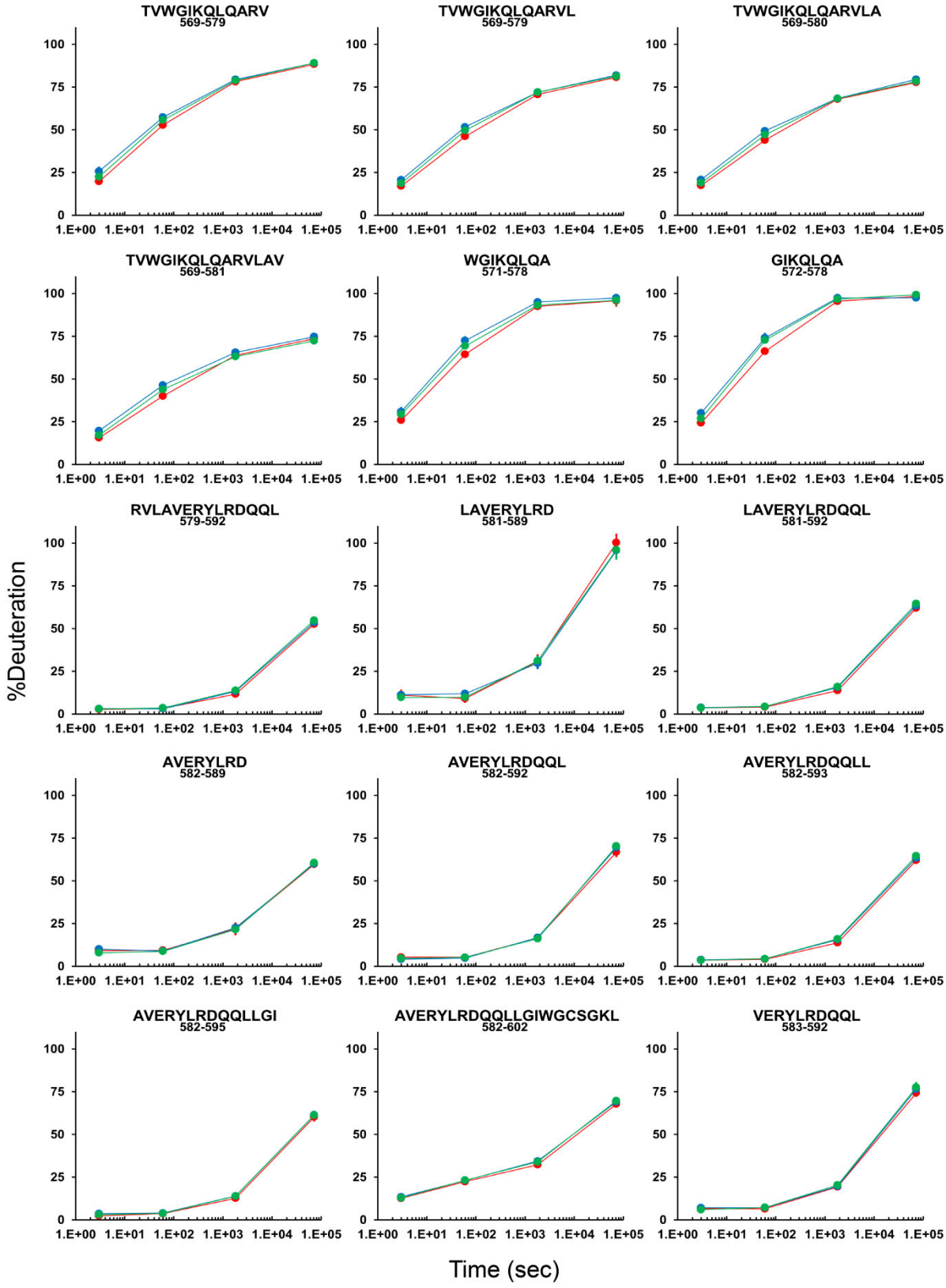
TVWGIKQLQARV
569-579
TVWGIKQLQARVL
569-579
TVWGIKQLQARVLA
569-580
TVWGIKQLQARVLAV
569-581
WGIKQLQA
571-578
GIKQLQA
572-578
RVLAVERYLRDQQL
579-592
LAVERYLRD
581-589
LAVERYLRDQQL
581-592
AVERYLRD
582-589
AVERYLRDQQL
582-592
AVERYLRDQQLL
582-593
AVERYLRDQQLLGI
582-595
AVERYLRDQQLLGIWGCSGKL
582-602
VERYLRDQQL
583-592
100
75
50
25
0
1.E+00
1.E+01
1.E+02
1.E+03
1.E+04
1.E+05
%Deuteration
Time (sec)

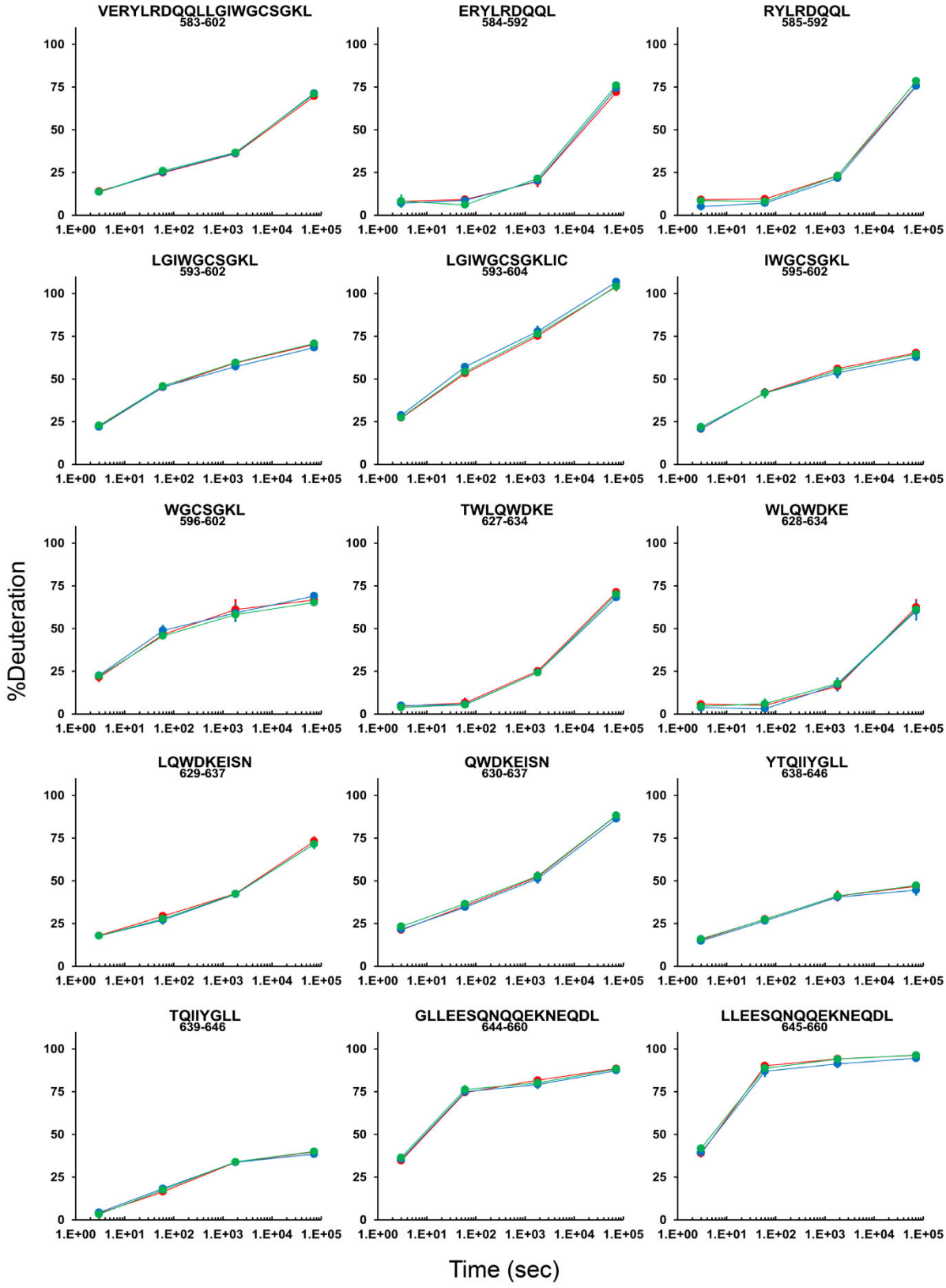
VERYLRDQQLLGIWGCSGKL
583-602
ERYLRDQQL
584-592
RYLRDQQL
585-592
LGIWGCSGKL
593-602
LGIWGCSGKLIC
593-604
IWGCSGKL
595-602
WGCSGKL
596-602
TWLQWDKE
627-634
WLQWDKE
628-634
LQWDKEISN
629-637
QWDKEISN
630-637
YTQIIYGLL
638-646
TQIIYGLL
639-646
GLLEESQNQQEKNEQDL
644-660
LLEESQNQQEKNEQDL
645-660
%Deuteration
Time (sec)
0
25
50
75
100
1.E+00
1.E+01
1.E+02
1.E+03
1.E+04
1.E+05

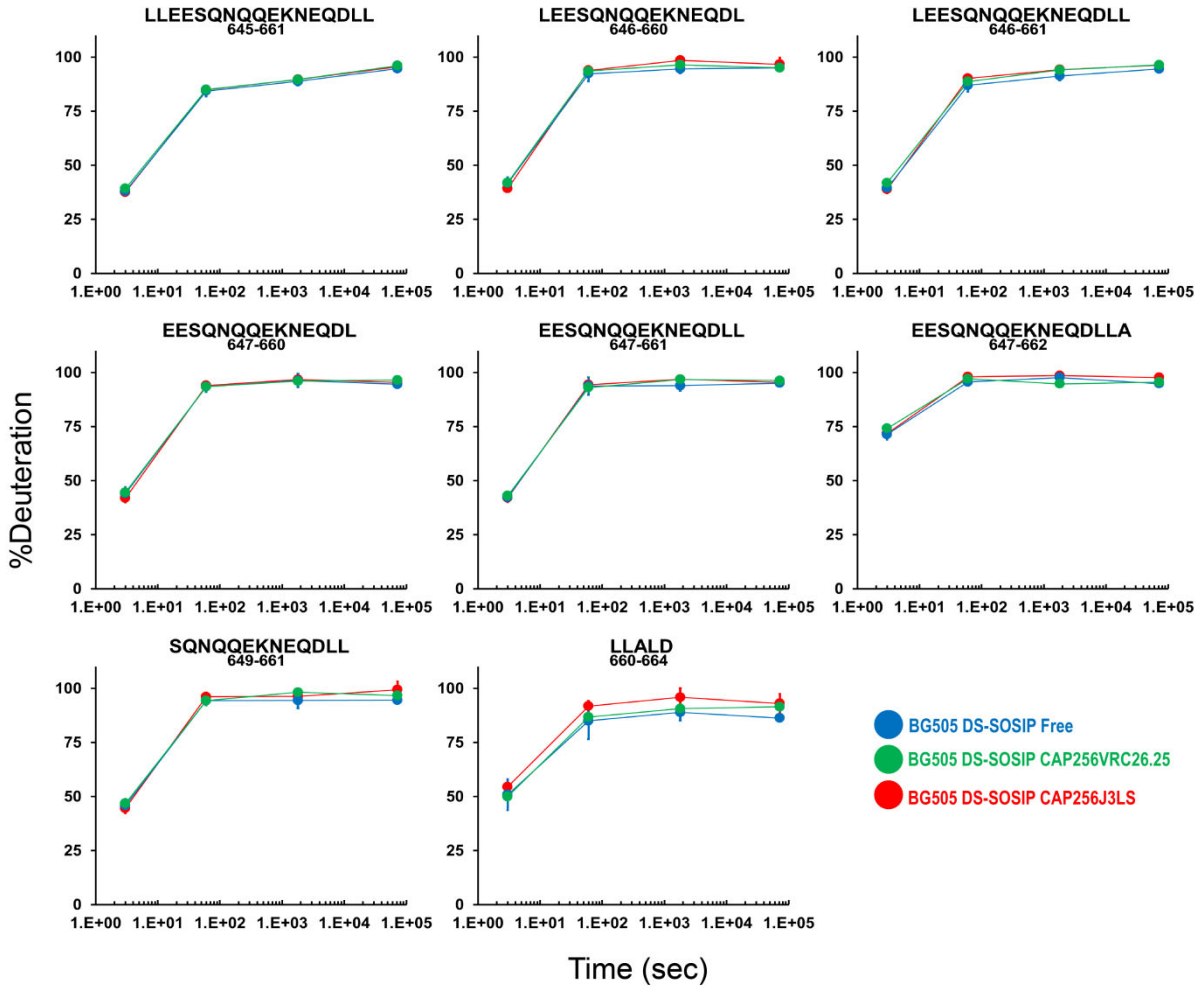

Figure S5.1. HDX plots comparing unbound BG505, BG505 bound to VRC26.25, and BG505 bound to CAP256J3LS. Deuterium uptake plots show backbone amide protection across time (3secs, 1min, 30min, 20hr) in free BG505, BG505-VRC26.25, and BG505-J3LS (blue, green, and red circles respectively). Each point on the plot is the average percent deuteration of two replicates normalized to a fully deuterated control with standard deviation bars.